A Thesis for the Degree of Ph.D. in Engineering

Sensorless Cutting Force Estimation in Ball-screw-drive System and Its Application to Chatter Avoidance

August 2017

Graduate School of Science and Technology
Keio University

Yuki Yamada

Table of contents

Table of contents i

Nomenclature iv

1. Introduction 1
   1.1 Key technology for a self-optimizing machine tool 1
   1.2 Process monitoring technology 3
   1.3 Cutting force monitoring technique 6
      1.3.1 Sensor-based approach 6
      1.3.2 Sensorless approach 8
      1.3.3 New challenges 10
   1.4 Chatter monitoring and avoidance technique 11
      1.4.1 Chatter avoidance technique in single tool cutting 11
      1.4.2 Chatter monitoring technique 14
      1.4.3 Chatter avoidance techniques in parallel turning 15
      1.4.4 New challenges 16
   1.5 Research purpose 16
   1.6 Organization of the dissertation 17

2. Sensorless cutting force estimation technique using multi-encoder 20
   2.1 Introduction 20
   2.2 Physical model of ball-screw-driven stage 20
   2.3 Cutting force estimation technique based on disturbance observer 23
      2.3.1 Disturbance observer 23
      2.3.2 Application to cutting force estimation 24
      2.3.3 Frequency response of cutting force observer 25
   2.4 Cutting force estimation technique based on multi-encoder-based disturbance observer 26
      2.4.1 Estimation principle for cutting force 26
      2.4.2 Compensation of phase lag elements 28
   2.5 Mode decoupled cutting force estimation technique 29
      2.5.1 Diagonalization of dual-inertia model 29
      2.5.2 Estimation principle for cutting force 33
   2.6 Extension to multi-inertia system 34
      2.6.1 Estimation principle for cutting force 34
      2.6.2 Frequency response of cutting force observer 38

2.7 Summary 40

3. Simulator and experimental setup for evaluating cutting force observer 41
3.1 Configuration of ball-screw-driven stage 41
3.2 Configuration of control system 44
3.3 Frequency response of ball-screw-driven stage 45
3.3.1 Frequency response between motor and stage 45
3.3.2 Stage-side frequency response 48
3.4 Position-dependent characteristics of disturbance force 49
3.5 Summary 54

4. Influence of error factors in sensorless cutting force estimation . 56
4.1 Introduction 56
4.2 Evaluation of error factors by time-domain simulator 56
4.2.1 Extraction of error factors 56
4.2.2 Frequency response of cutting force observer 59
4.2.3 Estimation characteristics against milling force 63
4.3 Experimental evaluation through end milling tests 68
4.3.1 Experimental procedure 68
4.3.2 Evaluation of multi-encoder-based cutting force estimation 69
4.3.3 Influence of identification error of parameters and output error 75
4.4 Summary 83

5. Evaluation of mode-decoupled and sensorless cutting force estimation technique 85
5.1 Introduction 85
5.2 Evaluation of estimation performance using time-domain simulator 85
5.2.1 Frequency response of cutting force observer 85
5.2.2 Estimation characteristics against milling force 90
5.3 Position-dependent characteristics of relative displacement between motor and stage 92
5.4 Experimental evaluation through end milling tests 94
5.4.1 Estimation result for feed force component 94
5.4.2 Estimation result for cross-feed force component 98
5.5 Summary 108

6. Monitoring and avoidance of chatter in parallel turning 110
6.1 Introduction 110
6.2 Configuration of multi-tasking machine tool with multi-turret 110

6.3 Chatter monitoring applying estimated cutting force in parallel turning 113
6.4 Proposal of chatter avoidance technique by unequal pitch turning 117
6.4.1 Concept of unequal pitch turning 117
6.4.2 Optimization of pitch angle 119
6.4.3 Construction of in-process chatter avoidance system 121
6.5 Chatter avoidance test 123
6.5.1 Unequal pitch turning at optimum pitch angle difference 123
6.5.2 Robustness of pitch angle difference 125
6.5.3 Chatter avoidance based on in-process measurement of chatter frequency 128
6.6 Summary 129
7. Conclusions 131
Appendix 136
References 139
Acknowledgement 149

Nomenclature

Roman symbols

a	Axial depth of cut
A	Section area of cylindrical workpiece
a_{cm}	Equivalent angular acceleration at counter-motor in translational motion
$a_m(= R\alpha_m)$	Equivalent value of α_m in translational motion
a_n	Acceleration of nut
a_t	Acceleration of stage
C_a	Total damping coefficient in rigid body motion
C_k	Damping coefficient of structure
C_n	Damping coefficient at nut interface
$C_r(= D_r/R^2)$	Equivalent value of D_r in translational motion
C_t	Damping coefficient of translational element
C_ω	Equivalent damping coefficient between motor and nut
d	Diameter of workpiece
D_r	Viscous friction coefficient of rotational element
$D(s)$	Denominator of transfer function for motion equation
E	Young modulus
f_c	Chatter frequency
f_n	Natural frequency of first bending mode
F_{cut}	Cutting force
F_{dis}	Disturbance force
F_{fric}	Friction force
F_n	Load force at nut interface
g_{cut}	Cutoff coefficient of a low-pass filter in cutting force observer
g_{dis}	Cutoff coefficient of a low-pass filter in disturbance observer
g_{LPF}	Cutoff coefficient of a low-pass filter in pseudo differential
I	Second moment of area
I_a	Motor current
I_a^{comp}	Compensation current for disturbance force
J_r	Total inertia of motor, coupling, and ball-screw
k	Frequency in discrete Fourier transform
K_r	Total stiffness of feed screw system
K_t	Torque coefficient
K_ω	Equivalent torsional stiffness of feed screw system in translational motion
L	Length of workpiece
ℓ	Pitch length
l_1, l_2	Number of wave within central angle θ_1 and θ_2

M_a	Total movable mass in rigid body motion
$M_r(=J_r/R^2)$	Equivalent value of J_r in translational motion
M_t	Movable mass
M_n	Mass of nut interface including inertia of ball-screw
Q	Ratio of nominal value to actual value
r	Radial depth of cut
R	Transform coefficient for rotational to translational motion $(=\ell/2\pi)$
S	Spindle speed
$S_k[n]$	Discrete Fourier transform from $y[n]$ to $y[n+N-1]$
T_{fric}	Friction torque
T_s	Dead time for servo amplifier
T_m	Summation of dead time in numerical differential and signal transmission at motor side
T_t	Summation of dead time in numerical differential and signal transmission at stage side
$T_1,\ T_2,\ T_3$	Dead time for phase lag compensation
$x_m(=R\theta_m)$	Equivalent value of θ_m in translational motion
x_n	Displacement of nut
x_t	Displacement of stage
$y[k]$	Analyzed signal
$v_m(=R\omega_m)$	Equivalent value of ω_m in translational motion
v_n	Velocity of nut
v_t	Velocity of stage

Greek symbols

$\alpha(=M_t/M_r)$	Inertia ratio
α_c, β_c	Constant for proportional damping
α_m	Angular acceleration
ΔC_a	Variation in total damping coefficient
ΔK_t	Variation in torque coefficient
ΔM_a	Variation in total movable mass
$\Delta\varepsilon(=\varepsilon_2-\varepsilon_1)$	Phase difference between regenerative waves
$\Delta\theta$	Optimum pitch angle difference
ε	Phase difference
$\varepsilon_1, \varepsilon_2$	Phase delay of tool 1 (2) against tool 2 (1)
ζ_k	Damping ratio of structure
ζ_r	Damping ratio of rotational elements
ζ_t	Damping ratio of translational elements
η	Constant determined by boundary condition and mode number
θ_1, θ_2	Pitch angle between tool 1 (2) and tool 2 (1)

θ_{cm}	Angle of counter motor
θ_m	Angle of motor
λ	Eigenvalue
$\lambda\varepsilon$	
ρ	Specific weight
φ	Phase of chatter frequency component left on one circumference of workpiece
φ_1, φ_2	Phase of chatter frequency component within central angle θ_1 and θ_2
ω_{cc}	Bandwidth of current loop
ω_m	Angular velocity of motor
ω_s	Resonance frequency in dual-inertia system
ω_t	Anti-resonance frequency at motor side

Matrix and vector

$\boldsymbol{F}$	Force vector
$\boldsymbol{M}, \boldsymbol{C}, \boldsymbol{K}$	Mass, damping, stiffness matrix
$\boldsymbol{x}, \boldsymbol{v}, \boldsymbol{a}$	Displacement, velocity, and acceleration vector
$\boldsymbol{\phi}$	Modal matrix

Subscript

$modal$	Value in modal coordinate system
n	Nominal value
$rigid$	Value in rigid body mode
vib	Value in vibration mode
$vib(1st)$	Value in 1st vibration mode
$vib(2nd)$	Value in 2nd vibration mode

Superscripts

cmd	Command value
ref	Reference value
res	Response value
^ (hat)	Estimated value

Abbreviations

AE	Acoustic Emission
CSSV	Continuous Spindle Speed Variation
DOB	Disturbance Observer
DSST	Discrete Spindle Speed Tuning
FFT	Fast Fourier Transform
FRF	Frequency response function

LPF	Low-pass filter
MDoF	Multi-Degree-of-Freedom
MEDOB	Multi-encoder based Disturbance Observer
NC	Numerical Control
PLC	Programmable Logic Controller
PSD	Power Spectrum Density
SDFT	Sliding Discrete Fourier Transform
SDoF	Single-Degree-of-Freedom
STFT	Short Time Fourier Transform
SLD	Stability Lobe Diagram

1. Introduction

1.1 Key technology for a self-optimizing machine tool

The accuracy of mechanical parts is determined by the motion accuracy of a machine tool. In machining, a desired shape is generated by the relative motion between a cutting tool and a workpiece. Therefore, increasing the motion accuracy of a feed drive mounting spindle or a workpiece is indispensable in increasing machining accuracy. For a long time, the motion of the feed drive was manually controlled by an operator. The introduction of numerical control (NC) contributed to the automation of a machine tool as well as simultaneous multiple-axis control. Additionally, it led to a more uniform quality of products, and production speed/cost decreased due to mass production. The feed drive of the machine tool has kept high-speed and high-accuracy due to progress in trajectory generation, control algorithms, mechanical drives and guideways, amplifiers, and sensors [1].

Machine tool manufacturers actively work toward technological development for process integration. Multi-tasking machine tools, in which both turning and milling are possible in one chucking, are a typical example of this. A 5-axis machine tool that equips two additional rotary axes makes it possible to machine complex parts such as molds, aerospace parts and implants. Recently, commercially available machine tools can perform both cutting and additive manufacturing [2], or both cutting and quenching [3]. The progress in process integration has been remarkable.

Advances in control techniques including multiple-axis and machine elements facilitate high precision machining of complex shaped parts. There is a variation in customer needs and an increasing shortening in product lifecycles. It is necessary for machine tool manufacturers in high-wage countries, such as Japan, Germany, and the U.S., to cope with the shortening of the development period as well as various other needs [4]. Recently, significant technological progress was observed in emerging countries. It is difficult for high-wage nations to achieve a sufficient technological advantage as in previous years if they only pursue high-speed, high-precision, and automation based on mass production. Breakthroughs beyond existing technology are expected.

Virtual manufacturing technology [5,6] is an example of enhancing competitiveness. In developing a machine tool, performance was traditionally evaluated by making prototypes and conducting time-consuming tests. In virtual manufacturing, manufacturers can significantly reduce total costs, because they can reduce the development period by conducting a series of operations in a virtual space, from design

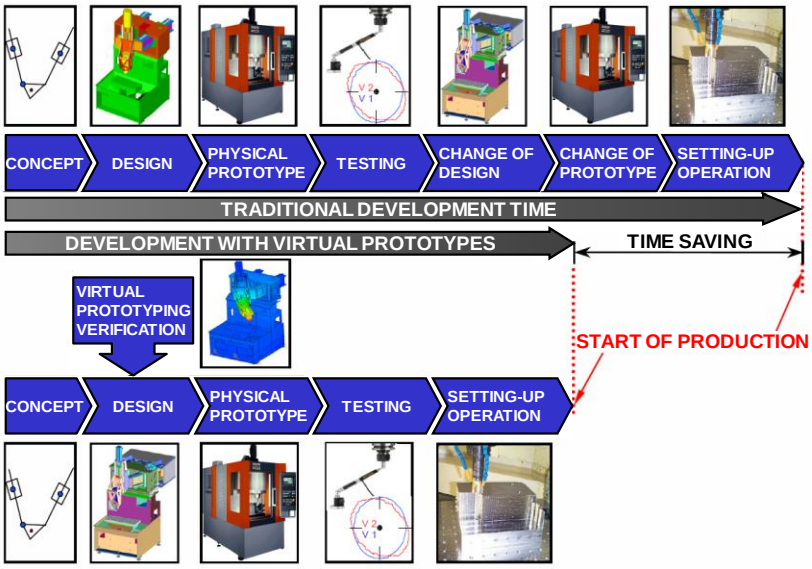

Fig. 1-1 Comparison of the traditional design process and the design process with virtual prototypes [5] (Y. Altintas, C. Brecher, M. Weck, and S. Witt, CIRP Annals, Vol.54, No.2, pp. 115–138, (2005). The figure is used with permission from Elsevier.)

to performance assessment, as shown in Fig. 1-1. Additionally, the quality of the product and the interference between the tool and workpiece can be checked by performing virtually machining on a simulator, which considers a process model of cutting and the dynamics of the machine tool. Virtual machining can be a powerful tool in terms of production planning. However, virtual manufacturing is a model reference approach based on an initial condition. Therefore, virtual manufacturing does not consider variations in the environment or state. Virtual manufacturing may not lead to an increase in productivity when the state variation is non-negligible.

A changeover from mass production to mass customization can constitute another approach for strengthening competitiveness, and the application of Internet of Things (IoT) technology is expected. Industrie 4.0 in Germany is a work that has attracted attention because of its high potential to change business models in manufacturing. The utilization of IoT typically involves storing various types of data (collected using a network) as big data in the cloud, and these data are analyzed to generate additional value.

In mass customization, it is necessary for a production system to adjust to a small lot order to the equivalent cost and efficiency in mass production, while considering changes in customers' needs, environments, and states. It is necessary for a production system to be flexible, robust, and autonomous at every level (i.e., management, manufacturing, and assembly). This suggests that analysis of the big data in the cloud based on IoT is not sufficient for mass customization. The establishment of a self-optimizing production system is important for mass customization, which can monitor and promptly judge the

current state and adopt an appropriate action. Both judgment of the state and process control are conducted based on the result of process monitoring, and thus accuracy of process monitoring is especially important. Hence, process monitoring is the main focus of this dissertation.

In industry, machine tool manufacturers actively work on developing production systems by introducing IoT technology. Secure and reliable communication among different companies is feasible with the unification of communications standards or co-development between the manufacturers and a networking company. Machine tools are connected to a network at the shop floor level such as the Field System from Fanuc [7] and Smartbox from Mazak [8]. There is a paucity of discussions on the optimization of machining, despite progress in monitoring operational statuses of factory and production management, such as stock management. Data analysis at the cloud level is not necessarily welcomed because of security and processing speed. The importance of data analysis at the edge level is pointed out [7]. Self-optimizing techniques at the machine tool level are promising in terms of both security and processing speed.

This dissertation deals with a sensorless cutting force estimation technique for process monitoring. Additionally, an in-process chatter avoidance technique based on the estimated cutting force was developed. The proposed cutting force estimation technique did not require additional sensors, and thus, manufacturers can avoid increase in cost and decrease in reliability to the maximum possible extent. Furthermore, the proposed estimation technique can be installed into existing machine tools as add-on. Stable condition is searched responding to the state in the proposed chatter avoidance technique, which leads to self-optimization in the future. This chapter reviews existing cutting force monitoring techniques and chatter avoidance techniques, and the purpose of the dissertation is presented.

1.2 Process monitoring technology

With respect to process monitoring, it is necessary to select appropriate sensors based on the observation objects or installation points of the sensors. Simultaneously, signal processing techniques and strategies for decision making are important for process monitoring. Therefore, the process monitoring is one of the major subjects for many researchers [9]. Due to increase in the performance and downsizing of sensors, monitoring object diversifies as well. With respect to the state monitoring of mechanical elements, Möhring et al. monitored wear of a ball-screw by measuring the preload of double-nut by using a thin film-like sensor [10]. In a previous study [11], condition monitoring by a material in itself was performed in which a tiny strain gauge and a wireless tip were installed. However, this section reviews sensor-based tool condition

monitoring techniques to limit the scope of this dissertation.

There are two different methods for process monitoring, namely, direct and indirect methods. Laser beam, cameras, and optical sensors are used in direct methods, and these sensors are effective in examining the profile of the cutting edge, tool breakage detection, or predicting surface quality. However, these sensors are expensive and difficult to apply in a machining environment due to cutting fluid, chips, and illumination [9].

In indirect methods, auxiliary quantities such as the cutting force are measured. Indirect methods are more economical and practical although they have lower accuracy when compared with direct methods. Generally, acoustic emission (AE), vibration acceleration, and cutting force are measured for process monitoring [12].

The AE ranges from kilohertz to megahertz, and this corresponds to the main characteristic points. Thus, AE is separated from cutting force and circumstantial noise, because the frequency of the AE significantly exceeds those of them. Additionally, AE sensors are not expensive, which is also an advantage. Conversely, uncertainty in physical understanding and difficulty of selecting an appropriate installation point constitute disadvantages of this method [12].

Vibration monitoring using an accelerometer is the most common method because of its ease in handling and low cost. An ordinary accelerometer is not suitable for measuring DC or low frequency components. Additionally, a scatter of chips could hit the accelerometer which may lead to failure and misreading. Although accelerometers are not as accurate and reliable as AE sensors and piezoelectric dynamometers (force sensor), the abovementioned advantages make acceleration sensors extremely practical for process monitoring.

Cutting force is known as one of the most important process-related indicators [13]. As shown in Table 1-1, the cutting force is closely related to various tool failures [14], and this indicates the validity of the process monitoring based on the cutting force. The cutting force can be applied to monitor relatively slow events, such as tool wear, as well as relatively fast events, such as chatter vibration. Hence, this study focuses on cutting force monitoring. Existing cutting force monitoring techniques are reviewed in the next section. Cutting force measurement using a piezoelectric dynamometer corresponds to the de-facto standard. However, the use of a dynamometer leads to an increase in the

Table 1-1 Troubles and physical quantities involved in cutting process

	Force (Torque)	Motive power	Sound, vibration	Temperature
Chatter	✓		✓	
Tool breakage	✓	✓	✓	
Tool wear	✓	✓	✓	✓
Built-up edge	✓	✓		
Chip evacuation	✓	✓	✓	
Collision	✓	✓	✓	

cost, limitations in workpiece size, and reduction of loop stiffness between the tool and the workpiece. Further, this results in a reduction of machining accuracy. Additionally, it is difficult to ignore the low thermal stability and lack of overload protection in case of collisions. Therefore, dynamometers are restricted to laboratory use.

In terms of practical application, the method of incorporating a sensor's signal into the control system of a machine tool is also important in conjunction with a method to measure physical variables. With respect to wideband process monitoring, it is necessary to acquire variables at a high sampling rate. Simultaneously, a high-capacity storage system is also required to utilize the variables as big data. Machine tool I/O signal lines are frequently connected to a programmable logic controller (PLC). However, an ordinary PLC is not suitable for acquiring analog signals at a high sampling rate. Furthermore, several machine tool manufacturers adopt an NC system provided by NC manufacturers on behalf of an in-house developed NC system [15]. Accessibility to sensor signals is usually limited by NC manufacturers, and this makes it difficult to incorporate acquired signals into the control system of machine tools. Fujishima et al. developed a sensory machine tool as shown in Fig. 1-2 that equipped interface boards with sensor signal inputs and ethernet outputs to use NC or PLC [15]. In this regard, challenges with respect to feedback of sensor information to NC or servo systems and optimizing the process continue to exist. Further cooperative development among machine tool and NC manufacturers is necessary to realize self-optimization based on process monitoring utilizing sensors. Machine tools integrating multiple sensors will be commercially

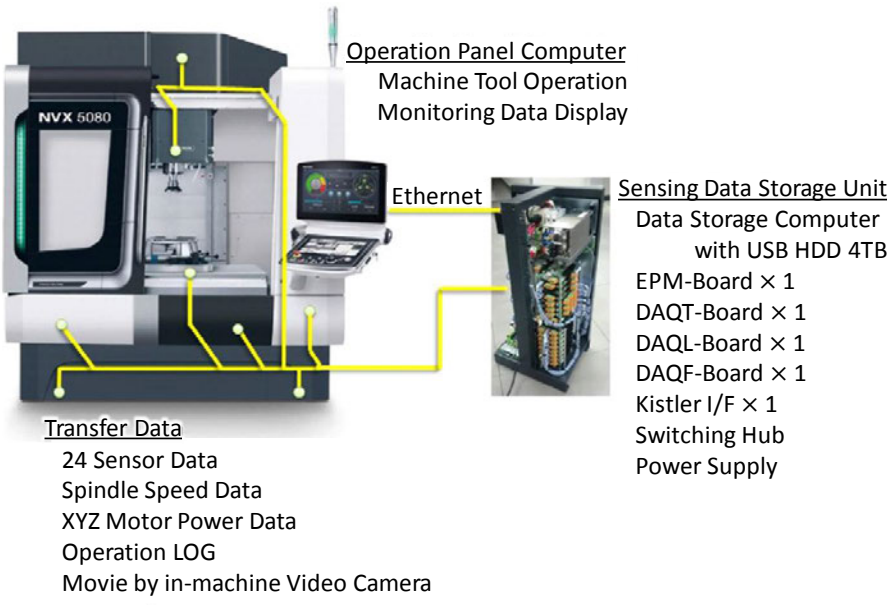

Fig. 1-2 Sensing data storage system [15] (M. Fujishima, K. Ohno, S. Nishikawa, K. Nishimura, M. Sakamoto, and K. Kawai, CIRP Journal of Manufacturing Science and Technology. Vol.14, pp. 71–75, (2016). The figure is used with permission from Elsevier.)

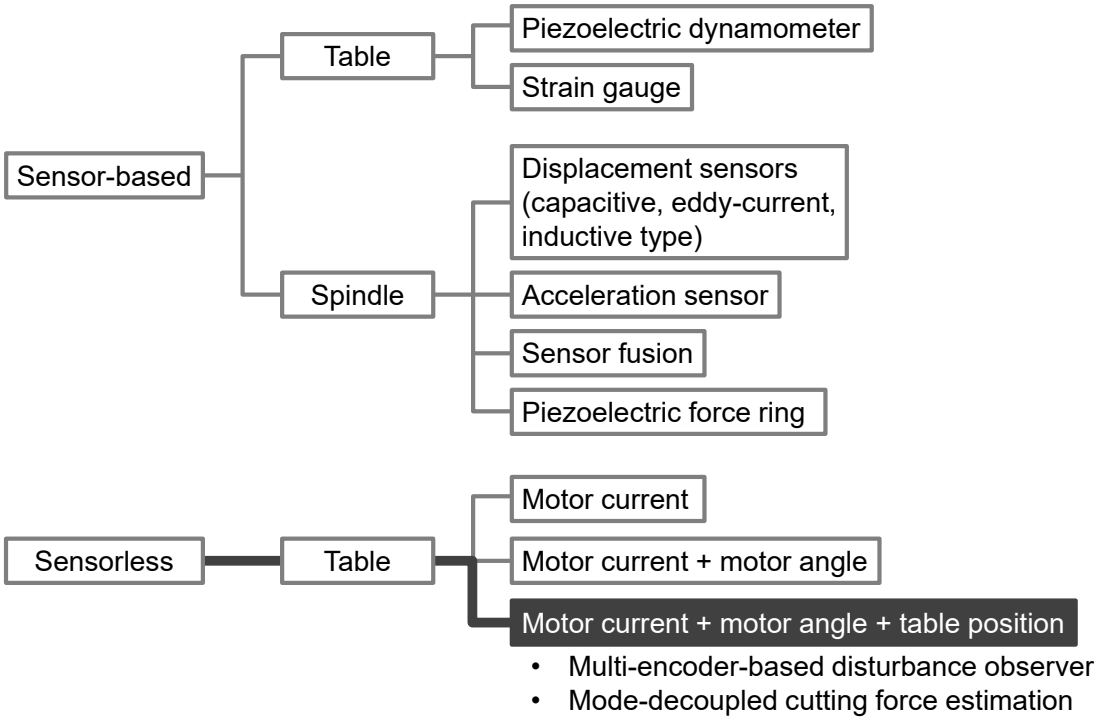

Fig. 1-3 An overview of the cutting force monitoring strategy

available in the future, although it takes time to penetrate into the shop floor.

Sensorless process monitoring using an inner sensor of the machine tool is inferior to sensor-based process monitoring in terms of accuracy. However, the former is superior to the latter in cost, reliability, and tool path design. Additionally, sensorless process monitoring can be installed on an existing machine tool as add-on. In terms of the intelligence of an existing machine tool, research and development of sensorless process monitoring technique is important in conjunction with those of sensor-based process monitoring. Considering that the machine tool can be operated for 10-20 years and is not frequently renovated, sensorless process monitoring is an ideal solution satisfying industrial needs.

1.3 Cutting force monitoring technique

1.3.1 Sensor-based approach

Numerous studies examine the cutting force monitoring technique [16]. Fig. 1-3 shows a classification of cutting force monitoring strategies. In sensor-based approaches, the cutting force is monitored at a table system or a spindle system. A piezoelectric dynamometer (in particular, a table-type dynamometer) is typically used for monitoring the cutting force. The force sensor in machining generally refers to a piezoelectric dynamometer. A workpiece is fixed on a dynamometer, and thus the available size of the workpiece is limited by that of the dynamometer. Therefore, it is difficult to attach the

dynamometer to large parts such as aircraft parts, which have a high demand for process monitoring.

Spindle-integrated and piezoelectric force sensors were also developed [17,18]. With respect to installation into the spindle system, the force sensor is generally attached to spindle housing that is stationary but at a distance from the cutting point. Recently, a force sensor attached to a rotational tool holder has become available due to the development of a wireless data transfer system. This increased the measurement bandwidth of the cutting force increased [18]. However, the spindle-integrated force sensor is more expensive than ordinal table-type force sensor. Additionally, it is necessary to design a spindle system such that the spindle-integrated force sensor can be attached to the same. Therefore, it is not suitable to mount the force sensor into the existing machine tools as an add-on.

In an alternative approach, displacement sensors, such as capacitive [19,20], eddy-current type [21], and inductive sensors [22], and acceleration sensors [23] are often attached to a spindle. In this approach, the cutting force is estimated by position/acceleration variation induced by a cutting force. Albrecht et al. compensated dynamics between the tool and rotating spindle shaft by using capacitive displacement sensors and enhanced the estimation bandwidth up to approximately 1 kHz [19]. Sarhan and Matsubara et al. used four spindle-integrated eddy-current displacement sensors. They considered thermal deformation and stiffness change due to high-speed rotation of the spindle [21]. Albertelli et al. employed inductive relative displacement sensors and a tri-axial accelerometer in order to estimate cutting force as well as tool tip vibration that was related to the surface-quality of the machined parts [22]. The sensors were attached to the spindle, and thus the mass variation of the workpiece did not influence on the measurement, in contrast with measurements using the dynamometer. The cutting force was accurately estimated using additional sensors. However, a decrease in reliability and an increase in the maintenance cost are inevitable with an increase in the number of sensors employed. The reduction in maintainability is non-negligible when sensors are embedded inside the spindle. Calibration of the thermal influence and spindle stiffness based on position is also necessary.

Strain gauges are also used for cutting force monitoring and are applied to detect chatter or tool failure [24–26]. Process monitoring from both the tool side and workpiece side is possible by attaching the strain gauges to the spindle system and fixtures of the workpiece [26]. However, cutting force monitoring by using strain gauges is less sensitive than other sensor-based methods.

1.3.2 Sensorless approach

Sensorless cutting force monitoring using inner information of the machine tools has attracted attention because of its sustainability. In this dissertation, sensorless cutting force monitoring refers to cutting force monitoring using signals for motion control of the machine tool. In milling, a cutting force is divided into feed force, cross-feed force, and axial force components. Sensorless cutting force estimation in milling typically focusses on the feed force component, which is comparatively easy to estimate. First, in this section, cutting force estimation techniques for the feed force component are reviewed. Next, estimation techniques for the cross-feed component are reviewed.

Sensorless cutting force estimation is broadly divided into current-based methods and observer-based methods. The current-based method is the most economical. Current signal during cutting is subjected to both cutting force and disturbance force with the exception of the cutting force. Disturbance force components, such as kinetic friction at sliding surfaces, are identified by idling motion. Thus, the estimation accuracy of the cutting force is influenced by the identification accuracy of the disturbance force. In the ball-screw-drive system, friction force/torque at the guideway, nut, and bearing can be considered influential factors in cutting force estimation.

Altintas et al. firstly established a cutting force monitoring methodology for a DC servomotor [27], and Lee et al. extended it to an AC servo drive [28]. In these studies, disturbance force components were eliminated by employing Coulomb and viscous friction models. The Stribeck friction model as well as the Coulomb and viscous friction models are also applicable [29]. In addition to employing Coulomb and viscous friction models, Sato et al. estimated the cutting force by eliminating the remaining disturbance force based on FFT and inverse FFT [30]. With respect to the accurate identification and compensation of disturbance force, current signals of the feed drive are applicable in estimating the cutting force in the feed direction within the bandwidth of the current control loop. For example, bandwidths of the current sensor in Ref. [27] and [28] is approximately correspond to 20 Hz and 62 Hz, respectively. The current-based method is practical. However, bandwidth of the cutting force estimation is narrow because dynamics of the movable mass are not directly considered.

With respect to the inertial force of the feed drive, the estimation bandwidth and accuracy could be enhanced using a position/angle in addition to the current. Cutting force estimation applying disturbance observer (DOB) [31] is especially effective when the observer is applied to the linear motor drive system that possesses a comparatively simple structure and is modeled as a rigid body. This is because DOB was originally proposed for a rigid body system. Additionally, the linear motor drive system is less subject to the friction force when compared with the ball-screw-drive system. Shinno et

al. successfully estimated the cutting force without the influence of temperature variations, in contrast to the case with a dynamometer [32]. Takei et al. presented cutting force monitoring in which the bandwidth surpassing the bandwidth of current loop was possible in a linear motor driven stage, and the estimation bandwidth reached 350 Hz [33]. The current reference cannot follow high frequency components of the cutting force. Nevertheless, more wideband estimation is possible by compensating for the inertial force. Ibaraki et al. indicated that the gravitational force exerted a greater influence on the cutting force estimation when compared with the friction force in hexapod type machine tools [34]. The accurate identification and compensation of friction and gravitational force allows the estimation of cutting force components in three directions with respect to the static force component.

In previous studies, the ball-screw-driven stage was controlled by a semi-closed loop. In this case, a stage response is unavailable as servo information. Thus, the cutting force is estimated based on inner information of a rotational servomotor when DOB is applied to the semi-closed controlled ball-screw-driven stage. Jeong and Cho successfully estimated the cutting force at a bandwidth of 130 Hz [35]. However, it is difficult to establish a comparable bandwidth in the linear motor drive system because dynamic interaction between rotation and translation is ignored. Existence of multiple natural modes in the ball-screw-drive makes it increasingly difficult to estimate cutting force with high accuracy and bandwidth in the ball-screw-drive system. Even if it is not possible for the estimation accuracy of the cutting force to increase, signal processing techniques help in extracting an abnormal pattern included in estimated cutting force. Tool fracture [36,37], tool breakage [28,38,39] and tool collision [40,41] have been successfully detected in previous studies. Abnormal cutting can be detected given variations in the cutting force are comparatively high and transmitted to the rotational servomotor. However, it is difficult to apply existing sensorless cutting force estimation techniques to process monitoring for fast events, if the damping property of the machine structure is high such as large scale machine tools or machine tools equipping sliding guideways.

Monitoring the cross-feed (i.e., stopping) direction components of the cutting force is also important because they directly affect the quality of the machined surface. However, the following error factors distort the estimated cutting force components in the cross-feed direction [35]: the stick-slip friction, lower encoder resolution, and arbitrary property of the stationary feed motor current. Specifically, the arbitrary property directly leads to difficulties in accurately identifying the friction force. Therefore, cutting force estimation in the cross-feed direction is more challenging than that in the feed direction. Jeong and Cho asserted that motor current in the stopping axis was influenced by the

magnitude and frequency of the cutting force. Additionally, they mentioned that the cutting force could be estimated if the stick-slip friction is assumed as a constant influence [35]. Ibaraki et al. proposed an estimation method by geometrically combining force vectors given by the servomotor of the feed drive and the spindle [42]. The armature current in a spindle motor that was less affected by the non-linearity of friction was used for estimating only the tangential component of the cutting force. However, the cutting force estimation was quasi-static due to the rigid body based formulation. Sato et al. extracted the cutting force components included in motor current by an inverse transformation from the frequency domain to the time domain [30]. The cutting force components in the cross-feed direction were successively estimated if the cutting force exceeded the static friction force.

1.3.3 New challenges

Several studies focused on a sensorless cutting force estimation technique for the ball-screw-drive system. However, most studies focused on eliminating DC or low-frequency components of friction force/torque included in servo information. In order to monitor the chatter or the tool fracture in addition to tool wear or tool breakage, wideband process monitoring needs to be realized, based on a sensorless cutting force estimation technique. Conversely, it is difficult to enhance bandwidth of cutting force estimation by only using inner information of the servomotor. A new methodology is necessary for estimating the cutting force.

The far from the cutting point, the more attenuated the vibration at the cutting point is, because there is damping among mechanical components. As a result, process monitoring based on the inner information is more difficult. Recently, a full-closed ball-screw-driven stages mounting linear encoder was widely used for high-end or large-scale machine tools. When indirect cutting force estimation using servo information from a full-closed controlled ball-screw-driven stage is considered, the following three pieces of information are available as servo signals of the feed drive: the motor current reference, rotation angle of the motor, and displacement of the stage. Only a few studies focused on in-process cutting force estimation methods that integrated the three aforementioned signals. Integration of the displacement of the stage into the observer can also increase the estimation bandwidth of the cutting force. In contrast, in terms of practical applications, it is not desirable to increase the order of the observer, and a formulation based on a simple model is desirable. Additionally, there is room for discussion with respect to the identification and compensation methods for disturbance force including friction force. Generally, the disturbance force is modeled based on a feed rate such as the Stribeck model. However, the disturbance force varies periodically, based on the lead

length of a ball-screw and the position of the nut, while the position-dependent characteristics were highly repeatable [43,44]. Furthermore, the disturbance force varies in response to the workpiece mass and the use of a chip cover [29]. Thus, it is difficult to ignore the influence of the disturbance force, and suitable compensation methods should be discussed.

An estimation technique for the cross-feed component of the cutting force is also important, in addition to the feed component. A new estimation technique that is less influenced by static friction force is necessary. The estimation of all components of the cutting force predicts the quality of the machined surface in addition to process monitoring in the future by integrating it with virtual manufacturing technology.

In order to enhance the estimation accuracy of the cutting force, the influence of several error factors (with the exception of friction or multiple structural modes) should be evaluated and compensated such as time delay in sampling, quantization error in angle/position measurement, and torque ripple. However, their influence is not sufficiently evaluated in past studies.

1.4 Chatter monitoring and avoidance technique

1.4.1 Chatter avoidance technique in single tool cutting

Chatter vibration resulting from dynamic interactions between the tool and workpiece leads to a reduction in surface quality and tool damage. It is desirable to increase the depth of a cut for higher material removal rate, which often incurs chatter. Although there are several sources of chatter, regenerative chatter becomes particularly problematic [45]. Fig. 1-4 shows a schematic of plunge cutting by assuming a single degree of freedom system. In each tooth pass, waviness is generated on the machined surface. Chip thickness varies during the process if a phase difference exists between inner modulation and outer modulation. Amplitude of the cutting force varies based on variations in the chip thickness. Machine structure is also excited by the dynamic cutting force. Vibration of the machine is transferred to the machined surface, and thus a new phase difference is generated. A feedback loop is included in the cutting process itself, and the phase difference between inner and outer modulation influences process stability.

Fig. 1-5 shows the relationship between the cutting force and displacement of the tool with respect to phase difference of waves [14]. If there is no phase difference (Fig. 1-5 (a)), cutting force becomes a constant value because the chip thickness is also maintained at a constant value. If the phase difference ε is $\pi/2$, the chip thickness increases when the tool cuts into the workpiece. In contrast, the chip thickness decreases when the tool leaves the workpiece. As a result, the work performed by the machine structure exceeds

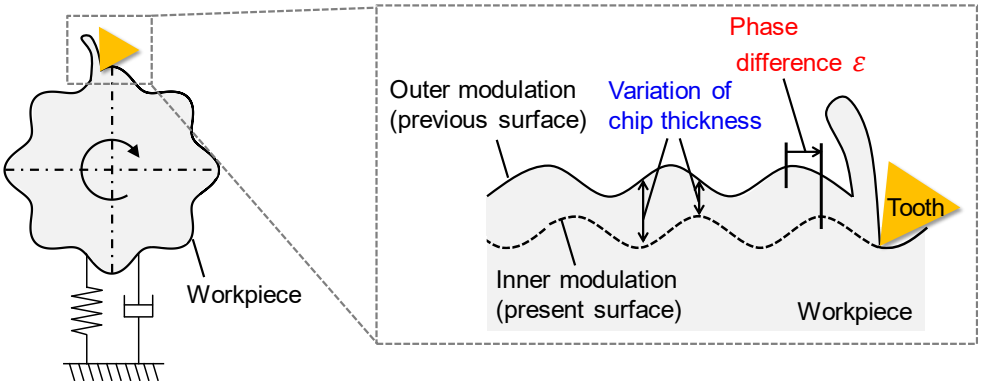

Fig. 1-4 Schematic of plunge cutting in a single degree of freedom system

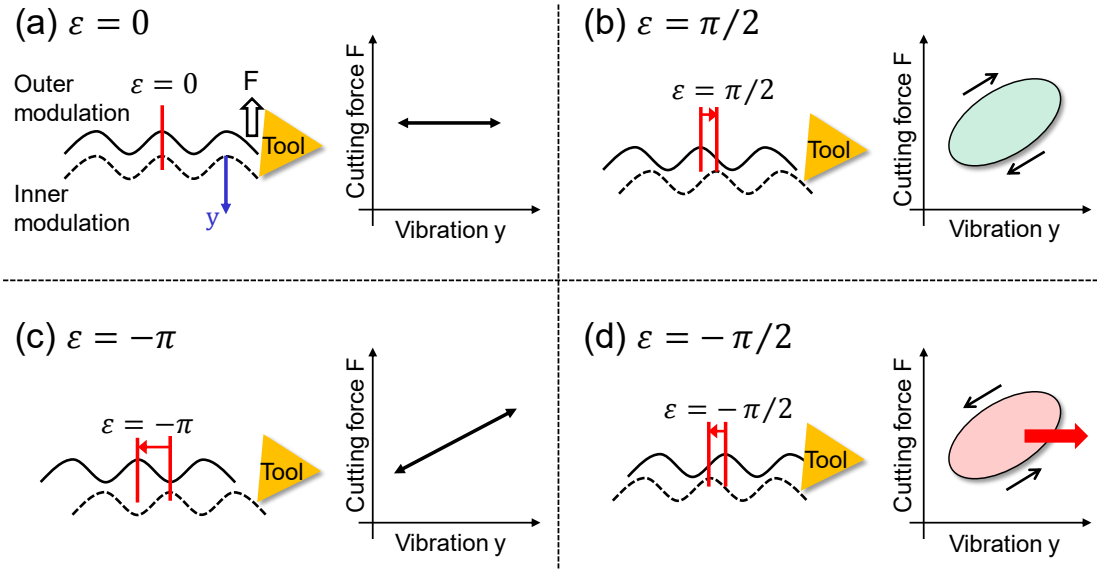

Fig. 1-5 Relationship between cutting force and vibration displacement of the tool with respect to phase difference of waves, ε (a) $\varepsilon = 0$ (b) $\varepsilon = \pi/2$ (c) $\varepsilon = \pi$ (d) $\varepsilon = -\pi/2$

that of the cutting process. Thus, chatter does not occur because energy is consumed in the cutting process. If the phase difference ε is $-\pi$, the cutting force varies during the process, while total work per cycle becomes zero. Therefore, a regenerative wave does not develop, and the process remains stable. Conversely, if the phase difference is $-\pi/2$, the chip thickness increases when the tool leaves the workpiece. In this case, mechanical energy flows into the machine structure. Vibration of the tool repeatedly develops unless its amplitude exceeds the depth of the cut. Although the mechanism of chatter has been clarified, it is still impossible to perfectly avoid chatter. Several studies continue to focus on avoidance techniques for chatter.

The most general method for avoiding chatter involves predicting stable and unstable cutting conditions based on a stability lobe diagram (SLD). As shown in Fig. 1-6, SLD indicates the border between a stable and unstable region responding to spindle speed and depth of cut. In order to calculate the SLD, it is necessary to accurately identify the

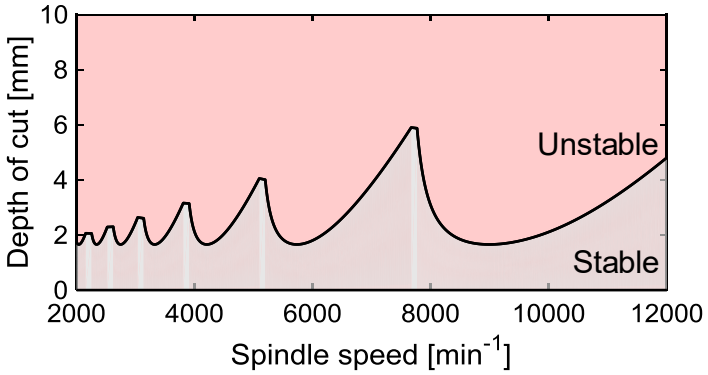

Fig. 1-6 Stability lobe diagram

shape of the tool, cutting coefficient of workpiece's material, and modal parameters of mechanical components. The calculation method of SLD is broadly divided into time domain based methods [46–48] and frequency domain based methods [49–51]. Time domain based methods are suitable for accounting for the non-linear effect of the process such as tool engagement, process damping, and variation of cutting coefficient [52]. When compared with time domain methods, frequency domain methods are comparatively simple and aid in a faster calculation of the stability boundary, although accuracy is sacrificed in some cases. The SLD is an effective tool for predicting stable cutting condition at the planning stage. Conversely, SLD is not robust with respect to variations in the parameters that should be preliminarily and accurately identified. For example, the frequency response of the spindle is different between rotation and stopping [53] while the frequency response is generally identified by hammering tests with stopping spindle rotation. Additionally, in case of thin wall machining, the frequency response of the workpiece changes due to material removal. Thus, it is difficult to perfectly avoid prediction error of the chatter.

In milling, the use of special tool cancels the regenerative effect such as variable pitch tools [54–57], variable helix tools [58–60], and serrated tools [61–63]. Specifically, chatter avoidance techniques based on variable pitch tools attract attention because they are comparatively easy to model and can be applied to the finishing process. In case of variable pitch tools, the phase difference between inner and outer modulation is not constant, and this reduces the modulation of chip thickness and increases stability against chatter. Budak developed an analytical model for designing a pitch angle that canceled regenerative effect [56]. The results indicated that the chatter free condition changed in response to the flute number of the tool, and chatter was avoided by setting phase difference ε to π, irrespective of the flute number. Additionally, the optimum pitch angle difference is sensitive to variation of chatter frequency, and it is determined more accurately if the chatter frequency and the spindle speed are known prior to designing the tool. Recently, Suzuki et al. proposed a design method for irregular

(variable) pitch tools by considering multiple vibration modes and variations in dynamics [57]. They introduced an index termed as Regenerative Factor for quantifying the regenerative effect, and revealed that robustness relative to the variation in chatter frequency is improved by adopting the proposed design method.

The regenerative effect can be canceled by changing spindle speed discretely or continuously for varying tooth-pass frequency [64–67]. In discrete spindle speed tuning (DSST), the spindle speed was regulated such that tooth-pass frequency or its harmonics correspond to chatter frequency [64]. This method is effective when the chatter frequency is close to the natural frequency of the dominant mode. Additionally, DSST is particularly useful in a comparatively high speed zone, in which wide stability pockets exist. In continuous spindle speed variation (CSSV), spindle speed is dynamically changed at several Hz [65–67]. In contrast to DSST, CSSV is adopted in a low spindle speed region because small variations in spindle speed can create large variations in the phase difference between inner and outer modulations. Furthermore, responsiveness of the servomotor limits application of CSSV to a high spindle speed region [52]. Although CSSV is comparatively easy to integrate into the control system, the selection of the amplitude and the frequency is not an easy task [65].

1.4.2 Chatter monitoring technique

An alternative approach is also discussed to detect chatter as fast as possible and adopt an appropriate countermeasure corresponding to the chatter state. Most chatter monitoring and detection techniques use additional sensors or inner sensors of the machine tool. Shimana et al. measured tool vibration by using laser displacement sensors and calculated the pseudo auto-correlation function for chatter detection in high-speed milling without frequency analysis [68]. Li et al. detected both tool wear and chatter based on a coherence function between two acceleration signals [69]. Cao et al. used acceleration sensors and defined two indicators by considering the non-linearity and non-stationary property of the chatter [70]. The cutting force signal is optimal for detecting chatter because it directly indicates the relative vibration between the tool and workpiece that causes regenerative chatter vibrations [13]. Mitsuishi et al. monitored the locus of the force vector by using a specially designed force sensor of the strain gauge type [24]. Frumuşanu et al. proposed an early chatter detection method in turning by predicting the features of the cutting force signal based on a logistic model [71].

In the sensorless techniques, servo information of spindle control system is frequently used. Lamraoui et al. [72] developed a chatter indicator in the angular domain by using the angular velocity calculated from the spindle rotary encoder, and the angular velocity is theoretically applicable to a system operated at variable spindle speeds. Kakinuma et

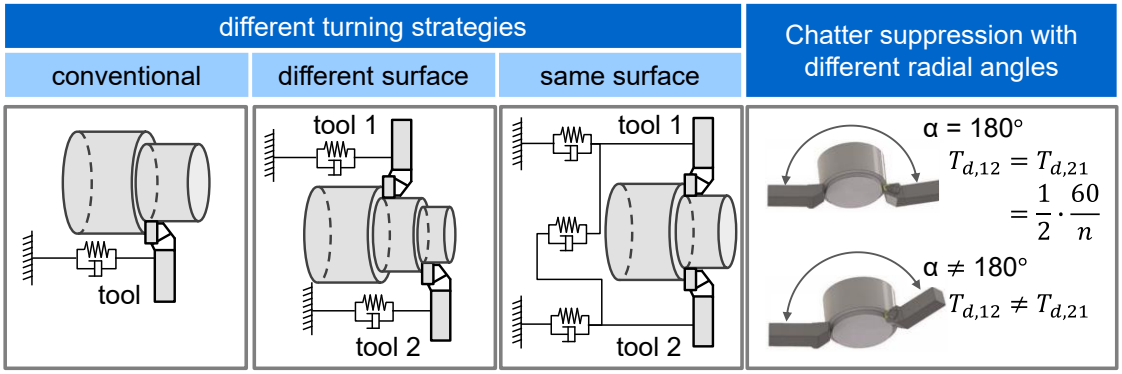

Fig. 1-7 Comparison of turning strategies [52] (J. Munoa, X. Beudaert, Z. Dombovari, Y. Altintas, E. Budak, C. Brecher, and G. Stepan, CIRP Annals. Vol.65, No.2, pp. 785–808, (2016). The figure is used with permission from Elsevier.)

al. applied the DOB theory to a spindle control system to estimate the cutting torque and successfully detected chatter vibrations, differentiating self-excited chatter vibrations from forced chatter vibrations in milling [73]. In order to reduce calculation loads in frequency analysis, Koike et al. proposed a chatter detection method using Moving Variance and Moving Fourier Transform [74].

1.4.3 Chatter avoidance techniques in parallel turning

Most studies focused on standard cutting processes, such as single-tool turning and milling. Recently, stability prediction models have been developed to represent the dynamics and stability of advanced cutting processes, such as parallel turning [75–78], parallel milling [79–82], and turn-milling [83,84]. These processes are termed as simultaneous machining and involve the use of multiple cutting tools for cutting the same or different surfaces of the workpiece. The simultaneous use of multiple cutting tools offers the possibility of higher material removal rates. Thus, simultaneous machining technology has attracted research attention as an important technique for future multi-axis and multi-tasking machine tools. Specifically, this study focuses on parallel turning. Budak and Ozturk formulated the dynamics of parallel turning in the feed direction with two tools cutting the same surface. They reported that the dynamic interaction between the tools could increase the stability limits when compared to single-tool turning operations with respect to the selection of appropriate cutting conditions. Brecher et al. developed a model by considering dynamic coupling through machine structure and waviness on a shared cutting surface as shown in Fig. 1-7 [76]. The radial angle between tools influences the dead time between two successive cuts, and this affects the stability limits under dynamic coupling. Thus, the stability limits may be increased by changing the spindle speed as well as the radial angle between the tools. Ozturk et al. used time and frequency domain simulations to reveal that the maximum

decrease in stability limits are observed when the natural frequency of the tool systems is identical [77]. The stability increases by adding or subtracting mass to the tool holder or by changing its length. Stepan et al. clarified, in both theoretical calculation and cutting tests, that the stability increases with changes in the overhang of the each tool holder [78]. In their experimental setup, the range of the optimum ratio of the natural frequencies was 0.7 – 0.8.

1.4.4 New challenges

Basically, existing chatter monitoring technique is intended for single tool cutting, and inner information of the spindle control system are often used in the sensorless approaches. Chatter cannot be necessarily detected by the spindle control system when resolution of angle measurement is low or users are not permitted to access inner information. In that case, application of inner information from the feed drive is expected. It is difficult to ignore the effect of the guideway, which can influence on the damping property of the machine tool. However, the effect of the guideway in chatter monitoring is out of focus in the past studies.

Existing chatter avoidance technique in parallel turning is basically the prediction method based on the process model. These techniques are especially effective if the model is perfectly identified, and the validity of the model is experimentally confirmed in literature. However, these techniques assume that chatter results from dynamics of the tool side and not the workpiece. The stiffness of the tool system in the feed direction (i.e., rotation axis) was low. Thus, it is not possible to apply these techniques while machining a slender workpiece, which is flexible in the radial direction and is likely to incur chatter. Additionally, in case of machining a slender workpiece, variation in the dynamics of the workpiece due material removal is non-negligible, and this is not considered in the prediction method. Therefore, a chatter avoidance technique with real-time process monitoring is also required, considering the variation in stability during cutting. If the chatter can be detected at the control system of the feed drive, appropriate avoidance techniques can be applied as a response to the actual process, which can lead to self-optimization of existing machine tools.

1.5 Research purpose

The aim of this study involves developing a sensorless cutting force estimation technique for a ball-screw-drive system with full-closed loop control. Additionally, an in-process chatter avoidance technique is developed by applying the estimated cutting force, which is intended for parallel turning.

Two sensorless cutting force estimation techniques are developed to enhance accuracy

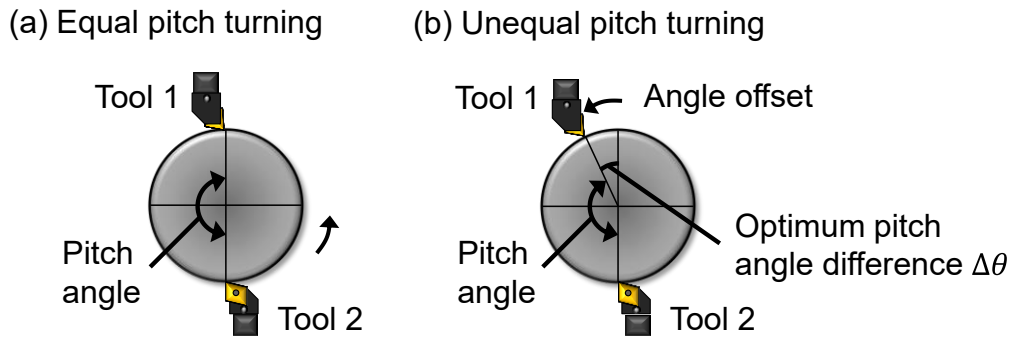

Fig. 1-8 Comparison of parallel turning method (a) equal pitch turning (b) unequal pitch turning

and bandwidth by applying a multi-encoder-based disturbance observer (MEDOB) [85] and mode-decoupling. The stage position in conjunction with the inner information of the rotational servomotor is used to estimate cutting force considering dynamic interactions between the rotation and translation of the ball-screw-driven stage. Although the MEDOB is a valid method to accurately estimate a load force in multi-inertia system, it is difficult to directly apply the MEDOB to cutting force estimation in the ball-screw-drive system. This is because the frequency of the cutting force is high and the motion of the ball-screw-drive is subjected to the friction force/torque. In the proposed MEDOB-based cutting force estimation method, therefore, the observer is designed by considering the following factors: compensation of the disturbance force by considering its repeatability, and phase lag elements in the control system. It is indispensable to construct the estimation system considering these factors to enhance accuracy and bandwidth of the cutting force estimation. In terms of practical application, error factors and their compensation techniques were also evaluated through end milling tests, idling tests, and numerical simulation.

A new cutting method termed as unequal pitch turning was developed to avoid chatter in parallel turning. In this method, the regenerative effect is canceled by providing an angle offset to one tool in the circumferential direction as shown in Fig. 1-8. The optimum pitch angle difference can be calculated from the chatter frequency and the spindle speed. The chatter frequencies can be calculated during the process owing to the sensorless cutting force estimation technique by using multiple encoders. Thus, chatter can be adeptly avoided by changing pitch angle even if the chatter state might change during the process.

1.6 Organization of the dissertation

Fig. 1-9 summarizes the organization of the dissertation. In Chapter 1, process monitoring techniques for self-optimizing machine tools and chatter avoidance techniques are introduced. With respect to process monitoring, the dissertation focuses

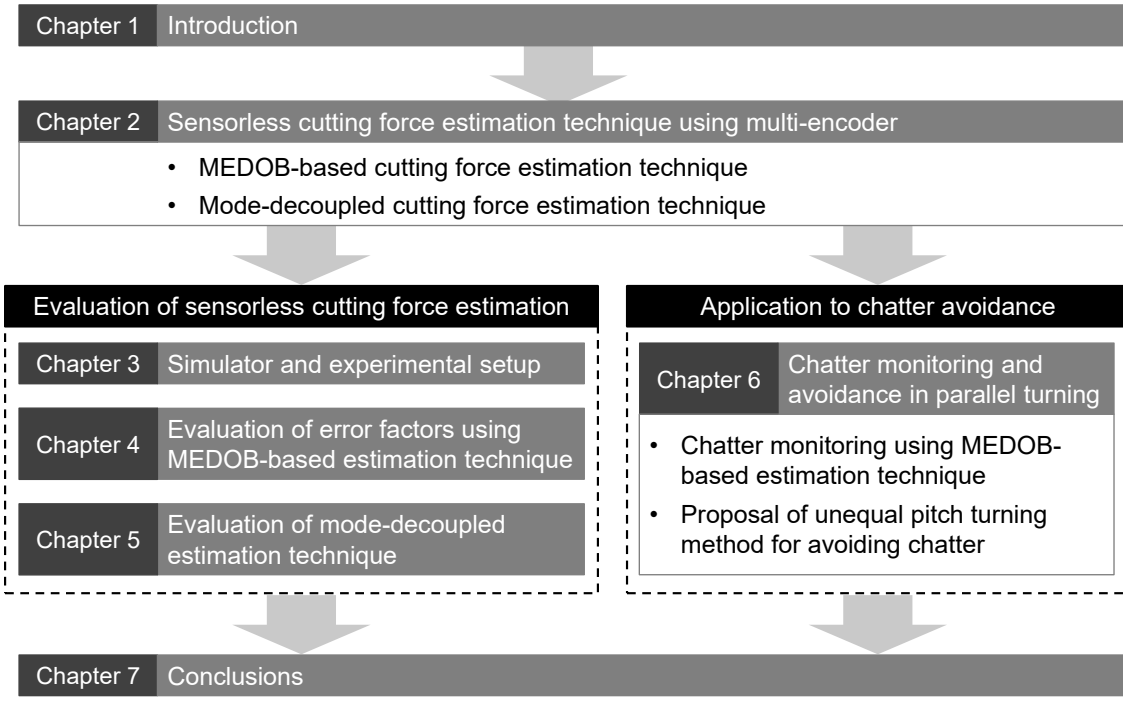

Fig. 1-9 Organization of dissertation

on cutting force and describes state-of-the-art technologies for cutting force monitoring. Furthermore, problems of the prediction method for chatter avoidance are explained, and the necessity of an in-process avoidance technique is presented. Finally, the purpose of this dissertation is declared.

Chapter 2 provides the fundamentals for two types of cutting force estimation techniques using a multi-encoder. Problems of a conventional estimation technique, which is rigid body-based formulation, are described through a theoretical calculation of a transfer function. A MEDOB-based cutting force estimation technique is introduced to include dynamic interaction of the ball-screw-drive system and by using inner information in a more effective manner. In mode-decoupled cutting force monitoring, the cutting force is independently estimated in the rigid body and the vibration mode. Specifically, with respect to the vibration mode, both feed and cross-feed components of the cutting force are estimated, and this is impossible in the MEDOB-based estimation method.

Chapter 3 summarizes the simulator and experimental setup for evaluating cutting force estimation. The frequency response of the ball-screw-driven stage is investigated in detail, and this may determine estimation bandwidth of the cutting force. Additionally, position/rotation dependent characteristics of the disturbance force and high frequency variations from encoder signals are also investigated, and the compensation method of them is described.

In Chapter 4, the influence of the error factors is evaluated both in a time domain

simulation and end milling tests. In the time domain simulation, the following factors are evaluated: difference of estimation method, identification error of mechanical parameters and phase lag elements, and resolution of the encoder. It is possible to increase the estimation bandwidth of the cutting force by employing a MEDOB-based cutting force estimation, which was confirmed by end milling tests with changes in the spindle speed.

In Chapter 5, the validity of the mode-decoupled cutting force estimation technique is evaluated using both a time domain simulation and end milling tests. The cutting force is estimated based on the relative displacement between the motor and the stage in the vibration mode, and thus position/rotation dependent characteristics of relative displacement are investigated. Estimation performances of both the feed and cross-feed components is evaluated through several end milling tests.

Chapter 6 describes monitoring and avoidance of chatter in parallel turning by applying the estimated cutting force. Initially, monitoring performance is evaluated based on the type of guideway (i.e., sliding, rolling) and estimation method of the cutting force (i.e., DOB, MEDOB). A chatter avoidance technique employing unequal pitch turning is introduced, considering an analogy between milling by using a variable pitch tool and unequal pitch turning. The optimum pitch angle differences between two tools are calculated from the spindle speed and the chatter frequency, which are measured by applying the estimated cutting force. Validity of the proposed method, including robustness, is evaluated by performing several cutting tests. The experimental results indicate that chatter is avoided based on the in-process measurement of the chatter frequency.

In Chapter 7, conclusions of the dissertation are summarized.

2. Sensorless cutting force estimation technique using multi-encoder

2.1 Introduction

This chapter describes methodology for cutting force estimation using multi-encoder. Estimating equations for the cutting force are derived from a dual-inertia model of the ball-screw-driven stage. In the MEDOB-based method, cutting force is estimated by considering motion of each mechanical element. On the other hand, in the mode-decoupled method, cutting force is estimated by separating rigid body component and vibration component with the use of modal matrix. In constructing the cutting force estimation system, synchronization errors resulting from phase lag elements in the control system are also considered, which can be error sources for wideband estimation. If additional sensors are available, the propose method can extend to multi-inertia system. Estimation principle in multi-inertia system is also presented for both estimation methods.

2.2 Physical model of ball-screw-driven stage

There are numerous works to model dynamic behavior of the ball-screw-driven stage [86–93]. While high-order model can effectively describe the dynamic behavior, low order model such as dual-inertia model [91–93] shown in Fig. 2-1 is generally employed. This is because the model is simple and intuitive. When the dual-inertia model is applied to the ball-screw-driven stage, both rotational and translational elements are represented by one inertia, respectively. Here, rotational elements refer to motor, mechanical coupling, and screw, which are regarded as one inertia by assuming that torsional stiffness of rotational elements is infinite. Dynamic interaction between rotational and translational elements is modeled by considering that elastic deformation of a nut interface is observed in axial direction. Since engineers who work on control of the ball-screw-driven stage are familiar

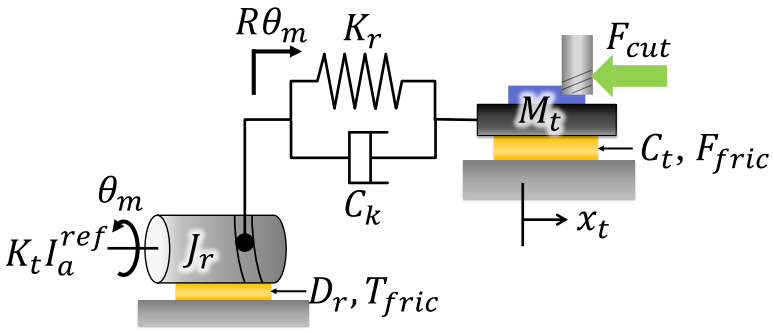

Fig. 2-1 Dual-inertia model of ball-screw-driven stage

with the model, cutting force estimation based on the model is more preferable than high-order model. In dual-inertia model, vibration mode resulting from axial stiffness is considered by combining axial stiffness of the ball-screw, bearing, and nut. On the other hand, vibration mode resulting from torsional stiffness is ignored [93]. This is because natural frequency resulting from torsional stiffness is much higher than that from axial stiffness in many NC machine tools. However, wideband estimation, surpassing the frequency of torsional modes, is difficult based on the cutting force estimation referring dual-inertia model. In addition to torsional stiffness, the following can be error factors: yawing, pitching, and rocking mode, and deformation of workpiece. When the dual-inertia model is applied to the stage of the spindle, dynamics between the tool and the stage is also non-negligible, which is modeled as rigid body when applying the dual-inertia model. As described above, there are multiple error factors only focusing on modeling method of the feed drive. However, the following can be error factors as well: friction force/torque, synchronization errors, and quantization error of position/angle measurement, and identification error of mechanical parameters. To realize accurate and wideband cutting force estimation, these error factors need to be considered in constructing the estimation system. In this study, estimation performance of the cutting force is evaluated where the ball-screw-driven stage is modeled as dual-inertia system, and modeling error of the feed drive is comparatively small.

Dynamic equation of the dual-inertia model is as follows:

$$J_r\alpha_m = K_t I_a^{ref} - K_r(R\theta_m - x_t)R - C_k(R\omega_m - v_t)R - D_r\omega_m - T_{fric} \quad (2\text{-}1)$$

$$M_t a_t = K_r(R\theta_m - x_t) + C_k(R\omega_m - v_t) - C_t v_t - F_{fric} - F_{cut} \quad (2\text{-}2)$$

where θ_m is angle of motor, ω_m is angular velocity of motor, α_m is angular acceleration of motor, x_t is displacement of stage, v_t is velocity of stage, a_t is acceleration of stage, J_r is total inertia of motor, coupling, and ball-screw, M_t is movable mass, K_t is torque coefficient, I_a^{ref} is motor current reference, K_t is total stiffness of feed screw system, C_k is damping coefficient of structure, D_r is damping coefficient of rotational element, C_t is damping coefficient of translational element, F_{fric} is friction force, T_{fric} is friction torque, and R is transform coefficient for rotational to translational motion. Here, it is assumed that armature current corresponds to current reference I_a^{ref}, considering bandwidth of the current control loop is sufficiently high. In addition, Coriolis force and centrifugal force are neglected because they are much smaller than cutting force and friction force/torque. Eq. (2-1) and Eq. (2-2) are rearranged as follows:

$$\begin{bmatrix} J_r & 0 \\ 0 & M_t \end{bmatrix}\begin{Bmatrix} \alpha_m \\ a_t \end{Bmatrix} + \begin{bmatrix} D_r + C_k R^2 & -C_k R \\ -C_k R & C_t + C_k \end{bmatrix}\begin{Bmatrix} \omega_m \\ v_t \end{Bmatrix} + \begin{bmatrix} K_r R^2 & -K_r R \\ -K_r R & K_r \end{bmatrix}\begin{Bmatrix} \theta_m \\ x_t \end{Bmatrix} = \begin{Bmatrix} K_t I_a^{ref} - T_{fric} \\ -F_{fric} - F_{cut} \end{Bmatrix} \quad (2\text{-}3)$$

To make frequency analysis simpler, Eq. (2-3) is rearranged in the Laplace domain, and the friction terms (F_{fric}, T_{fric}) are not considered for simplification. As a result, the following equation is obtained:

$$\begin{aligned} \begin{Bmatrix} R\theta_m \\ x_t \end{Bmatrix} &= \frac{\alpha}{M_t s D(s)}\begin{bmatrix} M_t s^2 + (C_t + C_k)s + K_r & C_k s + K_r \\ C_k s + K_r & (J_r/R^2)s^2 + (D_r/R^2 + C_k)s + K_r \end{bmatrix}\begin{Bmatrix} \frac{1}{R}K_t I_a^{ref} \\ -F_{cut} \end{Bmatrix} \\ &= \frac{\alpha}{M_t s D(s)}\begin{bmatrix} s^2 + 2(\zeta_t + \zeta_k)\omega_t s + \omega_t^2 & \omega_t(2\zeta_k s + \omega_t) \\ \omega_t(2\zeta_k s + \omega_t) & \frac{1}{\alpha}s^2 + 2(\zeta_r + \zeta_k)\omega_t s + \omega_t^2 \end{bmatrix}\begin{Bmatrix} \frac{1}{R}K_t I_a^{ref} \\ -F_{cut} \end{Bmatrix} \end{aligned} \quad (2\text{-}4)$$

where

$$\begin{aligned} D(s) = s^3 &+ 2\omega_t\{\alpha\zeta_r + (\alpha+1)\zeta_k + \zeta_t\}s^2 \\ &+\{\omega_s^2 + 4\alpha(\zeta_r\zeta_t + \zeta_r\zeta_k + \zeta_t\zeta_k)\omega_t^2\}s + 2\alpha(\zeta_r + \zeta_t)\omega_t^3 \end{aligned} \quad (2\text{-}5)$$

$$\omega_t = \sqrt{\frac{K_r}{M_t}}, \omega_s = \sqrt{\alpha+1}\omega_t, \zeta_r = \frac{D_r/R^2}{2\omega_t M_t}, \zeta_k = \frac{C_k}{2\omega_t M_t}, \zeta_t = \frac{C_t}{2\omega_t M_t} \quad (2\text{-}6)$$

ω_t is anti-resonance frequency at motor side, ω_s is resonance frequency in dual-inertia system, ζ_k, ζ_r, and ζ_t are damping ratio of structure, rotational elements, and translational elements, respectively. The dual-inertia model can describe both rigid body motion and first vibration mode of the ball-screw-driven stage. If only the rigid body motion is considered, the dual-inertia model can be simplified by assuming axial stiffness $K_r = \infty$. Because the axial stiffness is sufficiently large, there is no deformation in spring element of the dual-inertia model. In that case, therefore, stage response x_t corresponds to equivalent stage response calculated from motor angle $R\theta_m$. Dynamic equation of single-inertia model is derived as follows:

$$M_a a_m = \frac{1}{R}K_t I_a^{ref} - C_a v_m - \frac{1}{R}T_{fric} - F_{fric} - F_{cut} \quad (2\text{-}7)$$

where

$$\begin{aligned} M_a = J_r/R^2 + M_t, C_a = D_r/R^2 + C_t \\ x_m = R\theta_m, v_m = R\omega_m, a_m = R\alpha_m \end{aligned} \quad (2\text{-}8)$$

M_a is total movable mass in rigid body motion, C_a is total damping coefficient in rigid body motion, x_m, v_m, and a_m are equivalent value of θ_m, ω_m, and α_m in translational motion, respectively.

2.3 Cutting force estimation technique based on disturbance observer

2.3.1 Disturbance observer

Disturbance observer (DOB) theory was originally constructed for rigid body system. Robust motion control against load and parameter variations can be achieved by feedback of the compensation current equivalent to the disturbance [31,94]. Eq. (2-7) is rearranged so that parameter variation from the nominal parameters explicitly expressed as follows:

$$(M_{an} + \Delta M_a)a_m = \frac{1}{R}(K_{tn} + \Delta K_t)I_a^{ref} - (C_{an} + \Delta C_a)v_m - \frac{1}{R}T_{fric} - F_{fric} - F_{cut} \tag{2-9}$$

where

$$K_t = K_{tn} + \Delta K_t, M_a = M_{an} + \Delta M_a, C_a = C_{an} + \Delta C_a \tag{2-10}$$

Disturbance force F_{dis} is defined as sum of the friction terms, the load force (i.e. F_{cut}), and the parameter variations in the force dimension as follows:

$$F_{dis} \equiv \frac{1}{R}T_{fric} + F_{fric} + F_{cut} - \Delta K_t I_a^{ref} + \Delta M_a a_m + \Delta C_a v_m \tag{2-11}$$

By assuming Eq. (2-11), disturbance force can be calculated by using nominal parameters as follows:

$$F_{dis} = \frac{1}{R}K_{tn}I_a^{ref} - M_{an}a_m - C_{an}v_m \tag{2-12}$$

In order to reduce high frequency noise resulting from numerical differential, a low-pass filter ($g_{dis}/(s + g_{dis})$) was applied in estimating disturbance force as follow:

$$\hat{F}_{dis} = \frac{g_{dis}}{s + g_{dis}}\left(\frac{1}{R}K_{tn}I_a^{ref} - M_{an}\hat{a}_m - C_{an}\hat{v}_m\right) \tag{2-13}$$

where ^ indicates estimated value.

2.3.2 Application to cutting force estimation

As explained in the last section, the disturbance force is introduced from the dynamic equation. Similarly, the cutting force can be introduced from the dynamic equation. By solving the dynamic equation Eq. (2-9), the cutting force F_{cut} can be calculated as follows:

$$F_{cut} = \frac{1}{R}(K_{tn} + \Delta K_t)I_a^{ref} - (M_{an} + \Delta M_a)a_m - (C_{an} + \Delta C_a)v_m - \frac{1}{R}T_{fric} - F_{fric} \tag{2-14}$$

If mechanical parameters are identified accurately, the parameter variations in the force dimension are regarded as zero. In that case, estimating equation of the cutting force can be introduced as follows:

$$\hat{F}_{cut} = \frac{g_{cut}}{s + g_{cut}}\left(\frac{1}{R}K_{tn}I_a^{ref} - M_{an}\hat{a}_m - C_{an}\hat{v}_m - \frac{1}{R}\hat{T}_{fric} - \hat{F}_{fric}\right) \tag{2-15}$$

In this regard, identification of friction torque and friction force are necessary to apply Eq. (2-15). Based on Eq. (2-15), block diagram of cutting force observer is introduced as shown in Fig. 2-2. In calculating angular velocity in translational motion v_m, pseudo differential is conducted for eliminating high-frequency noise.

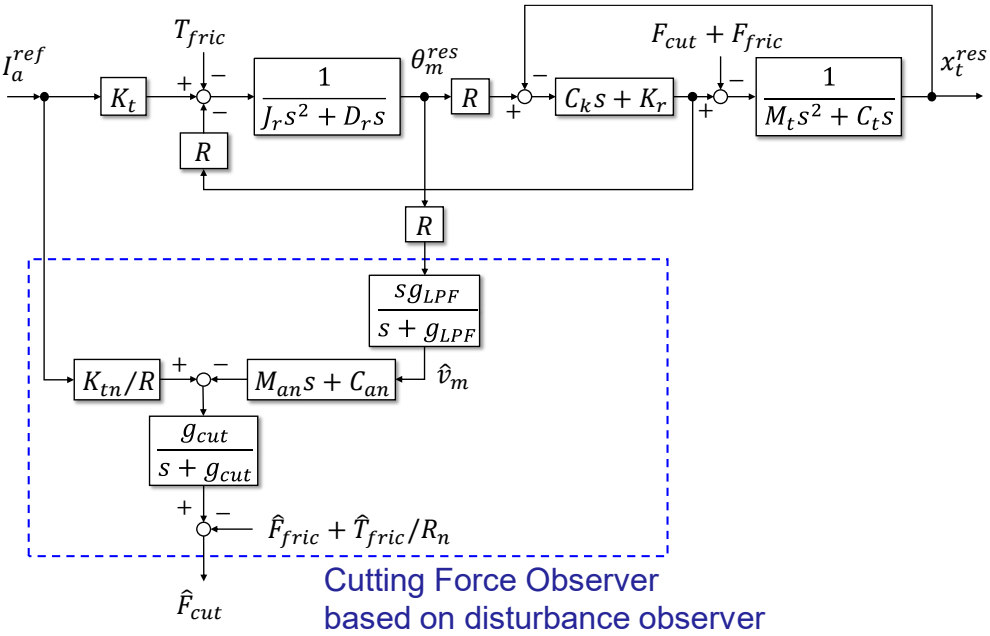

Fig. 2-2 Block diagram of cutting force observer based on disturbance observer

2.3.3 Frequency response of cutting force observer

In this section, frequency response of the cutting force observer based on DOB is calculated analytically. Eq. (2-15) is rearranged in the Laplace domain as follows:

$$\hat{F}_{cut} = \frac{g_{cut}}{s + g_{cut}} \left\{ \frac{1}{R} K_t I_a^{ref} - (M_a s^2 + C_a s) x_m \right\} \tag{2-16}$$

For simplification, friction force and torque are ignored. In addition, identification and quantization error are not considered. By refereeing Eq. (2-4), $x_m (= R\theta_m)$ can be expressed by using thrust force reference $K_t I_a^{ref}/R$ and cutting force F_{cut} as follows:

$$x_m = \frac{\alpha}{M_t^2 s D(s)} \left[\{ M_t s^2 + (C_t + C_k) s + K_r \} \frac{K_t I_a^{ref}}{R} - (C_k s + K_r) F_{cut} \right] \tag{2-17}$$

By substituting Eq. (2-17) into Eq. (2-16), the estimated cutting force is introduced after lengthy calculation as follows:

$$\begin{aligned} \hat{F}_{cut} = & -\frac{g_{cut}}{s + g_{cut}} \cdot \frac{\alpha (s + 2\zeta_t \omega_t)^2 s^2}{s D(s)} \cdot \frac{K_t I_a^{ref}}{R} \\ & + \frac{g_{cut}}{s + g_{cut}} \cdot \frac{2\zeta_k \omega_s s^3 + \{ 4\alpha \zeta_k (\zeta_r + \zeta_t) \omega_t^2 + \omega_s^2 \} s^2 + 2\alpha (\zeta_r + \zeta_t) \omega_t^3 s}{s D(s)} \cdot F_{cut} \end{aligned} \tag{2-18}$$

Thus, transfer function $\hat{F}_{cut}/F_{cut}$ can be calculated by neglecting the term of I_a^{ref} as follows:

$$\frac{\hat{F}_{cut}}{F_{cut}} = \frac{g_{cut}}{s + g_{cut}} \cdot \frac{2\zeta_k \omega_s s^3 + \{ 4\alpha \zeta_k (\zeta_r + \zeta_t) \omega_t^2 + \omega_s^2 \} s^2 + 2\alpha (\zeta_r + \zeta_t) \omega_t^3 s}{s D(s)} \tag{2-19}$$

Based on Eq. (2-19), frequency response of the cutting force observer is calculated. The result is shown in Fig. 2-3, and parameters used in the calculation are listed in Table 3-3. The gain of the estimated cutting force $\hat{F}_{cut}/F_{cut}$ is close to 0 dB at low frequencies in which the dual-inertia model presents rigid body characteristics against the cutting force. On the other hand, both the amplitude and the phase vary widely around the undamped natural frequency ω_s. In high frequencies, the estimated cutting force $\hat{F}_{cut}$ cannot follow cutting force reference F_{cut}, and the gain of $\hat{F}_{cut}/F_{cut}$ drastically decreases. In the dual-inertia system, wideband cutting force monitoring is impossible under rigid body-based formulation using inner information of only servomotor. The use of position response in

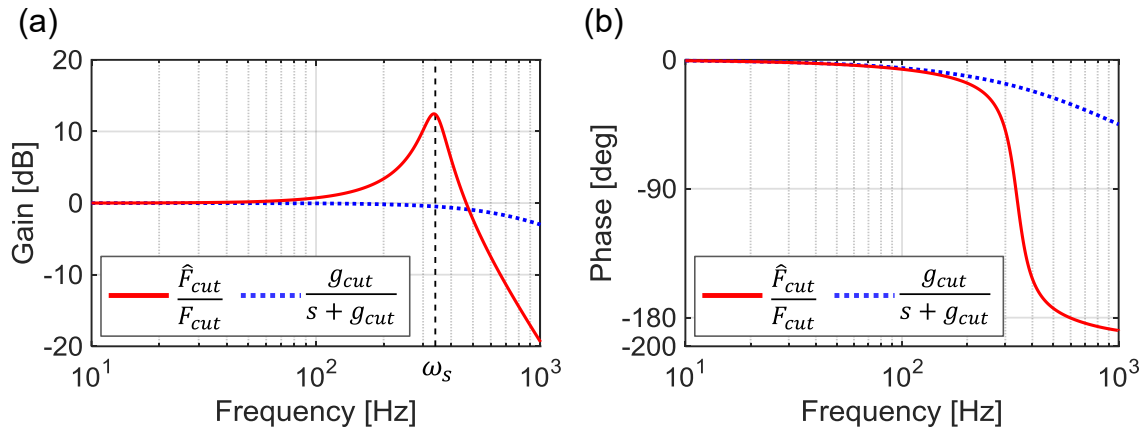

Fig. 2-3 Frequency response of cutting force observer based on disturbance observer (a) gain characteristics (b) phase characteristics

addition to angular response is beneficial for increasing estimation bandwidth of the cutting force.

When an inverse filter in discrete time domain is designed from the transfer function in Laplace domain (Eq. (2-19)), it is theoretically possible to estimate the cutting force using inner information of only servomotor. However, additional filter to make the system proper is necessary, which leads to additional lag in estimation, increase in calculation cost, and complication of the estimation system. In terms of practical application, it is more preferable and valuable to make use of available inner information at a maximum and to try to simplify the whole estimation system. The same is true of the cutting force estimation using the current reference and the position response. Therefore, this study focuses on development of the cutting force estimation method using the current, the angle, and the position.

2.4 Cutting force estimation technique based on multi-encoder-based disturbance observer

2.4.1 Estimation principle for cutting force

Multi-encoder-based disturbance observer (MEDOB) was originally proposed for estimating load-side external force of flexible robots [85]. Based on MEDOB, cutting force is introduced by solving Eq. (2-1) and Eq. (2-2), so that elastic force $K_r(R\theta_m - x_t)$ and damping force $C_k(R\omega_m - v_t)$ can be erased as follows:

$$F_{cut} = \frac{1}{R}\left(K_t I_a^{ref} - J_r\alpha_m - D_r\omega_m - T_{fric}\right) - M_t a_t - C_t v_t - F_{fric} \tag{2-20}$$

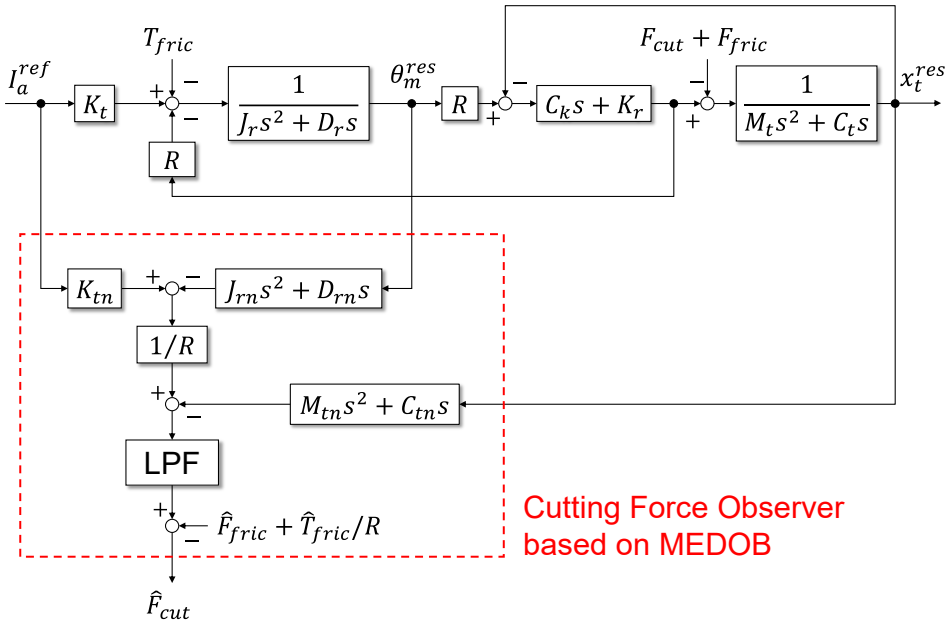

Fig. 2-4 Block diagram of cutting force observer based on multi-encoder based disturbance observer

If cutting force is calculated from Eq. (2-2), the stiffness K_r needs to used, which varies depending on the displacement of the stage. On the other hand, cutting force is expressed without using the stiffness K_r in Eq. (2-20). Therefore, it is unnecessary to identify the stiffness in calculating cutting force based on MEDOB. As in the case of cutting force observer based on DOB, the estimating equation of the cutting force can be introduced as follows:

$$\hat{F}_{cut} = \frac{g_{cut}}{s + g_{cut}} \left\{ \frac{1}{R} \left(K_{tn} I_a^{ref} - J_{rn} \hat{\alpha}_m - D_{rn} \hat{\omega}_m - \hat{T}_{fric} \right) - M_{tn} \hat{a}_t - C_{tn} \hat{v}_t - \hat{F}_{fric} \right\} \tag{2-21}$$

Fig. 2-4 shows block diagram of cutting force observer based on MEDOB. In the figure, the low-pass filter $g_{cut}/(s + g_{cut})$ is rewritten as LPF. In the MEDOB-based estimation technique, load force is extracted by independently considering each mechanical element on behalf of considering interaction between mechanical elements (i.e. rotation and translation). The cutting force can be accurately estimated based on Eq. (2-21), when there is no identification error of parameters and the disturbance force, and the stage behaves as ideal dual-inertia system.

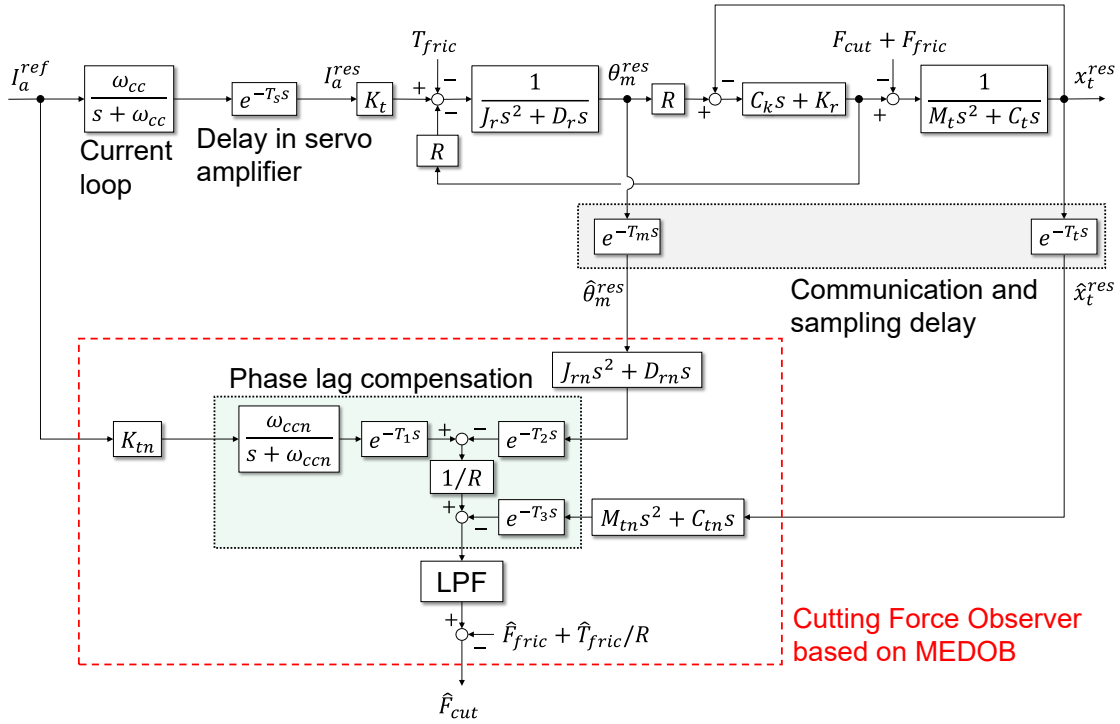

Fig. 2-5 Block diagram of cutting force observer with phase lag compensation

2.4.2 Compensation of phase lag elements

Generally, phase lag elements in the control system are not considered in designing of the cutting force observer. However, their effect is non-negligible when estimating high frequency components of the cutting force, because phase lag increases with increase of the frequency. The phase lag elements alter both gain and phase characteristics of $I_a^{ref} \rightarrow \theta_m$ and $I_a^{ref} \rightarrow x_t$ particularly in high frequencies. Fig. 2-5 shows block diagram of the MEDOB-based cutting force observer with phase lag compensation. In this dissertation, the following three types of phase lag elements are considered: bandwidth of the current control loop ($\omega_{cc}/(s+\omega_{cc})$), dead time in servo amplifier ($e^{-T_s s}$), and the summation of delay in numerical differential and transmission of each encoder signal ($e^{-T_m s}, e^{-T_t s}$). Phase lag compensation was carried out by delaying signals so that the total amount of dead time became equal. In Machine B, for example, dead times for T_s, T_m, and T_t are set to 0.2 s. That indicates that $R\hat{\theta}_m^{res}$ and $\hat{x}_t^{res}$ are delayed signals against I_a^{ref}. Thus, I_a^{ref} was delayed to compensate phase lag by setting $(T_1, T_2, T_3) = (0.2,\ 0,\ 0)$ ms. Identification procedure of parameters will be explained in section 3.3.1.

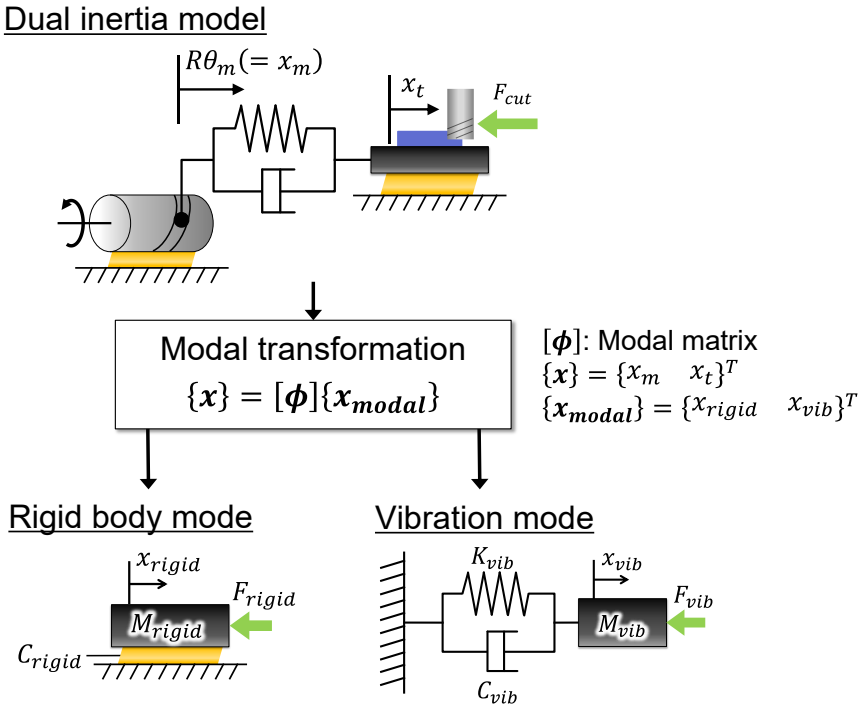

Fig. 2-6 Concept of mode-decoupled cutting force estimation

2.5 Mode decoupled cutting force estimation technique

2.5.1 Diagonalization of dual-inertia model

Fig. 2-6 shows concept of mode-decoupled cutting force estimation. As mentioned before, the dual-inertia model includes both rigid body motion and first vibration mode of the ball-screw-driven stage. With the use of modal matrix, the rigid body and the vibration mode are introduced, which are mutually independent. The cutting force is estimated in each modal space. In other words, multi-inertia plant can be decoupled into multiple equivalent single-inertia plants. The process monitoring in the equivalent single-inertia system is theoretically possible when employing mode-decoupled cutting force estimation technique. As a result, the process monitoring in the multi-inertia system can be easier and simpler. In this section, the modal matrix is analytically introduced for calculating modal parameters in each mode.

By transforming the dynamic equation in rotational motion to translational motion, Eq. (2-3) is rewritten as follows:

$$\begin{bmatrix} M_r & 0 \\ 0 & M_t \end{bmatrix}\begin{Bmatrix} a_m \\ a_t \end{Bmatrix} + \begin{bmatrix} C_r + C_k & -C_k \\ -C_k & C_t + C_k \end{bmatrix}\begin{Bmatrix} v_m \\ v_t \end{Bmatrix} + \begin{bmatrix} K_r & -K_r \\ -K_r & K_r \end{bmatrix}\begin{Bmatrix} x_m \\ x_t \end{Bmatrix} = \begin{Bmatrix} K_t I_a^{ref}/R - T_{fric}/R \\ -F_{fric} - F_{cut} \end{Bmatrix} \quad (2\text{-}22)$$

$$[\boldsymbol{M}]\{\boldsymbol{a}\} + [\boldsymbol{C}]\{\boldsymbol{v}\} + [\boldsymbol{K}]\{\boldsymbol{x}\} = \{\boldsymbol{F}\} \quad (2\text{-}23)$$

where

$$M_r = J_r/R^2\,, C_r = D_r/R^2$$
$$[\boldsymbol{M}] = \begin{bmatrix} M_r & 0 \\ 0 & M_t \end{bmatrix}, [\boldsymbol{C}] = \begin{bmatrix} C_r + C_k & -C_k \\ -C_k & C_t + C_k \end{bmatrix}, [\boldsymbol{K}] = \begin{bmatrix} K_r & -K_r \\ -K_r & K_r \end{bmatrix} \tag{2-24}$$
$$\{\boldsymbol{a}\} = \begin{Bmatrix} a_m \\ a_t \end{Bmatrix}, \{\boldsymbol{v}\} = \begin{Bmatrix} v_m \\ v_t \end{Bmatrix}, \{\boldsymbol{x}\} = \begin{Bmatrix} x_m \\ x_t \end{Bmatrix}, [\boldsymbol{F}] = \begin{Bmatrix} K_t I_a^{ref}/R - T_{fric}/R \\ -F_{fric} - F_{cut} \end{Bmatrix}$$

Modal matrix $[\boldsymbol{\phi}]$ of the dual-inertia model satisfies following equation:

$$\{\boldsymbol{x}\} = [\boldsymbol{\phi}]\{\boldsymbol{x_{modal}}\} \tag{2-25}$$

where $\{\boldsymbol{x_{modal}}\}$ represents modal vector. If the modal matrix is determined, a decoupled dynamic equation is introduced by multiplying $[\boldsymbol{\phi}]^T$ on the left side of Eq. (2-25) as follows:

$$[\boldsymbol{M_{modal}}]\{\boldsymbol{a_{modal}}\} + [\boldsymbol{C_{modal}}]\{\boldsymbol{v_{modal}}\} + [\boldsymbol{K_{modal}}]\{\boldsymbol{x_{modal}}\} = [\boldsymbol{\phi}]^T\{\boldsymbol{F}\} \tag{2-26}$$

where

$$[\boldsymbol{M_{modal}}] = [\boldsymbol{\phi}]^T[\boldsymbol{M}][\boldsymbol{\phi}]$$
$$[\boldsymbol{C_{modal}}] = [\boldsymbol{\phi}]^T[\boldsymbol{C}][\boldsymbol{\phi}]$$
$$[\boldsymbol{K_{modal}}] = [\boldsymbol{\phi}]^T[\boldsymbol{K}][\boldsymbol{\phi}]$$

The estimating equation of the cutting force in the modal space can be introduced by solving Eq. (2-26), which will be explained in the next section. In order to calculate modal matrix, eigenvector of the dual-inertia model needs to be calculated. Here, free vibration is considered assuming right-hand side of Eq. (2-22) to zero. Solution of the free vibration is assumed as follows:

$$\{\boldsymbol{x}\} = \{\boldsymbol{X}\}e^{\lambda t} \tag{2-27}$$

where

$$\{\boldsymbol{X}\} = \begin{Bmatrix} X_m \\ X_t \end{Bmatrix}$$

By substituting Eq. (2-27) into Eq. (2-22), the following equation is introduced as follows:

$$\left(\lambda^2 \begin{bmatrix} M_r & 0 \\ 0 & M_t \end{bmatrix} + \lambda \begin{bmatrix} C_r + C_k & -C_k \\ -C_k & C_t + C_k \end{bmatrix} + \begin{bmatrix} K_r & -K_r \\ -K_r & K_r \end{bmatrix}\right) \begin{Bmatrix} X_m \\ X_t \end{Bmatrix} = \begin{Bmatrix} 0 \\ 0 \end{Bmatrix} \tag{2-28}$$

In this dissertation, proportional damping is considered. Thus, damping matrix is expressed

as follows:

$$[\boldsymbol{C}] = \alpha_c[\boldsymbol{M}] + \beta_c[\boldsymbol{K}] \tag{2-29}$$

where

$$\begin{aligned} \alpha_c &= C_r/M_r = C_t/M_t \\ \beta_c &= C_k/K_r \end{aligned} \tag{2-30}$$

Thus, the following equation can be derived from Eq. (2-28):

$$\left((\lambda^2 + \alpha_c\lambda)\begin{bmatrix} M_r & 0 \\ 0 & M_t \end{bmatrix} + (\beta_c\lambda + 1)\begin{bmatrix} K_r & -K_r \\ -K_r & K_r \end{bmatrix}\right)\begin{Bmatrix} X_m \\ X_t \end{Bmatrix} = \begin{Bmatrix} 0 \\ 0 \end{Bmatrix} \tag{2-31}$$

By letting $p^2 = (\lambda^2 + \alpha_c\lambda)/(\beta_c\lambda + 1)$, Eq. (2-31) is rewritten as follows:

$$\left(p^2\begin{bmatrix} M_r & 0 \\ 0 & M_t \end{bmatrix} + \begin{bmatrix} K_r & -K_r \\ -K_r & K_r \end{bmatrix}\right)\begin{Bmatrix} X_m \\ X_t \end{Bmatrix} = \begin{Bmatrix} 0 \\ 0 \end{Bmatrix} \tag{2-32}$$

Determinant of coefficient matrix needs to be zero so that Eq. (2-32) may have solution other than $X_m = X_t = 0$:

$$\begin{aligned} &(p^2M_r + K_r)(p^2M_t + K_r) - K_r^2 = 0 \\ &\therefore p^2 = 0\,, -\frac{M_r + M_t}{M_rM_t}K_r \end{aligned} \tag{2-33}$$

By substituting Eq. (2-33) into Eq. (2-32), following two equations are introduced:

$$\begin{bmatrix} K_r & -K_r \\ -K_r & K_r \end{bmatrix}\begin{Bmatrix} X_m \\ X_t \end{Bmatrix} = \begin{Bmatrix} 0 \\ 0 \end{Bmatrix} \tag{2-34}$$

$$\begin{bmatrix} K_r/\alpha & K_r \\ K_r & \alpha K_r \end{bmatrix}\begin{Bmatrix} X_m \\ X_t \end{Bmatrix} = \begin{Bmatrix} 0 \\ 0 \end{Bmatrix} \tag{2-35}$$

According to Eq. (2-34) and Eq. (2-35), eigenvectors for rigid body and vibration mode are introduced as follows:

$$\{\boldsymbol{\phi_{rigid}}\} = \begin{Bmatrix} 1 \\ 1 \end{Bmatrix} \tag{2-36}$$

$$\{\boldsymbol{\phi_{vib}}\} = \begin{Bmatrix} 1 \\ -1/\alpha \end{Bmatrix} \tag{2-37}$$

Therefore, modal matrix can be defined as follows:

$$\begin{aligned}[\boldsymbol{\phi}] &= \left[\{\boldsymbol{\phi_{rigid}}\} \quad \{\boldsymbol{\phi_{vib}}\}\right] \\ &= \begin{bmatrix} 1 & 1 \\ 1 & -1/\alpha \end{bmatrix}\end{aligned} \tag{2-38}$$

By substituting Eq. (2-38) into Eq. (2-25), modal displacement vector $\{\boldsymbol{x_{modal}}\} = (x_{rigid} \quad x_{vib})^T$ is introduced as follows:

$$\begin{aligned}\{\boldsymbol{x_{modal}}\} &= [\boldsymbol{\phi}]^{-1}\{\boldsymbol{x}\} \\ \therefore \begin{Bmatrix} x_{rigid} \\ x_{vib} \end{Bmatrix} &= \frac{1}{\alpha + 1}\begin{Bmatrix} x_m + \alpha x_t \\ \alpha(x_m - x_t) \end{Bmatrix}\end{aligned} \tag{2-39}$$

Eq. (2-39) indicates that both displacement in the rigid body mode x_{rigid} and in the vibration mode x_{vib} can be calculated from servo information of the ball-screw-driven stage. Mass matrix $[\boldsymbol{M}]$, damping matrix $[\boldsymbol{C}]$, and stiffness matrix $[\boldsymbol{K}]$ can be diagonalized by using modal matrix $[\boldsymbol{\phi}]$ and its transpose $[\boldsymbol{\phi}]^T$ as follows:

$$\begin{aligned}[\boldsymbol{M_{modal}}] &= [\boldsymbol{\phi}]^T[\boldsymbol{M}][\boldsymbol{\phi}] \\ &= \begin{bmatrix} M_r + M_t & 0 \\ 0 & (1 + 1/\alpha)M_r \end{bmatrix} \\ [\boldsymbol{C_{modal}}] &= [\boldsymbol{\phi}]^T[\boldsymbol{C}][\boldsymbol{\phi}] \\ &= \alpha_c[\boldsymbol{M_{modal}}] + \beta_c[\boldsymbol{K_{modal}}] \\ [\boldsymbol{K_{modal}}] &= [\boldsymbol{\phi}]^T[\boldsymbol{K}][\boldsymbol{\phi}] \\ &= \begin{bmatrix} 0 & 0 \\ 0 & (1 + 1/\alpha)^2 K_r \end{bmatrix}\end{aligned} \tag{2-40}$$

As shown in Eq. (2-40), the non-diagonal elements of $[\boldsymbol{M_{modal}}]$, $[\boldsymbol{C_{modal}}]$ and $[\boldsymbol{K_{modal}}]$ became zero. Because (1, 1) component of $[\boldsymbol{K_{modal}}]$ is zero, (1, 1) components of Eq. (2-40) indicate parameters for the rigid body mode. Similarly, (2, 2) components indicate parameters for the vibration mode. By defining $[\boldsymbol{M_{modal}}] = \mathrm{diag}(M_{rigid}, M_{vib})$, $[\boldsymbol{C_{modal}}] = \mathrm{diag}(C_{rigid}, C_{vib})$, $[\boldsymbol{K_{modal}}] = \mathrm{diag}(0, K_{vib})$, modal parameters are introduced as follows:

$$\begin{aligned} M_{rigid} &= M_r + M_t \\ C_{rigid} &= \alpha_c M_{rigid} \\ M_{vib} &= (1 + 1/\alpha)M_r \\ C_{vib} &= \alpha_c M_{vib} + \beta_c K_{vib} \\ K_{vib} &= (1 + 1/\alpha)^2 K_r \end{aligned} \tag{2-41}$$

2.5.2 Estimation principle for cutting force

Estimating equation of the cutting force is derived from motion equation in the modal space shown in Eq. (2-26). Based on the calculated modal matrix $[\boldsymbol{\phi}]$, Eq. (2-26) is expanded by as follows:

$$\begin{bmatrix} M_{rigid} & 0 \\ 0 & M_{vib} \end{bmatrix} \begin{Bmatrix} a_{rigid} \\ a_{vib} \end{Bmatrix} + \begin{bmatrix} C_{rigid} & 0 \\ 0 & C_{vib} \end{bmatrix} \begin{Bmatrix} v_{rigid} \\ v_{vib} \end{Bmatrix} + \begin{bmatrix} 0 & 0 \\ 0 & K_{vib} \end{bmatrix} \begin{Bmatrix} x_{rigid} \\ x_{vib} \end{Bmatrix} = \begin{bmatrix} 1 & 1 \\ 1 & -1/\alpha \end{bmatrix} \begin{Bmatrix} K_t I_a^{ref}/R - T_{fric}/R \\ -F_{fric} - F_{cut} \end{Bmatrix} \tag{2-42}$$

By solving Eq. (2-42), the cutting force component in the rigid body and vibration modes can be calculated as follows:

$$F_{cut(rigid)} = \frac{1}{R} K_t I_a^{ref} - M_{rigid} a_{rigid} - C_{rigid} v_{rigid} - \frac{1}{R} T_{fric} - F_{fric} \tag{2-43}$$

$$F_{cut(vib)} = \alpha \left\{ M_{vib} a_{vib} + C_{vib} v_{vib} + K_{vib} x_{vib} - \frac{1}{R} K_t I_a^{ref} + \frac{1}{R} T_{fric} - \frac{1}{\alpha} F_{fric} \right\} \tag{2-44}$$

In practice, a low-pass filter is implemented to eliminate higher frequency noise as in the case of MEDOB-based cutting force estimation.

Fig. 2-7 shows block diagram of the cutting force observer in modal space with phase lag compensation. Compensation process of the phase lag is identical to that in MEDOB-based method written in the section 2.4.2.

As can be seen in Eq. (2-39), the modal displacement in the vibration mode x_{vib} is calculated from the relative displacement between the stage x_t and the motor x_m. Thus, the cutting force estimation in vibration mode is based on relative displacement, velocity, and acceleration. The relative displacement is used in load-side disturbance observer (LDOB [95,96]), which is also applicable to the cutting force estimation. However, equivalent single-inertia system cannot be introduced in employing LDOB. In terms of simplifying the process monitoring, it is preferable to employ the proposed mode-decoupled estimation technique. Application of the mode decoupling is not limited to the cutting force estimation. In the literature, mode decoupling is applied to analyze the damping property of the relative velocity feedback control [97].

In the MEDOB-based method, as mentioned before, the cutting force can be estimated without using the stiffness K_r. Cutting force estimation in the rigid body mode is essentially the same as the MEDOB-based method. In other words, the stiffness independent

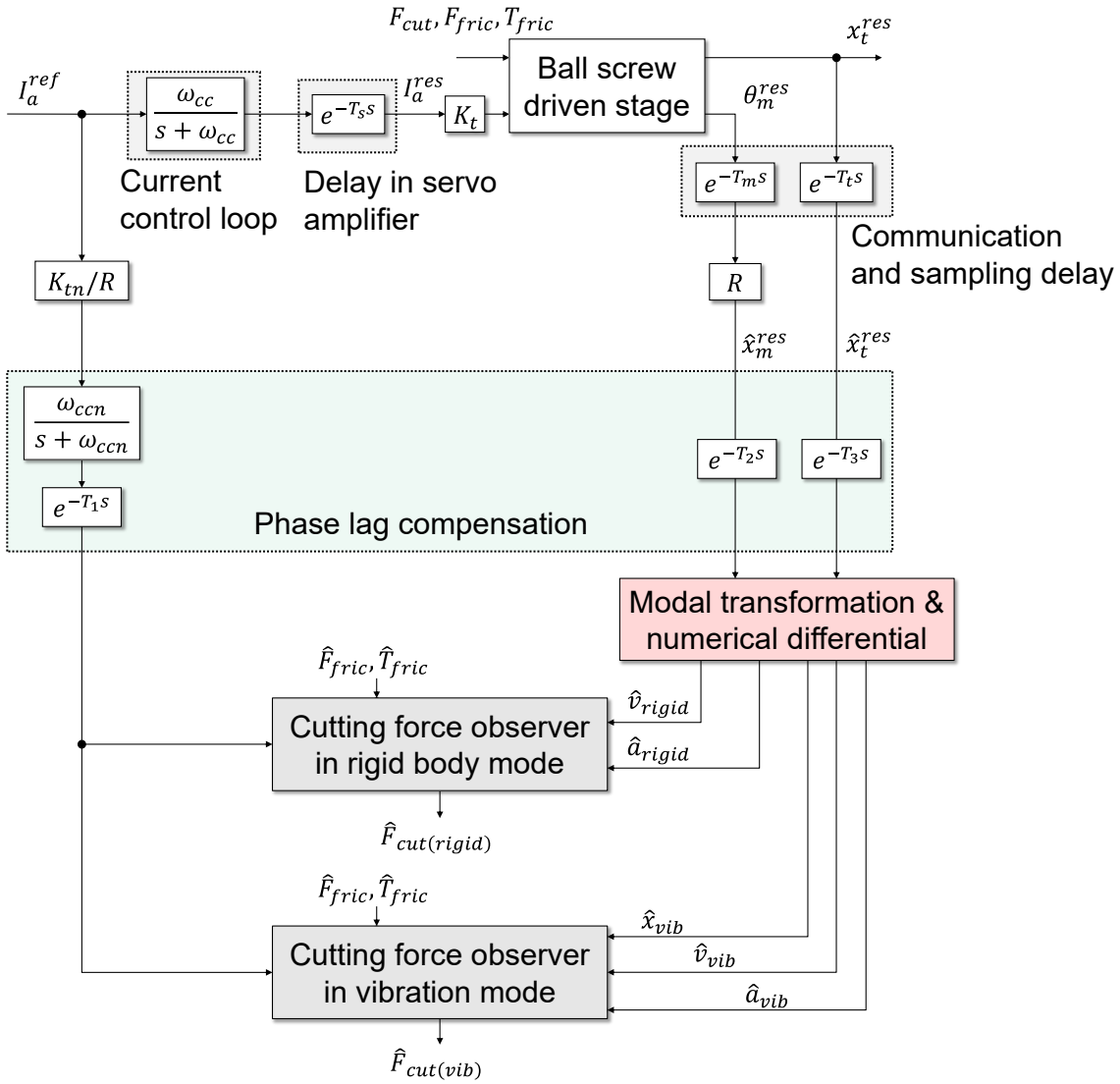

Fig. 2-7 Block diagram of cutting force observer in modal space with phase lag compensation

estimation is possible in MEDOB, because the rigid body motion of the ball-screw-driven stage is extracted by applying MEDOB. The equivalence of two estimation methods is analytically proved in Appendix.

2.6 Extension to multi-inertia system

2.6.1 Estimation principle for cutting force

It is possible to extend the basic idea of the proposed method to a multi-inertia system. Displacement (or acceleration) sensors are then required, corresponding to the number of degrees of freedom to extract eigenmode. In this section, estimation principle of the cutting force is explained based on the triple-inertia model, which considers torsional vibration

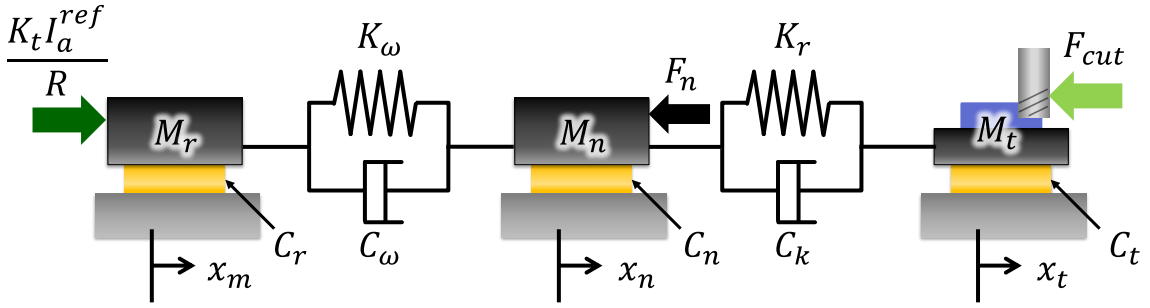

Fig. 2-8 Triple-inertia model of ball-screw-driven stage

between motor and nut. The triple-inertia model is shown in Fig. 2-8. In the figure, rotational elements are transformed to translational elements for simplification. Dynamic equations are introduced as follows:

$$M_r a_m = K_t I_a^{ref}/R + K_\omega(x_n - x_m) + C_\omega(v_n - v_m) - C_r v_m \tag{2-45}$$

$$M_n a_n = K_r(x_t - x_n) - K_\omega(x_n - x_m) + C_k(v_t - v_n) - C_\omega(v_n - v_m) - C_n v_n - F_n \tag{2-46}$$

$$M_t a_t = -K_r(x_t - x_n) - C_k(v_t - v_n) - C_t v_t - F_{cut} \tag{2-47}$$

where M_n is mass of nut interface including inertia of ball-screw, K_ω is equivalent torsional stiffness of feed screw system in translational motion, C_n is damping coefficient at nut interface, C_ω is equivalent damping coefficient between motor and nut, and F_n is load force at nut interface. In Eq. (2-45) ~ (2-47), friction torque at the motor and friction force at the linear guideway are ignored. In the MEDOB-based cutting force estimation, the dynamic equations are solved, so that elastic and damping forces can be erased as follows:

$$F_{cut} = \frac{1}{R} K_t I_a^{ref} - M_r a_m - M_n a_n - M_t a_t - C_r v_m - C_n v_n - C_t v_t - F_n \tag{2-48}$$

Thus, estimating equation of the cutting force applying MEDOB is written as follows:

$$\hat{F}_{cut} = \frac{g_{cut}}{s + g_{cut}} \left\{ \frac{1}{R} K_{tn} I_a^{ref} - M_{rn}\hat{a}_m - M_{nn}\hat{a}_n - M_{tn}\hat{a}_t - C_{rn}\hat{v}_m - C_{nn}\hat{v}_n - C_{tn}\hat{v}_t - \hat{F}_n \right\} \tag{2-49}$$

In mode-decoupled cutting force estimation technique, the modal matrix $[\boldsymbol{\phi}]$ needs to be calculated to decouple (i.e. diagonalize) the triple-inertia model. The dynamic equations shown in Eq. (2-45) ~ (2-47) are rewritten as matrix form as follows:

$$[\boldsymbol{M}]\{\boldsymbol{a}\} + [\boldsymbol{C}]\{\boldsymbol{v}\} + [\boldsymbol{K}]\{\boldsymbol{x}\} = \{\boldsymbol{F}\} \tag{2-50}$$

where

$$[\boldsymbol{M}]=\begin{bmatrix}M_r & 0 & 0\\ 0 & M_n & 0\\ 0 & 0 & M_t\end{bmatrix},[\boldsymbol{C}]=\begin{bmatrix}C_r+C_\omega & -C_\omega & 0\\ -C_\omega & C_n+C_\omega+C_k & -C_k\\ 0 & -C_k & C_c+C_k\end{bmatrix},$$
$$[\boldsymbol{K}]=\begin{bmatrix}K_\omega & -K_\omega & 0\\ -K_\omega & K_\omega+K_r & -K_r\\ 0 & -K_r & K_r\end{bmatrix},[\boldsymbol{F}]=\begin{Bmatrix}K_t I_a^{ref}/R\\ -F_n\\ -F_{cut}\end{Bmatrix},\{\boldsymbol{a}\}=\begin{Bmatrix}a_m\\ a_n\\ a_t\end{Bmatrix},\{\boldsymbol{v}\}=\begin{Bmatrix}v_m\\ v_n\\ v_t\end{Bmatrix},\{\boldsymbol{x}\}=\begin{Bmatrix}x_m\\ x_n\\ x_t\end{Bmatrix} \tag{2-51}$$

By assuming proportional damping, Eq. (2-50) can be rewritten as follows:

$$[\boldsymbol{M}]\{\boldsymbol{a}\}+(\alpha_c[\boldsymbol{M}]+\beta_c[\boldsymbol{K}])\{\boldsymbol{v}\}+[\boldsymbol{K}]\{\boldsymbol{x}\}=\{\boldsymbol{F}\} \tag{2-52}$$

where

$$\alpha_c=\frac{C_r}{M_r}=\frac{C_n}{M_n}=\frac{C_t}{M_t},\beta_c=\frac{C_\omega}{K_\omega}=\frac{C_k}{K_r} \tag{2-53}$$

As in the case of the dual-inertia system, the free vibration is assumed and Eq. (2-27) is substituted into Eq. (2-53). As a result, the following equation is obtained as follows:

$$\begin{aligned}\{(\lambda^2+\alpha_c\lambda)[\boldsymbol{M}]+(\beta_c\lambda+1)[\boldsymbol{K}]\}\{\boldsymbol{X}\}e^{\lambda t}=\{\boldsymbol{0}\}\\ \therefore (p^2[\boldsymbol{M}]+[\boldsymbol{K}])\{\boldsymbol{X}\}=\{\boldsymbol{0}\}\end{aligned} \tag{2-54}$$

where

$$p^2=\frac{\lambda^2+\alpha_c\lambda}{\beta_c\lambda+1} \tag{2-55}$$

Determinant of coefficient matrix needs to be zero so that Eq. (2-54) may have solution other than $\{\boldsymbol{X}\}=\{\boldsymbol{0}\}$. Therefore, p^2 satisfies following equation:

$$p^2\left\{p^4+\left(\frac{K_\omega}{M_r}+\frac{K_\omega+K_r}{M_n}+\frac{K_r}{M_t}\right)p^2+K_\omega K_r\left(\frac{1}{M_rM_n}+\frac{1}{M_nM_t}+\frac{1}{M_tM_r}\right)\right\}=0 \tag{2-56}$$

Three eigenmodes can be calculated by solving Eq. (2-56) and substituting the solution into Eq. (2-54). When solution of Eq. (2-54) is assumed as $p^2=P$, eigenmode of triple-inertia model can be expressed as follows:

$$\begin{Bmatrix}\phi_r\\ \phi_n\\ \phi_t\end{Bmatrix}=\begin{Bmatrix}1\\ 1+\dfrac{M_r}{K_\omega}P\\ \dfrac{K_r}{K_\omega}\cdot\dfrac{M_m}{M_t}\cdot\dfrac{P+K_\omega/M_m}{P+K_r/M_t}\end{Bmatrix} \tag{2-57}$$

Thus, modal matrix $[\boldsymbol{\phi}]$ can be expressed as follows:

$$[\boldsymbol{\phi}] = \begin{bmatrix} \begin{Bmatrix} \phi_r \\ \phi_n \\ \phi_t \end{Bmatrix}_{rigid} & \begin{Bmatrix} \phi_r \\ \phi_n \\ \phi_t \end{Bmatrix}_{vib(1st)} & \begin{Bmatrix} \phi_r \\ \phi_n \\ \phi_t \end{Bmatrix}_{vib(2nd)} \end{bmatrix} \equiv \begin{bmatrix} \phi_{1,1} & \phi_{1,2} & \phi_{1,3} \\ \phi_{2,1} & \phi_{2,2} & \phi_{2,3} \\ \phi_{3,1} & \phi_{3,2} & \phi_{3,3} \end{bmatrix} \tag{2-58}$$

Although the modal matrix of the dual-inertia model can be expressed with simple formula (i.e. Eq. (2-38)), it is difficult to analytically calculate the modal matrix of multi-inertia model. In multi-inertia system, the modal matrix needs to be calculated based on the numerical calculation algorithm.

Because modal displacement vector $\{\boldsymbol{x_{modal}}\} = (x_{rigid} \quad x_{vib(1st)} \quad x_{vib(2nd)})^T$ is calculated by $\{\boldsymbol{x_{modal}}\} = [\boldsymbol{\phi}]^{-1}\{\boldsymbol{x}\}$, decoupled dynamic equation can be expressed as in the case of dual-inertia model:

$$[\boldsymbol{M_{modal}}]\{\boldsymbol{a_{modal}}\} + [\boldsymbol{C_{modal}}]\{\boldsymbol{v_{modal}}\} + [\boldsymbol{K_{modal}}]\{\boldsymbol{x_{modal}}\} = [\boldsymbol{\phi}]^T\{\boldsymbol{F}\} \tag{2-59}$$

where

$$\begin{aligned} [\boldsymbol{M_{modal}}] &= [\boldsymbol{\phi}]^T[\boldsymbol{M}][\boldsymbol{\phi}] = \mathrm{diag}\left(M_{rigid}, M_{vib(1st)}, M_{vib(2nd)}\right) \\ [\boldsymbol{C_{modal}}] &= [\boldsymbol{\phi}]^T[\boldsymbol{C}][\boldsymbol{\phi}] = \mathrm{diag}\left(C_{rigid}, C_{vib(1st)}, C_{vib(2nd)}\right) \\ [\boldsymbol{K_{modal}}] &= [\boldsymbol{\phi}]^T[\boldsymbol{K}][\boldsymbol{\phi}] = \mathrm{diag}\left(0, K_{vib(1st)}, K_{vib(2nd)}\right) \\ \{\boldsymbol{v_{modal}}\} &= (v_{rigid} \quad v_{vib(1st)} \quad v_{vib(2nd)})^T \\ \{\boldsymbol{a_{modal}}\} &= (a_{rigid} \quad a_{vib(1st)} \quad a_{vib(2nd)})^T \end{aligned} \tag{2-60}$$

Therefore, the cutting force in each mode can be introduced by solving Eq. (2-59) as follows:

$$F_{cut(rigid)} = \frac{1}{\phi_{3,1}}\left\{\phi_{1,1}\frac{K_t I_a^{ref}}{R} - M_{rigid}a_{rigid} - C_{rigid}v_{rigid} - \phi_{2,1}F_n\right\} \tag{2-61}$$

$$F_{cut(vib1)} = \frac{1}{\phi_{3,2}}\left\{\phi_{1,2}\frac{K_t I_a^{ref}}{R} - M_{vib(1)}a_{vib(1)} - C_{vib(1)}v_{vib(1)} - K_{vib(1)}x_{vib(1)} - \phi_{2,2}F_n\right\} \tag{2-62}$$

$$F_{cut(vib2)} = \frac{1}{\phi_{3,3}}\left\{\phi_{1,3}\frac{K_t I_a^{ref}}{R} - M_{vib(2)}a_{vib(2)} - C_{vib(2)}v_{vib(2)} - K_{vib(2)}x_{vib(2)} - \phi_{2,3}F_n\right\} \tag{2-63}$$

2.6.2 Frequency response of cutting force observer

Frequency response of the cutting force observer is calculated based on the triple-inertia model of the ball-screw-driven stage. There are two resonance points in the triple-inertia model. Parameters are determined so that the first mode is resulting from axial stiffness between the nut and the stage (i.e. K_r), and the second mode is resulting from torsional stiffness between the motor and the nut (i.e. K_ω). Calculation procedure is the same as that shown in section 4.2.2. For comparison, the frequency responses of DOB and MEDOB with dual-inertia model are also calculated. In order to reduce degree of freedom, relative motion between motor and nut is ignored (i.e. $x_m = x_n$) for MEDOB with dual-inertia model. In other words, dynamics between the nut and the stage is modeled by applying the dual-inertia model. Similarly, the rigid body motion is assumed for DOB with single-inertia model. Estimation equations of the cutting force are expressed as follows:

DOB based on single-inertia model

$$\hat{F}_{cut} = (\text{LPF}) \cdot \left\{ \frac{1}{R} K_t I_a^{ref} - (M_r + M_n + M_t)\hat{a}_m - (C_r + C_n + C_t)\hat{v}_m \right\} \tag{2-64}$$

MEDOB based on dual-inertia model

$$\hat{F}_{cut} = (\text{LPF}) \cdot \left\{ \frac{1}{R} K_t I_a^{ref} - (M_r + M_n)\hat{a}_m - M_t\hat{a}_t - (C_r + C_n)\hat{v}_m - C_t\hat{v}_t \right\} \tag{2-65}$$

Following estimating equation in the vibration modal space is introduced by assuming $x_m = x_n$ as well as MEDOB with dual-inertia model.

$$\hat{F}_{cut} = (\text{LPF}) \cdot \alpha \left(M_{vib} a_{vib} + C_{vib} v_{vib} + K_{vib} x_{vib} - \frac{1}{R} K_t I_a^{ref} \right) \tag{2-66}$$

where

$$\begin{aligned} \alpha &= M_t/(M_r + M_n) \\ M_{vib} &= M_r + M_n + M_t/\alpha^2 \\ C_{vib} &= \alpha_c M_{vib} + \beta_c K_{vib} \\ K_{vib} &= (1 + 1/\alpha)^2 K_r \\ x_{vib} &= \frac{\alpha}{\alpha + 1}(x_m - x_t) \end{aligned} \tag{2-67}$$

M_r in Eq. (2-41) is replaced to $M_r + M_n$ in Eq. (2-67), which is true of modal matrix $[\boldsymbol{\phi}]$.

Fig. 2-9 shows the frequency response of the cutting force observer. Butterworth 4th order

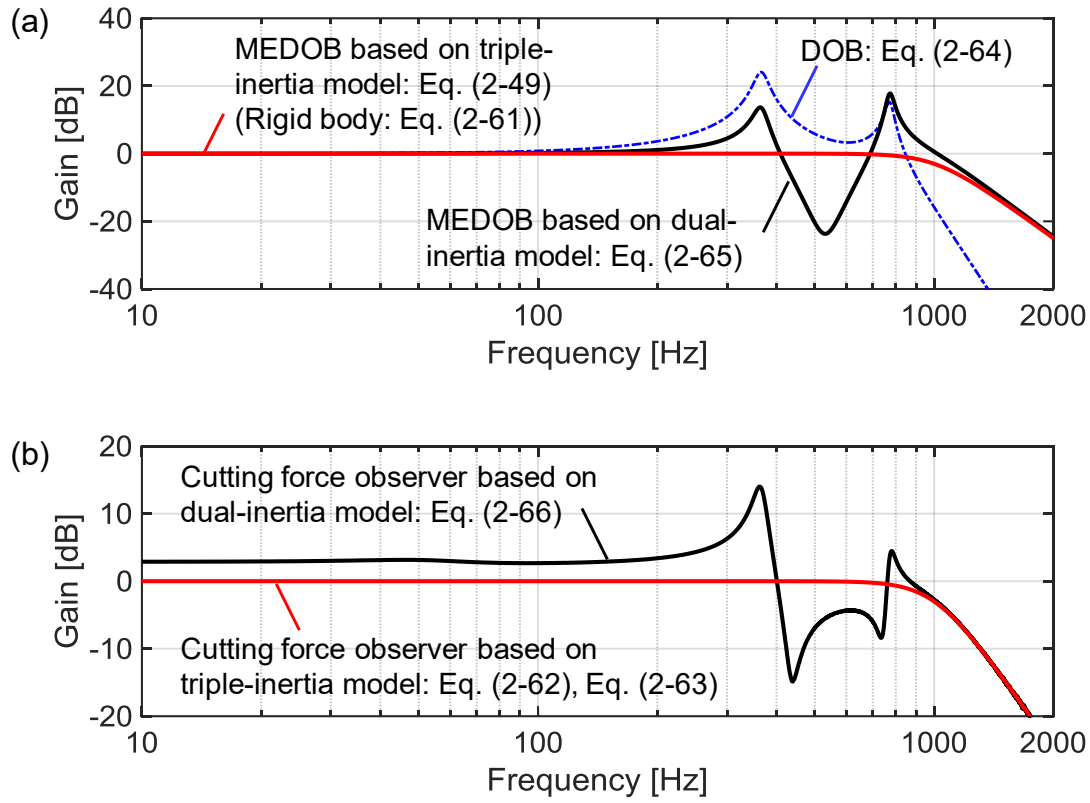

Fig. 2-9 Frequency response of cutting force observer under triple-inertia system (a) DOB and MEDOB (b) mode-decoupled monitoring in vibration mode

low pass filter (LPF) whose cutoff frequency was 1 kHz was employed. When DOB or MEDOB is applied, low frequency components of the applied cutting force can be estimated accurately regardless of estimation method as shown in Fig. 2-9 (a). On the other hand, estimation accuracy decreases near the resonance frequencies (i.e. 366 Hz, 770 Hz) under single- or dual-inertia model-based formulation. As for the vibration mode, the estimated cutting force based on the dual-inertia model is highly distorted up to the second resonance frequency. Even if the dual-inertia model that considers the axial dynamics is applied, estimation accuracy can decrease near the first resonance frequency, which is true of both MEDOB and mode-decoupled method. It is preferable to correspond the number of sensors to the order of the plant model for wideband and accurate cutting force estimation.

Although frequency response of the cutting force observer under the triple-inertia plant was discussed in the above paragraphs, the proposed estimation method can be extended to multi-inertia system. As for MEDOB-based method, estimating equation of the cutting force can be introduced by solving the motion equation, so that elastic and damping forces can be erased. As for mode-decoupled method, calculating the modal matrix of the multi-inertia plant is necessary in order to extract eigenmode and introduce modal space. The cutting force is similarly estimated by solving the motion equation in each modal space.

2.7 Summary

This chapter describes methodology for the cutting force estimation using multi-encoder, which are available under the full-closed control. The contents are summarized as follows.

1. By applying multi-encoder based disturbance observer (MEDOB), the estimating equation for the cutting force is derived from the dual-inertia model of the ball-screw-driven stage. In the MEDOB-based method, the cutting force is estimated by extracting rigid body motion of the ball-screw-driven stage. In addition, the method does not require the stiffness value, which can vary depending on the stage position.
2. In constructing the cutting force estimation system, the phase lag elements in the control system are considered, which are non-negligible when estimating high frequency components of the cutting force. Delay in the servo amplifier, the numerical differential, and the signal transmission are considered, and the phase lags are compensated by delaying the signal(s) so that the total amount of the phase lags becomes equal.
3. Mode-decoupled cutting force estimation technique using the modal matrix is introduced, which independently estimates the cutting force components in the rigid body and vibration mode. The cutting force estimation in the rigid body mode is essentially the same as the MEDOB-based method. In contrast to general estimation technique, the cutting force estimation technique in the vibration mode makes use of the relative displacement, velocity, and acceleration between the stage and the motor.
4. Estimation principles of the cutting force in multi-inertia system are presented for both estimation method, taking triple-inertia system as an example. If there is discrepancy in degrees of freedom between the plant model and the cutting force observer, the estimation error can increase around the resonance frequencies of the plant.

3. Simulator and experimental setup for evaluating cutting force observer

3.1 Configuration of ball-screw-driven stage

Fig. 3-1 and Fig. 3-2 show the prototype of ball-screw-driven machine tools, that are, Machine A and Machine B. Machine B was built to enhance estimation accuracy of the cutting force based on the simulation results shown in section 4.2. The proposed estimation technique can be implemented in the control system of all axes. In this dissertation, however, the estimation performance was mainly evaluated in the X-direction at the workpiece side, which can be compared with the result of the piezoelectric dynamometer (Type9129A, from Kistler). Specification of the dynamometer is listed in Table 3-1, and major specification of Machine A and Machine B is presented

Table 3-1 Specification of piezoelectric dynamometer

	Fx	Fy	Fz
Dynamic resolution [N]	< 0.01	< 0.01	< 0.01
Sensitivity [pC/N]	8	4.1	8
Natural frequency [kHz]	3.5	4.5	3.5
Linearity, all ranges [%FSO]	±< 0.3	±< 0.3	±< 0.3

Table 3-2 Major specification of experimental setup

	Machine A	Machine B
Ball screw		
Lead length [mm]	5	5
Diameter [mm]	15	15
Support type	Single anchor	Double anchor
Preload type	Oversized ball	Oversized ball
Stroke [mm]	210	200
Sampling frequency [kHz]	20	10
Pole number of motor	8	10
Slot number of motor	9	12
Bandwidth of current control loop [rad/s]	3000	5000
Linear encoder		
Signal type	Square wave	Sine wave
Resolution [nm]	20	0.24
Grating period [μm]	8	8
Signal period after interpolation at scanning head [μm]	0.08	4
Rotary encoder		
Resolution [bit]	17	23
Equivalent resolution in translational motion [nm]	38	0.60
Signal period [count/rev]	512 (= 2^9)	512 (= 2^9)
Interpolation times	256 (= 2^8)	16384 (= 2^{14})

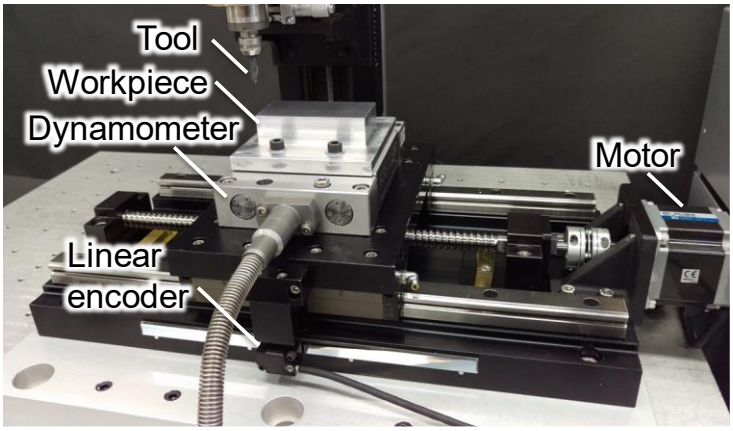

Fig. 3-1 Experimental setup for Machine A

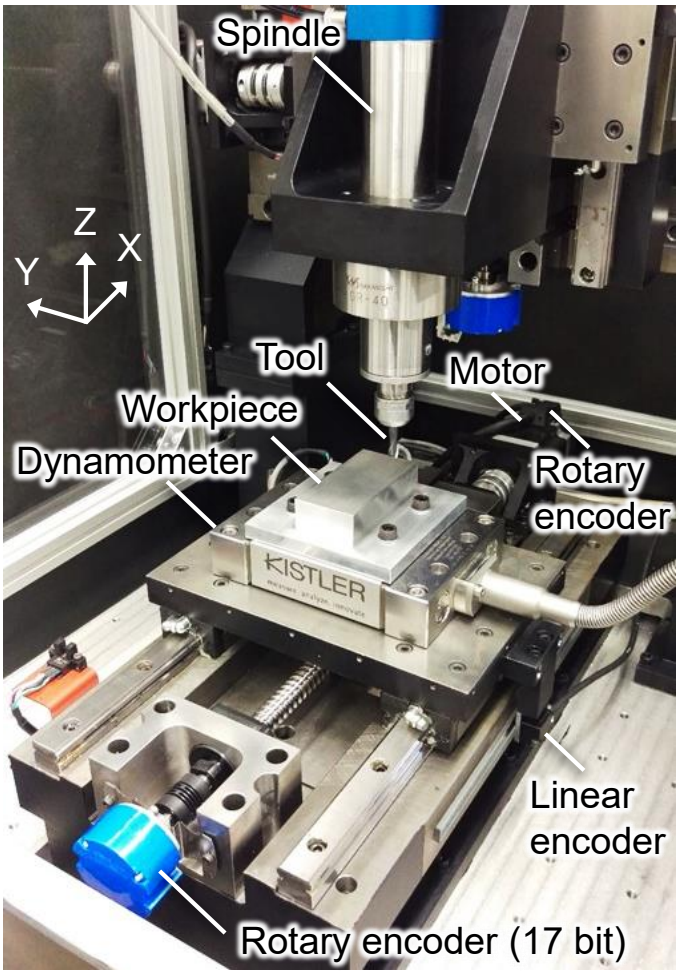

Fig. 3-2 Experimental setup for Machine B

in Table 3-2. Ball-screws are directly connected to synchronous AC servomotors via disk-type couplings. To reduce variation of disturbance force during feed motion, ball-screws with small torque variation are employed in Machine B, which was experimentally confirmed by preliminary inspection of manufacturer. The motion of the tables is supported by ball guideways. Feedback signals for the controllers are provided by linear

encoders and rotary encoders. Square wave-type linear encoder (LIF471R, from Heidenhain) is used in Machine A, and 20 nm resolution is realized by quadrupling pulse signal in counter circuit of counter board (PCI-632206, from Interface). In Machine B, sine wave-type linear encoder (LIF481R, from Heidenhain) is used, which can provide 244 pm resolution by interpolating the encoder signal 16384 times. Similarly, high-resolution rotary encoder is adopted in Machine B to reduce measurement error of velocity and acceleration. In Machine B, another rotary encoder (resolution: 17 bit) is mounted at the counter-motor side, which is not used for cutting force estimation but for generating the electrical angle of the servomotors.

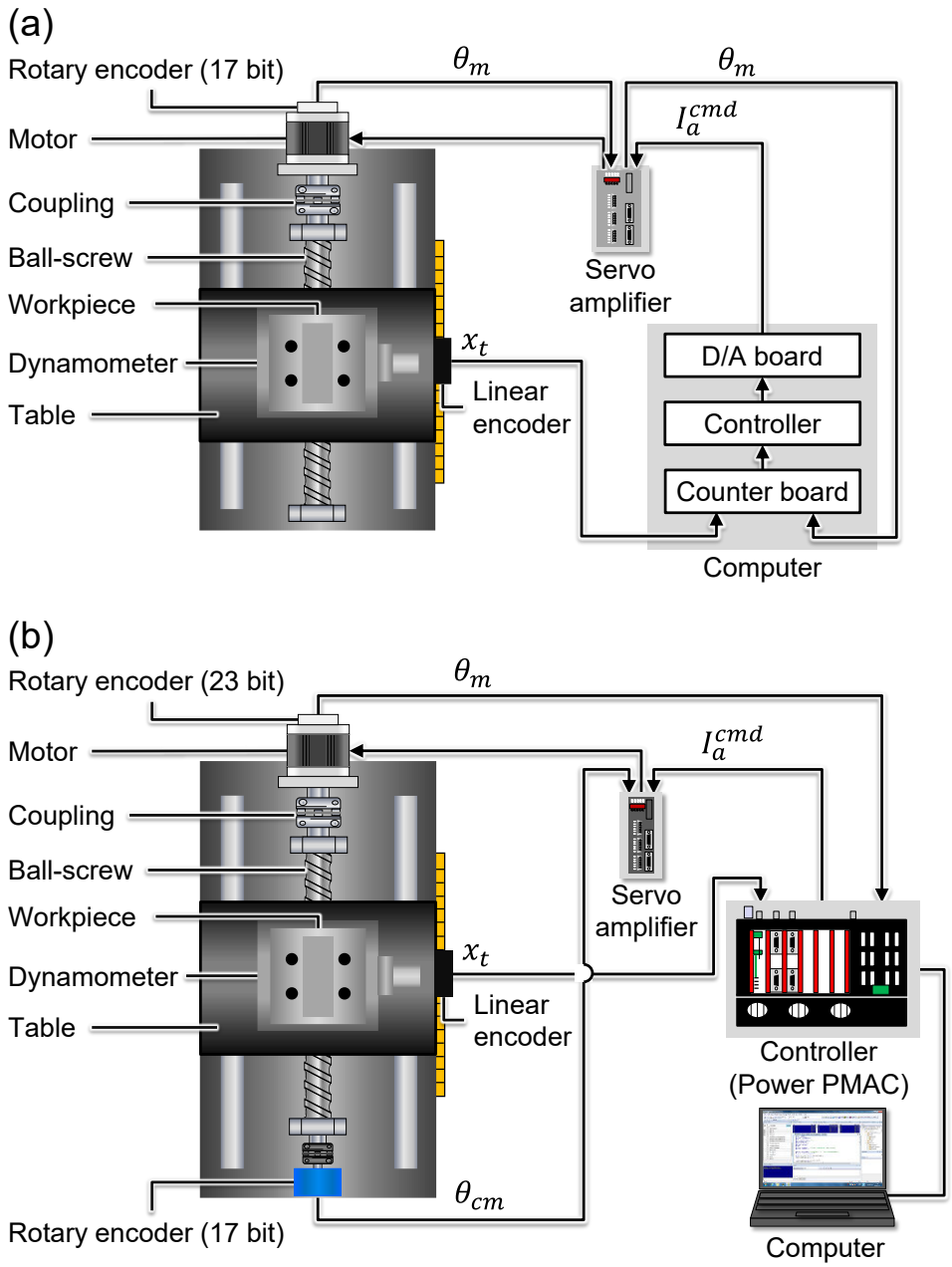

Fig. 3-3 System configuration of experimental setup (a) Machine A (b) Machine B

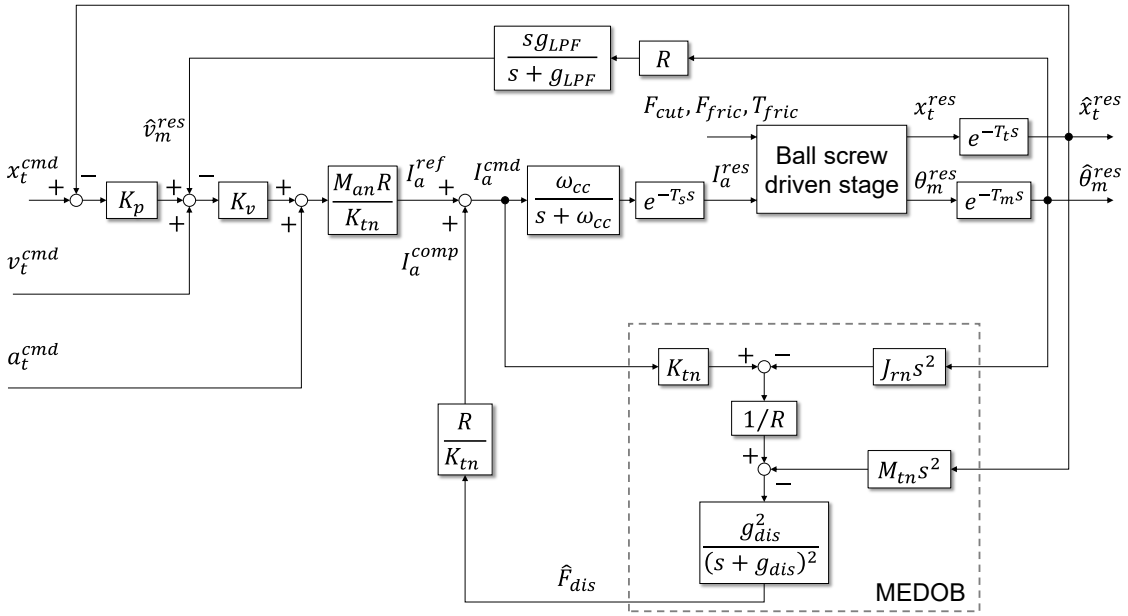

Fig. 3-4 Block diagram of entire control system

3.2 Configuration of control system

The system configuration of the experimental setup is shown in Fig. 3-3. In Machine A, control algorithm is implemented into computer. Because motor angle θ_m is fed back to computer via servo amplifier, θ_m is more subjected to dead time of the servo amplifier compared with Machine B. Thus, there are synchronization errors between θ_m and x_t in Machine A. In Machine B, the control algorithm is implemented to the motion controller (Power PMAC, from Delta Tau). Servo amplifiers of both machines are operated under torque control mode, and torque command input voltage after D/A conversion is applied to the servo amplifiers.

Fig. 3-4 shows block diagram of entire control system. Position control was performed by the combination of the position-P velocity-P controller and the MEDOB. Cutoff frequency of the low-pass filter in MEDOB is set to become lower than the resonance frequency as the dual-inertia system. This is because disturbance cancellation by MEDOB is performed for rigid body motion of the drive system. In addition, phase lag compensation is not conducted in MEDOB for disturbance cancellation. Both in the experimental verification and simulation, control algorithm was constructed based on the block diagram shown in Fig. 3-4.

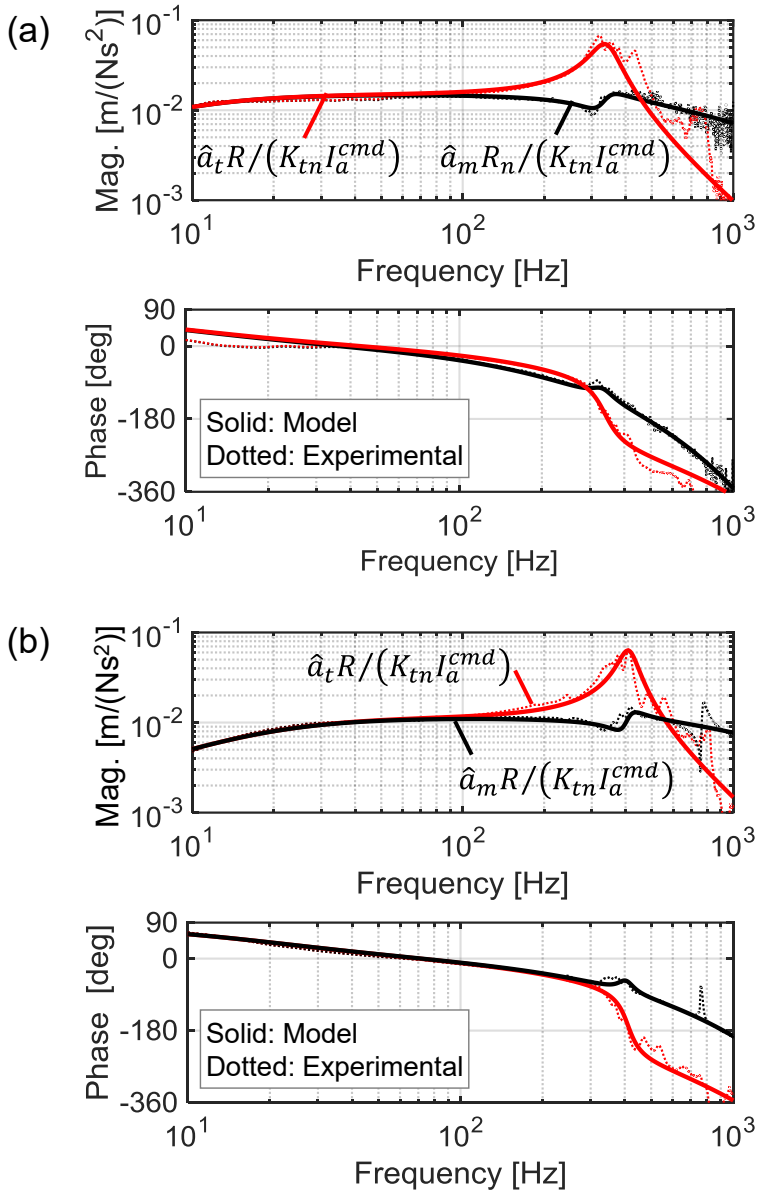

Fig. 3-5 Frequency response of ball-screw-driven stage (a) Machine A (b) Machine B

3.3 Frequency response of ball-screw-driven stage

3.3.1 Frequency response between motor and stage

An accurate identification of mechanical parameters is one of the most important factors for accurate cutting force estimation. In addition to mechanical parameters, quantity of phase lag in the control system needs to be identified as well. In this dissertation, the parameters were identified based on the swept sine excitation. Sinusoidally varying velocity command whose frequency was 0.1 Hz - 1 kHz was applied, while position feedback loop was eliminated for avoiding destabilization.

Fig. 3-5 shows measured and identified frequency response function (FRF). If there is

Table 3-3 Identified parameters by swept sine excitation

	Machine A	Machine B
Resonance frequency [Hz]	335	408
Total inertia of motor, coupling, and ball screw J_{rn} [kg・m^2]	3.8×10^{-5}	5.2×10^{-5}
Total movable mass M_{tn} [kg]	6.2	6.6
Inertia ratio α [-]	0.103	0.080
Damping coefficient of translational element C_{tn} [N・s/m]	3.7×10^{2}	8.2×10^{2}
Damping coefficient of mechanism C_{kn} [N・s/m]	2.5×10^{3}	1.8×10^{3}
Damping coefficient of rotational element D_{rn} [N・m・s/rad]	2.3×10^{-3}	6.5×10^{-3}
Axial stiffness of feed screw system K_{rn} [N/μm]	25.7	40.5
Dead time T_s, T_m, T_t [ms]	0.35, 0.45, 0.1	0.2, 0.2, 0.2
Dead time for phase lag compensation T_1, T_2, T_3 [ms]	0.8, 0, 0.35	0.4, 0, 0

no phase lag element and the ball-screw-driven stage can be modeled as ideal dual-inertia plant, phase shift between current command and angular acceleration (i.e. $\hat{a}_m R/(K_{tn} I_a^{cmd})$) does not fall below 0°. In the same manner, phase shift between current command and stage acceleration (i.e. $\hat{a}_t R/(K_{tn} I_a^{cmd})$) does not fall below -180°. However, it is difficult to ignore the effect of phase lag elements, and phase lag increases in high frequencies. The identified parameters are listed in Table 3-3. Bandwidth of the current control loop ω_{cc} was determined from nominal value from manufactures. In Machine B, dead time of servo amplifier T_s was determined by considering nominal value from manufactures. In Machine A, on the other hand, dead time of servo amplifier T_s were experimentally determined, because actual result presented larger phase lag than catalog value (250 μs). Dead times at encoder side T_m and T_t were experimentally determined so as to follow the phase characteristics. Mechanical parameters were identified by applying differential iteration method [98,99], which was a sort of least square method in frequency domain. Non-linear terms of measured FRF were linearized by performing Taylor expansion around initial value. Modal parameters were iteratively calculated, while ω_{cc}, T_s, T_m and T_t were excluded from iterative calculation. These parameters were used for both numerical simulation and experimental verifications. Dead time for phase lag compensation was determined according to the procedure written in section 2.4.2.

Although it is preferable to experimentally identify the phase characteristics between current command and acceleration response, some users hesitate to excite machine tools in fear of their damage. In that case, quantity of the phase lag in each element needs to be investigated in detail.

Based on the identified mechanical parameters and resolution of encoders, minimum detectable force fluctuation per sampling period is calculated, and the result is shown in Table 3-4. In this calculation, velocity and acceleration terms were calculated by

Table 3-4 Minimum detectable force fluctuation per sampling period

	Machine A	Machine B
Inertia force of rotational elements, $M_r a_m$ [N]	922.4	4.38
Inertia force of translational elements, $M_t a_t$ [N]	49.8	0.16
Damping force of rotational elements, $C_r v_m$ [N]	2.77	0.06
Damping force of translational elements, $C_t v_t$ [N]	0.15	0.002
Inertia force in vibration modal space, $M_{vib} a_m$ [N]	483.6	2.00
Damping force in vibration modal space, $C_{vib} v_{vib}$ [N]	11.96	0.08
Elastic force in vibration modal space, $K_{vib} x_{vib}$ [N]	5.51	0.13
Sampling frequency [kHz]	20	10
Resolution of stage response [nm]	20.0	0.244
Resolution of angular response [nm]	38.1	0.596

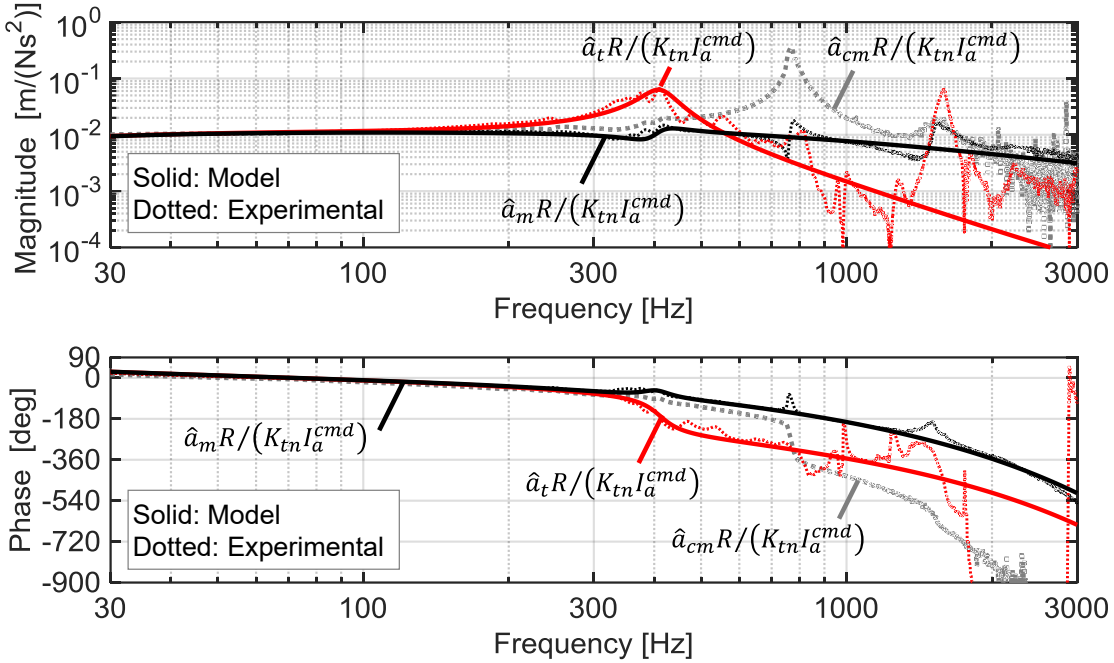

Fig. 3-6 Frequency response of Machine B in high frequencies

backyard differential and low pass-filters were not applied. In Machine A, inertia force of rotational elements can significantly reduce estimation accuracy of the cutting force because of the low encoder resolution. In Machine B, the minimum detectable force fluctuation can be drastically improved by employing high resolution encoders.

As mentioned before, the dual-inertia can describe only rigid body mode and first vibration mode. However, there are several natural modes in high frequencies. Fig. 3-6 shows frequency response of $I_a^{cmd} \rightarrow \hat{a}_m$, $I_a^{cmd} \rightarrow \hat{a}_t$, and $I_a^{cmd} \rightarrow \hat{a}_{cm}$. As shown in the figure, frequency response between current command and angular acceleration at counter-motor side (i.e. $\hat{a}_{cm} R/(K_{tn} I_a^{cmd})$) indicates sharp resonance peak at 778 Hz. That natural mode is resulting from torsional stiffness of screw-system, while it is not considered in the dual-inertia model. Thus, estimation bandwidth is limited by the

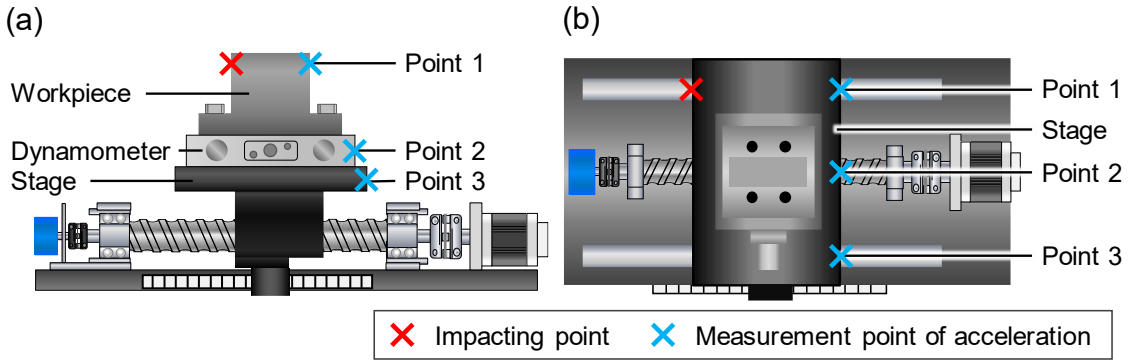

Fig. 3-7 Impact and measurement points in impacting tests
(a) Case I: pitching mode (b) Case II: yawing mode

torsional mode. In the experimental verification, cutoff frequency of the observers was set to 500 Hz to avoid the effect of the structural dynamics in high frequencies.

3.3.2 Stage-side frequency response

In addition to torsional dynamics of the screw system, pitching and yawing of the table can be error factors of the cutting force estimation, while they are not considered in the dual-inertia model. The pitching and yawing modes were identified by impulse response method. Fig. 3-7 shows schematic of the impacting tests. In Case I, the pitching mode was identified by impacting workpiece and measuring acceleration signals at three points as shown in Fig. 3-7 (a). Similarly, in Case II, yawing mode was identified by impacting the stage as shown in Fig. 3-7 (b).

Fig. 3-8 shows measurement result of the frequency response in Case I. As shown in the figure, characteristic peaks are observed at 1598 Hz and 1779 Hz. Considering phase characteristics among three measurement points are different, these modes were judged to come from the pitching mode of the stage.

Fig. 3-9 shows measurement result of the frequency response in Case II. Both side of the stage is oscillating at 805 Hz, while there is no significant peak at center of the stage (Point 2). That suggests that the natural mode at 805 Hz is resulting from yawing of the stage.

As presented in the above, both the pitching and yawing modes are problematic in estimating high frequency component of cutting force. However, in this dissertation, the influence of these modes as well as the torsional modes are eliminated by setting cutoff frequency of the low-pass filter to 500 Hz. In addition, cutting tests were conducted around center of the stage in order to avoid the influence of yawing mode.

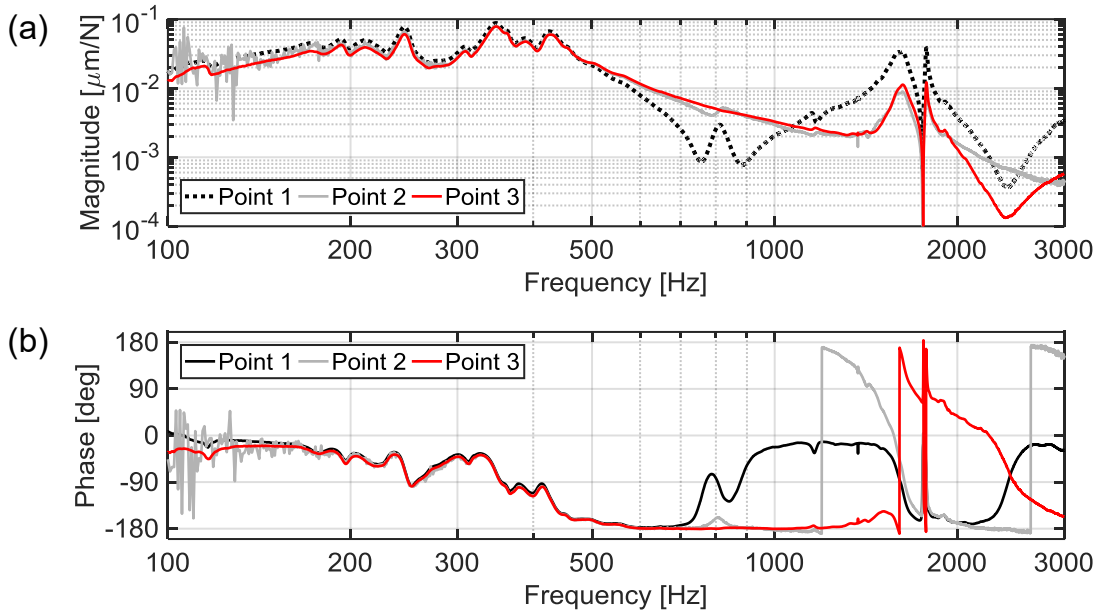

Fig. 3-8 Table-side frequency response in Case I (a) magnitude (b) phase

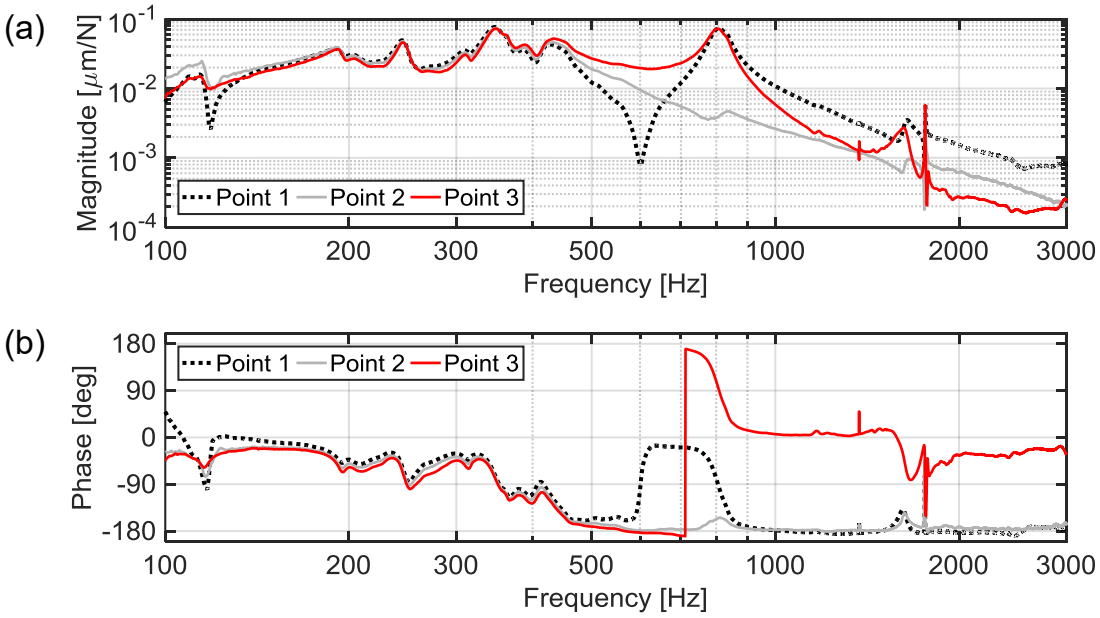

Fig. 3-9 Table-side frequency response in Case II (a) magnitude (b) phase

3.4 Position-dependent characteristics of disturbance force

Variation of the disturbance force is non-negligible for accurate cutting force estimation. That variation is resulting from runout and geometrical error of ball-screw, circulation of ball, and disturbance in the control system [44]. In addition, that variation ranges from submillimeter to millimeter. On the other hand, variation of disturbance force has position-dependency and repeatability. In this section, the position dependent

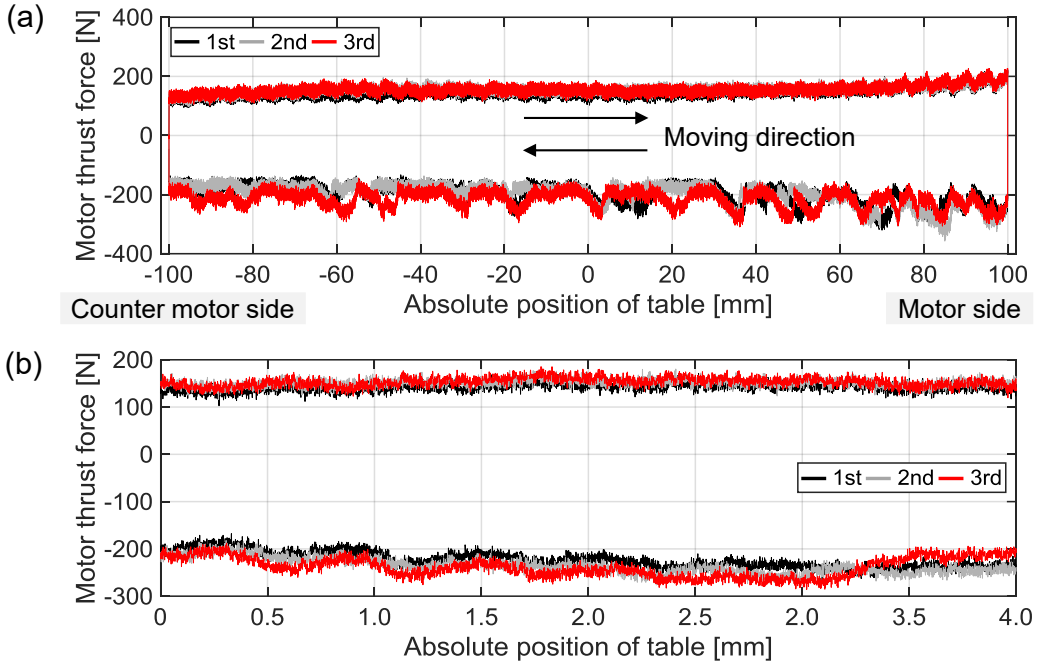

Fig. 3-10 Position dependent characteristics of thrust force in Machine A at 5 mm/s (a) overall view (b) expanded view

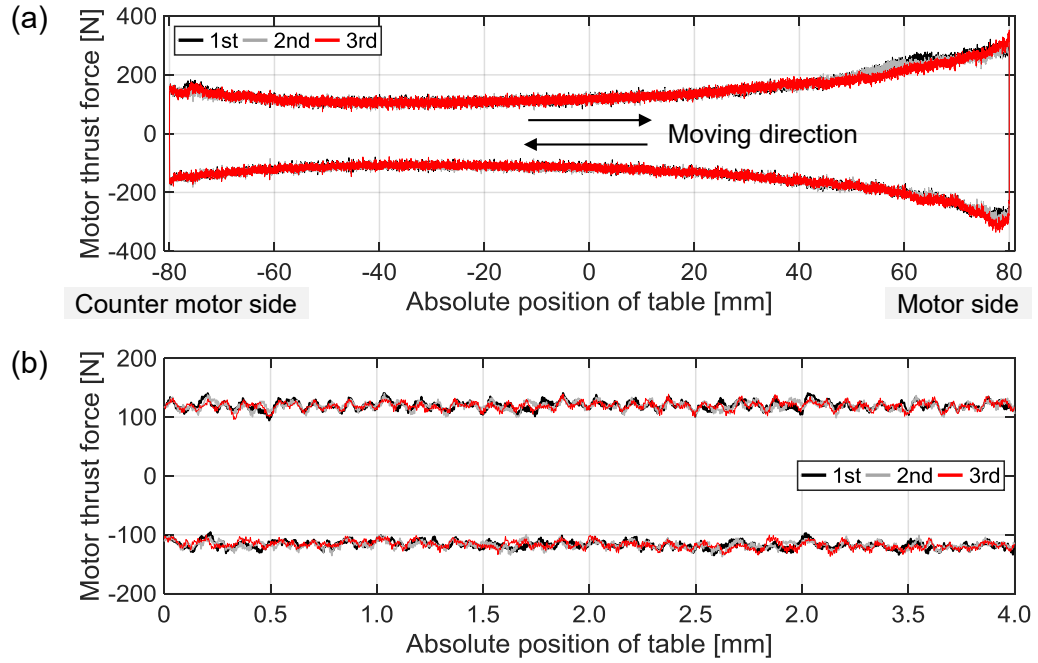

Fig. 3-11 Position dependent characteristics of thrust force in Machine B at 5 mm/s (a) overall view (b) expanded view

characteristics are analyzed for determining appropriate compensation method of the disturbance force.

When the stage was moved at constant feed rate without additional load, such as the cutting force, the motor thrust force was assumed equal to the disturbance force, which included the friction force and friction torque. Here, inertia and viscous terms were

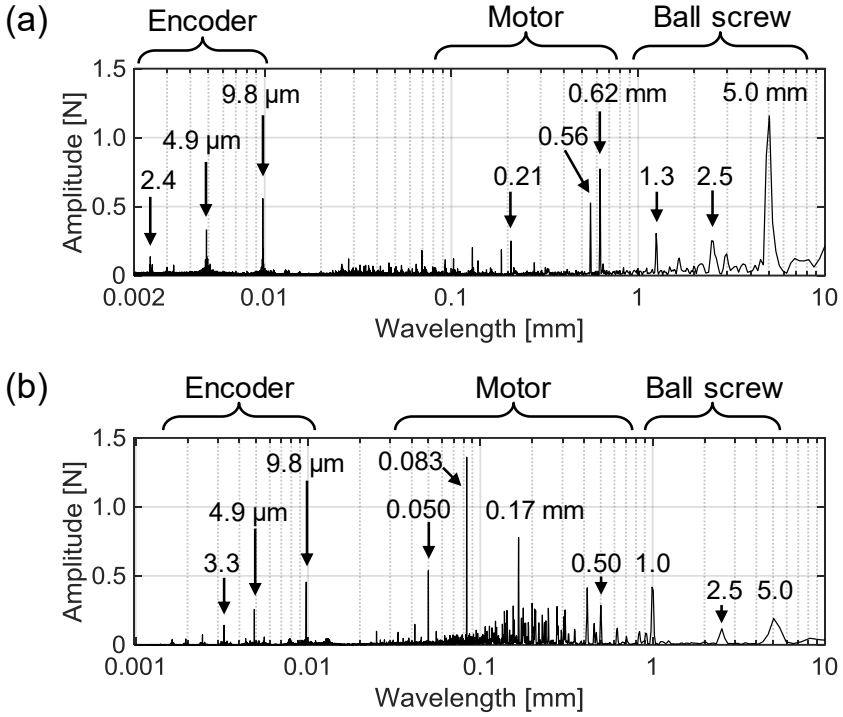

Fig. 3-12 Thrust force spectrum at 5 mm/s in wavelength domain
(a) Machine A (b) Machine B

ignored. Fig. 3-10 and Fig. 3-11 show motor thrust force command $K_{tn}I_a^{cmd}/R$ of Machine A and Machine B at constant feed rate and no additional load. The motor thrust force varied depending on the table position, and fluctuated periodically at the same phase in each motion. On the other hand, the thrust force command presents high repeatability particularly in Machine B, when feed rate and motion trajectory are identical in each trial. The thrust force is analyzed in wavelength domain, and the result is shown in Fig. 3-12. The calculation is based on the fact that wavelength of the variations can be calculated by dividing feed rate by frequency of variations. Analyzed area was limited to the case of moving the stage from counter-motor to motor side, where the thrust force presented high repeatability both in Machine A and Machine B. In millimeter region, periodical fluctuations depending on lead of the ball-screw (5.0 mm) and its harmonics are generated, which are noticeable in Machine A. In sub-millimeter region, periodical fluctuations depending on circulation of the balls and disturbance in the control system can be induced [44]. For instance, the wavelength that is related to the ball circulation in Machine B is calculated as 0.610 mm. In the experimental setup, torque ripples of the servomotors presented higher spectrum than them. For instance, 30 and 60 times periodical fluctuations per revolution of the motor (i.e. wavelength: 0.167 mm, 0.083 mm) are observed in Machine B, which equips 10-poles and 6-slots AC servomotors. Wavelength of fluctuations changes depending on the pole number and slot number of the servomotor. When the frequency of the fluctuation comes close to that of the cutting

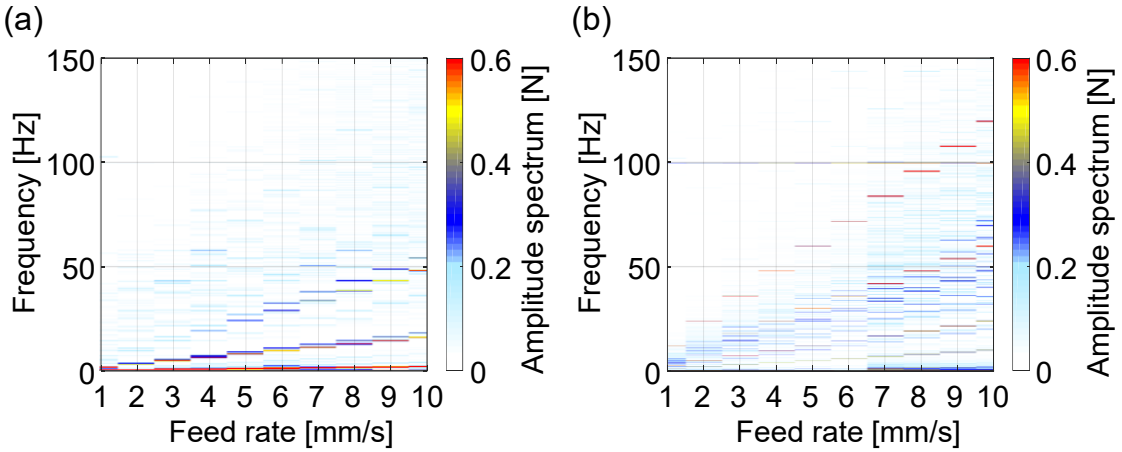

Fig. 3-13 Frequency analysis result of motor thrust force at different feed rates
(a) Machine A (b) Machine B

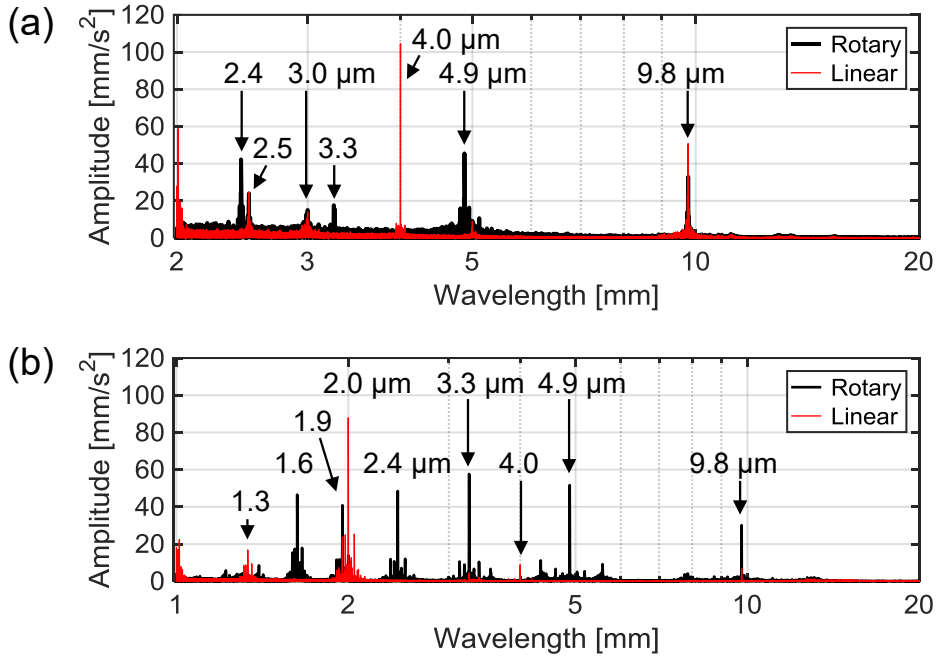

Fig. 3-14 Acceleration spectrum at 5 mm/s in wavelength domain
(a) Machine A (b) Machine B

force, the estimated cutting force might be distorted because of thrust force fluctuation. As shown in Fig. 3-13, the dominant frequencies in each feed rate linearly increases and are likely to approach the frequency of the cutting force. At the same time, the intensity of the spectrum changes responding to feed rate. These results suggested that the feed rate could influence the estimation accuracy of the cutting force as well as the position dependent fluctuations. In this dissertation, velocity dependent variations were eliminated by idling tests, which will be explained later in this section.

In micrometer region, high frequency variations resulting from encoders are dominant. Acceleration signals calculated from encoder signals are analyzed in wavelength domain,

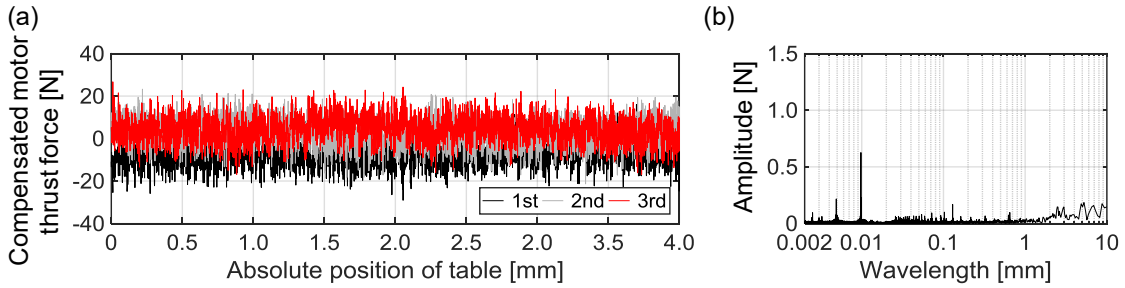

Fig. 3-15 Compensated motor thrust force by average value in Machine A
(a) position domain (b) wavelength domain

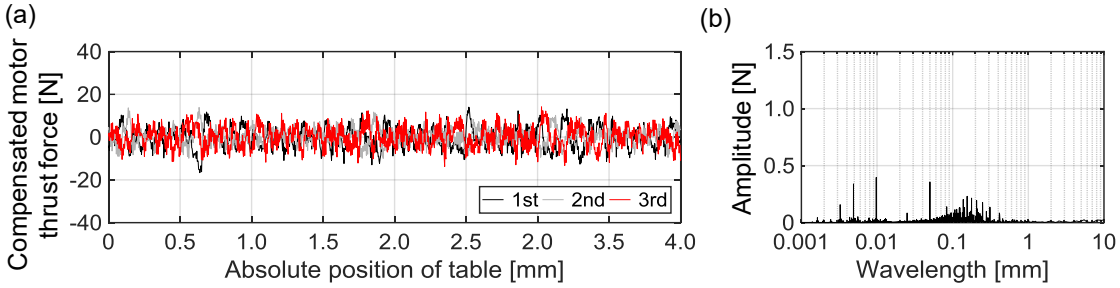

Fig. 3-16 Compensated motor thrust force by average value in Machine B
(a) position domain (b) wavelength domain

and the result is shown in Fig. 3-14. In Machine A, angular acceleration of the motor includes 9.8 μm, 4.9 μm, and 2.4 μm period components (Fig. 3-14 (a)). The same wavelength components are also included in the motor thrust force as described in Fig. 3-12 (a). Considering that signal period of the rotary encoder is 512 count/rev (wavelength: 9.77 μm) as presented in Table 3-2, it is assumed that these fluctuations result from angular measurement. Acceleration of the stage includes high frequency (i.e. short wavelength) components as well. Harmonic components of grating period (8.0 μm) are observed in Machine A, which equips square wave encoder. In Machine B with sine wave encoders, the high frequency components synchronizing signal period (4.0 μm) are observed. These variations are induced by numerical differential of position/angle, which are non-negligible for wideband cutting force estimation using position/angle-based observer.

As for the motor thrust force shown in Fig. 3-10, mean value of the thrust forces was subtracted from each data depending on table position. The result for Machine A is shown in Fig. 3-15. In the figure, the higher repeatability of the disturbance force is, the closer to zero the compensated motor thrust force is. Although low frequency (i.e. long-wave) variations were dominant in motion as shown in Fig. 3-12 (a), periodical variations reduced by subtracting depending on the position. By acquiring variation in disturbance force as numerical data or modeling the variation, comparatively low frequency components can be eliminated. On the other hand, high frequency variations resulting from the encoders are little eliminated. The same analysis was carried out for Machine

B, and the result is shown in Fig. 3-16. There are high frequency components of the motor thrust force as in the case of Machine A. This is because it is difficult to subtract the motor thrust force in phase in high frequencies. While identification of the disturbance force including phase is difficult in high frequencies, it is possible to eliminate high frequency components by signal processing, because the frequency of the variations can be predicted if the wavelength and the feed rate are known. In this regard, it is difficult to extract cutting force components if the frequency of the variations comes close to that of the cutting force.

In this dissertation, disturbance force was identified by idling (air cutting) tests based on the position dependent and repeatable characteristics. The output of the observer in idling motion was regarded as the disturbance force except for the cutting force. Idling tests were performed three times before the cutting test in each cutting condition. In order to exploit position dependency, the position trajectory and velocity in the idling tests need to correspond as much as possible with those in the cutting tests. When high frequency variations resulting from the encoders are non-negligible, notch filters are applied to enhance estimation accuracy of the cutting force.

As well as position of the stage, its weight including the workpiece is also influencing factor on the friction characteristics [29]. On the other hand, the experimental setup is desktop size, and available mass is limited because of the table size. Therefore, the influence of stage weight on the disturbance force was not considered in this dissertation.

3.5 Summary

This chapter describes simulator and experimental setup, which were used for evaluating the proposed cutting force observer. The contents are summarized as follows.

1. Frequency response of the ball-screw-driven stage was analyzed, and nominal parameters of the cutting force observer were determined based on it. In addition to axial dynamics between the motor and the stage, torsional dynamics, yawing and pitching mode were also identified for specifying modeling error of the dual-inertia model.
2. Position dependent characteristics of the disturbance force was analyzed in both position and wavelength domain. In millimeter and sub-millimeter region, variations of the disturbance force are resulting from mechanical elements, such as the ball-screw and the motor. In micrometer region, high frequency variations resulting from the encoders are dominant, which correspond to the signal period or the grating period.
3. By acquiring variation in the disturbance force as numerical data or modeling the

variation as mathematical model, comparatively low frequency components can be eliminated owing to the position-dependency and the repeatability. On the other hand, high frequency variations resulting from the encoders are little eliminated, because it is difficult to subtract the disturbance force in phase. High frequency variations need to be eliminated by the signal processing, considering the wavelength of the variations.

4. Influence of error factors in sensorless cutting force estimation

4.1 Introduction

In sensorless cutting force estimation, cutting force is indirectly estimated based on the model of feed drive and control system. Thus, modeling accuracy of the feed drive and the control system directly influences the estimation accuracy of the cutting force. In this chapter, the influence of the error factors was evaluated through time domain simulation and end milling tests. In the simulation, frequency response of the cutting force observer was evaluated regarding following error factors: difference of the estimation method (i.e. DOB, MEDOB), identification error of the movable mass, synchronization error of the control signal due to the phase lag elements, and quantization error of the angle measurement. In addition to frequency response, estimation characteristics against the milling force was also evaluated in the simulation. Estimation performance of the cutting force and influence of the error factors were experimentally evaluated by conducting actual end milling tests. In the experimental verification in this chapter, not cross-feed component but feed force component was focused.

4.2 Evaluation of error factors by time-domain simulator

4.2.1 Extraction of error factors

The estimated cutting force by MEDOB (Eq. (2-21)) is constituted from four kinds of forces (i.e. motor thrust, inertia, damping and friction forces). The proportion of the forces used in estimating the cutting force varies responding to frequency. Thus, the estimation accuracy of the cutting force is influenced by the most dominant force. In the simulation, a sinusoidal load force (simulating the cutting force) was applied as a reference value. The time-domain simulator was constructed based on the block diagram shown in Fig. 3-4. The FRF between the cutting force reference and the estimated cutting force by the observer was investigated by continuously varying the frequency of the cutting force from 1 Hz to 1 kHz. The amplitude of the cutting force reference was set to 20 N. In order to evaluate dynamic response against the cutting force, position, velocity, and acceleration command were not applied as well as another disturbance force, such as friction force/torque. Simulation parameters were determined according to the

Table 4-1 Simulation parameters for control system

Cutoff frequency of low-pass filter in DOB- and MEDOB-based cutting force observer g_{cut} [Hz]	1000.0
Cutoff frequency of low-pass filter in MEDOB for disturbance cancellation g_{dis} [rad/s]	1000.0
Cutoff frequency of low-pass filter in pseudo differential g_{LPF} [rad/s]	5000.0
Sampling frequency [kHz]	20.0
Position proportional gain K_p	50.0
Velocity proportional gain K_v	200.0

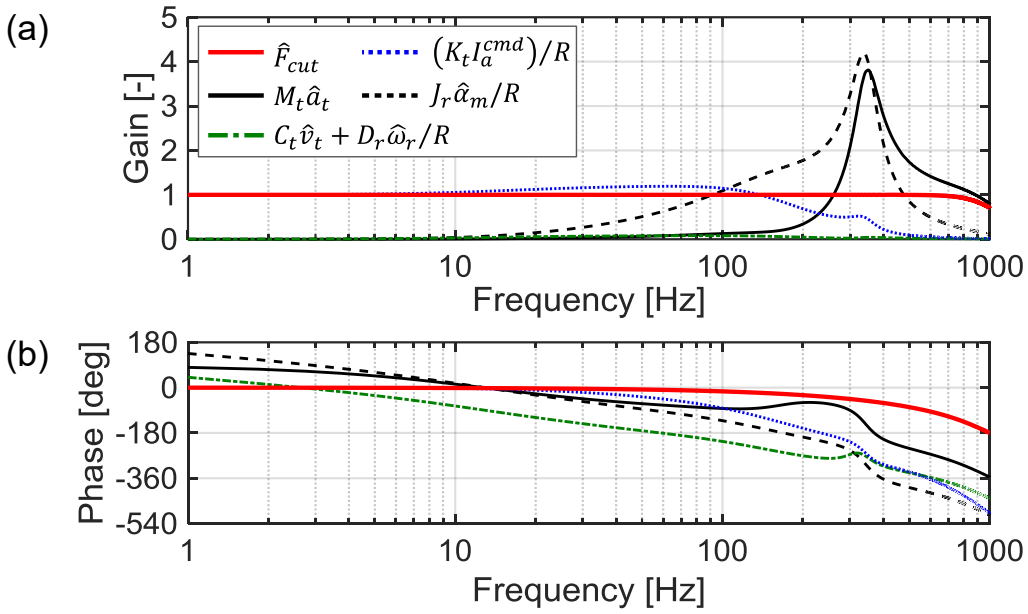

Fig. 4-1 Frequency response of each force constituting estimated cutting force

characteristics of Machine A. Parameters for the control system and the filters are listed in Table 4-1. The nominal mechanical parameters are listed in Table 3-3. The parameters were changed from the nominal value in reference condition responding to evaluation item. Here, reference condition denotes the condition where there are not any of identification error of the parameters, synchronization error, or quantization error in position/angle measurement.

Frequency response of motor thrust, inertia, damping and estimated forces are described in Fig. 4-1. In low frequencies including DC, the estimated cutting force $\hat{F}_{cut}$ and the motor thrust force $(K_t I_a^{cmd})/R$ are identical in both gain and phase, which indicates current signal is applicable to estimate cutting force components in low frequencies. However, gain of the motor thrust force decreases in high frequencies. The current signal cannot follow dynamic variation in the cutting force in the region. When some filters are applied to the current for attenuating vibration, the frequency response of the thrust force changes responding to that of the applied filters. In contrast to the

thrust force, gain of inertia forces is low in low frequencies, while it increase near the resonance frequency of the dual-inertia system (335 Hz). Because the inertia forces are dominant, estimation error increases in high frequencies when measurement error of acceleration or identification error of mass and inertia is large.

In this dissertation, following factors, which particularly influenced the cutting force estimation, were set to evaluation items: the difference of the estimation method, identification error of the movable mass including the workpiece M_t, synchronization error of the control signal due to the phase lag elements, and quantization error of the angle measurement.

As for the mechanical parameters such as movable mass, it is possible to calculate frequency response of the observer by transfer function on behalf of conducting time-domain simulation. When evaluating identification error of the movable mass, for example, Eq. (2-21) is rewritten by assuming $M_{tn} = QM_t$ and ignoring identification error of the other parameters and friction terms as follows:

$$\hat{F}_{cut} = \frac{g_{cut}}{s + g_{cut}} \left\{ \frac{1}{R} \left(K_t I_a^{ref} - J_r \hat{\alpha}_m - D_r \hat{\omega}_m \right) - QM_t \hat{a}_t - C_t \hat{v}_t \right\} \tag{4-1}$$

For simplifying calculation, $\hat{v}_t, \hat{\omega}_m, \hat{a}_t, \hat{\alpha}_m$ are changed to $v_t, \omega_m, a_t, \alpha_m$ by assuming that cutoff frequency of low-pass filter in pseudo differential is infinite. As a result, Eq. (4-1) is rearranged to Eq. (4-2) as follows:

$$\hat{F}_{cut} = \frac{g_{cut}}{s + g_{cut}} \left\{ \frac{1}{R} \left(K_t I_a^{ref} - J_r \alpha_m - D_r \omega_m \right) - QM_t a_t - C_t v_t \right\} \tag{4-2}$$

Since $v_t, \omega_m, a_t, \alpha_m$ are the numerical differential of x_t, θ_m, transfer function $\hat{F}_{cut}/F_{cut}$ is analytically calculated by erasing $v_t, \omega_m, a_t, \alpha_m$ based on the dynamic equation of the dual-inertia model. In calculating the transfer function, single input and single output system between reference and estimated cutting force was assumed. Detailed calculation procedure is written in Appendix. The frequency responses of the observer calculated by transfer function and by time-domain simulation almost coincided, which was confirmed in Appendix. In addition, the same was true of the other mechanical parameters. As for the phase lag elements and the resolution of encoders, however, transfer function-based evaluation is difficult. Considering that estimation characteristics against milling force were evaluated in section 4.2.3, the frequency response of the observer was evaluated based on the time-domain simulation in this chapter.

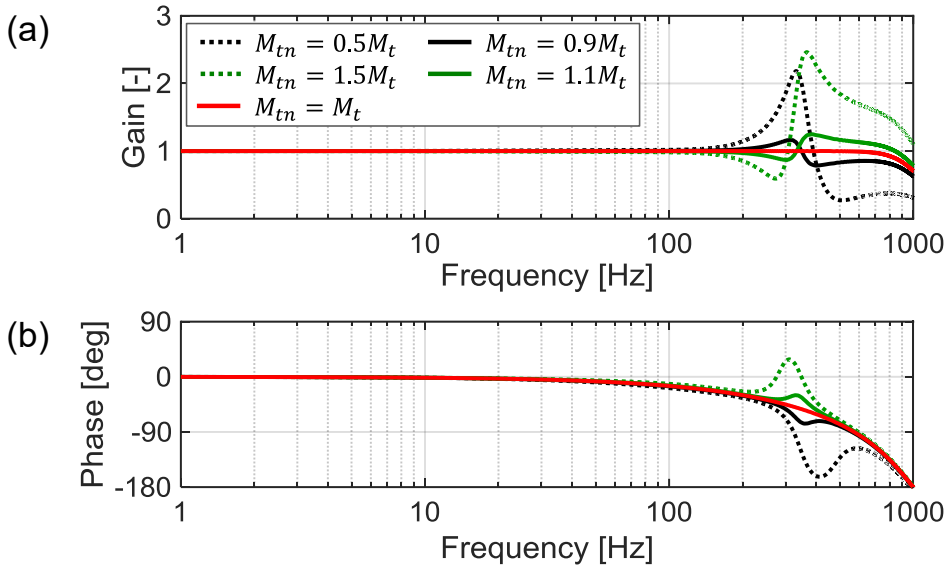

Fig. 4-2 Frequency response of cutting force observer corresponding to identification accuracy of movable mass

4.2.2 Frequency response of cutting force observer

Comparison result responding to the identification error of the movable mass is shown in Fig. 4-2. As described in the last section, identification error of the movable mass influences on the estimation accuracy. When the nominal mass is more than the actual mass (e.g. $M_{tn} = 1.5M_t$), the cutting force is also overestimated in high frequencies. In addition, the estimated cutting force entails phase lead around resonance frequency. In motion control, phase lead compensation by setting a higher nominal mass than the actual one is beneficial for stabilizing the multi-inertia system [100]. When estimating only DC or low frequency component, accurate identification of the movable mass is not necessarily required. Identification accuracy of the inertia of rotational elements J_r can influence on the estimation accuracy in high frequencies as well as the movable mass M_t.

Comparison result responding to the compensation error of the phase lag elements is shown in Fig. 4-3. Here, modeling error of the phase lag by current control loop was not considered. When phase lag compensation was carried out ($T_1 = 0.8, T_2 = 0, T_3 = 0.35$), the same gain characteristics as reference condition were obtained, while phase lag increased because of delaying signals. When the phase lag compensation was not conducted, the estimation accuracy by MEDOB decreases around 100 Hz and was lower than that by the motor thrust force. When the phase lag elements are ignored, the estimation bandwidth does not necessarily increase even if the observer is consturcted for increasing the estimation bandwidth. In some cases, estimation bandwidth of the observer becomes narrower than that of the motor thrust force. Estimation accuracy

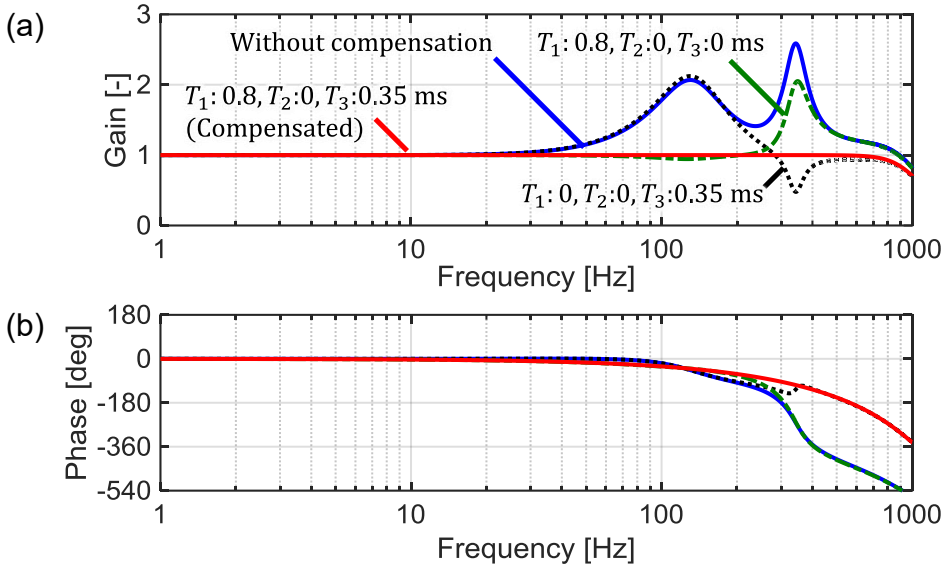

Fig. 4-3 Frequency response of cutting force observer corresponding to compensation error of phase lag elements

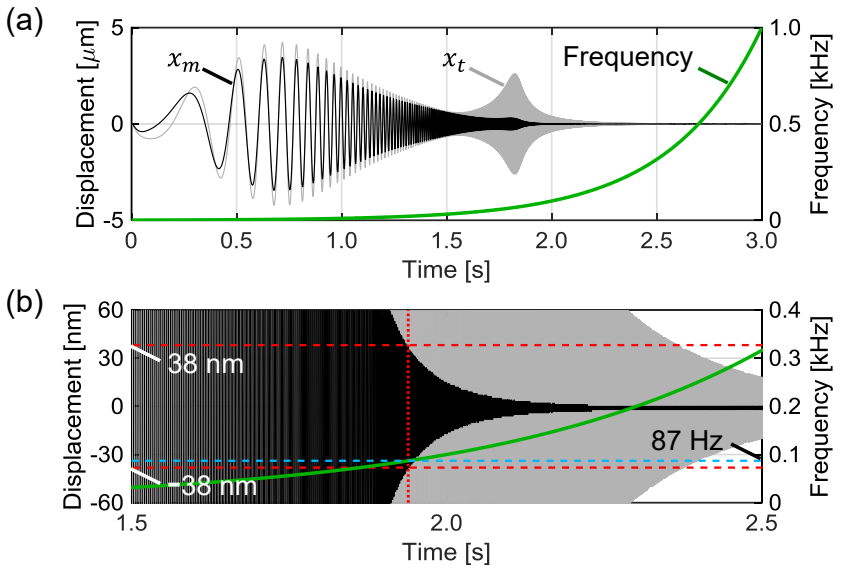

Fig. 4-4 Disturbance response and applied frequency under reference condition (a) overall view (b) expanded view

decreases at certain frequencies, when phase lag compensation was partially conducted among current-angle ($T_1 = 0.8, T_2 = 0, T_3 = 0$) and angle-position ($T_1 = 0, T_2 = 0, T_3 = 0.35$). Wideband cutting force estimation require elaborate modeling considering phase characteristics among the current, the angle, and the position.

Fig. 4-4 shows applied frequency, position x_t and angle response in translational motion x_m under reference condition. As the frequecy of the cutting force increased, variation amplitude of the angle drastically decreased compared with the position. When applied frequency exceeded 87 Hz, angle variation falled below resolution of the rotary encoder in Machine A (i.e. 17 bit, approx. 38 nm). Reduction of angle variation in high

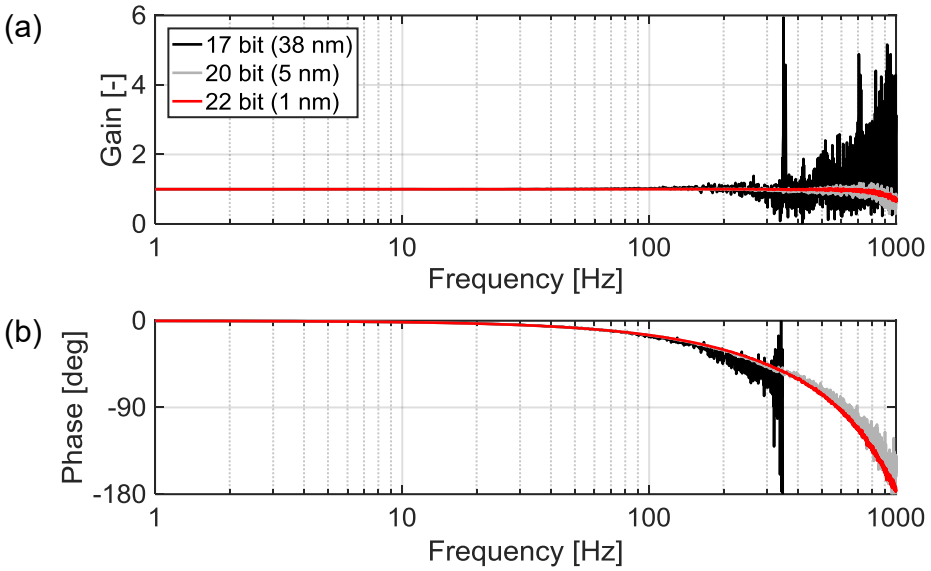

Fig. 4-5 Frequency response of cutting force observer corresponding to resolution of rotary encoder

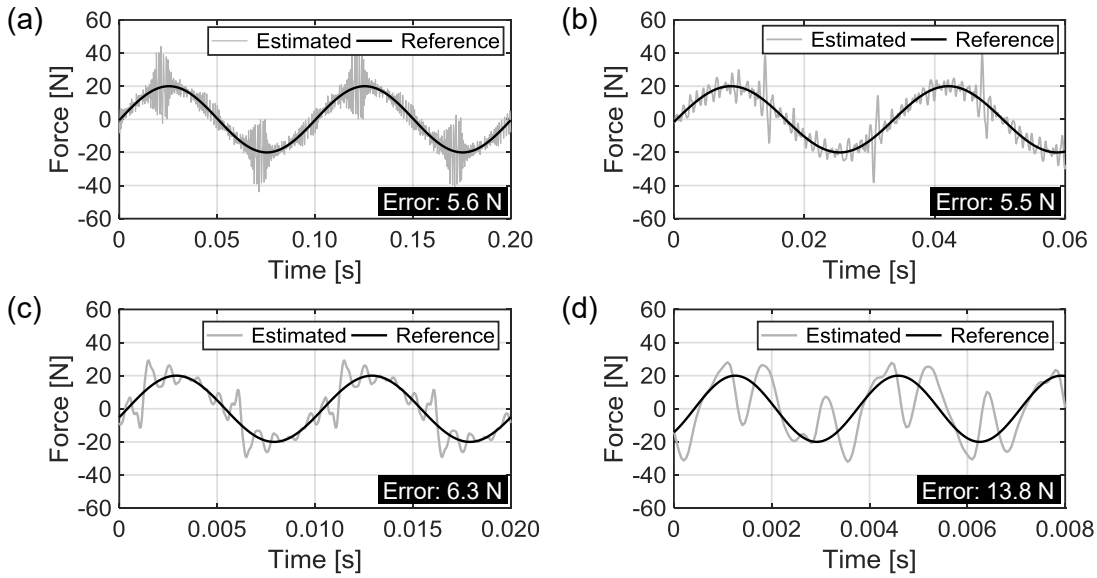

Fig. 4-6 Comparison of applied cutting force and estimated cutting force by MEDOB with 38 nm resolution of angle measurement (a) 10 Hz (b) 30 Hz (c) 100 Hz (d) 300 Hz (standard deviation of estimation error are presented in right bottom.)

frequencies is remarkable when the inertia ratio is small. In addition, damping of structure and sliding surface lead to reduction of angle variation, which makes it difficult to accurately measure angle in high frequencies. Fig. 4-5 shows comparison result of frequency response responding to resolution of the rotary encoder. As shown in the figure, estimation error drastically increased in high frequencies when 17 bit rotary encoder was assumed. In addition to quantazation error of angle measurement, inertia forces presented high portion of the estimation cutting force in high frequencies, which makes it further difficult for wideband cutting force estimation.

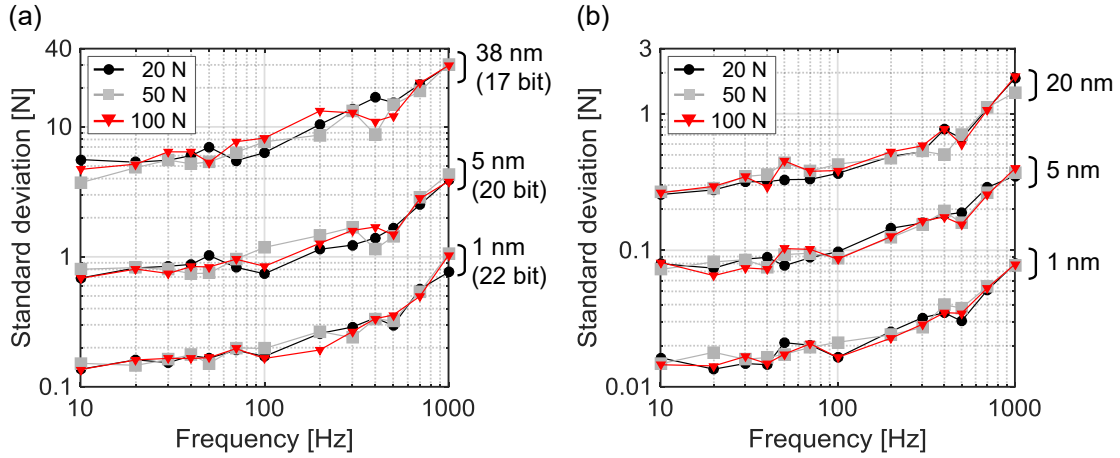

Fig. 4-7 Standard deviation of estimation error responding to amplitude of load force and resolution of angle/position measurement (a) resolution of angle measurement (b) resolution of position measurement

Standard deviation of estimation error against sinusoidal cutting force was copmared, corresponding to the resolution of the angle/position measurement. In the simulation, the frequency of the cutting force reference was changed, and the standard deviation of the estimation error was calculated in each frequency as shown in Fig. 4-6. For fair comparison, both the reference and the estimated cutting force were filtered by the same low-pass filter whose cutoff frequency was 1 kHz. In addition, there were neither the identification error of the parameters nor the synchronization error in the simulation. The results are shown in Fig. 4-7. When the resolution of angle measurement was 38 nm, the estimation error of the cutting force exceeds 10 N in high frequencies as shown in Fig. 4-7 (a). By increasing the resolution up to 1 nm (22 bit), the esimation error was less than 1 N within 1 kHz. As shown Table 3-2, in Machine B, the resolution of the rotary encoder is increased to 23 bit (approx. 0.60 nm) by interpolating the original encoder signal 16384 (= 2^{14}) times. Thus, minimum detectable unit (i.e. resolution) was assumed sufficiently small. However, measurement error synchronizing the signal period of the rotary encoder (9 bit) is inevitble in the experimental setup, which will be experimentally shown in the section 4.3. On the other hand, resolution of the position measurement less influences on the estimation accuracy as shown in Fig. 4-7 (b). For instance, estimation error is less than 1 N up to 700 Hz even if the resolution of the position measurement is 20 nm. When the resolution increases to 5 nm, the estimation error is suppressed less than 0.5 N within 1 kHz. The resolution of the rotary encoder is more influential on the estimation accuracy of the cutting force than that of the linear encoder.

Dynamic variation of the cutting force can be captured by using the position response from the linear encoder near the cutting point in addition to angular response from the rotary encoder. In the full-closed control ball-screw-driven stage, resolution of the linear encoder is often enhanced for improving positioning performance. In terms of cutting

Table 4-2 Cutting conditions for milling simulations

Condition number	#1	#2	#3	#4
Spindle speed [min^{-1}]	2000	6000	2000	6000
Feed rate [mm/s]	2	6	2	6
Milling type	Down	Down	Slotting	Slotting
Radial depth of cut [mm]	1	1	6	6
Axial depth of cut [mm]	1			
Feed per tooth [mm/tooth]	0.030			
Tool diameter [mm]	ϕ 6.0			
Number of flute	2			
Cutting coefficient				
tangential [MPa]	1800			
radial [MPa]	820			
axial [MPa]	170			

force estimation, resolution of the rotary encoder is also important as well as that of the linear encoder.

4.2.3 Estimation characteristics against milling force

In milling, the cutting force often includes multiple frequency components due to the intermittent nature of the process. In this section, estimation characteristics against milling force was evaluated by applying milling force to the dual-inertia plant in the simulator. Mechanistic model [101] was employed as milling force model. Table 4-2 shows cutting condition. Spindle speed was changed considering that estimation accuracy was influenced by the frequency of the cutting force. Radial depth of cut was also changed to evaluate estimation characteristics under different immersion (intermittency). The lower the depth of the cut is, the more intermittent cutting force becomes and the estimation gets difficult. Estimation performance of the milling force was compared responding to error factors in order. When conducting frequency analysis, the number of sampled data was set to 16384 (= 2^{14}). The sampling frequency (10 kHz) and other simulation parameters of the control system were not changed from those used in the last section.

Fig. 4-8 shows comparison result of the estimated, the motor thrust and the inertia forces at condition #1. Inertia force of the rotational ($J_r\hat{\alpha}_m/R$) and the translational elements ($M_t\hat{a}_t$) presented different response, which suggested difficulty of rigid body based-formulation. In this cutting condition, the amplitude of the motor thrust force and that of the cutting force reference became approximately equal. On the other hand, phase delay of the motor thrust force was larger than that of the estimated cutting force by MEDOB. Comparison result of DOB- and MEDOB-based method at the same condition is shown in Fig. 4-9. When DOB was applied, cutting force was overestimated around

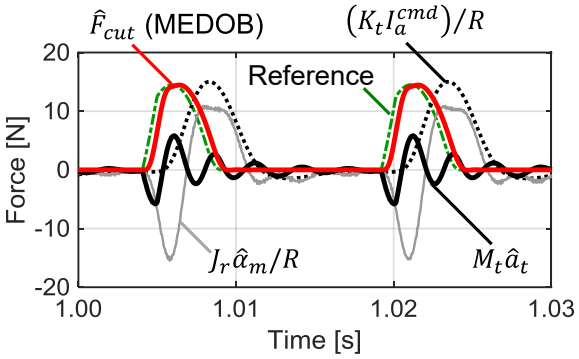

Fig. 4-8 Comparison of each force against milling force at condition #1

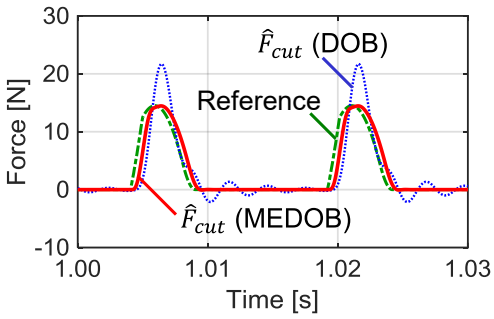

Fig. 4-9 Milling force estimation result by DOB and MEDOB at condition #1

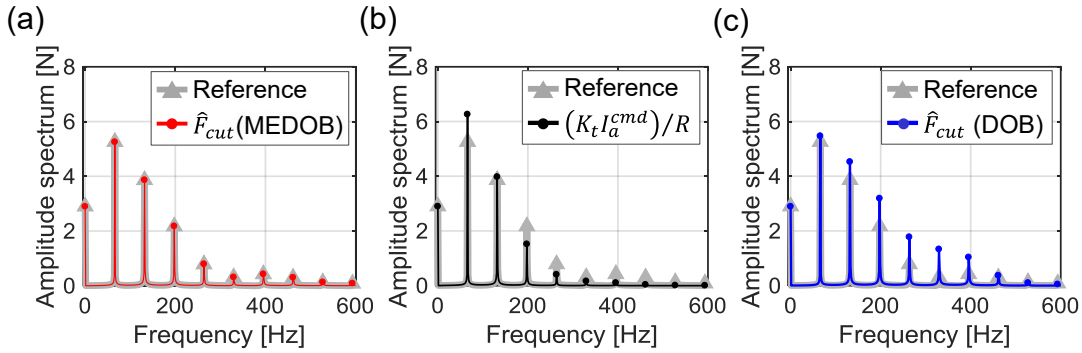

Fig. 4-10 Frequency analysis result of reference and estimated forces at condition #1 (a) MEDOB (b) motor thrust force (c) DOB

local maximum value where variation of the inertia forces got larger (see Fig. 4-8). As presented in frequency analysis result shown in Fig. 4-10, DOB overestimated high frequency components, while MEDOB could capture all components of the cutting force reference. As for the motor thrust force, high frequency components are underestimated.

When spindle speed increased, difference of the estimation result among motor thrust force, DOB-, and MEDOB-based method got larger. Comparison result of reference and estimated cutting force at condition #2 is presented in Fig. 4-11. Both the motor thrust force and the estimated force by DOB were apparently different from the cutting force reference.

Fig. 4-12 shows comparison results in slotting. In contrast to the case of smaller radial depth at condition #1 and #2, the cutting forces were sinusoidal, which included only DC and tooth-pass frequency components. Tooth-pass frequencies at condition #3 and #4 were 66.7 Hz and 200 Hz, respectively. In condition #3 where spindle speed was comparatively low, there was little difference between the estimated forces by DOB and MEDOB. This is because the dual-inertia model presents rigid body motion against the applied cutting force. When the number of the frequency components is a few such as

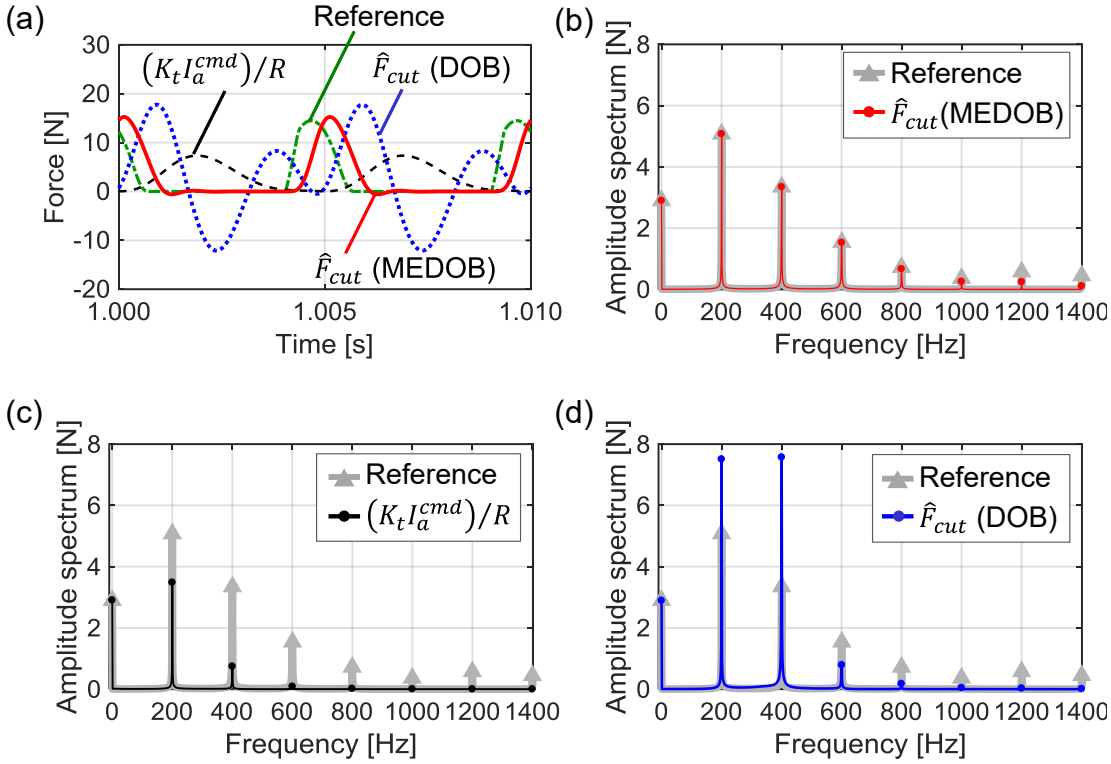

Fig. 4-11 Comparison result of reference and estimated cutting force at condition #2 ((a) time domain data, and frequency analysis result of (b) MEDOB (c) motor thrust force (d) DOB)

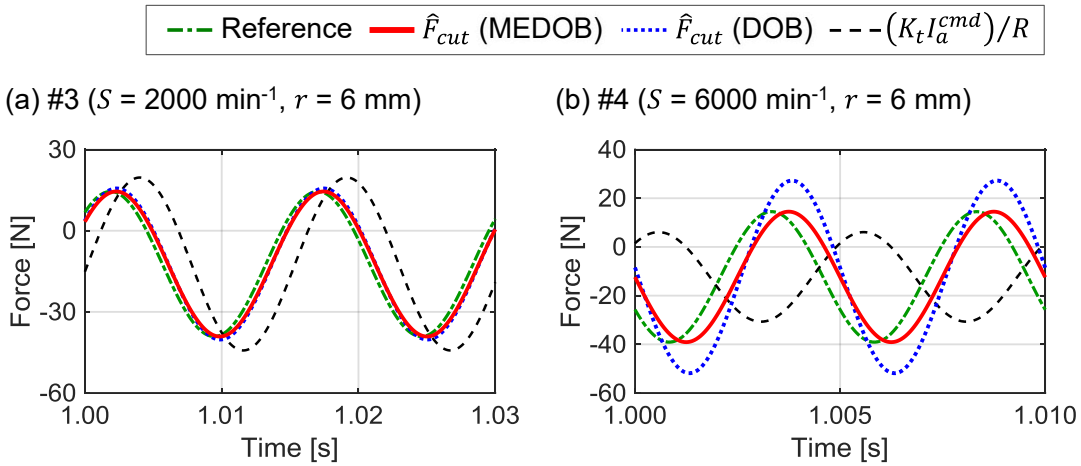

Fig. 4-12 Comparison result of reference and estimated cutting force in slotting (a) condition #3 (b) condition #4

slotting and the spindle speed is low, DOB is applicable to estimate cutting force. When radial depth is small and the cutting process is highly intermittent, on the other hand, estimation error of the cutting force by DOB can increase even if the spindle speed is low as shown in Fig. 4-9. By employing MEDOB, multiple frequency components of the cutting force can be estimated.

In Fig. 4-13, estimation results in each condition are compared responding to identification error of movable mass. Setting of the nominal mass particularly influences

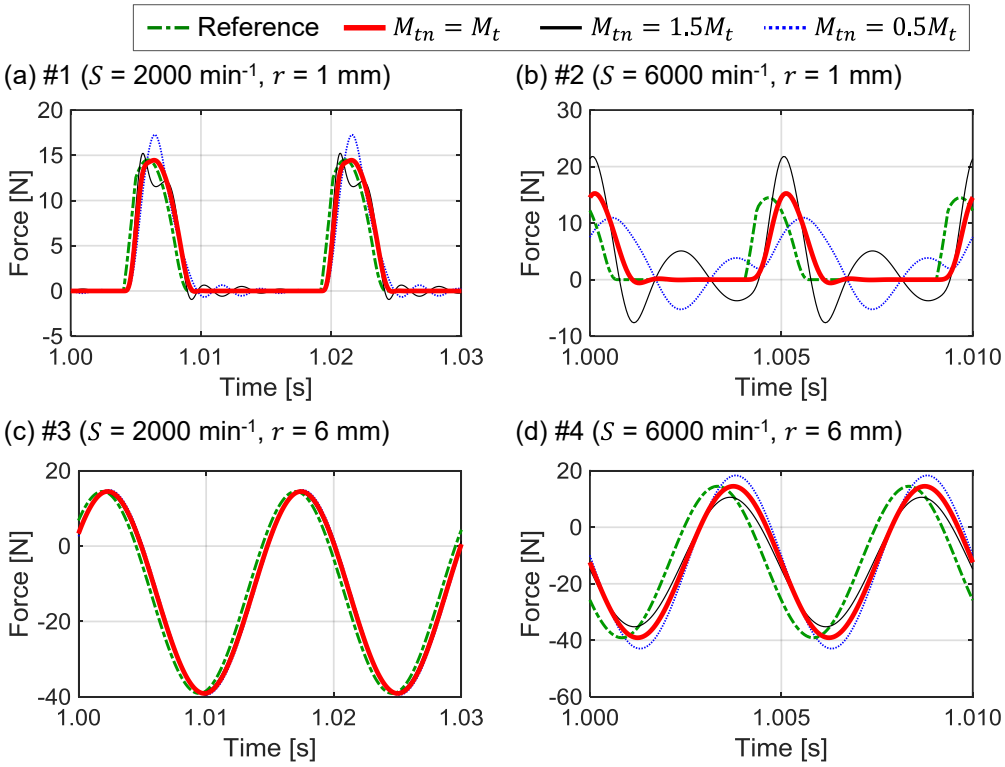

Fig. 4-13 Estimation results of milling forces responding to identification error of movable mass (a) condition #1 (b) condition #2 (a) condition #3 (b) condition #4

on the estimation result at higher spindle speed (i.e. Fig. 4-13 (b) and (d)), where inertia force accounts for high portion of the estimated cutting force. Estimation error especially increases at the instant when the cutting force becomes local maximum value and cutting edge comes out of the workpiece.

Estimation results responding to synchronization errors are described in Fig. 4-14. When the process was intermittent and phase lag compensation was not conducted, waveform of the estimated force was largely distorted. Phase lag compensation between current and angle (i.e. $T_1 = 0.8, T_2 = 0, T_3 = 0$ ms) is not sufficient for estimating intermittent cutting force, including high frequency components as shown in Fig. 4-14 (b). For accurate cutting force estimation, phase lag compensation among both current-table and current-angle (i.e. $T_1 = 0.8, T_2 = 0, T_3 = 0.35$ ms) is required. In slotting where the process is less intermittent, on the other hand, cutting force can be estimated when phase lag compensation between only current and angle is carried out. The more intermittent the process is by reducing radial depth, the severer phase lag compensation is required.

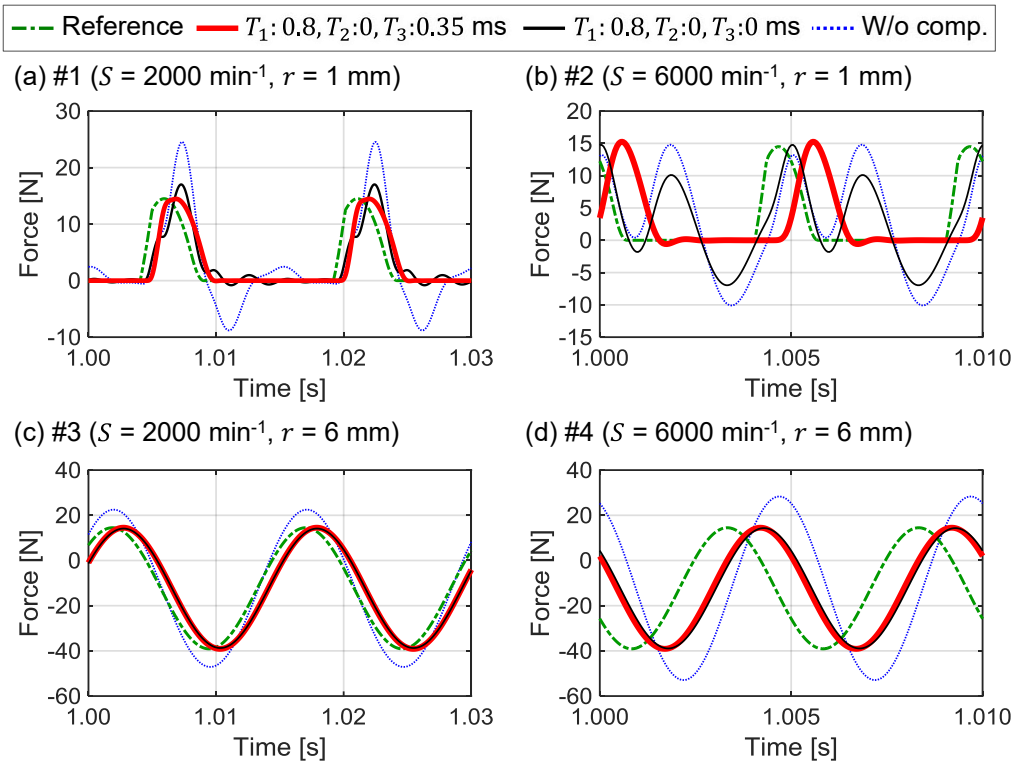

Fig. 4-14 Estimation results of milling forces responding to synchronization errors (a) condition #1 (b) condition #2 (a) condition #3 (b) condition #4

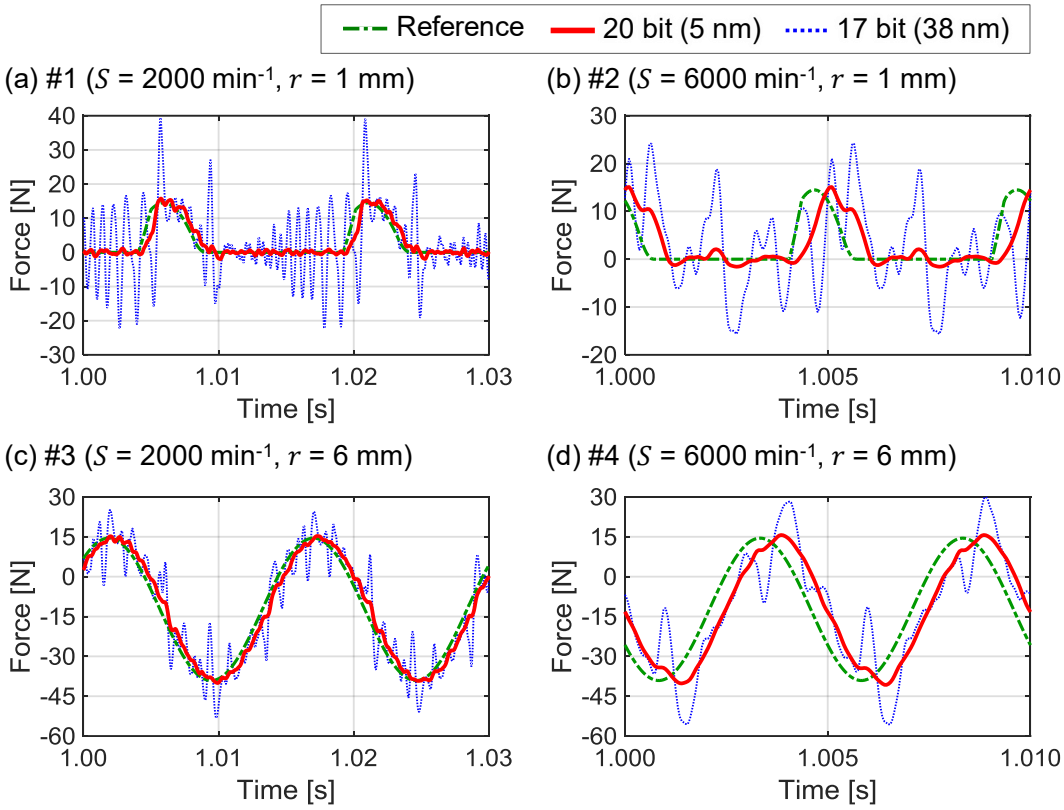

Fig. 4-15 Estimation results of milling forces responding to resolution of rotary encoder (a) condition #1 (b) condition #2 (a) condition #3 (b) condition #4

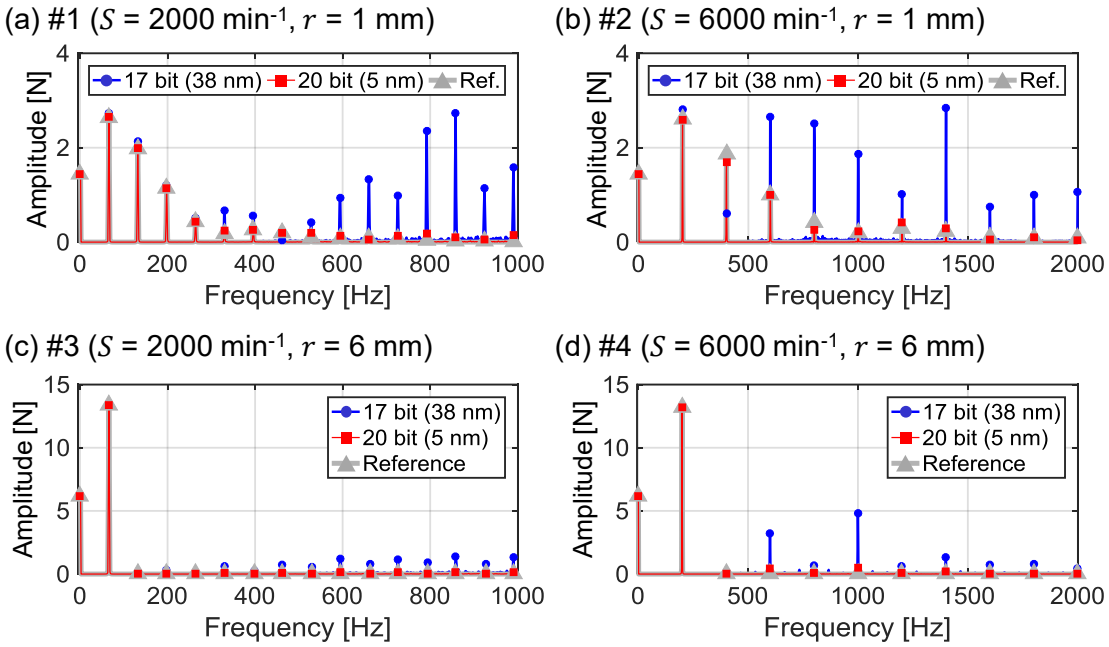

Fig. 4-16 Comparison of frequency analysis results responding to resolution of rotary encoder (a) condition #1 (b) condition #2 (a) condition #3 (b) condition #4

Estimation results responding to resolution of the rotary encoders are presented in Fig. 4-15. When 17 bit rotary encoder was assumed, high frequency noises were included in the estimated cutting force. Especially, the noises were remarkable during air cutting region in intermittent cutting, where variation in angle against cutting force decreased. As shown in Fig. 4-16, high frequency noises develop around the higher harmonics of the cutting force reference. In order to estimate intermittent cutting force and enhance estimation bandwidth, output error needs to be minimized by increasing resolution of the encoders.

High frequency noises are likely to be included when estimating cross-feed (i.e. stationary axis) components of the cutting force, which are remarkable when sliding guideway is employed. As mentioned before, the above simulation was conducted referring specification of Machine A. Machine B was developed based on the simulation results. Encoders' resolution of Machine B is sufficiently enhanced as shown in Table 3-2 in order to reduce quantization error of the encoder signals.

4.3 Experimental evaluation through end milling tests

4.3.1 Experimental procedure

For verifying the validity of the cutting force observer based on MEDOB, end milling tests were carried out using the prototype ball-screw-driven machine tools. In the end milling tests, the workpiece was machined at a constant feed rate and depth of cut

Table 4-3 Parameters of control system in Machine B

Cutoff frequency of low-pass filter in DOB-based and MEDOB-based cutting force observer g_{cut} [Hz]	500.0
Cutoff frequency of low-pass filter in MEDOB for disturbance cancellation g_{dis} [rad/s]	1000.0
Cutoff frequency of low-pass filter in pseudo differential g_{LPF} [rad/s]	3000.0
Sampling frequency and control interval [kHz]	10.0
Position proportional gain K_p	80.0
Velocity proportional gain K_v	320.0

without lubricant. The X-stage was moved, and the cutting force component in X-direction was estimated in order to evaluate the estimation performance in feed direction. As for load condition, small depth of cut was applied so that the cutting force became less than kinetic friction to show that smaller cutting force was observable. The parameters of the control system in Machine B are listed in Table 4-3. The cutoff frequency of the low-pass filter was set to 500 Hz, and it was 4th order Butterworth filter. For fair comparison, both the estimated cutting force and the force measured by the dynamometer were filtered. The disturbance force was identified according to the procedure in section 3.4.

At first, estimation results of DOB- and MEDOB-based method were compared as a function of the frequency of the applied cutting force. Secondly, influence of the error factors were experimentally evaluated.

4.3.2 Evaluation of multi-encoder-based cutting force estimation

Experimental conditions are listed in Table 4-4. The spindle speeds were varied between 1000 min^{-1} and 12000 min^{-1} in order to evaluate the estimation accuracy as a function of the frequency of the applied cutting forces. Cutting forces were estimated by MEDOB, DOB, and the motor current (motor thrust force). Phase lag compensation was performed and disturbance force was compensated for all estimation methods. Notch filters were applied to the estimated cutting forces in order to eliminate high frequency noises. Considering wavelength of variations in angle measurement (9.8 μm, 4.9 μm, 3.3 μm, 2.4 μm), notch frequencies were changed responding to the spindle speed as shown in Table 4-5. In addition, torsional vibration of the screw system was eliminated from the estimated cutting force when it was non-negligible. Influence of phase lag compensation and high frequency noises is discussed in the next section.

Table 4-4 Experimental conditions for evaluating multi-encoder-based cutting force estimation

Axial depth of cut [mm]	1.5
Radial depth of cut [mm]	0.5, 1.5
Spindle speed [min^{-1}]	1000 ~ 12000
Milling type	Down
Feed per tooth [mm/tooth]	0.030
Tool diameter [mm]	ϕ 6.0
Number of flute	2
Material of workpiece	Al alloy (A5052)

Table 4-5 Cutoff frequencies of notch filters

Source		Interpolation error of rotary encoder				Torsional mode
Spindle speed [min^{-1}]	1000	-	204.7 [Hz]	307.1 [Hz]	409.4 [Hz]	-
	2000	204.7 [Hz]	409.4 [Hz]	614.1 [Hz]	-	-
	3000	307.1 [Hz]	614.1 [Hz]	-	-	-
	4000	409.4 [Hz]	818.8 [Hz]	-	-	-
	5000	512.1 [Hz]	1023.5 [Hz]	-	-	-
	6000	614.1 [Hz]	-	-	-	-
	7000	716.5 [Hz]	-	-	-	-
	8000	818.8 [Hz]	-	-	-	778.5 [Hz]
	9000	921.2 [Hz]	-	-	-	778.5 [Hz]
	10000	1023.5 [Hz]	-	-	-	778.5 [Hz]
	11000	1125.9 [Hz]	-	-	-	-
	12000	1228.2 [Hz]	-	-	-	-
Wavelength [μm]		9.8	4.9	3.3	2.4	-

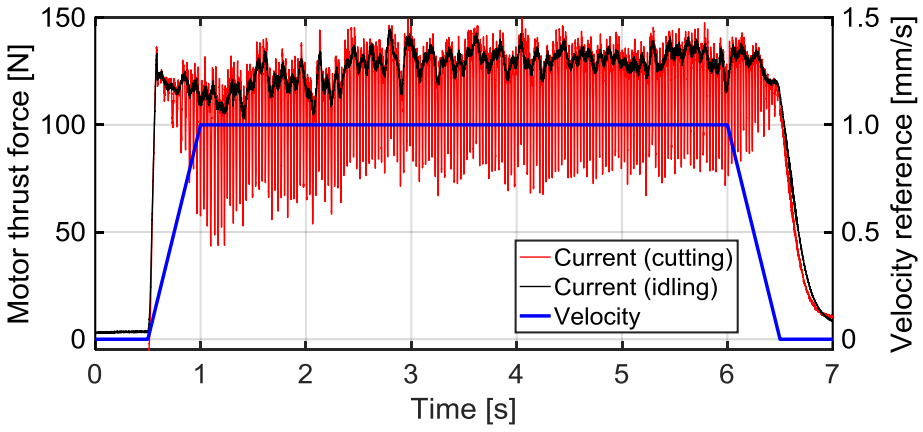

Fig. 4-17 Overall view of estimated and measured cutting forces and velocity reference at 1000 min^{-1} spindle speed and 1.5 mm radial depth of cut

Fig. 4-17 shows velocity reference and the motor thrust force in idling and cutting before compensating the disturbance force with 1000 min^{-1} spindle speed and 1.5 mm radial depth of cut. As shown in the figure, the motor thrust force fluctuates depending on the position of the table. Because the cutting force was smaller than the disturbance force, the motor thrust force in cutting kept positive value during feed motion. In Fig. 4-

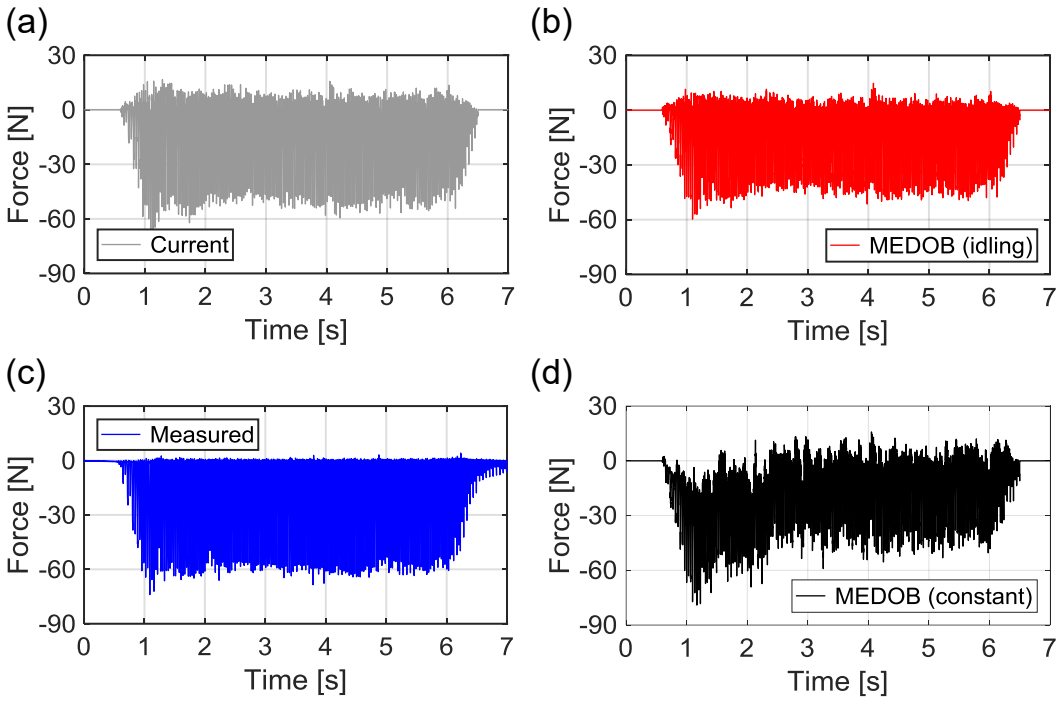

Fig. 4-18 Overall view of estimated ((a), (b), and (d)) and measured cutting forces (c) (a) current command (b) MEDOB compensating disturbance force by idling test (c) measured value (d) MEDOB compensating disturbance force by constant value

18, measured and estimated cutting forces are compared under the same condition. For comparison, the estimated cutting force by MEDOB is also presented when the disturbance force is assumed constant value, 120 N. While amplitude of the estimated cutting forces does not perfectly coincide with the measured cutting force, the estimated cutting forces with idling tests are in reasonable agreement with the measured cutting force. When the disturbance force is assumed constant value, it is difficult to eliminate the position dependent fluctuations. Fig. 4-19 indicates that the estimated cutting forces can capture dynamic variations responding to tooth-pass. In addition, there is no significant difference between DOB and MEDOB in this cutting condition, which is true of both time and frequency domain data. In calculating amplitude spectrum, 32768 (= 2^{15}) points FFT was conducted. Because the frequency of the cutting force was comparatively low, the rigid body-based formulation was sufficient for estimating dynamic cutting force.

When the frequency of the cutting forces increased by setting spindle speed to 4000 min^{-1}, another result was observed. As shown in Fig. 4-20, the amplitude of the estimated cutting force by DOB was larger than both the measured and the estimated force by MEDOB. The second harmonic component of 267 Hz was overestimated in DOB, which was similar result observed in simulation results shown in Fig. 4-10 and Fig. 4-11.

The estimated and the measured cutting forces for a spindle speed of 10000 min^{-1} are

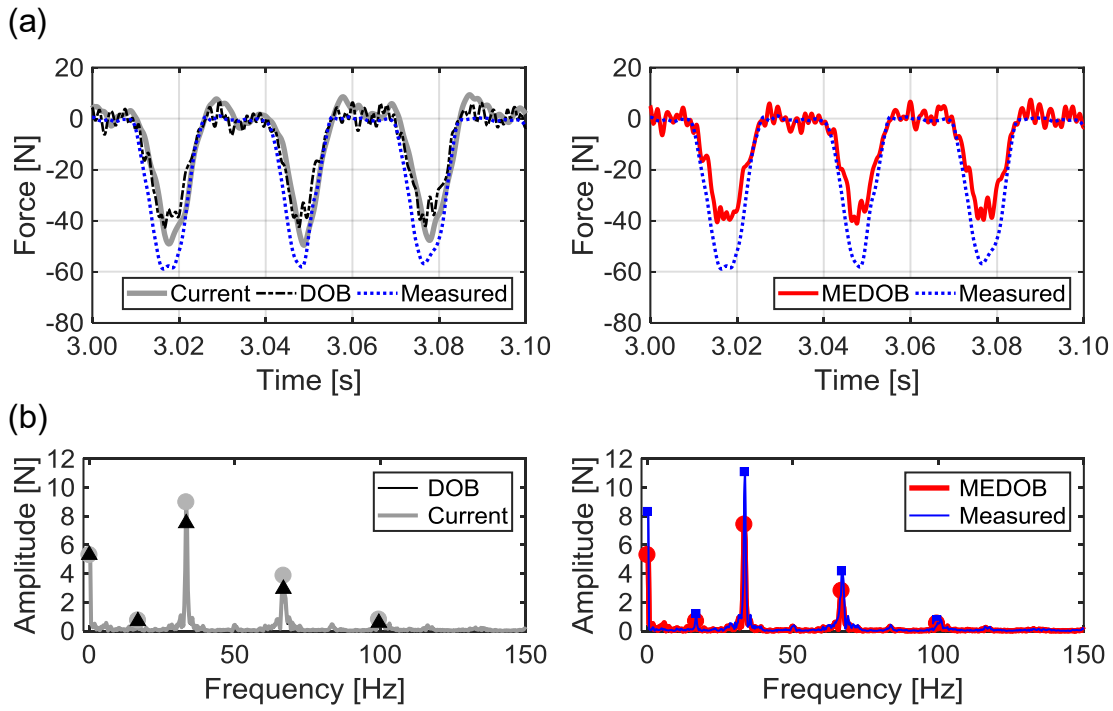

Fig. 4-19 Estimated and measured cutting forces at 1000 min^{-1} spindle speed and 1.5 mm radial depth of cut (a) time domain (b) frequency domain

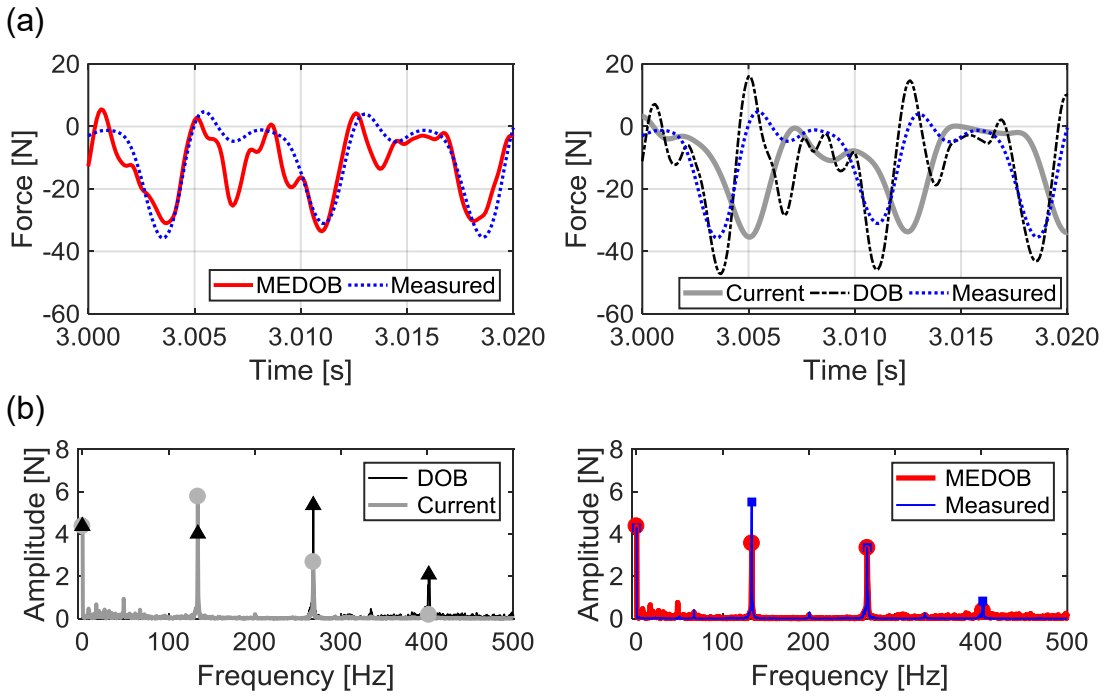

Fig. 4-20 Estimated and measured cutting forces at 4000 min^{-1} spindle speed and 1.5 mm radial depth of cut (a) time domain (b) frequency domain

described in Fig. 4-21. In this cutting condition, the tooth-pass frequency of the cutting force (333 Hz) came close to resonance frequency of the ball-screw-driven stage. In that case, the amplitude of the estimated cutting force by DOB was much higher than that of

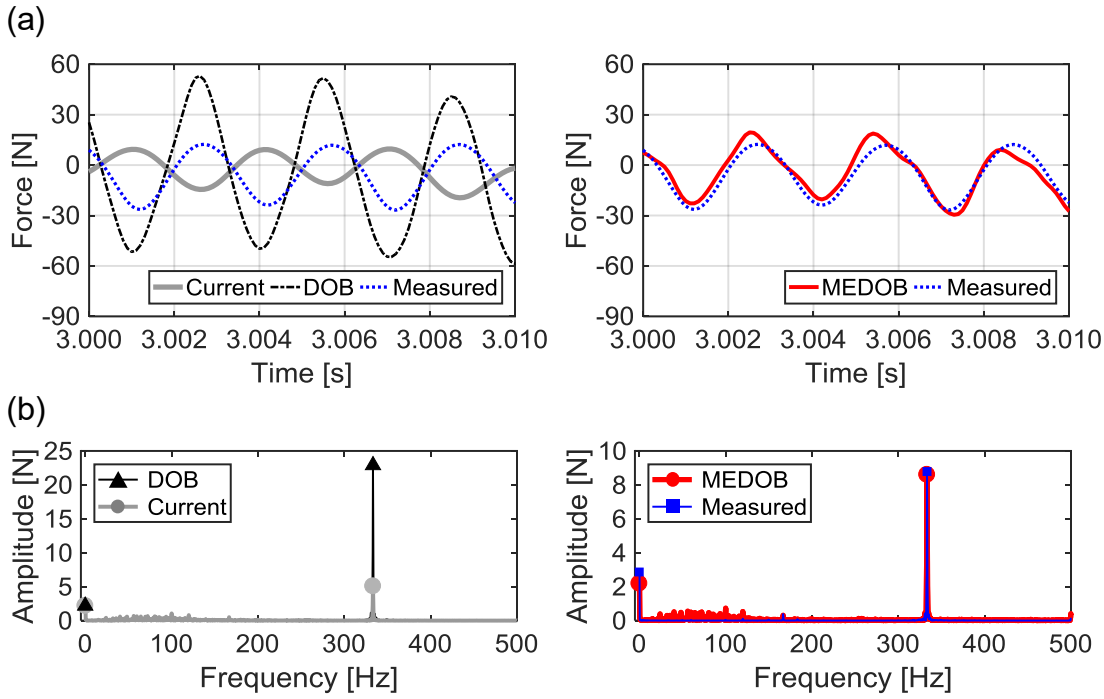

Fig. 4-21 Estimated and measured cutting forces at 10000 min^{-1} spindle speed and 1.5 mm radial depth of cut (a) time domain (b) frequency domain

the measured cutting force. By applying MEDOB, it is possible to monitor high-frequency variation of the cutting force with the frequency of 333 Hz.

Estimation bandwidth of the cutting force is compared with existing estimation techniques in the following. In Chapter 1, Ref. [27], [28] and [30] were cited to show existing current signal-based estimation techniques in the ball-screw-drive system. In each study, estimation performance was evaluated when tooth-pass frequencies were 18 Hz, 20 Hz, and 20 Hz, respectively. In addition, the estimation bandwidth in [27] and [28] was concluded to approximately 20 Hz and 62 Hz, respectively. In Ref. [35], inertia force of the feed drive was eliminated by employing observer. The estimation result at tooth-pass frequencies of 15 Hz and 100 Hz were presented, and the bandwidth of the estimation was concluded to 130 Hz, which corresponded to bandwidth of current sensor. In the literatures regarding sensorless cutting force estimation in the ball-screw-drive system, estimation performance of the cutting force was evaluated under lower spindle speed. In Ref. [33], cutting force estimation whose bandwidth was 350 Hz was accomplished in the linear motor driven stage by applying DOB. Even if the cutting force is estimated in the ball-screw-drive system, it is possible to enhance estimation bandwidth comparable to linear motor drive system by employing the proposed estimation method. In this regard, decrease in the estimation bandwidth is inevitable in general NC machine tool, because the resonance frequency as dual-inertia system is lower than the desktop size experimental setup. In case of large-scale machine tool, for example, the resonance frequency is limited to several tens of hertz, and it is difficult to

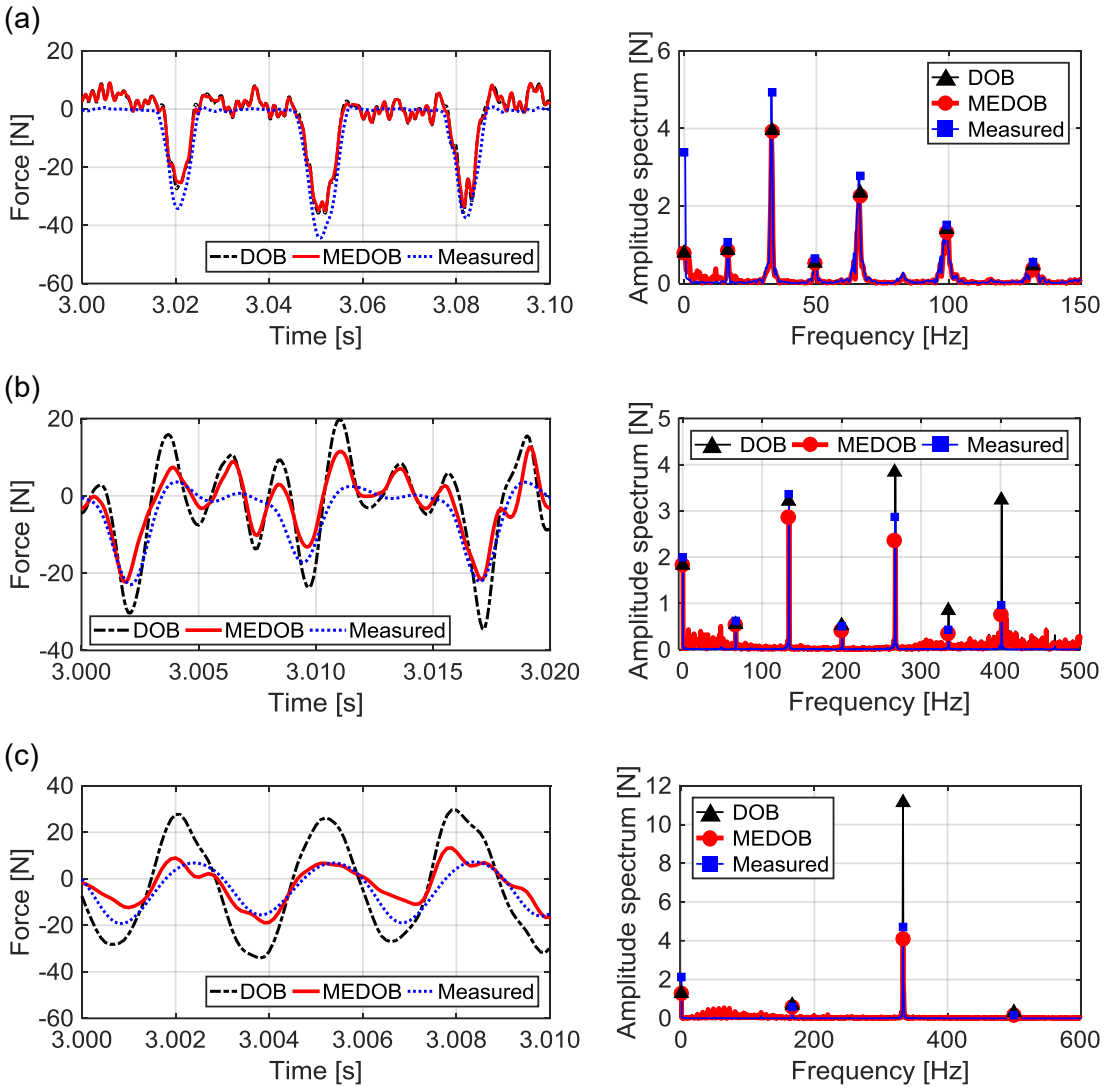

Fig. 4-22 Estimated and measured cutting forces at 0.5 mm radial depth of cut
(a) 1000 min^{-1} (b) 4000 min^{-1} (c) 10000 min^{-1}

increase it comparable to Machine B. Evaluation of the estimation bandwidth in general machine tool is remaining issue.

Fig. 4-22 shows estimated and measured cutting forces at lower radial depth and the same axial depth of cut. The cutting forces became smaller and more intermittent compared with the case of 1.5 mm radial depth. In 1000 min^{-1}, waveform of intermittent cutting force can be replicated, and the cutting force components up to fourth harmonic can be monitored. Although the dominant cutting force components can be monitored as shown in the frequency analysis results, waveforms of the cutting force in 4000 min^{-1} and 10000 min^{-1} are more distorted. Because the cutting force was smaller than that in 1.5 mm radial depth of cut, uncompensated extenal force is more influential to the cutting force estimation. The smaller the cutting force is, the more difficult it is to estimate cutting force components.

Standard deviations of the estimation error in each cutting conditions are summarized

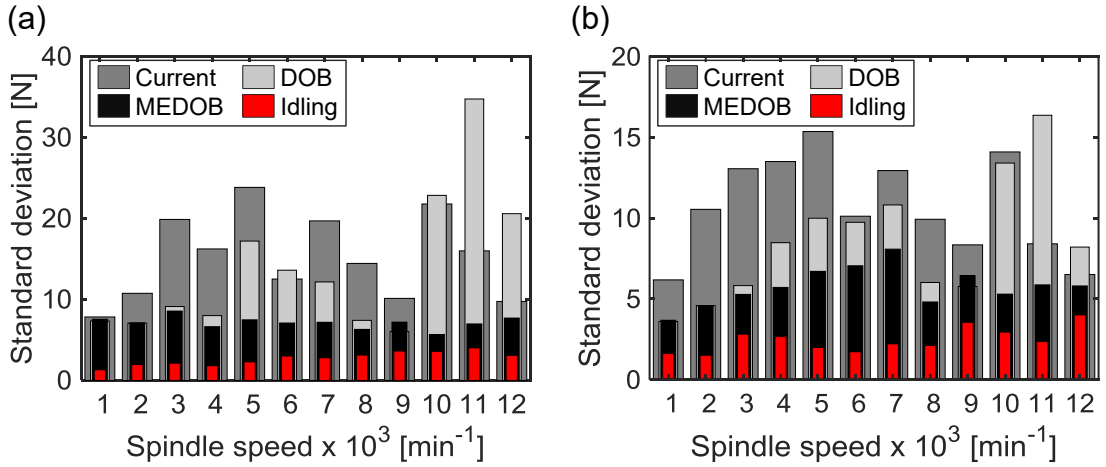

Fig. 4-23 Standard deviation of estimation error and compensation error of disturbance force in each cutting condition (a) radial depth: 1.5 mm (b) radial depth: 0.5 mm

in Fig. 4-23. In the figure, standard deviation of compensated disturbance force, calculated from the motor thrust force in idling tests, is denoted as "Idling" in the graph legend. The calculation procedure of the uncompensated disturbance force is identical to what is shown in Fig. 3-15 (a) and Fig. 3-16 (a). The standard deviation of "Idling" indicates inevitable estimation error in the cutting force estimation. At lower spindle speeds, the discrepancy of the standard deviation between DOB and MEDOB was comparatively small. However, the estimation accuracy of the DOB-based method falls at higher spindle speeds. By employing MEDOB-based method, the standard deviation of the estimation errors was less than 10 N under the cutting condition shown in Table 4-4.

4.3.3 Influence of identification error of parameters and output error

Experimental conditions are listed in Table 4-6. Condition <1> is set as reference condition. Owing to accurate identification of mechanical parameters and suitable phase lag compensation, dynamic variation of cutting force can be estimated as shown in Fig. 4-24. The parameters are changed from their nominal value and the estimated cutting force at condition <1> is recalculated in order to evaluate influence of identification error of the parameters. In addition, other conditions <2> ~ <5> were selected as condition where the following error factors became non-negligible: the identification error of the movable mass for condition <2>, the synchronization error for condition <3>, the output error resulting from the encoder for condition <4>, and the output error due to modeling error of the torsional dynamics for condition <5>. A part of estimation result at condition <5> is identical to the result shown in Fig. 4-21.

Table 4-6 Experimental conditions for evaluating identification error of parameter and output error

Condition number	<1>	<2>	<3>	<4>	<5>
Spindle speed [min^{-1}]	2000	10000	1000	1000	10000
Axial depth of cut [mm]	0.5	0.5	0.5	0.3	2.0
Radial depth of cut [mm]	0.5	6.0	1.5	1.5	1.5
Milling type	Down	Slotting	Down	Down	Down
Feed rate [mm/s]	2.0	8.0	1.0	1.0	10.0
Used machine	B	B	A	B	B
Tool diameter [mm]			ϕ 6.0		
Number of flute			2		
Material of workpiece			Al alloy (A5052)		

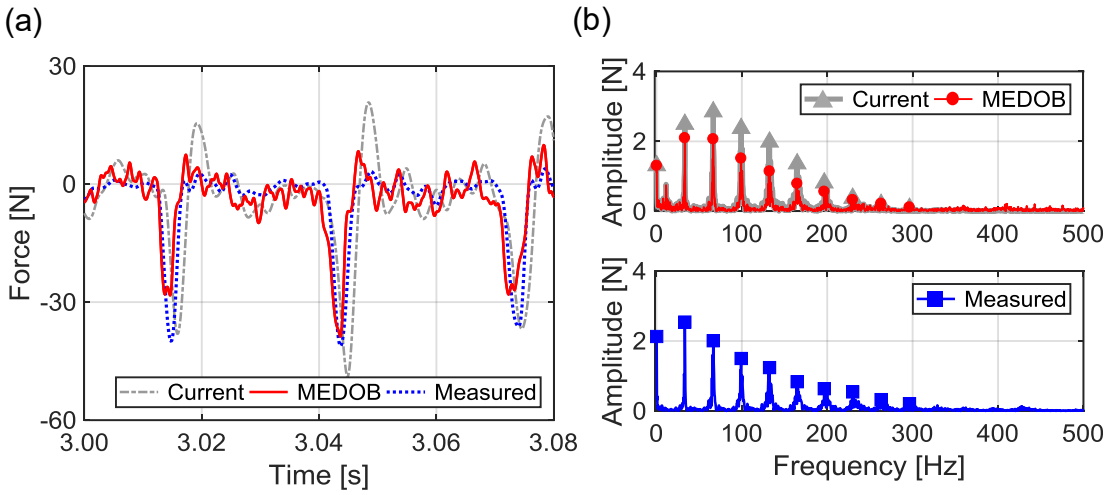

Fig. 4-24 Estimated and measured cutting forces at condition <1> (a) time domain (b) frequency domain

Fig. 4-25 shows estimation results at condition <1> and <2> responding to nominal value of movable mass. When fundamental frequency of the cutting force is much lower than resonance frequency as the dual-inertia system as condition <1>, selection of the nominal movable mass little influences on the cutting force estimation as shown in Fig. 4-25 (a). When spindle speed increases and fundamental frequency comes close to resonance frequency as condition <2>, on the other hand, identification error of the movable mass is non-negligible. This is because the inertia forces presented high portion of the estimated cutting force in high frequencies. These results are coincident with the simulation results shown in section 4.2. As mentioned before, the resonance frequency in the general NC machine tool is lower than that in desktop size machine tool like Machine A and B. Thus, bandwidth where the identification error of the movable mass is negligible is limited and becomes narrow.

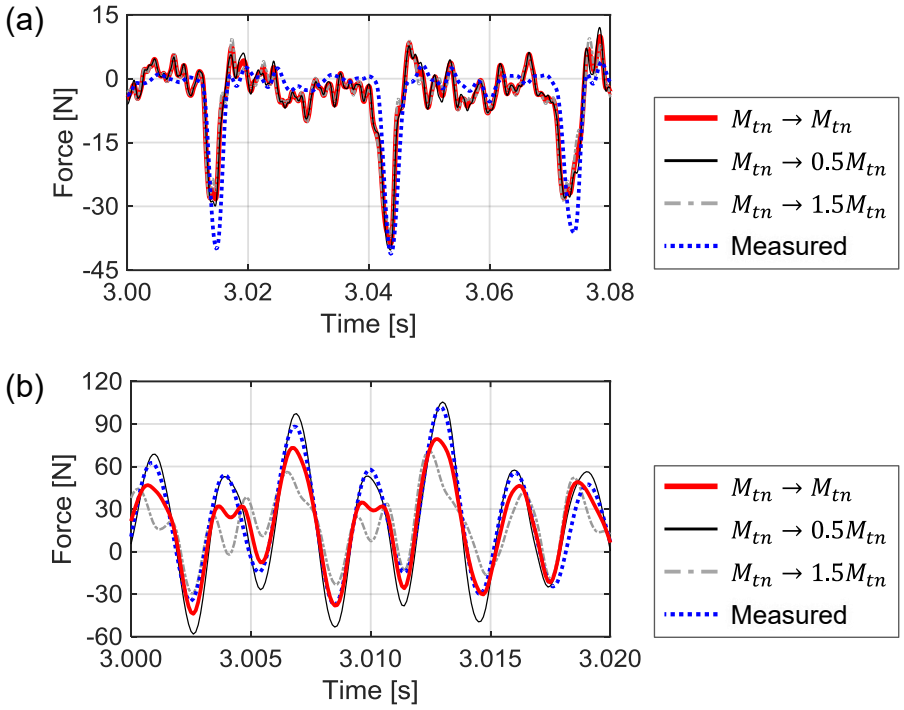

Fig. 4-25 Estimated and measured cutting forces responding to identification error of movable mass (a) condition <1> (b) condition <2>

Fig. 4-26 shows estimation results at condition <1> and <3> responding to the synchronization error of the control signals. When the phase lag compensation is not carried out, estimation error increases at the instant when cutting edge comes out of the workpiece. This is because higher harmonics components were overestimated as shown in frequency analysis results. In Machine A, high frequency noises are remarkable during air cutting region as shown in Fig. 4-26 (b). Considering simulation results shown in section 4.2, it is believed that insufficient resolution of the rotary encoder excited high frequency noises.

Fig. 4-27 presents estimated cutting forces at condition <4> where the output error of the encoder signal is non-negligible. As shown in Fig. 4-27 (a), high frequency noises are included in the estimated cutting force applying MEDOB. In contrast to the measured cutting force using dynamometer, both current signal and the estimated force by MEDOB included variable components irrelevant to actual cutting force, whose frequencies were 204 Hz, 307 Hz, 410 Hz, and 512 Hz. Considering that feed rate at condition <4> was 1.0 mm/s, wavelengths of the variations were 4.90 μm, 3.26 μm, 2.44 μm, 1.95 μm, respectively. Their wavelengths are coincident with those of angular acceleration shown in Fig. 3-14. In addition, the frequency of third harmonic (i.e. 100 Hz) came close to that of acceleration variation with a period of 9.8 μm (i.e. 102 Hz), and cutting force component of 100 Hz was overestimated. When acceleration/angular acceleration are calculated by numerical differential of position/angle, high frequency variation of acceleration signal is non-negligible in some cutting condition, and the

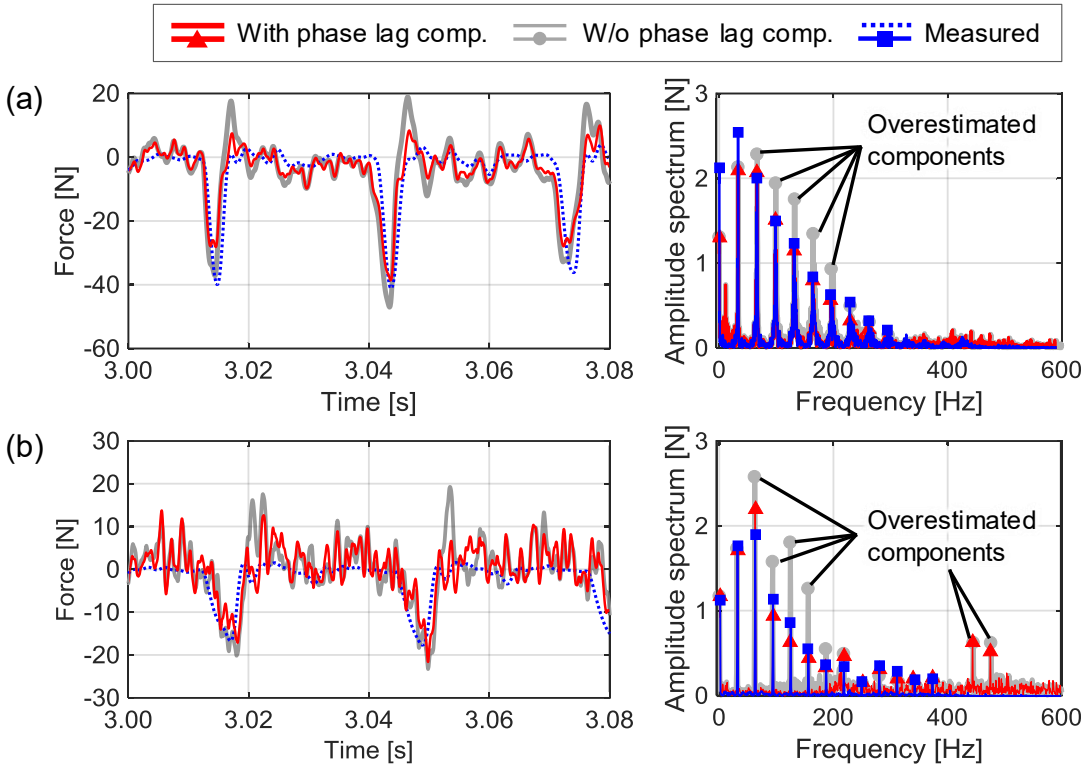

Fig. 4-26 Estimated and measured cutting forces responding to compensation error of dead time elements (a) condition <1> (b) condition <3>

estimation accuracy of the cutting force decreases. Particularly, output error from encoders is particularly influential in low feed rate where frequency of the cutting force is likely to come close to that of the output error. In addition, chatter vibration might be miss-detected when frequency of the output error comes close to resonance frequency of the mechanical components. Although amplitude of the output error is difficult to predict, its frequency is predictable. By employing notch filters, high frequency noises can be reduced as shown in Fig. 4-27 (b).

Fig. 4-28 describes estimated cutting forces at condition <5> where the output error due to the modeling error of the torsional dynamics is non-negligible. As shown in Fig. 4-28 (c), 778 Hz and 1024 Hz components are included in the estimated cutting force by MEDOB. 778 Hz component was resulting from torsional stiffness of the screw-system, which was observed swept sine excitation result shown in Fig. 3-6. Although cutoff frequency of the low-pass filter in MEDOB was set to 500 Hz, high frequency variation at 778 Hz was unable to be attenuated. Considering that the feed rate was 10 mm/s, angular variation with a period of 9.8 μm corresponded to 1024 Hz in frequency domain. When targeting frequency range of the cutting force estimation was less than the frequency of the torsional mode, notch filters are applicable. As shown in Fig. 4-28 (b), tooth-pass frequency (333 Hz) component of the cutting force can be captured by applying the notch filters.

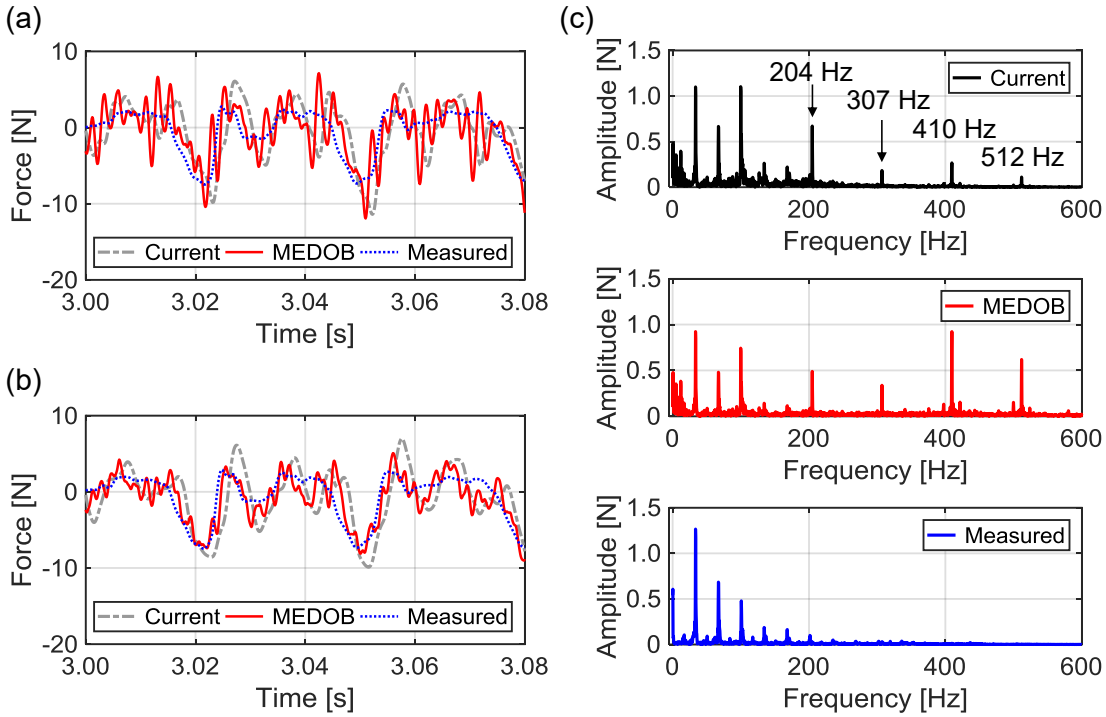

Fig. 4-27 Estimated and measured cutting forces at condition <4> (a) without notch filters (b) with notch filters <3> frequency analysis result before applying notch filters

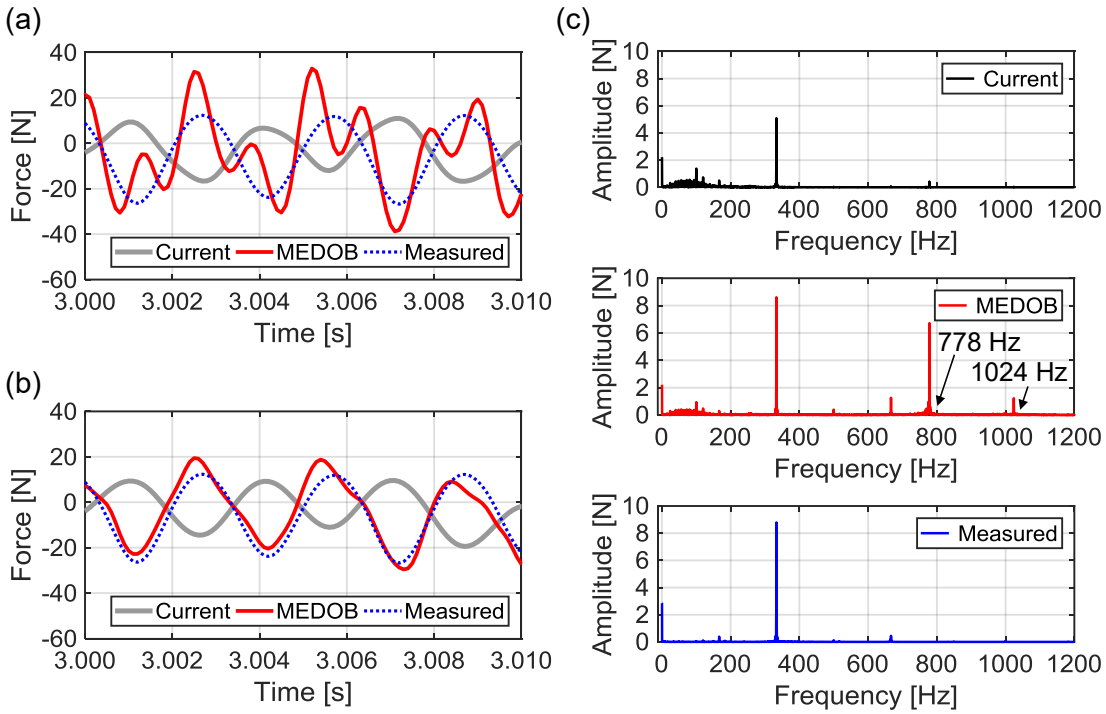

Fig. 4-28 Estimated and measured cutting forces at condition <5> (a) without notch filters (b) with notch filters <3> frequency analysis result before applying notch filters

Table 4-7 Standard deviation of estimation error and compensated disturbance force

Condition number	<1>	<2>	<3>	<4>	<5>
Compensated disturbance force [N]	2.0	3.3	2.4	1.5	3.6
With phase lag compensation [N]	5.7	-	5.6	-	-
Without phase lag compensation [N]	8.2	-	7.4	-	-
$M_{tn} \rightarrow M_{tn}$ [N]	5.7	11.4	-	-	-
$M_{tn} \rightarrow 0.5M_{tn}$ [N]	5.4	11.3	-	-	-
$M_{tn} \rightarrow 1.5M_{tn}$ [N]	6.4	19.2	-	-	-
With notch filters [N]	-	-	-	2.5	5.7
Without notch filters [N]	-	-	-	3.3	11.8
Thrust force (motor current) [N]	10.4	17.4	8.8	3.7	21.7

Standard deviations of estimation error are summarized in Table 4-7. Because the disturbance force needs to be preliminarily identified and eliminated, it is difficult to estimate the cutting force less than the variation in the disturbance force. As shown in the table, estimation accuracy of the cutting force is less than the variation in compensated disturbance force. In some condition, it is possible to estimate cutting force component with the accuracy of several N.

As for the estimated cutting forces shown in the last section, the influence of the error factors in each cutting condition was evaluated by calculating the standard deviations, and the results are shown in Fig. 4-29 ~ Fig. 4-31. As shown in Fig. 4-29, identification error of movable mass tends to increase the estimation errors when spindle speed increases. In order to increase estimation bandwidth of the cutting force, it is inevitable to accurately identify the nominal value of the movable mass.

In contrast to identification error of the movable mass, the synchronization errors can influence the estimation accuracy of the cutting force at various spindle speeds as shown in Fig. 4-30. In Machine B, the synchronization error between current command and acceleration response was identified as 0.4 ms. By compensating the synchronization error, the estimation accuracy of the cutting force can be enhanced.

Influence of the output errors on the estimation accuracy is summarized in Fig. 4-31. When the notch filters were not applied, estimation error drastically increased at 1.5 mm radial depth and 10000 min^{-1}, because the torsional vibration was induced as presented in Fig. 4-28. The torsional vibration was also induced at 0.5 mm radial depth and 9000 min^{-1}. Compared with the torsional vibration, high frequency variations resulting from encoder signals less influenced the cutting force estimation under the evaluated cutting condition.

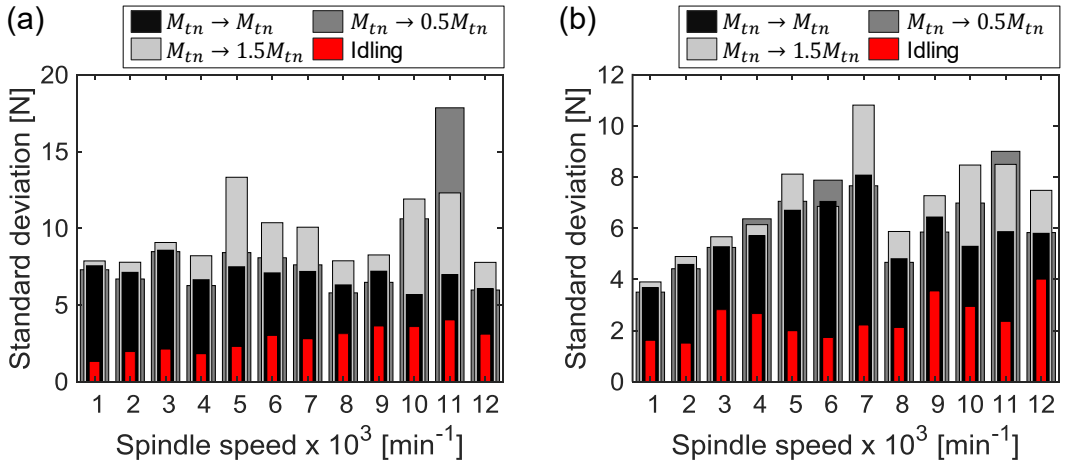

Fig. 4-29 Influence of identification error of movable mass on estimation accuracy of cutting forces (a) radial depth: 1.5 mm (b) radial depth: 0.5 mm

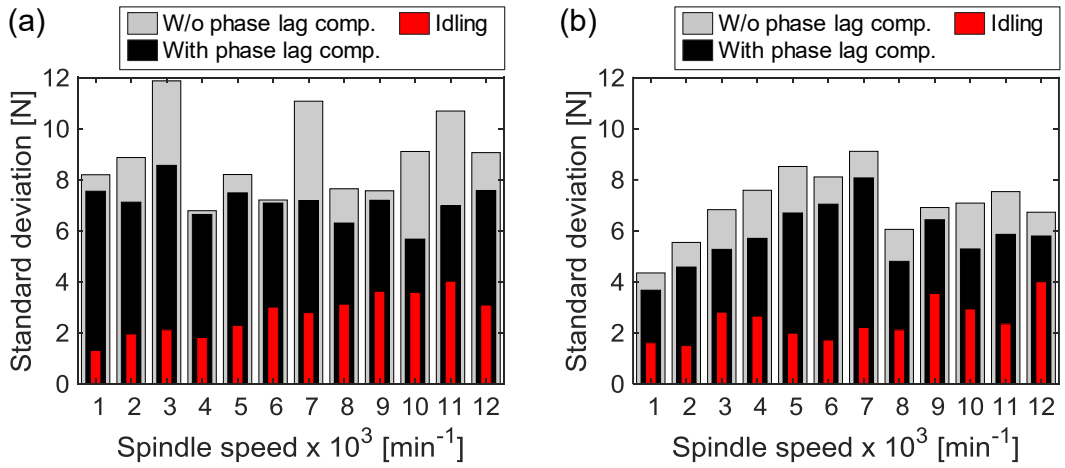

Fig. 4-30 Influence of synchronization errors on estimation accuracy of cutting forces (a) radial depth: 1.5 mm (b) radial depth: 0.5 mm

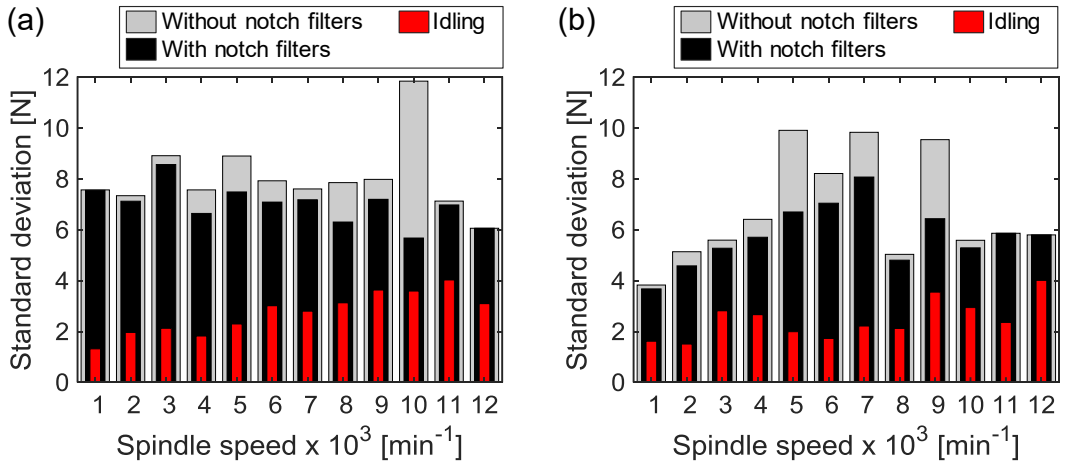

Fig. 4-31 Influence of output errors on estimation accuracy of cutting forces (a) radial depth: 1.5 mm (b) radial depth: 0.5 mm

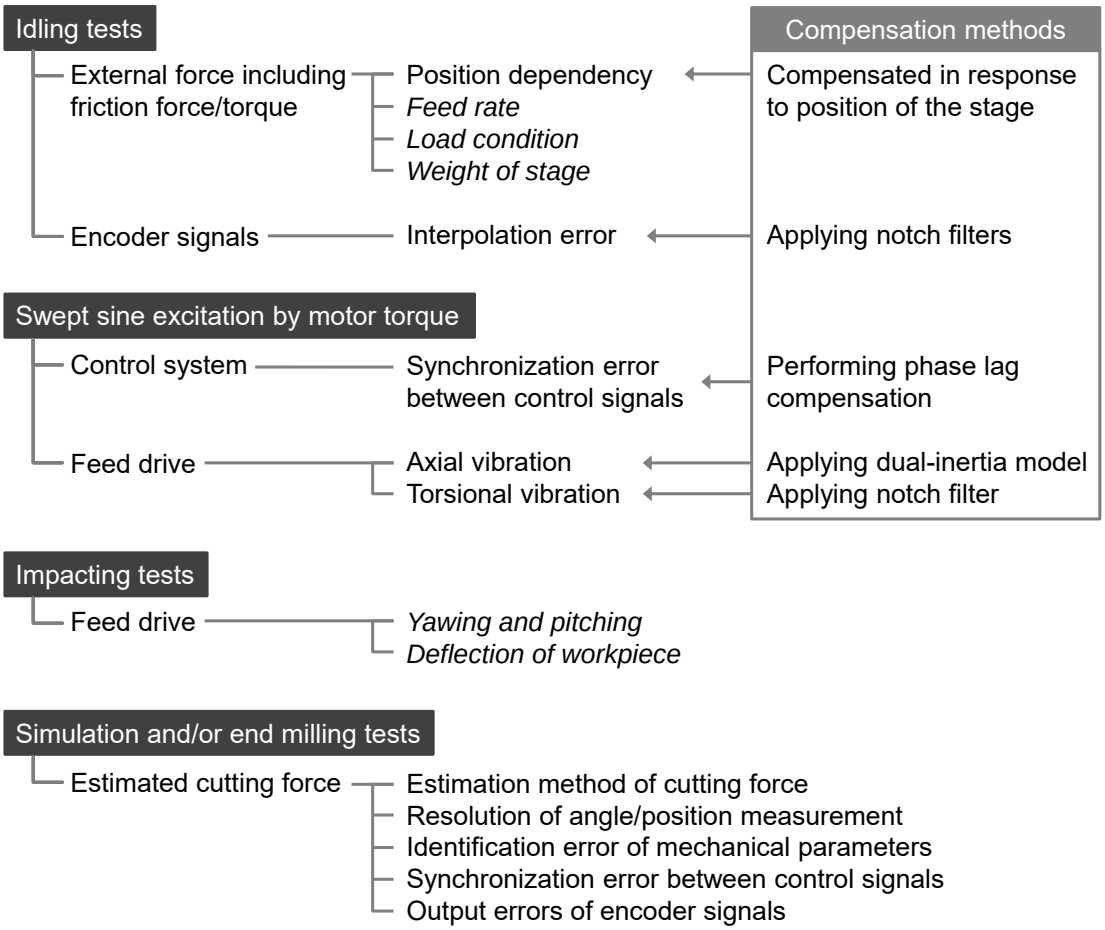

Fig. 4-32 Summary of methods for extracting error factors in case of cutting force estimation at workpiece side (oblique type: uncompensated error factors)

In Fig. 4-32, methods for extracting the major error factors, which were evaluated in this research, are summarized. Since the cutting force is estimated based on the servo information (i.e. current, angle, position) during feed motion, detailed analysis of them is important as well as evaluation of the estimation accuracy through simulation and/or experiment. In addition, experimental or theoretical structural analysis is helpful to predict the probable estimation bandwidth under the dual-inertia model-based formulation. When excitation tests were carried out based on the servo information, it is possible to perform the phase lag compensation, because the phase lag between input and output signals can be identified. Although some of the above error factors are not considered in the general cutting force estimation, detailed analysis of them contributes to enhance the estimation accuracy of the cutting force.

Without using a piezoelectric force sensor, it is possible to avoid increase in sensor's cost, which is usually more than several hundred yen. On the other hand, performance of mechanical elements, such as encoders, need to be enhanced to monitor dynamic cutting force whose frequency often surpasses 100 Hz. To reconstruct waveform of the

cutting force as time domain data, it is preferable to enhance sampling frequency at least 10 times higher than the frequency of the cutting force. In order to monitor high frequency components of the cutting force, resolution of the encoders needs to be increased to reduce measurement error of the acceleration. For example, in Machine A, estimation error resulting from quantization error of position/angle measurement can reduce less than 1 N within 1 kHz when resolution of encoders is higher than 1 nm. On the other hand, angle of the motor is not necessarily incorporated into the control system due to lack of compatibility to servo amplifier, which can be a restraint condition. When applying the dual-inertia model, resolution of the rotary encoder at the motor side has higher priority than that at the counter-motor side. Two rotary encoders at the motor and the counter-motor side are beneficial when modeling torsional dynamics of the screw system.

4.4 Summary

This chapter describes the influence of the error factors in sensorless cutting force estimation based on the time domain simulation and the end milling tests. The contents are summarized as follows.

1. By using the time-domain simulation, the frequency response of the cutting force observer and estimation characteristics of the milling forces were evaluated regarding following error factors: the difference of the estimation method, the identification error of the movable mass, the quantization error of the angle measurement, and synchronization errors due to the phase lag elements.
2. When measurement error of acceleration or identification error of the movable mass is large, estimation error of the cutting force increases in high frequencies, because the inertia forces are dominant in the region. To increase the resolution of the rotary encoder is important, because vibration amplitude of the angle response against the cutting force drastically decreases in high frequencies, compared with the position response of the stage.
3. When the phase lag elements are ignored, estimation bandwidth of the cutting force might become narrower than that of current signal-based estimation even if MEDOB is employed. For wideband cutting force etsimation, suitable phase lag compensation is required based on the frequency response among the current, the angle, and the table.
4. According to the simulation result, MEDOB can capture dynamic variation of intermittent milling force in contrast to DOB. The identification error of mass and the synchronization error can evoke estimation error of the milling force at the

instant when the cutting force becomes local maximum value and cutting edge comes out of the workpiece.

5. The high frequency noises due to quantization error of angle measurement is remarkable during air cutting region in intermittent cutting. In addition, the high frequency noises develop around the higher harmonics of the applied cutting force.
6. By constructing the estimation system that considered above error factors, the proposed MEDOB-based method could increase the estimation bandwidth compared with the conventional DOB-based method. In addition, it was possible to estimate high-frequency variation of the actual cutting force with the frequency of 333 Hz. The obtained result was comparable to previous work evaluated in the linear motor driven stage. The standard deviation of the estimation errors was less than or comparable to 10 N under the evaluated cutting condition.
7. Estimation accuracy of the cutting force might decrease due to the high frequency noises of acceleration signal, which is amplified by the numerical differential of position/angle. Although it is difficult to predict their amplitude, their frequency is predictable considering the feed rate and the signal period of the encoder. In addition, the torsional vibration of the screw-system in high frequencies can be an error factor of the estimation. When targeting estimation bandwidth is less than the frequency of torsional mode, it is possible to enhance the estimation accuracy by applying the notch filters.

5. Evaluation of mode-decoupled and sensorless cutting force estimation technique

5.1 Introduction

As presented in Chapter 4, both estimation accuracy and bandwidth increase by employing MEDOB-based method on behalf of conventional DOB-based method. On the other hand, evaluation of the estimation performance is limited to feed force components. Presented MEDOB-based estimation technique is not necessarily applicable to estimate cross-feed component of the cutting force as explained later in this chapter. This is why cutting force estimation technique in the vibration mode is introduced, applying the mode-decoupling. In the mode-decoupled estimation technique in the vibration mode, both feed and cross-feed components are observable. In addition, high frequency variations of acceleration resulting from the output error of encoders can be reduced owing to the relative motion-based cutting force estimation. In this chapter, the validity of the mode-decoupled method was evaluated both in time domain simulation and end milling tests, in which both feed and cross-feed were estimated. Considering that cutting force estimation in the rigid body mode is essentially the same as the MEDOB-based method, validity of the estimation in the vibration mode is mainly evaluated.

5.2 Evaluation of estimation performance using time-domain simulator

5.2.1 Frequency response of cutting force observer

Frequency response of the estimated cutting force in the vibration mode is calculated using the time domain simulator by applying a sinusoidal cutting force as a command value. Simulation condition and configuration are identical to those shown in section 4.2 except for the estimation method of the cutting force.

In the MEDOB-based method (i.e. rigid body mode), the motor thrust force, $K_t I_a^{cmd}/R$, consisted mostly of the estimated cutting force in lower frequencies as shown in Fig. 4-1. The friction force and torque mostly consist of DC and low frequency components, and the motor thrust force (i.e. motor current) is strongly affected by the frictions. On the other hand, in the vibration mode, the portion of motor thrust force is low as shown in Fig. 5-1, because the low inertia ratio (α: 0.103) is assumed in the simulation. Here, the proportion of motor thrust force is written as $\alpha K_t I_a^{cmd}/R$ by referring Eq. (2-44). Thus,

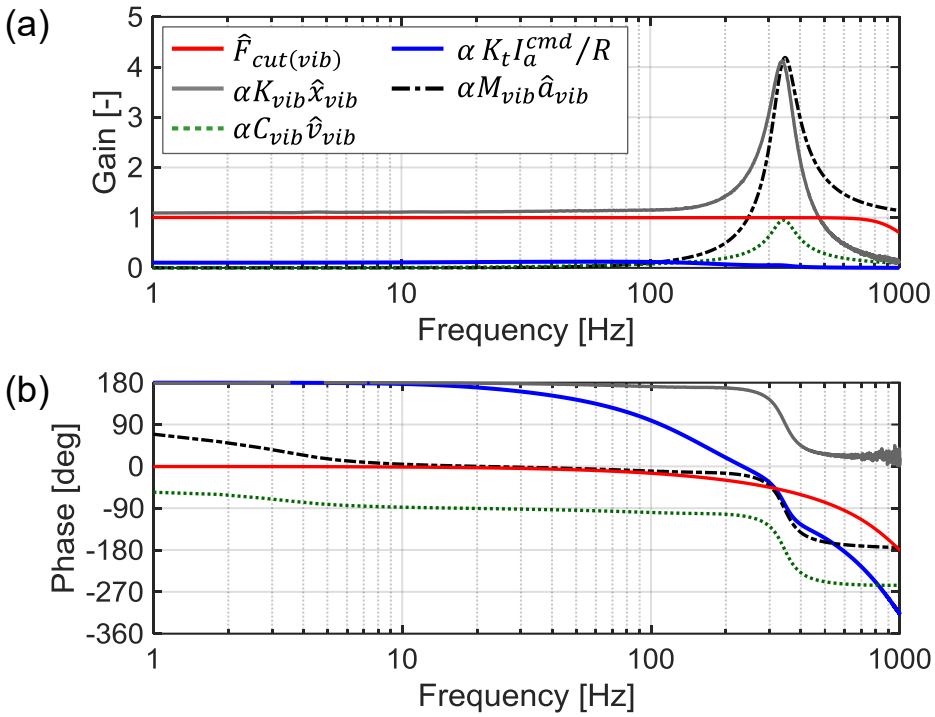

Fig. 5-1 Frequency response of each force constituting estimated cutting force in vibration mode (a) gain characteristics (b) phase characteristics

the estimation is less affected by the variation of the motor thrust force in the vibration mode. On the other hand, the elastic force, $\alpha K_{vib}\hat{x}_{vib}$, presented high proportion in a wide frequency range. Accurate identification of stiffness was important in the vibration mode. When the frequency components close to the resonance frequency were monitored, the damping force, $\alpha C_{vib}\hat{v}_{vib}$, was non-negligible in the vibration mode.

Frequency responses among applied cutting force and motor thrust, elastic, damping, and inertia forces are shown in Fig. 5-2 ~ Fig. 5-5, respectively. In calculating the frequency responses, the inertia ratio α was changed in each condition, while the resonance frequency (335 Hz) and the total mass M_a were kept by adaptively changing movable mass M_t, inertia J_r, and stiffness K_r. As shown in Fig. 5-2, the inertia ratio α plays important role in frequency response of the motor thrust force. When the inertia ratio is high, cutting force estimation in the vibration mode is subjected to variation of the motor thrust force resulting from the disturbance force. As described in Fig. 5-3, the elastic force is also subjected to the inertia ratio as well as the motor thrust force. In lower frequency, the applied cutting force balances the difference of the elastic and the motor thrust forces. In contrast to the motor thrust and the elastic forces, the damping and the inertia forces are less influenced by the inertia ratio in lower frequencies as shown in Fig. 5-4 and Fig. 5-5, respectively. As suggested from the above results, the value of the inertia ratio α can influence on the estimation performance of the cutting

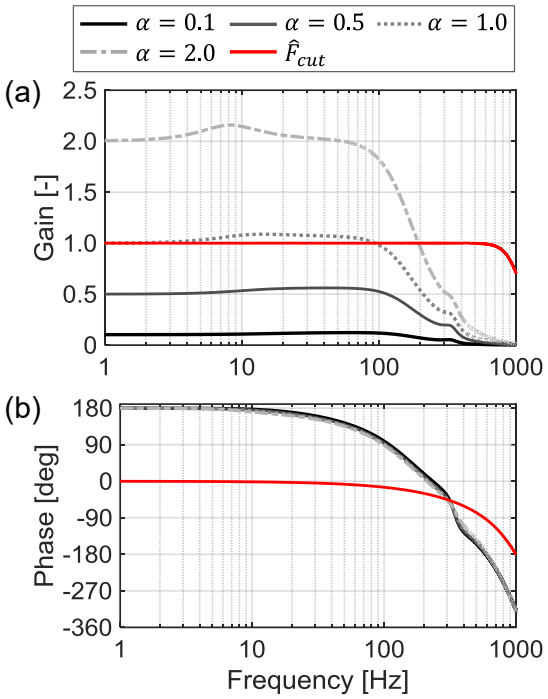

Fig. 5-2 Frequency response of thrust force $\alpha K_t I_a^{cmd}/R$ in vibration mode (a) gain (b) phase

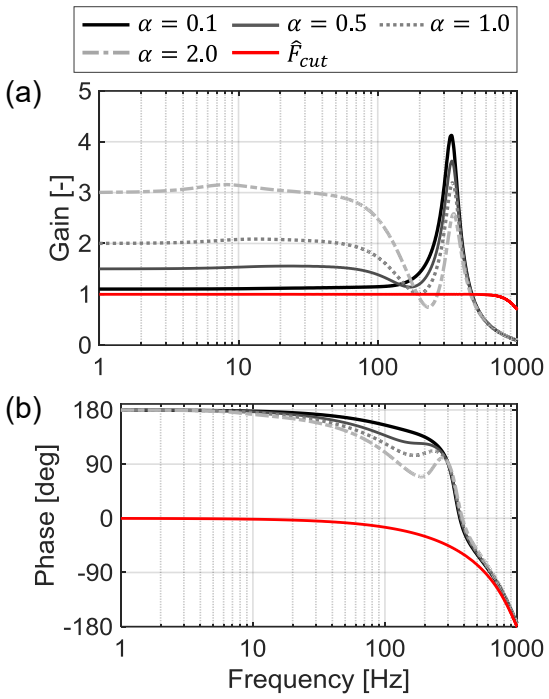

Fig. 5-3 Frequency response of elastic force $\alpha K_{vib}\hat{x}_{vib}$ in vibration mode (a) gain (b) phase

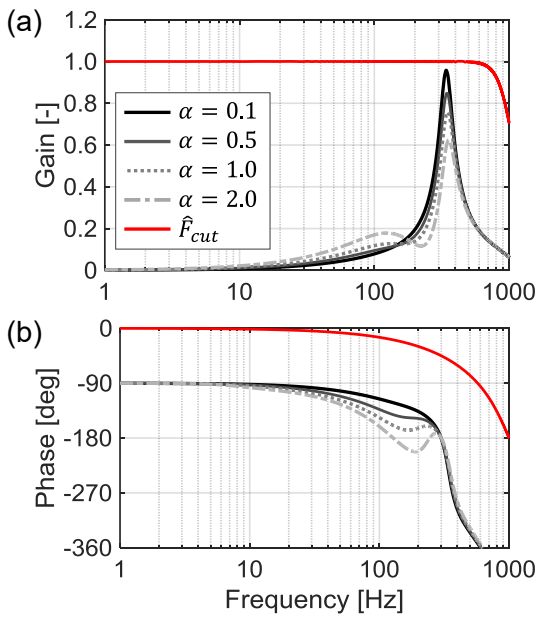

Fig. 5-4 Frequency response of damping force $\alpha C_{vib}\hat{v}_{vib}$ in vibration mode (a) gain (b) phase

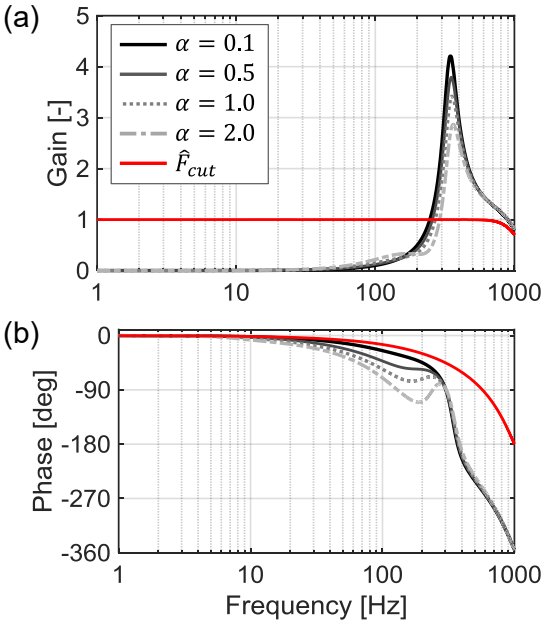

Fig. 5-5 Frequency response of inertia force $\alpha M_{vib}\hat{a}_{vib}$ in vibration mode (a) gain (b) phase

force. In the experimental setup, however, it is difficult to substantially change the inertia ratio α, because the experimental setup is desktop size, and available load mass is limited by the table size. Thus, the influence of the inertia ratio α is not discussed in

experimental verification presented in section 5.4.

As in the case of MEDOB-based method shown in section 4.2.2, frequency responses are compared responding to the identification error of the paramters. The results are shown in Fig. 5-6 ~ Fig. 5-9. As for the identification error of the movable mass shown in Fig. 5-6, there are no differences of the simulation results between in the vibration mode and in MEDOB-based method shown in Fig. 4-2. Identification error of the movable mass deteorites the estimation accuracy in high frequencies. As shown in Fig. 5-7, estimation accuracy decreases at certain frequencies when there is compensation error of the phase lag elements.

In Fig. 5-8, comparison result of frequency response corresponding to identification error of axial stiffness K_r is shown. In contrast to MEDOB-based method, identification error of stiffness alters frequency response from DC to high frequencies, which suggested the necessity for accurate identification of the stiffness value. That can be disadvantage of the proposed estimation technique, because the stiffness varies depending on the displacement of the stage, which is remarkable in the large-scale machine tool. However, position dependency of the stiffness is not considered in this dissertation, because Machine B is a desktop size machine tool.

In Fig. 5-9, comparison result of frequency response correspinding to resolution of the rotary encoder is presented. Compared with the result of MEDOB-based method shown in Fig. 4-5, estimation accuracy in high frequencies was improved when 17 bit rotary encoder was assumed. As written in Eq. (2-39), the modal displacement in vibration mode x_{vib} is calculated from the relative displacement between the stage x_t and the motor x_m. Because variation amplitude of the stage response against cutting force is larger than that of angle response in high frequencies, the relative velocity and acceleration are larger than angular velocity and acceleration. Therefore, the relative acceleration is less subjected to measurement error of angle response, and estimation accuracy under 17 bit rotary encoder is improved in the vibration mode.

Fig. 5-10 shows gain characteristics between the applied cutting force and the inertia force in each mode. In the rigid body mode, the inertia force calculating from the angle response ($M_{rigid}\,\hat{a}_m/(\alpha+1)$) composed a large part of the total inertia force ($M_{rigid}\hat{a}_{rigid}$). In the vibration mode, on the other hand, the proportion of the inertia force calculating from angle response ($\alpha^2 M_{vib}\,\hat{a}_m/(\alpha+1)$) was small. In other words, the proportion of $\hat{a}_m$ was larger in the rigid body mode, while that was smaller in the vibration mode. Thus, measurement error of angular response further amplified the estimation error of the cutting force in the rigid body mode. The cutting force estimation in the rigid body mode requires more accurate measurement of the angular response than in the vibration mode.

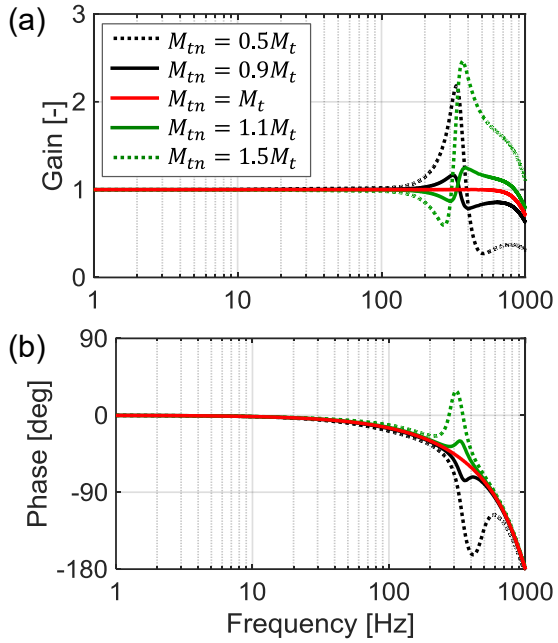

Fig. 5-6 FRF of estimated cutting force in vibration modal space corresponding to identification accuracy of movable mass (a) gain (b) phase

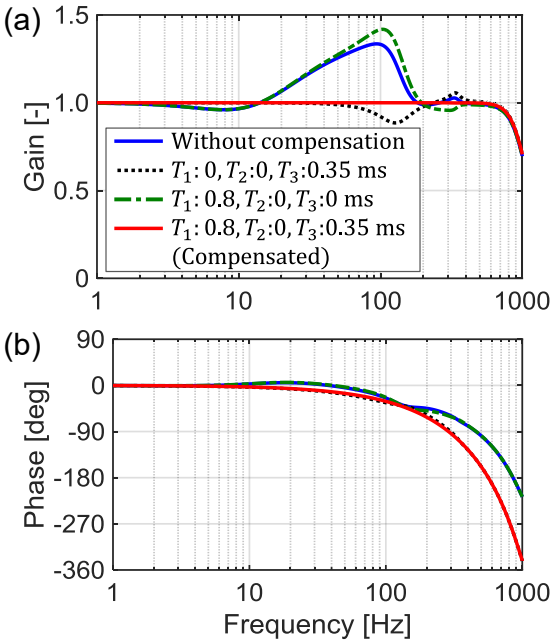

Fig. 5-7 FRF of estimated cutting force in vibration modal space corresponding to compensation method of dead time (a) gain (b) phase

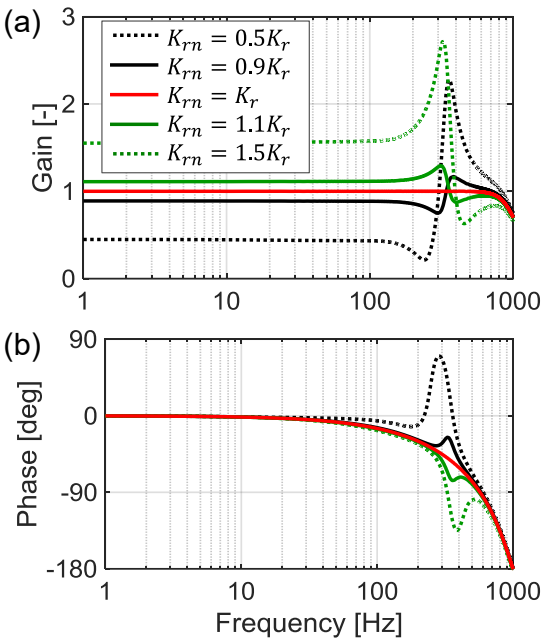

Fig. 5-8 FRF of estimated cutting force in vibration modal space corresponding to identification accuracy of axial stiffness (a) gain (b) phase

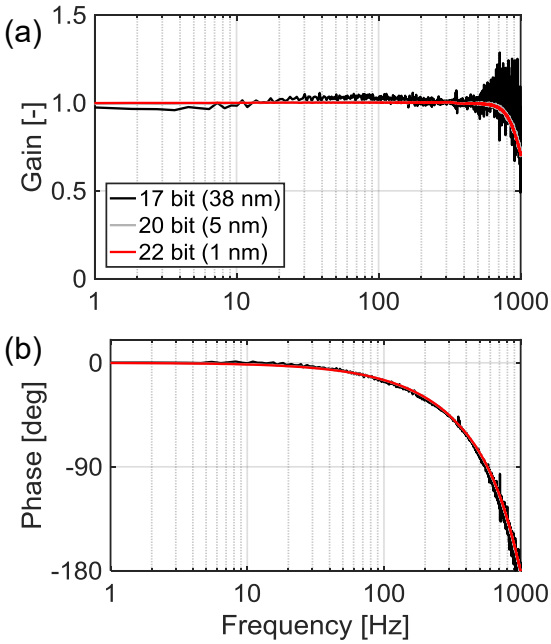

Fig. 5-9 FRF of estimated cutting force in vibration modal space corresponding to resolution of rotary encoder (a) gain (b) phase

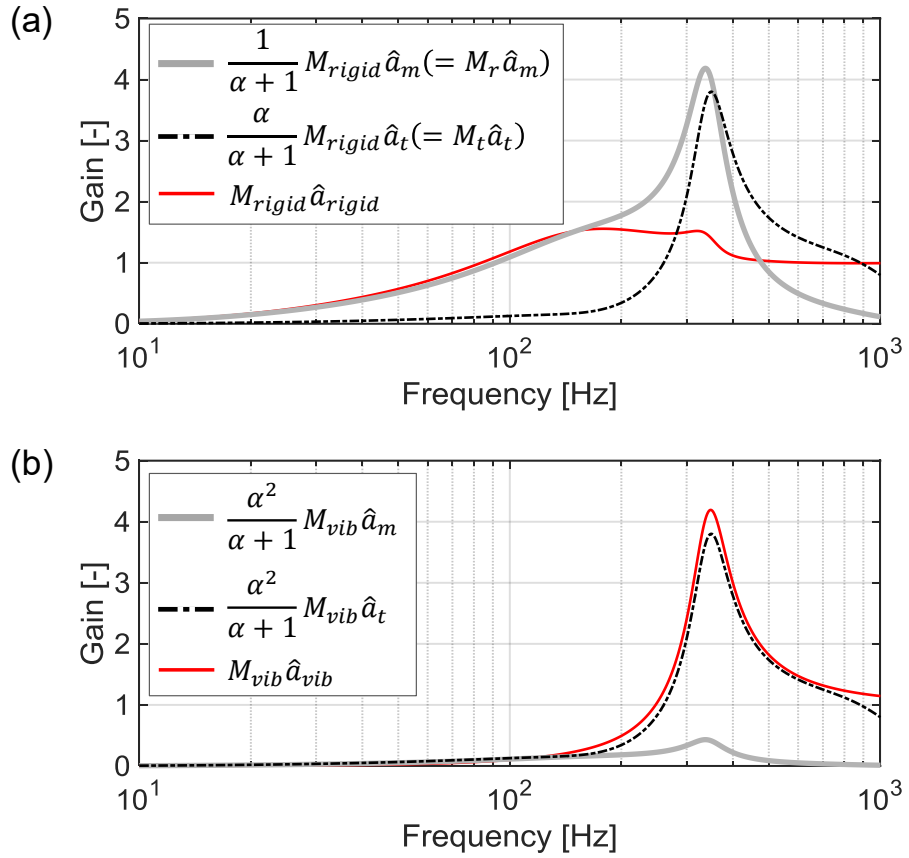

Fig. 5-10 Gain characteristics between applied load force and inertia forces in each mode (a) rigid body mode (b) vibration mode

5.2.2 Estimation characteristics against milling force

By applying the milling force to the dual-inertia mode plant in the simulator, estimation characteristics against milling force were confirmed as in the case of MEDOB-based method. In section 4.2.3, estimation characteristics were evaluated at condition #1 ~ #4. In order to keep conciseness, estimation characteristics at condition #1 and #2 were evaluated in this section, where the cutting forces were intermittent.

Estimation results at condition #1 are shown in Fig. 5-11. As suggested from frequency responses of the observer shown in the last section, identification error of the stiffness is the most influential factor in this cutting condition. Compared with the result of MEDOB-based method shown in Fig. 4-14 (a) and Fig. 4-15 (a), both phase lag elements and resolution of the rotary encoder are less influential on estimation accuracy of the cutting force.

In Fig. 5-12, estimation results at condition #2 are presented. As shown in Fig. 5-12 (a) and (d), the identification error of the movable mass and the stiffness distorts the estimated cutting force, and makes it difficult to distinguish whether the process is in

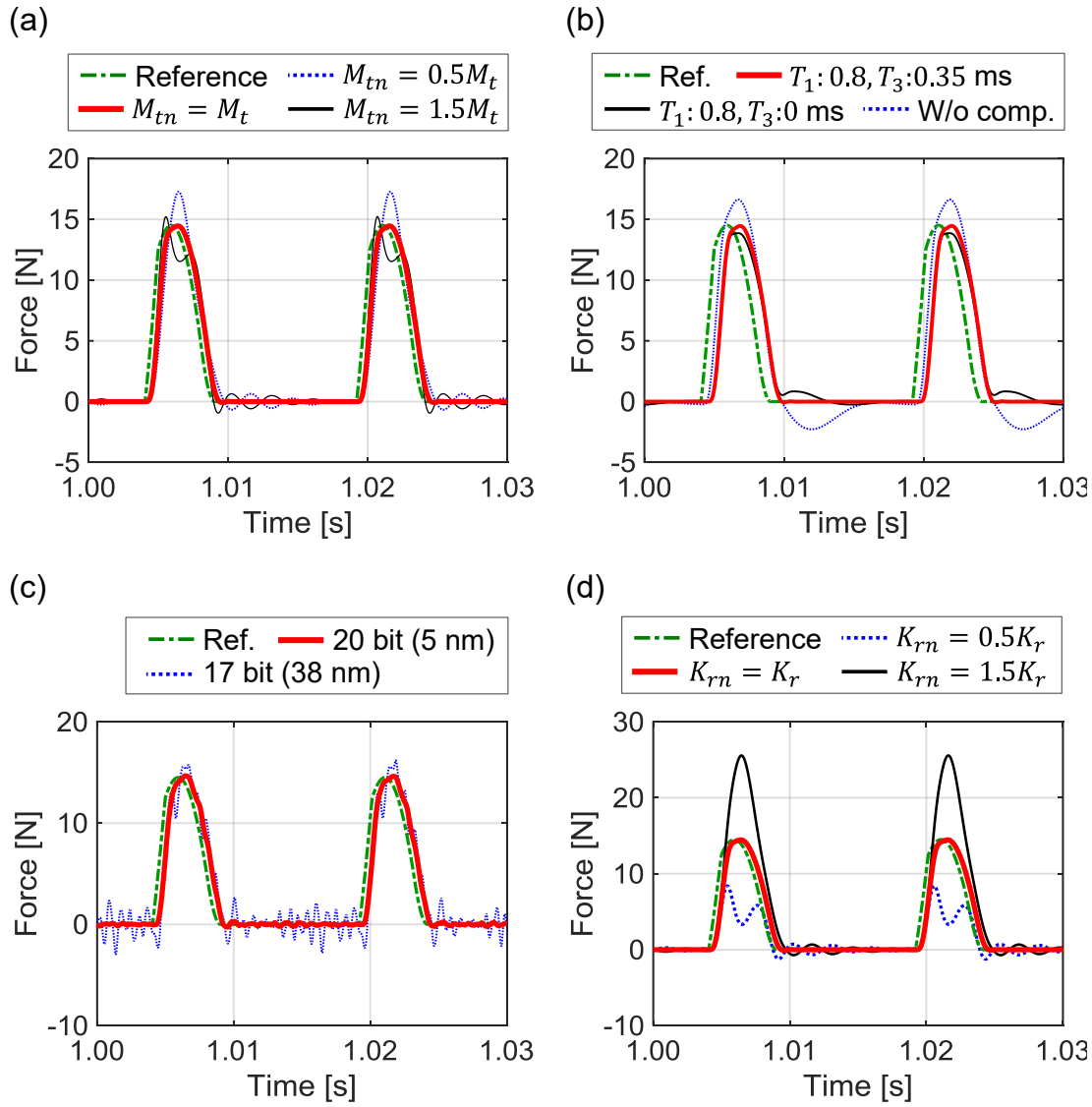

Fig. 5-11 Estimation results of milling forces responding to error factors at condition #1 (a) movable mass M_t (b) synchronization errors (c) resolution of rotary encoder (d) axial stiffness K_r

cutting or out of cutting. Even if the spindle speed increases, both phase lag elements and resolution of the rotary encoder are less influential on the estimation accuracy compared with the MEDOB-based method.

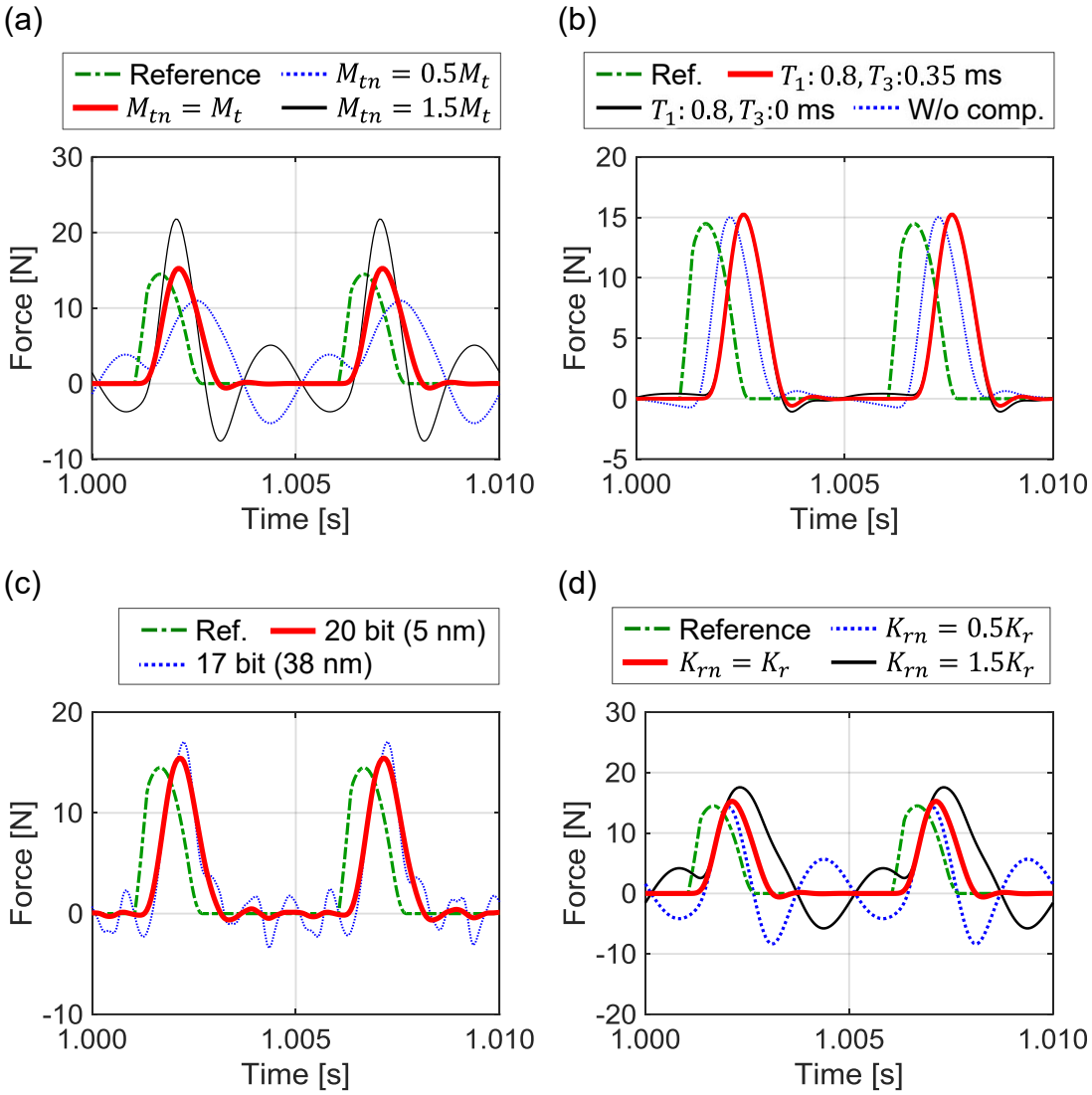

Fig. 5-12 Estimation results of milling forces responding to error factors at condition #2 (a) movable mass M_t (b) synchronization errors (c) resolution of rotary encoder (d) axial stiffness K_r

5.3 Position-dependent characteristics of relative displacement between motor and stage

Fig. 5-13 shows the relative displacement between the motor and the stage responding to position of the stage. As in the case of the motor thrust force, the relative displacement also varies depending on the position of the table, while it has repeatability. The relative displacement for the 1st data is analyzed in wavelength domain, and the result is shown in Fig. 5-14. In contrast to the motor thrust force, periodical fluctuations depending on the lead of the ball-screw (5.0 mm) and its harmonics are dominant. Therefore, estimated cutting force in the vibration mode may be distorted and fluctuate with a period of 5 mm when the periodical fluctuations are not compensated properly. As shown in Fig. 5-15,

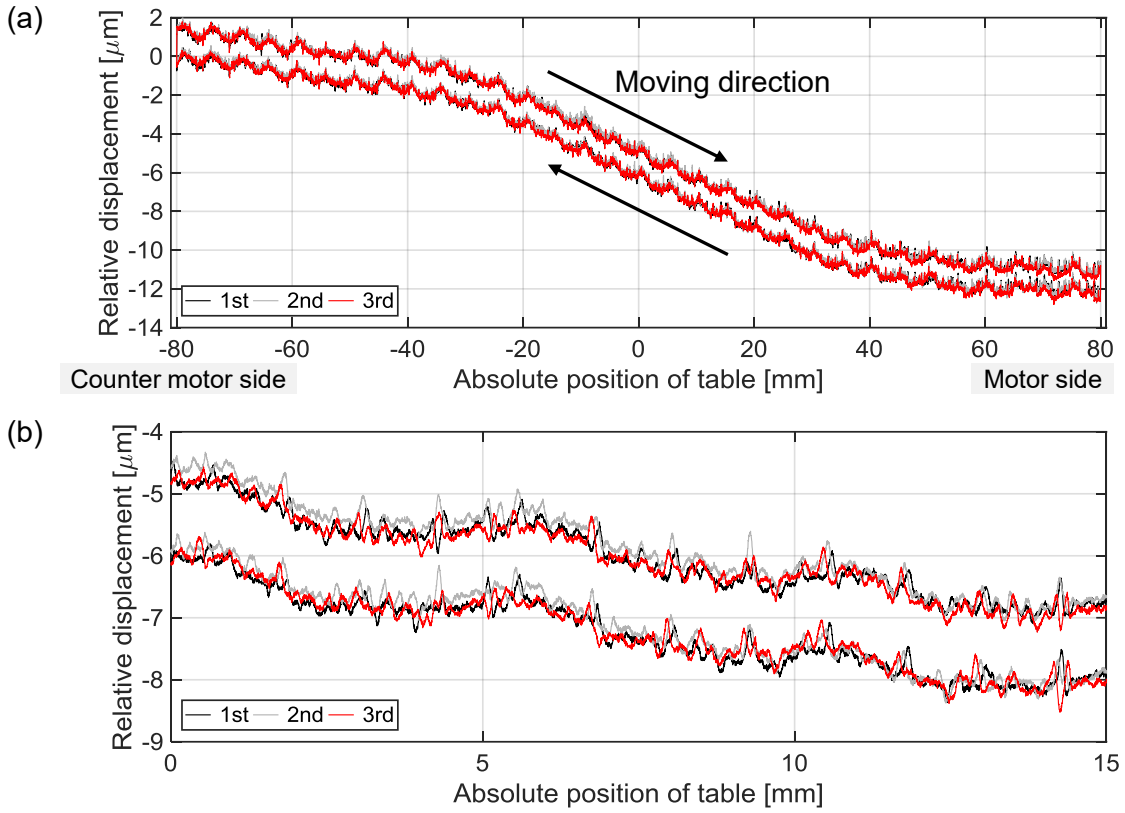

Fig. 5-13 Position dependent characteristics of relative displacement between motor and stage in Machine B at 5 mm/s (a) overall view (b) expanded view

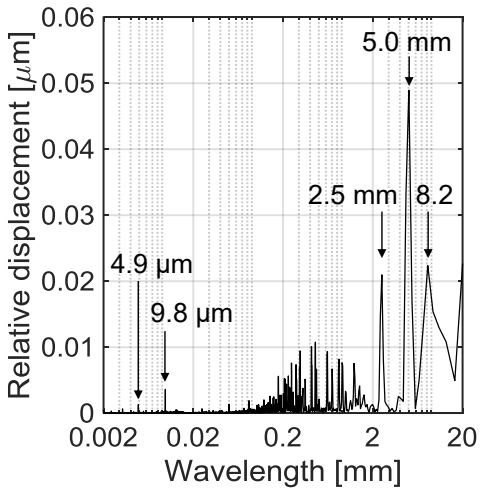

Fig. 5-14 Wavelength analysis result of relative displacement at 5 mm/s in Machine B

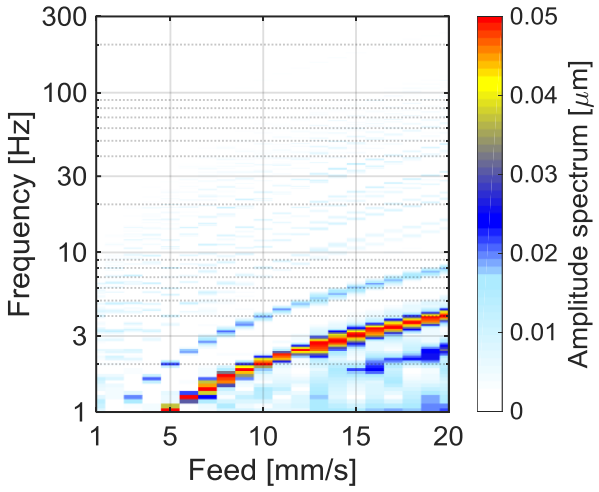

Fig. 5-15 Frequency analysis result of relative displacement at different feed rates in Machine B

fluctuations with a period of 5 mm are the most dominant at various feed rates. On the other hand, the frequency of the 5 mm-per fluctuations is low (e.g. 4 Hz at 20 mm/s) compared with that of the cutting force. Therefore, the 5 mm-per fluctuations little influence on estimation accuracy for the variable components of the cutting force.

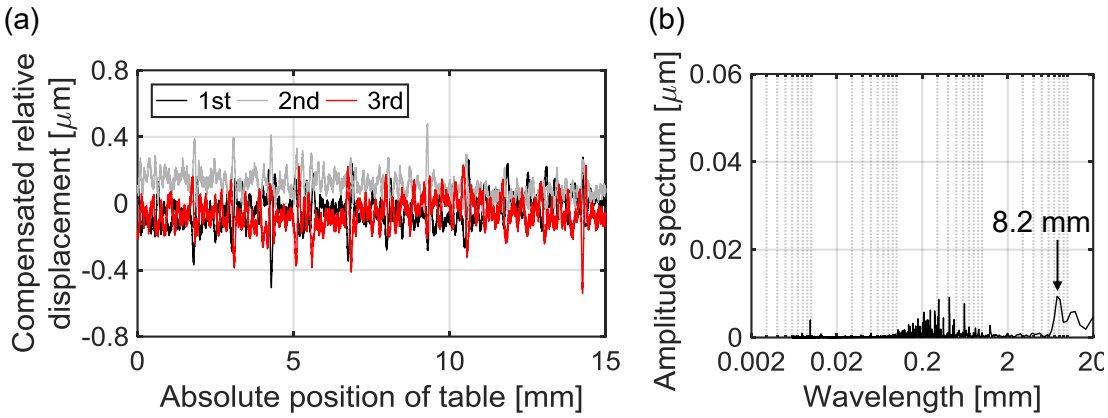

Fig. 5-16 Compensated relative displacement by average value for Machine B (a) position domain (b) wavelength domain

As for the relative displacement shown in Fig. 5-13, their mean value was calculated and is subtracted from each data depending on the stage position. The results in position and wavelength domain are shown in Fig. 5-16. As in the case of the motor thrust force, the 5 mm-per fluctuations can be eliminated as shown in the figure, while high frequency fluctuations cannot be eliminated. In addition, there are compensation errors in DC as shown in the 2nd result of the compensated relative displacement in Fig. 5-16. Assuming that the axial stiffness is 40.5 N/μm and compensation error of the relative displacement is 0.2 μm, the compensation error in force domain is 8.1 N. It is difficult to perfectly suppress the compensation error, which directly leads to estimation error of the cutting force.

5.4 Experimental evaluation through end milling tests

5.4.1 Estimation result for feed force component

Firstly, estimation performance of the feed force component was evaluated. In this section, the cutting force estimation in the vibration mode was evaluated by using the same data in Chapter 4. Cutting conditions are listed in Table 4-4. While the phase lag compensation and idling tests were preliminarily carried out, the notch filters were not applied for all condition, because they were unnecessary in the vibration mode.

Fig. 5-17 shows estimated and measured cutting forces at 1000 min^{-1} spindle speed and 1.5 mm radial depth of cut. As shown in the figure, the estimated value in the vibration mode can capture dynamic variation of the cutting force as well as that in the rigid body mode. In the figure, as in the case of section 4.3.2, the estimated value is shown when the disturbance force was compensated by constant value, 150 N. Since the relative displacement varied depending on the position as shown in the last section, the estimated cutting force compensated by the constant value also varied with low

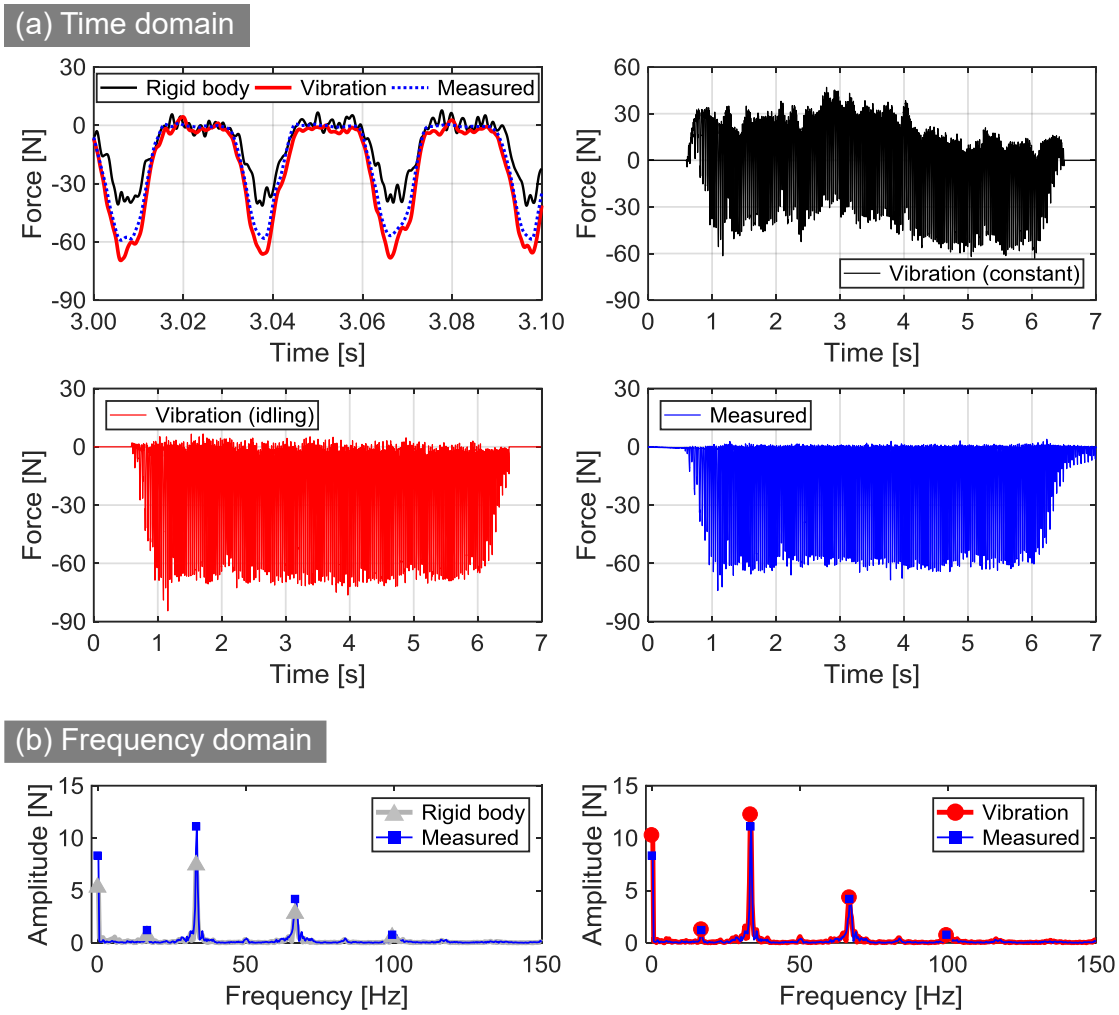

Fig. 5-17 Measured and estimated cutting forces by mode-decoupled method at 1000 min^{-1} spindle speed and 1.5 mm radial depth (a) time domain (b) frequency domain

frequency. By performing the idling test, position dependent fluctuation can be eliminated as in the case of MEDOB-based cutting force estimation. Seen from the frequency analysis result, the cutting force components can be captured by estimating in the vibration mode.

Measured and estimated cutting forces in each mode at 4000 min^{-1} and 10000 min^{-1} are shown in Fig. 5-18 and Fig. 5-19, respectively. In the rigid body mode, high frequency noises resulting from the angular measurement (409 Hz, 809 Hz, 1024 Hz) and the torsional mode (778 Hz) are included. On the other hand, they were not included in the estimated value in the vibration mode, and the temporal variation of the cutting force can be estimated accurately. As shown in the simulation result regarding resolution of the rotary encoder, the effect of angle measurement can be reduced when the cutting force is estimated in the vibration mode.

The estimation results of the cutting force under smaller radial depth of cut (0.5 mm)

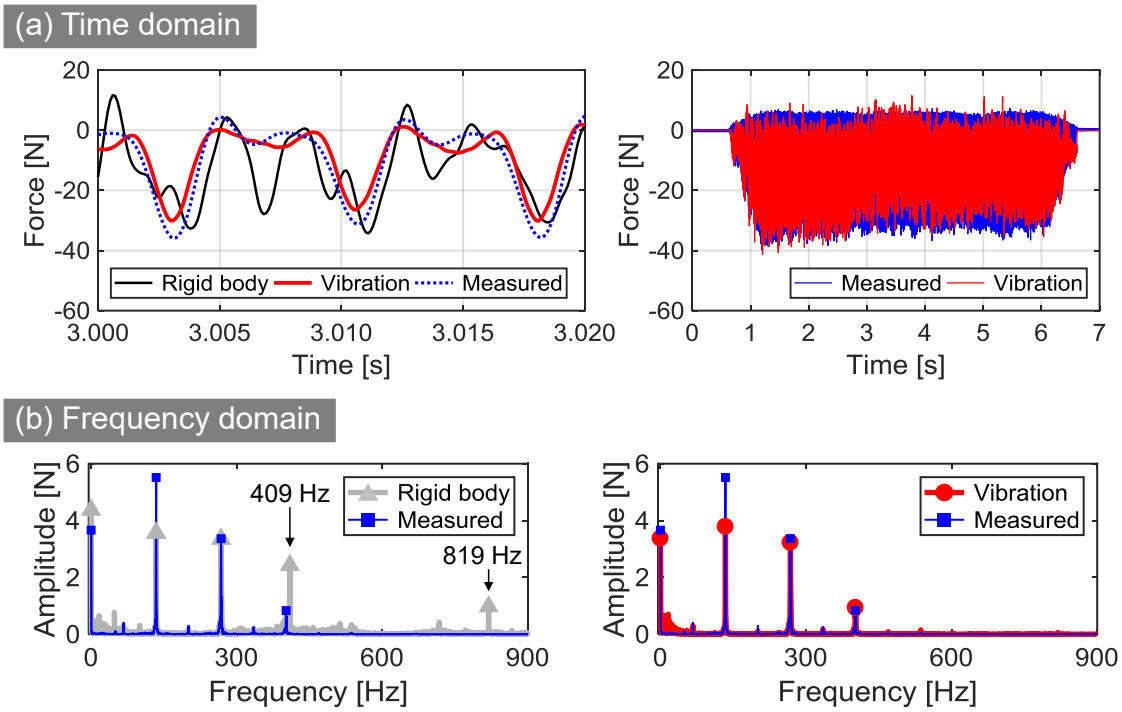

Fig. 5-18 Measured and estimated cutting forces by mode-decoupled method at 4000 min^{-1} and 1.5 mm radial depth (a) time domain (b) frequency domain

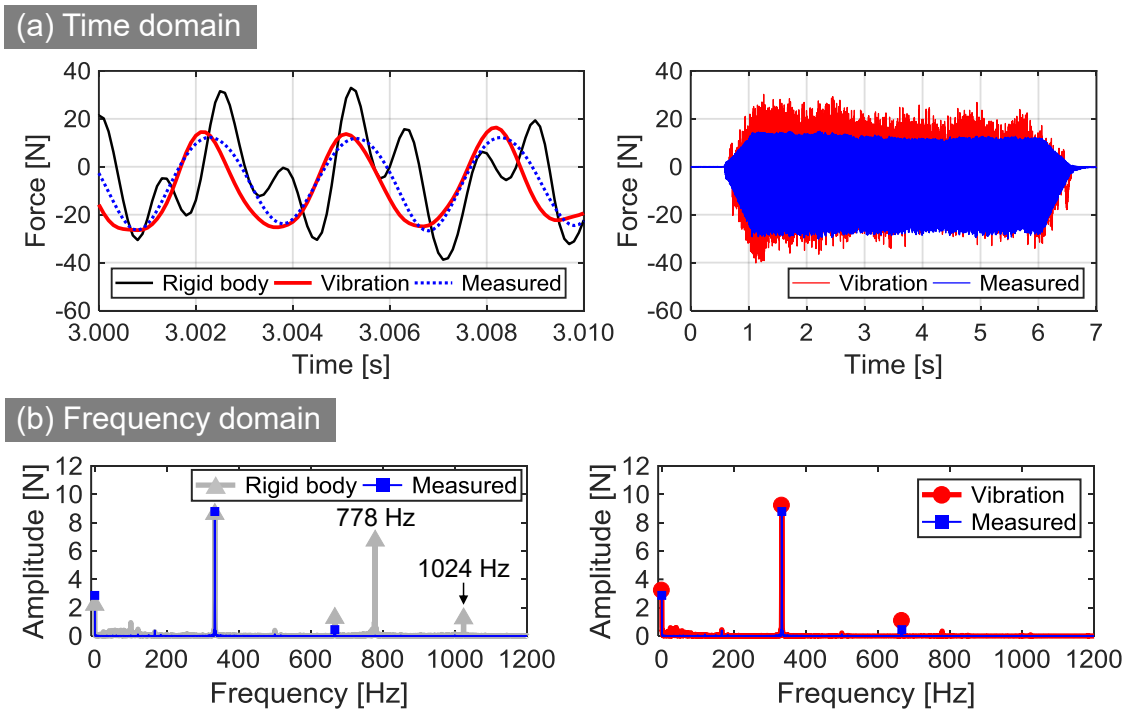

Fig. 5-19 Measured and estimated cutting forces by mode-decoupled method at 10000 min^{-1} and 1.5 mm radial depth (a) time domain (b) frequency domain

are shown in Fig. 5-20. Of all condition, the estimated cutting force in the vibration mode can capture dynamic variation of the cutting force without exciting high frequency noises.

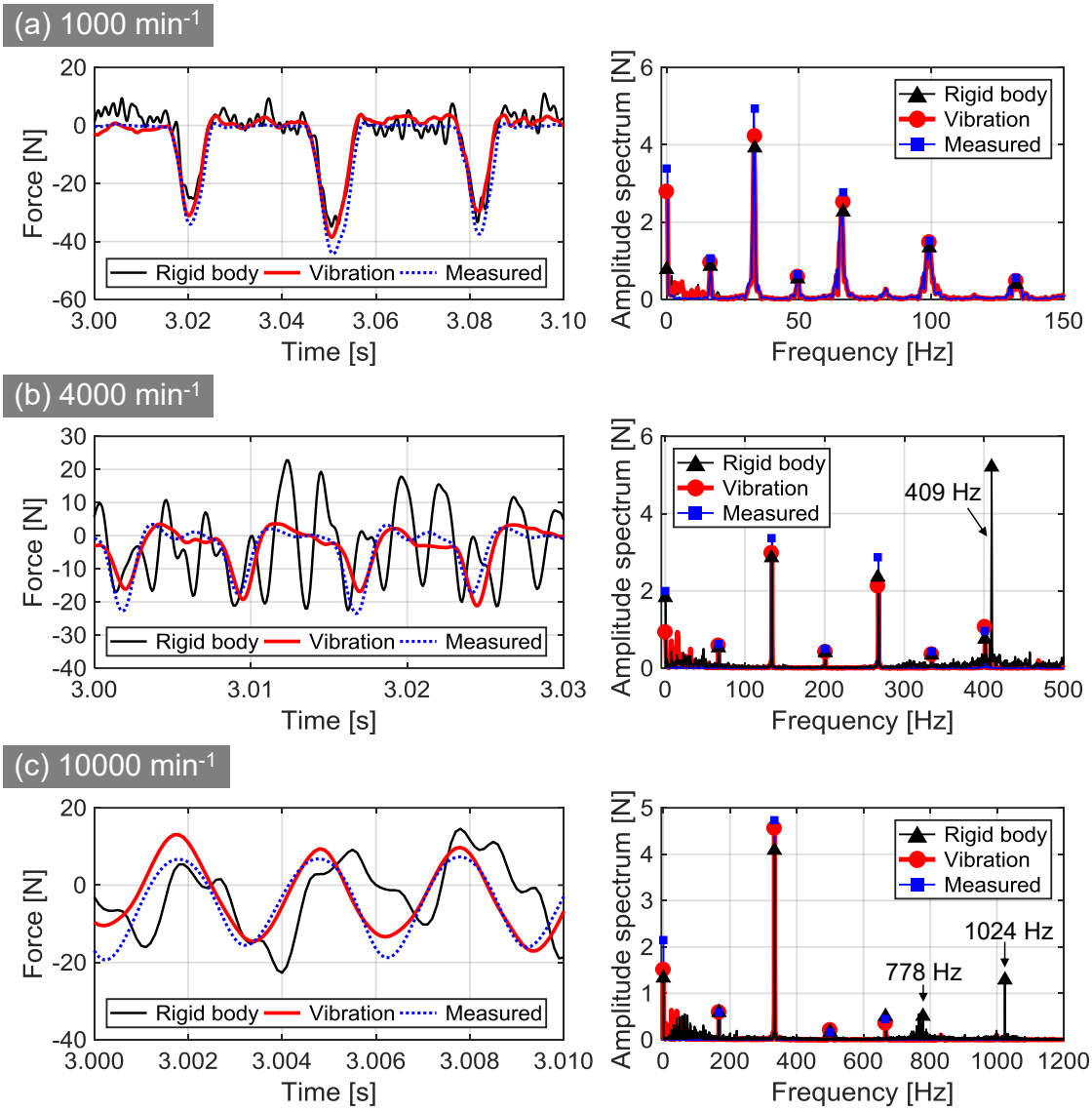

Fig. 5-20 Measured and estimated cutting forces by mode-decoupled method at 0.5 mm radial depth of cut (a) 1000 min-1 (b) 4000 min-1 (b) 10000 min-1

The standard deviations of the estimation error by the mode-decoupled method are summarized in Fig. 5-21. In the figure, the standard deviation of the compensated disturbance force in the vibration mode is denoted as “Idling” in the graph legend, which indicates the inevitable estimation error of the cutting force. In most condition, the standard deviation in the vibration mode was less than or comparable to that in the rigid body mode with notch filters. The relative motion-based estimation technique is also valid approach for monitoring the dynamic cutting force as well as the MEDOB-based estimation technique.

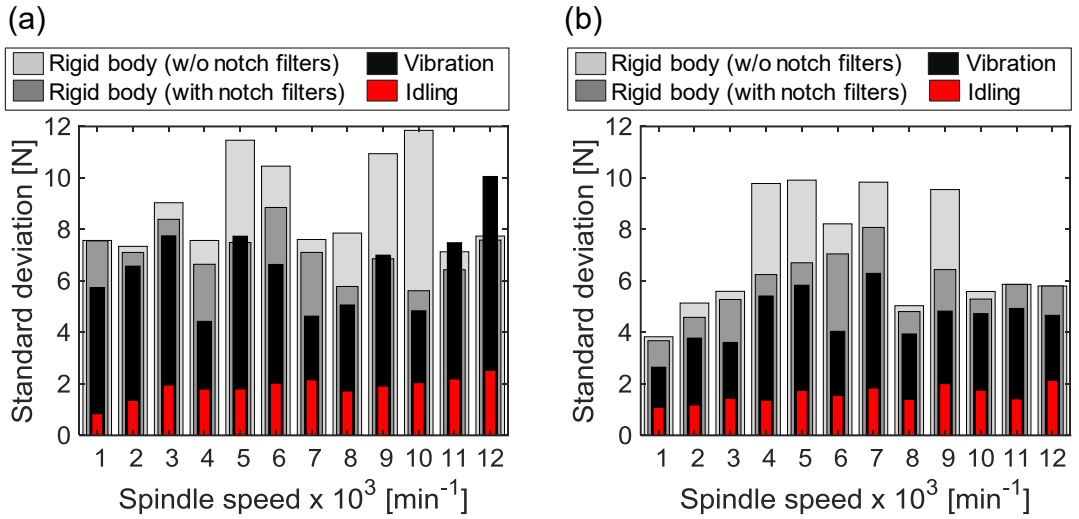

Fig. 5-21 Standard deviation of estimated cutting forces by mode-decoupled method (a) radial depth: 1.5 mm (b) radial depth: 0.5 mm

Table 5-1 Cutting conditions for cross-feed force estimation tests

Axial depth of cut [mm]	2.0	2.0	0.5
Radial depth of cut [mm]	1.5	0.5	6.0
Milling type	Down	Down	Full immersion
Spindle speed [min^{-1}]	1000 ~ 12000		
Feed per tooth [mm/tooth]	0.030		
Tool diameter [mm]	ϕ 6.0		
Number of flute	2		
Material of workpiece	Al alloy (A5052)		

5.4.2 Estimation result for cross-feed force component

In this section, estimation performance of the cross-feed direction component of the cutting force was evaluated. In the cutting tests, the Y-stage was moved, while the X-stage was commanded to fix, and the cutting force component in X-axis direction was monitored. Cutting conditions are listed in Table 5-1. In contrast to the estimation of the feed force component, the idling test was not conducted. The reason will be explained later in this section.

The measured and estimated cutting forces at 1000 min^{-1} spindle speed and 1.5 mm radial depth of cut are shown in Fig. 5-22. In the rigid body mode, the estimated cutting force was far from the measured cutting force. In addition, temporal variation in response to tooth-pass was not reflected to the estimated value. On the other hand, in the vibration mode, the cross-feed components could be estimated as well as the feed force components.

The large estimation error in rigid body mode was attributed to the response of the motor thrust force. Fig. 5-23 shows the motor thrust forces in cutting and idling tests in

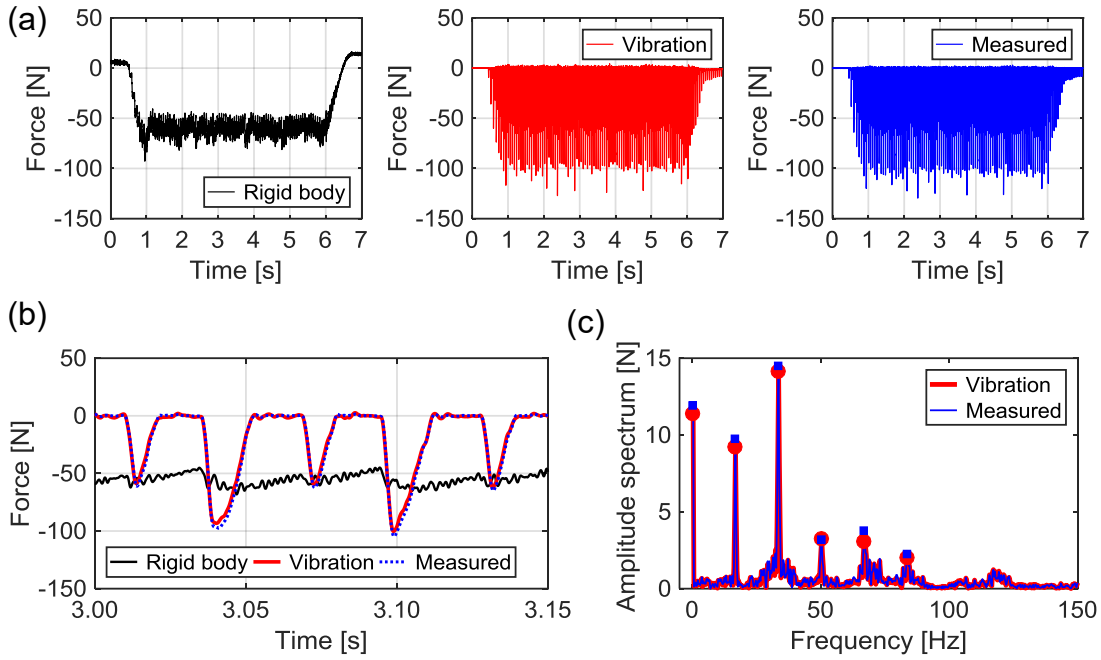

Fig. 5-22 Measured and estimated cutting forces in cross-feed direction with 1000 min^{-1} spindle speed and 1.5 mm radial depth of cut (a) overall view (b) expanded view (c) frequency analysis result

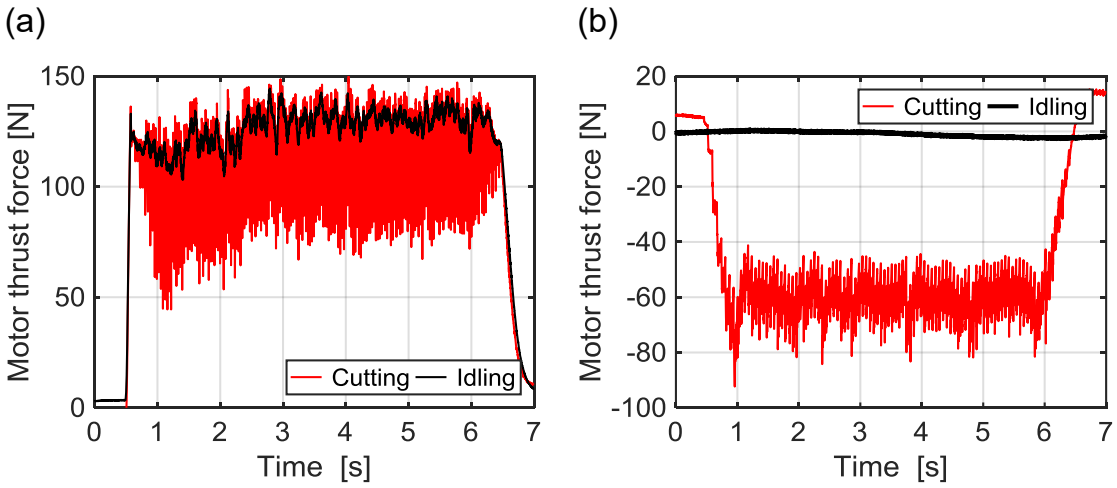

Fig. 5-23 Comparison of motor thrust force in X-axis at 1 mm/s feed rate, 1000 min^{-1} spindle speed, and 1.5 mm radial depth (a) feed direction (b) cross-feed direction

X-direction. As shown in Fig. 5-23 (a), the motor thrust forces in cutting and in idling were partially overlapping because of their high repeatability and position dependency. In this case, a motor thrust force of around 130 N was supplied in order to keep feed motion without stopping. Therefore, the total kinetic friction force of the X-stage was assumed to reach approximately 130 N. Fig. 5-23 (b) shows the cross-feed component of the motor thrust force under the same condition as Fig. 5-22. As shown in the figure, the motor thrust force was massed around -60 N during cutting and was smaller than the kinetic friction force of the X-stage. It is obvious that the motor thrust force in cross-feed

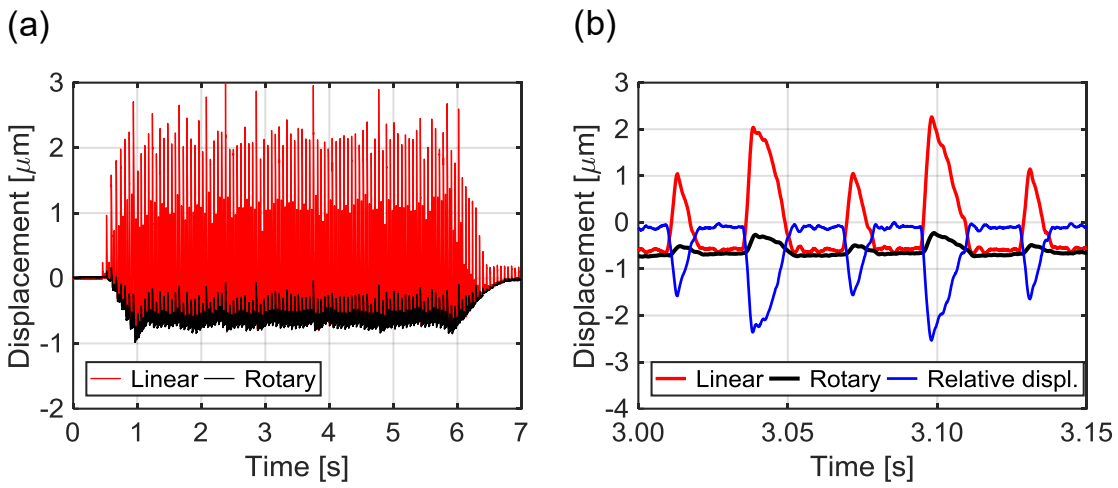

Fig. 5-24 Comparison of position response in cross-feed direction at 1000 min^{-1} spindle speed and 1.5 mm radial depth of cut (a) overall view (b) enlarged view

direction is subjected to the static friction force in the cutting test. The cutting force components in cross-feed direction is canceled out by the friction force, and it is not reflected to the motor thrust force [42]. Therefore, it is difficult to estimate the cross-feed components in rigid body mode. According to the literature [30], it is possible to estimate the cutting force by utilizing frequency analysis, when the cross-feed component of the cutting force is larger than the static friction force. However, the measured cutting force in cross-feed direction was less than the maximum static friction force. The previous study suggested difficulty of estimating the cross-feed components in the rigid body mode, which is also true of conventional DOB-based cutting force estimation. In the vibration mode, it is possible to estimate cross-feed component of the cutting force even if the cross-feed force is less than the maximum static friction force. The reason why it is possible to estimate the cross-feed components is presented in the following several paragraphs.

Fig. 5-24 shows the position response in cross-feed direction from the rotary and the linear encoders. The waveform of the angle response in Fig. 5-24 (a) was similar to that of the motor thrust force during cutting shown in Fig. 5-23 (b). While the variation of the motor angle was comparatively small, a large position variation was observed at the stage near the cutting point. In Fig. 5-24 (b), the relative displacement between the motor and the stage is presented in addition to the motor and the stage response. Seen from the figure, the waveform of the relative displacement is similar to the cutting force shown in Fig. 5-22 (b), which indicates that the relative displacement captured the dynamic variation of the cutting force. The cutting force components can be monitored when employing LDOB which uses the relative displacement. The estimation results by LDOB almost coincides with that in the vibration mode at the condition where the spindle speed and the inertia ratio are low, which was confirmed experimentally.

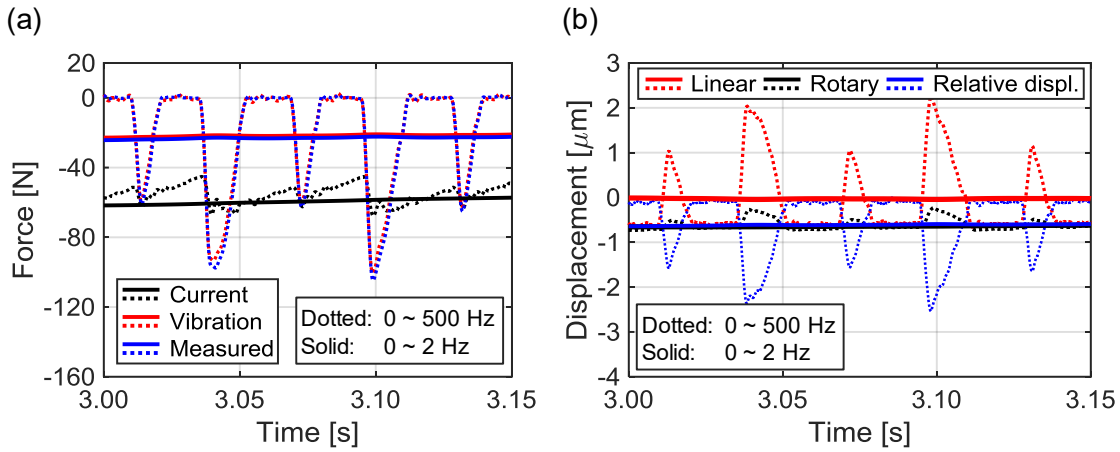

Fig. 5-25 Comparison of cutting forces and position responses responding to cutoff frequency of LPF (a) measured and estimated cutting forces (b) position responses (DC component of angular response almost coincides with that of relative displacement)

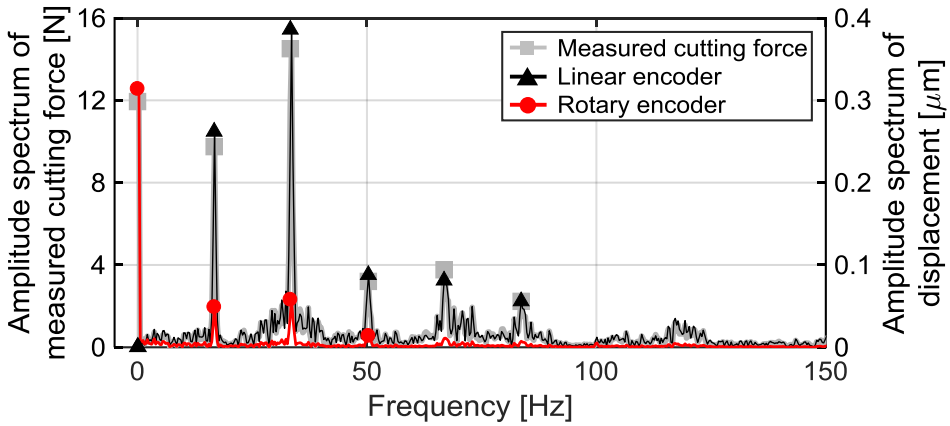

Fig. 5-26 Frequency analysis result of measured cutting force and position responses

DC components of the cutting forces and position responses are extracted by applying LPF with cutoff frequency of 2 Hz, and the results are presented in Fig. 5-25. In contrast to the monitoring of the feed force components, the current reference could not extract DC component of the cutting force in cross-feed direction as shown in Fig. 5-25 (a). DC components of the position responses are presented in Fig. 5-25 (b). Since the position response from the linear encoder was fed back to the controller and the stage position was commanded to keep zero position, DC component of the stage response was also kept zero. DC component of the cutting force provided both the angular response and the relative displacement with deviations from zero position. Thus, it is possible to approximately estimate DC component of the cutting force by using the angular response and stiffness value of the dual-inertia system K_r (e.g. 24.3 N = 40.5 N/μm × 0.60 μm). However, AC components of the cutting force less transmits to the angular response than the position response. Fig. 5-26 shows frequency components included in measured

cutting force, the position, and the angular responses. As shown in the figure, the angular response includes DC component much compared with AC components. When only using the angular response, it is difficult to reconstruct waveform of the measured cutting force. Although the position response does not include DC component, its amplitude spectrum for AC components corresponds to the amplitude spectrum of the measured cutting force. By combining table and angle responses, an accurate cutting force monitoring, including DC component, was accomplished in the vibration mode, even if the cutting force was less than the maximum static friction force.

In this cutting condition, comparatively large position error of 2 μm was evoked by the cutting force. One of the reasons is that the movable mass of the experimental setup is low (6.6 kg). Although the inertia ratio of the ball-screw-driven stage often exceeds 1, the inertia ratio of the experimental setup is 0.08. In the experimental setup, therefore, position variation of the stage was readily evoked by cutting load compared with general NC machine tools. The other reason is that position and velocity gains of the controller are not sufficiently enhanced. Estimation performance of the cutting force is influenced by the gain setting. For example, stronger high frequency variations resulting from the interpolation error of the encoder are observed when the gain value increases. However, this study focuses on design of observer and error factor in the control signals rather than influencing factors outside of the observer, such as gain setting. Thus, the influence of the gain setting is not evaluated with integrative manner in this study.

Estimation results of the cutting forces at another radial depth of cut are shown in Fig. 5-27 and Fig. 5-28. The estimated value in the rigid body mode could not capture dynamic variation of the cutting force. On the other hand, cutting force components could be estimated accurately in the vibration mode. When the frequency of the cutting force is comparatively low, the elastic force mostly occupies the estimated cutting force as explained in the simulation section. This is why the waveform of the relative displacement corresponds to that of the estimated cutting force in the vibration mode. By comparing the relative displacement and the measured cutting forces in cross-feed direction at low spindle speed, the stiffness value in the vibration mode can be experimentally determined. In this regard, synchronization error between angle and position signal should be minimized.

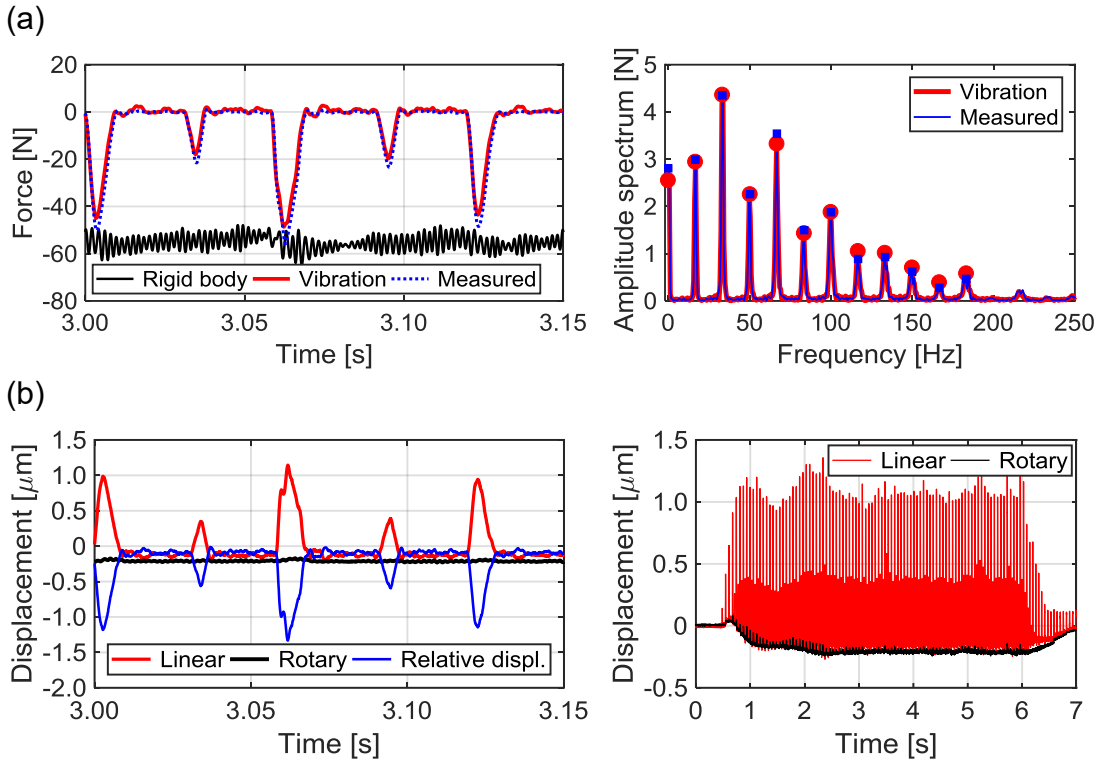

Fig. 5-27 Comparison of estimated cutting force and position response at 1000 min^{-1} and 0.5 mm radial depth (a) estimation result of cutting force (b) position response

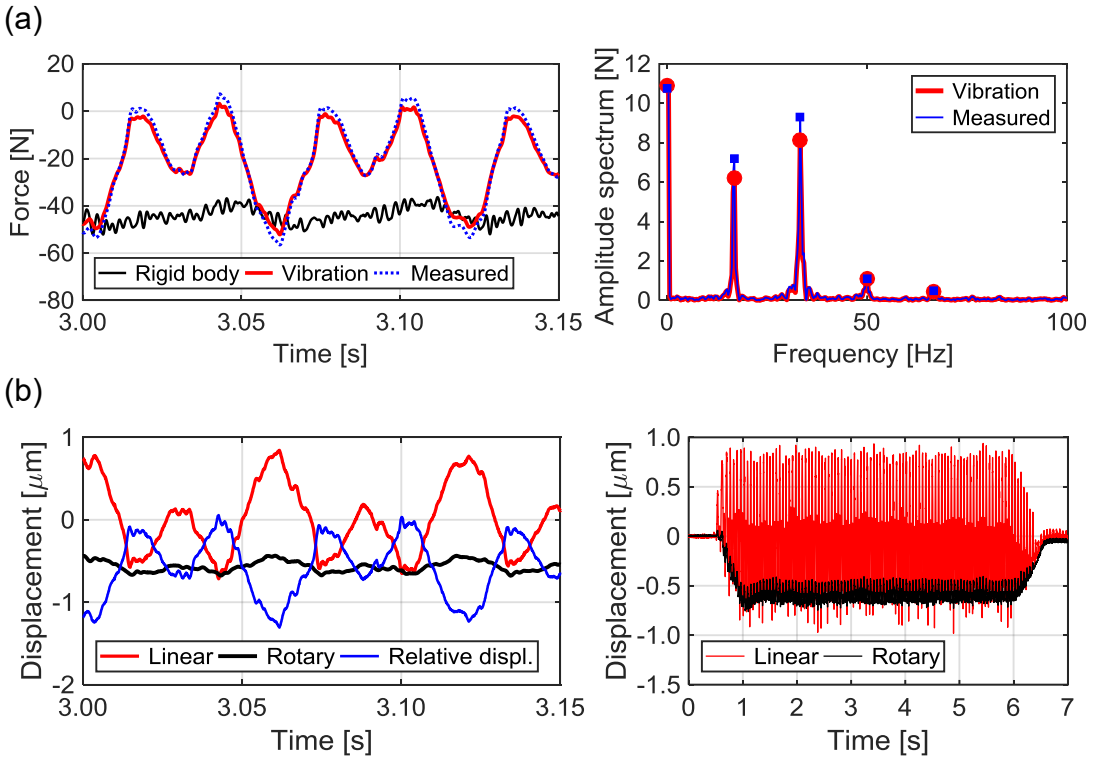

Fig. 5-28 Comparison of estimated cutting force and position response at 1000 min^{-1} and 6.0 mm radial depth (a) estimation result of cutting force (b) position response

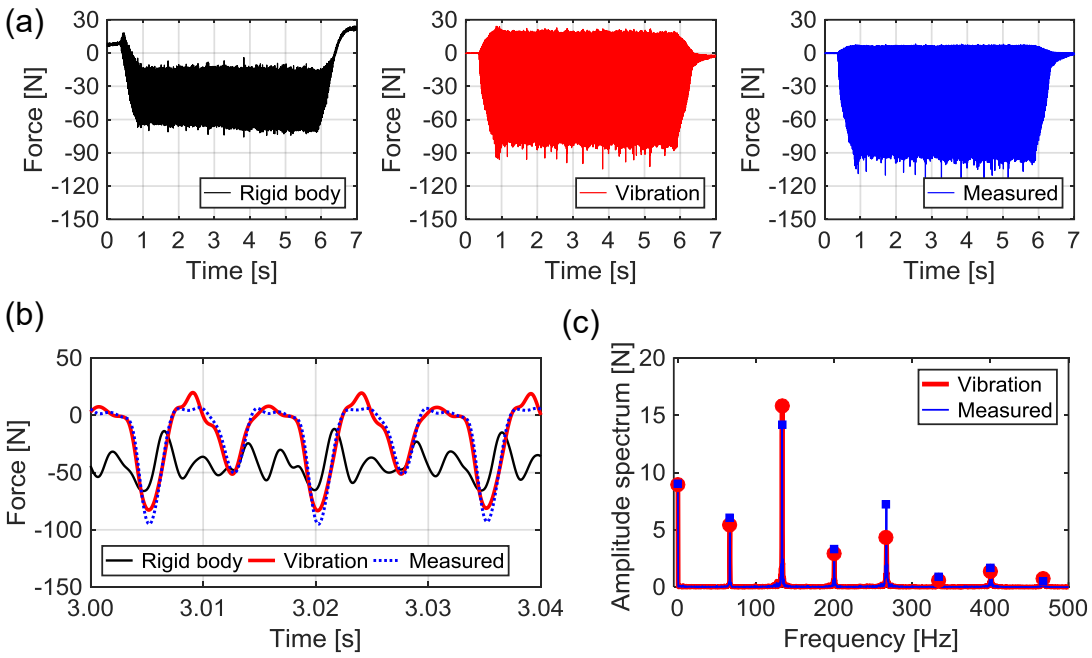

Fig. 5-29 Measured and estimated cutting forces in cross-feed direction with 4000 min^{-1} spindle speed and 1.5 mm radial depth of cut (a) overall view (b) expanded view (c) frequency analysis result

When the feed motion was applied to the stage, as mentioned before, the motor thrust force and the relative displacement periodically fluctuated depending on the rotation/position. However, the periodical fluctuation did not influence the estimation performance in cross-feed direction, because the stage was commanded to fix in the cutting tests. Cutting force monitoring in vibration mode can offer higher estimation accuracy in cross-feed direction than in feed direction. When monitoring only cross-feed components of the cutting force, it was unnecessary to perform idling tests before the cutting test, which was experimentally confirmed. In this regard, the relative displacement between the motor and the stage is not changed during idling motion.

Estimation result of the cutting force at 4000 min^{-1} is shown in Fig. 5-29. In the rigid body mode, the estimated value was distorted, and its variation in response to tooth-pass was small. On the other hand, the estimated value in the vibration mode could capture dynamic variation of cross-feed components as well as that of feed force components. As shown in Fig. 5-30, the estimated value in the rigid body mode fluctuated with tooth-pass frequency (333 Hz), when the spindle speed increased to 10000 min^{-1}. However, the estimation error in DC was remarkable in the rigid body mode. The relative motion-based formulation is effective for estimating the cross-feed component. In this section, estimation performance of the cutting force by DOB is abbreviated to keep conciseness. This is because DOB cannot capture high frequency components of the cutting force as described in section 4.3.2. In addition, the current reference mostly occupies DC component of the estimated cutting force, while the cross-feed component cannot be

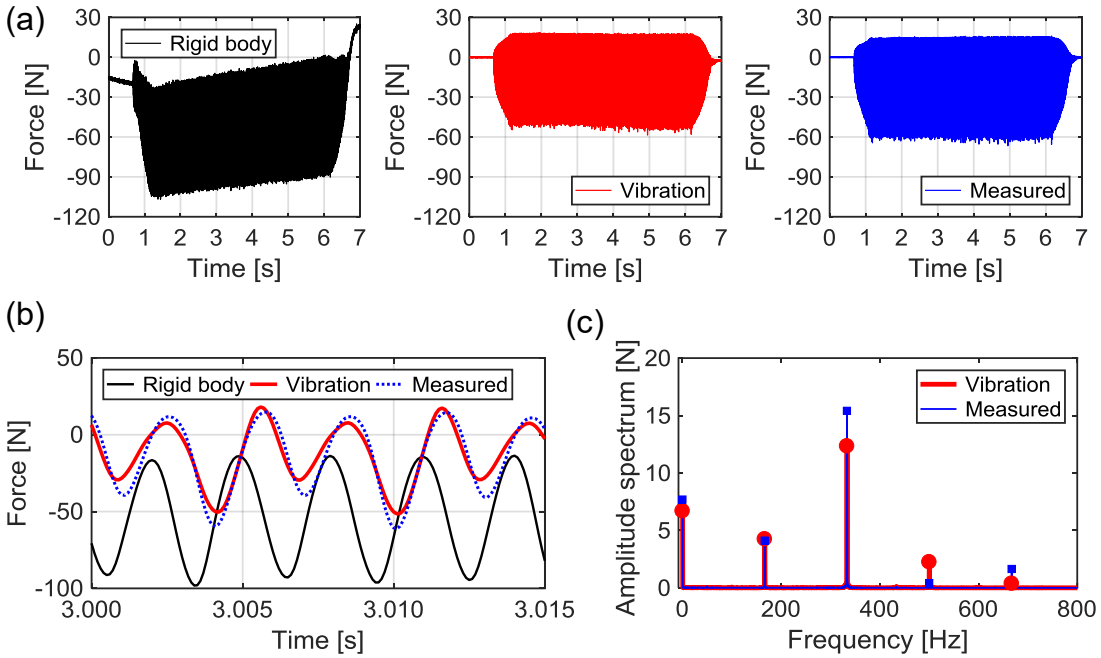

Fig. 5-30 Measured and estimated cutting forces in cross-feed direction with 10000 min^{-1} spindle speed and 1.5 mm radial depth of cut (a) overall view (b) expanded view (c) frequency analysis result

estimated by the current reference as mentioned before.

Mean value and standard deviation of the estimation error in each cutting condition are summarized in Fig. 5-31. In the figure, the standard deviation of the compensated disturbance force is not shown, because the idling test was not carried out in estimating cross-feed components. Alternatively, the standard deviation and the mean value of the measured cutting force in cross-feed direction are shown for comparison. Since the estimated value in the rigid body mode was influenced by the static friction force, the mean error of the estimated value was large. In addition, it was larger than the mean value of the measured cutting force under a lot of conditions. As presented in the above, the estimated value in the rigid body mode could not capture dynamic variation of the cutting force. The standard deviation of the estimation error in the rigid body mode was larger than or comparable to that of measured cutting force. In the vibration mode, on the other hand, both the standard deviation and mean value of the estimation errors were less than or comparable to 10 N under the evaluated cutting condition. In the vibration mode, it was possible to estimate cross-feed component less than the maximum static friction force.

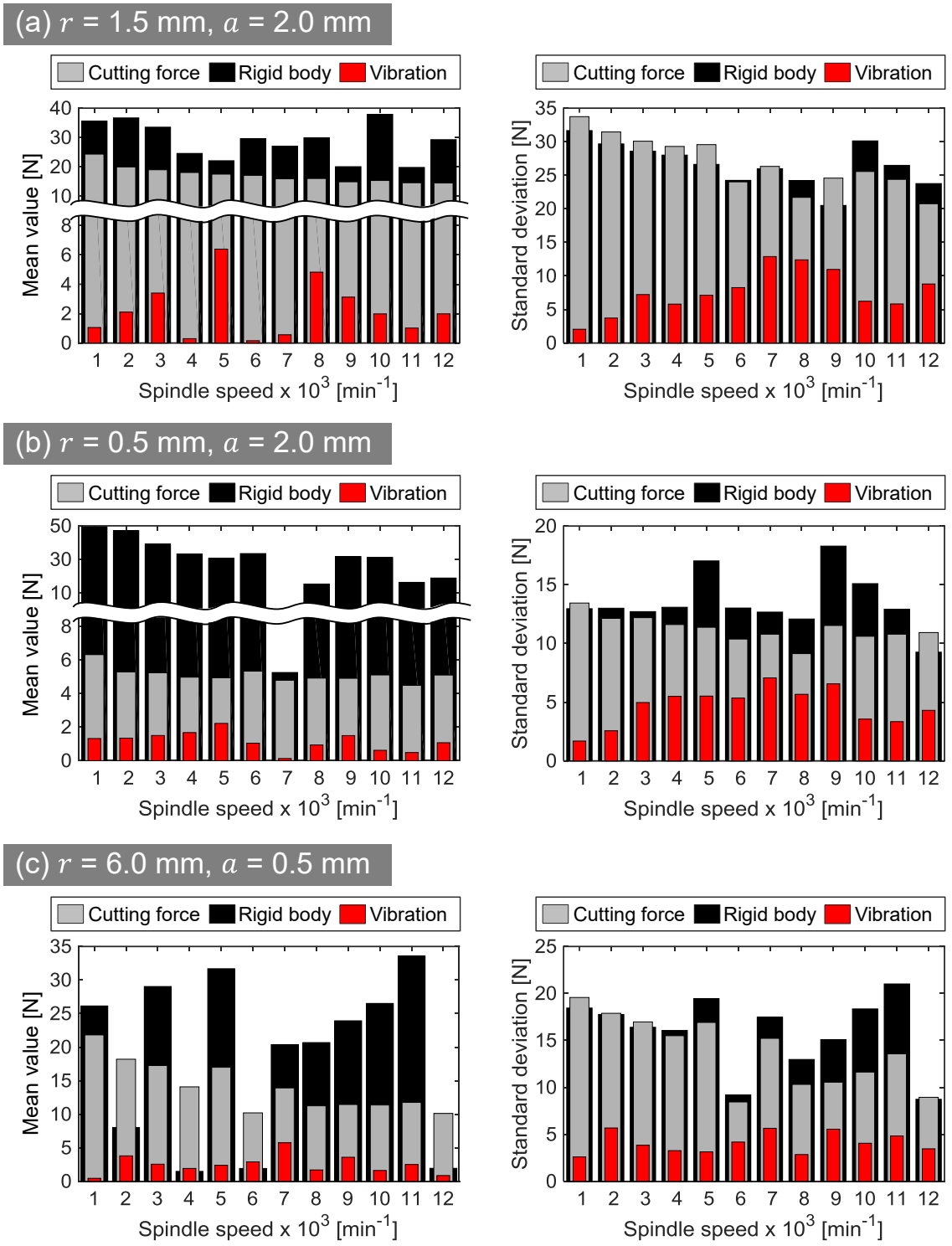

Fig. 5-31 Mean value and standard deviation of estimation error in each condition (a) radial depth: 1.5 mm, axial depth: 2.0 mm (b) radial depth: 0.5 mm, axial depth: 2.0 mm (c) radial depth: 6.0 mm, axial depth: 0.5 mm

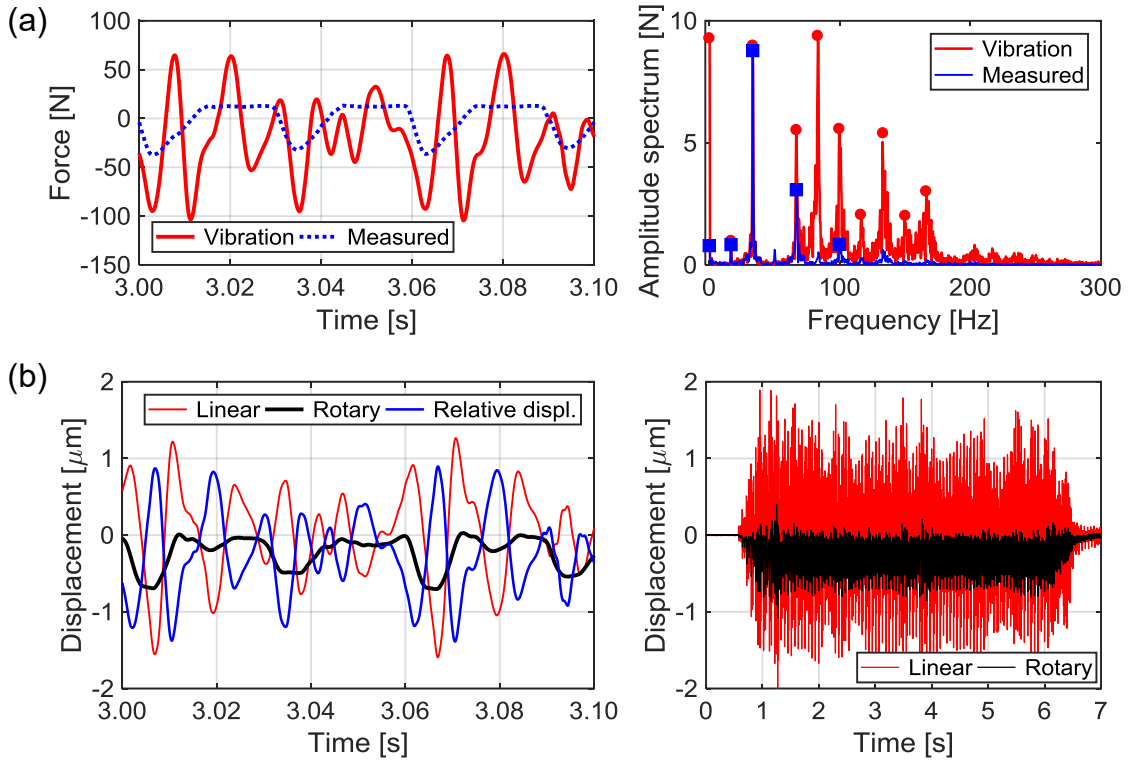

Fig. 5-32 Comparison of estimated cutting force and position response in Y-axis at 1000 min^{-1} and 1.5 mm radial depth (a) measured and estimated cutting forces (b) position response

The mode-decoupled cutting force estimation technique is applicable to the Y-axis and the Z-axis ball-screw-driven stages. Fig. 5-32 shows estimation result of cross-feed component and position response in Y-axis under the same condition as that shown in Fig. 4-19 and Fig. 5-17. The Y-axis ball-screw-driven stage equips the spindle and the Z-stage, which was regarded as the dual-inertia system. As shown in the frequency analysis result, tooth-pass frequency (33 Hz) component could be captured as well as in the case of the estimation result in X-axis. However, higher harmonics were overestimated and waveform of the estimated cutting force was apparently larger than the measured cutting force. In contrast to the estimation result in X-axis under the same spindle speed, the waveform of the measured cutting force did not correspond to that of relative displacement.

In Fig. 5-33, the estimation result and position response with full immersion milling are presented, where the process is less intermittent than the former case. As shown in the figure, the dynamic variation of the cutting force can be monitored, and the waveform of the measured cutting force corresponded to that of the relative displacement. When the frequency of the cutting force is comparatively low, it is possible to estimate the cross-feed component based on the servo information at the spindle side. However, the estimation accuracy decreased with higher spindle speed, because the presented dual-inertia model did not consider the dynamics between the tool and the stage. The

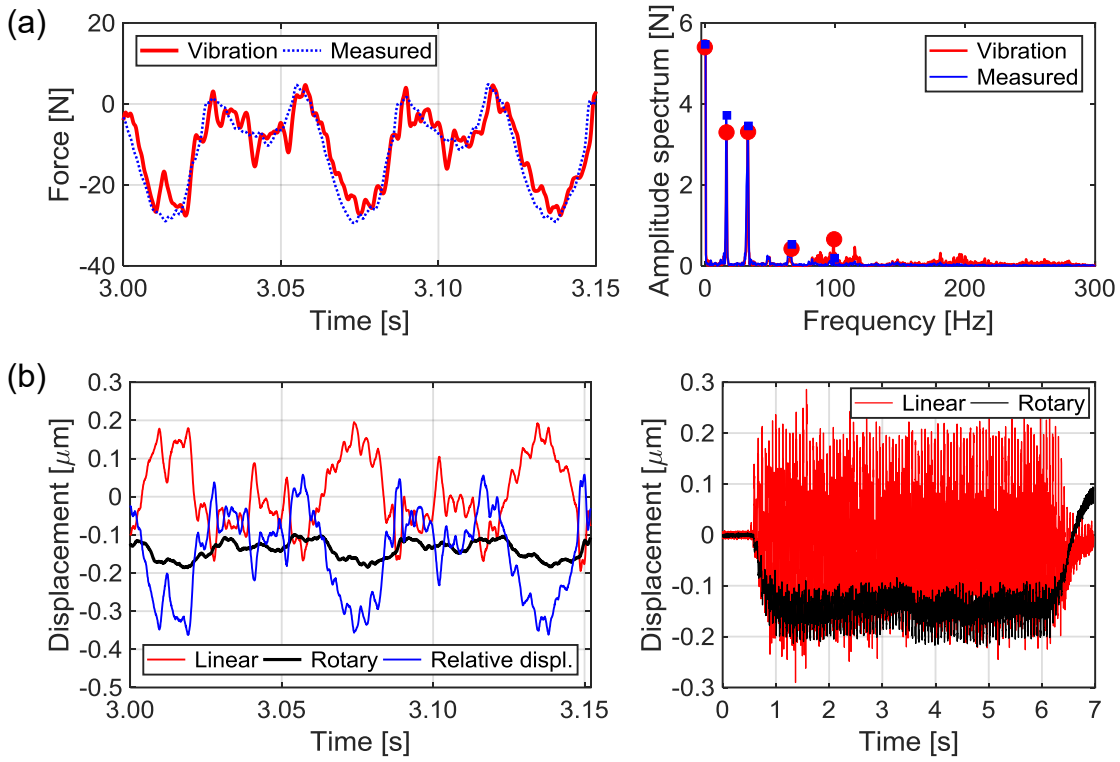

Fig. 5-33 Estimation result of cross-feed component and position response in Y-axis (spindle speed: 1000 min^{-1}, radial depth: 6.0 mm, axial depth: 0.3 mm, feed: 1 mm/s) (a) measured and estimated cutting forces (b) position response

extension to a multi-inertia model, using additional displacement/acceleration sensors, is one of the solutions.

5.5 Summary

In this chapter, the validity of the mode-decoupled method was evaluated by both time domain simulation and end milling tests, in which both feed and cross-feed components were estimated. Specifically, the estimation performance was mainly evaluated under the low inertia ratio condition. The contents are summarized as follows.

1. When the inertia ratio is low, the cutting force estimation in the vibration mode was less affected by the variation of the motor thrust force due to the disturbance force. On the other hand, the elastic force was proportionally high in a wide frequency range. Therefore, an accurate identification of the stiffness was important in the vibration mode.
2. In the vibration mode, the position dependency of the relative displacement rather than the motor thrust force can influence on the estimation accuracy of the cutting force. When the position dependent components are not properly compensated, the estimated cutting force might be distorted depending on the lead of the ball-screw

and its harmonics.

3. According to the result of the end milling tests, the temporal variation of the feed force can be estimated in the vibration mode as well as the MEDOB-based method. In the experimental setup, it is possible to decrease high frequency noises resulting from the output error of the rotary encoder owing to the relative motion-based cutting force estimation.
4. In the vibration mode, it is possible to estimate cross-feed component of the cutting force including higher harmonics, even if the cutting force is less than the maximum static friction force. In estimating the cross-feed components, the relative motion-based method is more effective than the general observer-based method. Both the standard deviation and mean value of the estimation errors were less than or comparable to 10 N under the evaluated cutting condition.

6. Monitoring and avoidance of chatter in parallel turning

6.1 Introduction

This chapter describes monitoring and avoidance of the chatter in parallel turning applying the estimated cutting force. Developed cutting force observer was implemented to actual multi-tasking machine tool. The estimated cutting force was particularly used for measuring chatter frequency during the process. Firstly, monitoring performance of chatter was evaluated between the proposed MEDOB- and the conventional DOB-based estimation method. Secondly, chatter avoidance technique by unequal pitch turning was introduced considering analogy between milling using the variable pitch tool and the unequal pitch turning. The optimum pitch angle difference between two tools can be calculated from the spindle speed and the chatter frequency. Validity of the proposed method including robustness was evaluated through several cutting tests.

6.2 Configuration of multi-tasking machine tool with multi-turret

As shown in Fig. 6-1, prototype multi-tasking machine tool (Super NTY3 from Nakamura-Tome Precision Industry Co., Ltd.) has three turrets and two work spindles. The cutting tools for parallel turning are attached to turrets 1 and 2, and each turret can move in three translational directions (X1, Y1, and Z1- axes for turret 1, and X2, Y2, and Z2- axes for turret 2). Since there is no rotational axis, posture of the turrets and the tools cannot be changed. In addition, the drive axes of each turret are not mutually perpendicular. As shown in Fig. 6-2, the X1- and X2-axes are tilted at 60 degrees from the horizontal plane. In addition, the angle between the X1- and Y1-axes is 45 degrees, as is the angle between the X2- and Y2-axes. Major specification of the multi-tasking machine tool is listed in Table 6-1. The type of guideway and drive system of each turret differ with the moving direction. The ball-screw-driven stages of the X2- and Y2-axes are connected with the servomotor through a belt, while the other stages employ mechanical coupling at the connection. An optical linear encoder (LC415, accuracy grade ±3 μm, from Heidenhain) is attached to the X1 and Y1 stages. A belt drive system is employed for the work spindle. A modular magnetic-type ring encoder (AK ERM 280, signal period approx. 400 μm, from Heidenhain) is installed inside the spindle. Control signals are generated from the motion controller (Power PMAC, from Delta Tau) shown in Fig. 6-2. Both control interval and sampling frequency are 9 kHz. For real-time chatter monitoring and

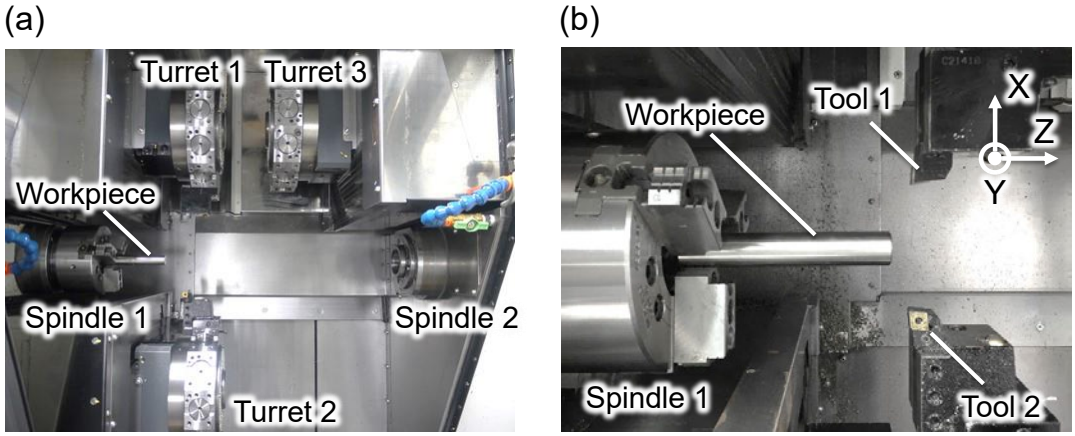

Fig. 6-1 Prototype of multi-tasking machine tool (a) front view (b) expanded view

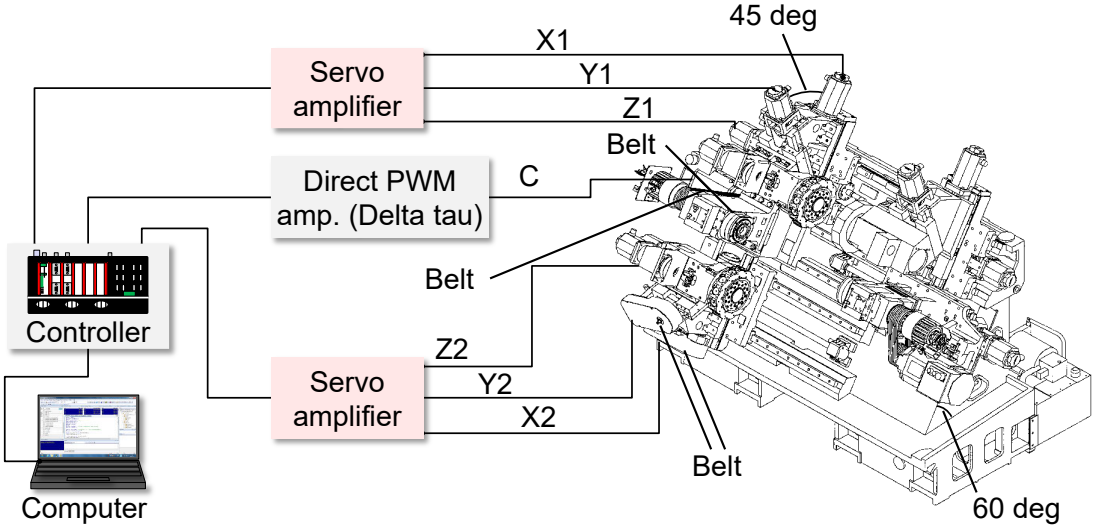

Fig. 6-2 System configuration of multi-tasking machine tool

Table 6-1 Major specification of prototype machine tool

	Unit	X1	Y1	Z1	X2	Y2	Z2	C
Type of guideway	-	Rolling	Sliding	Rolling	Rolling	Sliding	Rolling	-
Lead length	mm	8	6	12	8	6	12	-
Drive system	-	BS + coupling	BS + coupling	BS + coupling	BS + belt	BS + belt	BS + coupling	Belt
Reduction ratio	-	1	1	1	1	1	1	14/13
Resolution of encoders								
Linear encoder	nm	1	1	-	-	-	-	-
Rotary encoder	count/rev	120000	160000	80000	120000	160000	80000	262144
	nm	66.7	37.5	150	66.7	37.5	150	-
Ring encoder	count/rev	-	-	-	-	-	-	19660800

* BS: Ball-screw

avoidance, observers are placed in the control system of all axes. In the control system of X1 and Y1 stages, both DOB- and MEDOB-based cutting force observers can be implemented, because the linear encoders are attached to the stages. In real-time chatter avoidance, as explained later, the chatter frequencies were measured based on the

estimated cutting force components in Y1 direction for simplifying whole system and reducing calculation load. Therefore, discussion on chatter monitoring is limited to the result in X1 and Y1 direction in order to keep conciseness of this dissertation. The nominal parameters for the cutting force observers were determined from the designed values from the manufactures.

In the literatures [75–78], SLD was introduced based on the tool-side (i.e. turret-side) dynamics. Dynamics of the workpiece was ignored and it was modeled as rigid body. When machining slender workpiece in contrast to previous works, chatter is likely to develop due to flexibility of the workpiece rather than tool-side flexibility. Frequency response of the workpiece was measured by impacting test as shown in Fig. 6-3, and the result is presented in Fig. 6-4. As shown in the figure, the frequency of the first bending mode was 592 Hz, and that of second mode was 3611 Hz. Chatter develops around first mode rather than second mode because of the high flexibility of the first mode.

Before conducting cutting tests, the disturbance force was identified based on the idling test. The disturbance force is modeled as summation of the friction force, the friction torque in translational motion, and the gravity force. Position and velocity dependent characteristics were not considered in modeling the disturbance force, because they little influence on measurement of the chatter frequency at high frequencies.

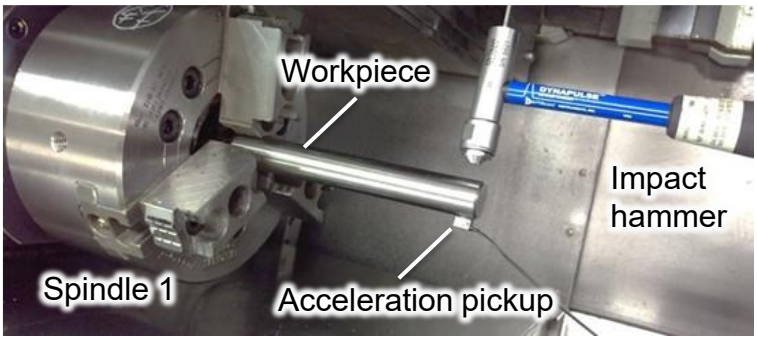

Fig. 6-3 Appearance of impacting test

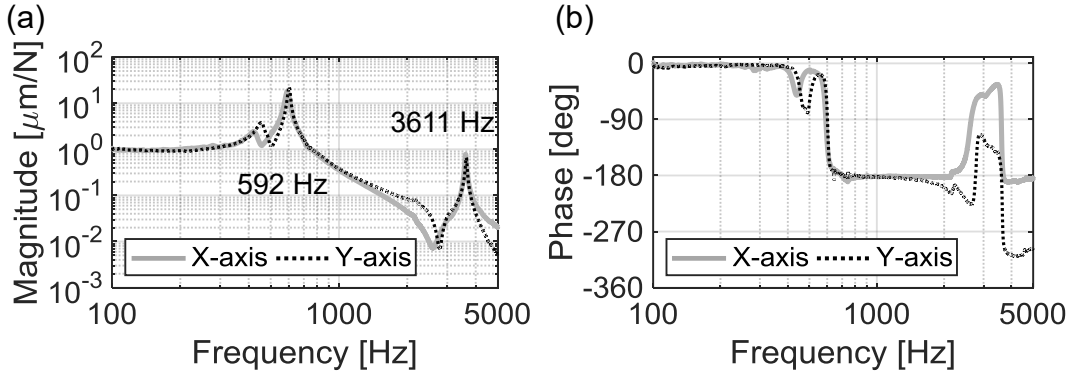

Fig. 6-4 Frequency response of cylindrical workpiece at tip (a) magnitude (b) phase

6.3 Chatter monitoring applying estimated cutting force in parallel turning

Parallel outside turning tests were performed to evaluate the monitoring of chatter. The experimental conditions are listed in Table 6-2. Both tools cut the same width. Turrets 1 and 2 were moved in the negative Z direction at constant speed, while the position remained fixed in the other directions. As shown in Fig. 6-5 (a), the tool tip positions in the Z-direction were set to equal for cutting the same surface, calibrated using a touch sensor before the cutting tests. To identify the dominant chatter frequencies, two triaxial acceleration pickups were attached behind the cutting tools. Time-frequency analysis result of acceleration response in Y1 direction is described in Fig. 6-5 (b) as an example. As shown in the figure, the most dominant chatter frequency was not constant, and shifted in response to the cutting point. While largest vibration developed in Y1 direction, the chatter frequency components were also observed in the other directions, which was confirmed.

Fig. 6-6 shows the machined surface and the estimated cutting force components in the X1 direction under chatter condition. Seen from the figure, chatter marks left on the

Table 6-2 Experimental conditions for chatter monitoring test

Spindle speed [min^{-1}]	1200
Depth of cut in each tool [mm]	0.2 (unstable), 0.3 (stable)
Feed rate [mm/rev]	0.15
Material of workpiece	JIS SUS303
Diameter of workpiece [mm]	25
Projection length [mm]	130
Cutoff frequency of a low-pass filter in cutting force observer [Hz]	1000

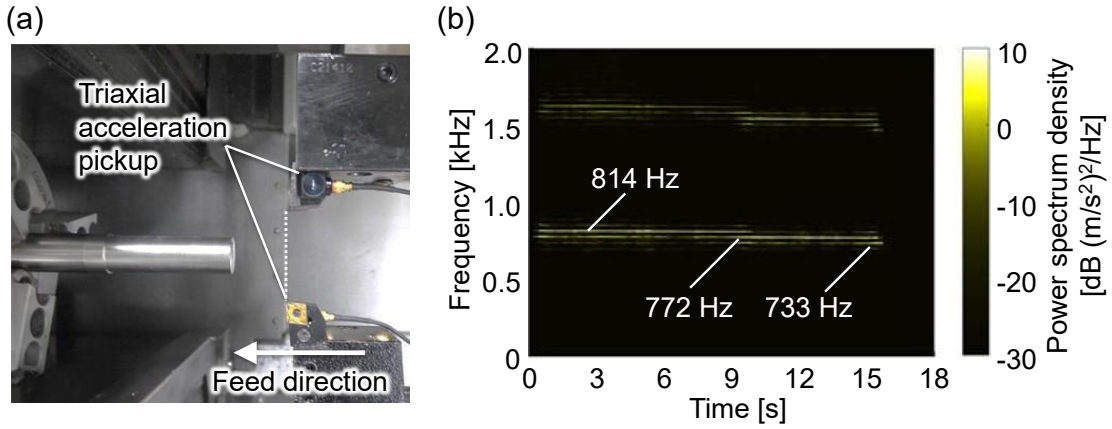

Fig. 6-5 Measurement result of acceleration response during chatter (a) attachment point of acceleration pickup (b) time-frequency analysis result in Y1 direction

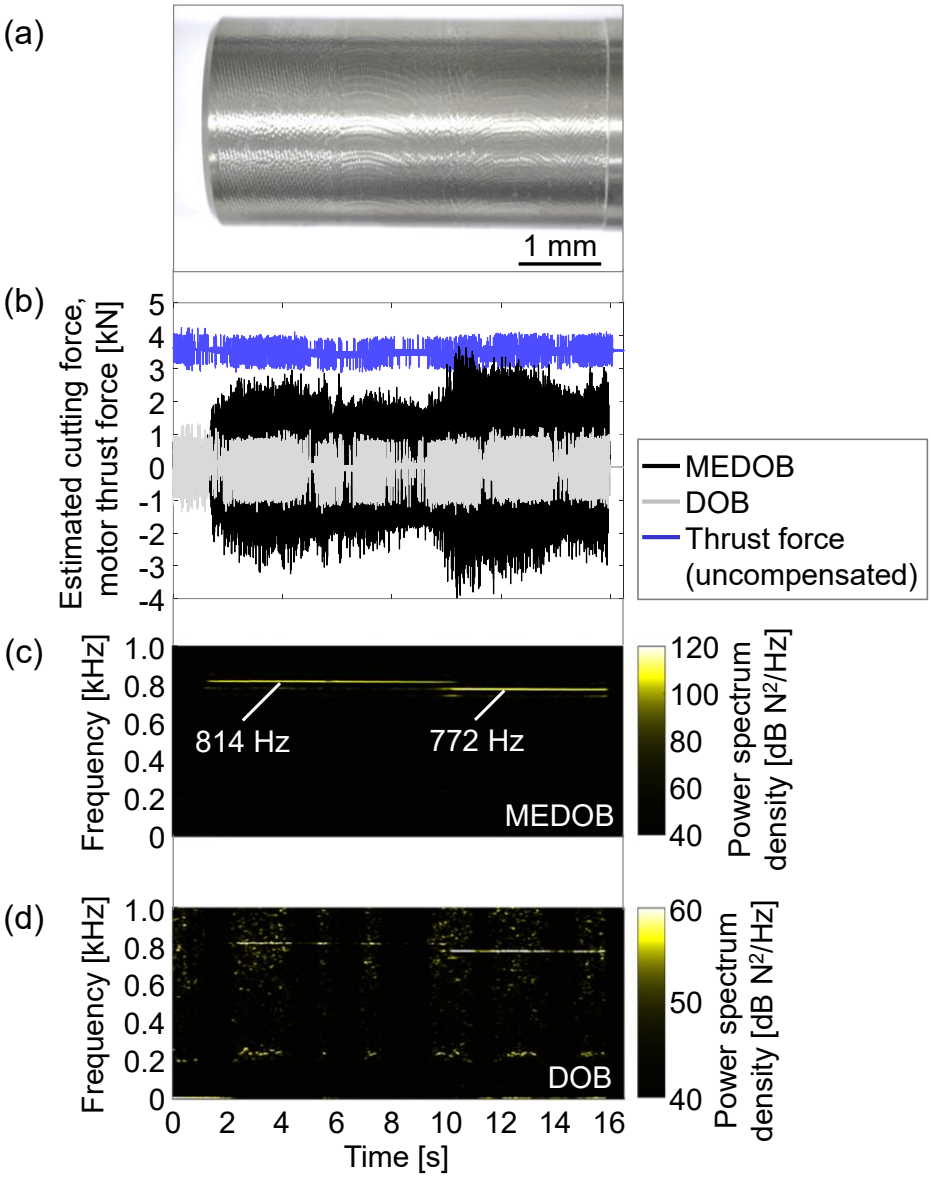

Fig. 6-6 Machined surface and experimental result in X1-axis with 0.2 mm width of cut (a) machined surface (b) time domain data of estimated cutting forces (c) time-frequency analysis result of estimated cutting force by MEDOB (d) time-frequency analysis result of estimated cutting force by DOB

machined surface change in response to the cutting point. A wavy surface results from the variation in the depth of cut, which suggests that the amplitude of the estimated cutting force should also vary in response to both the cutting points. As for the time-domain data of the estimated cutting force, dynamic variations are observed in the MEDOB-based method. In addition, the estimated value by MEDOB correlates with chatter marks left on the machined surface. On the other hand, these variations are not reflected to the time-domain data of the estimated value by DOB and the thrust force reference. The time-frequency analysis of MEDOB shows that the estimated cutting force can clearly capture the dominant chatter frequency components, as in the case of

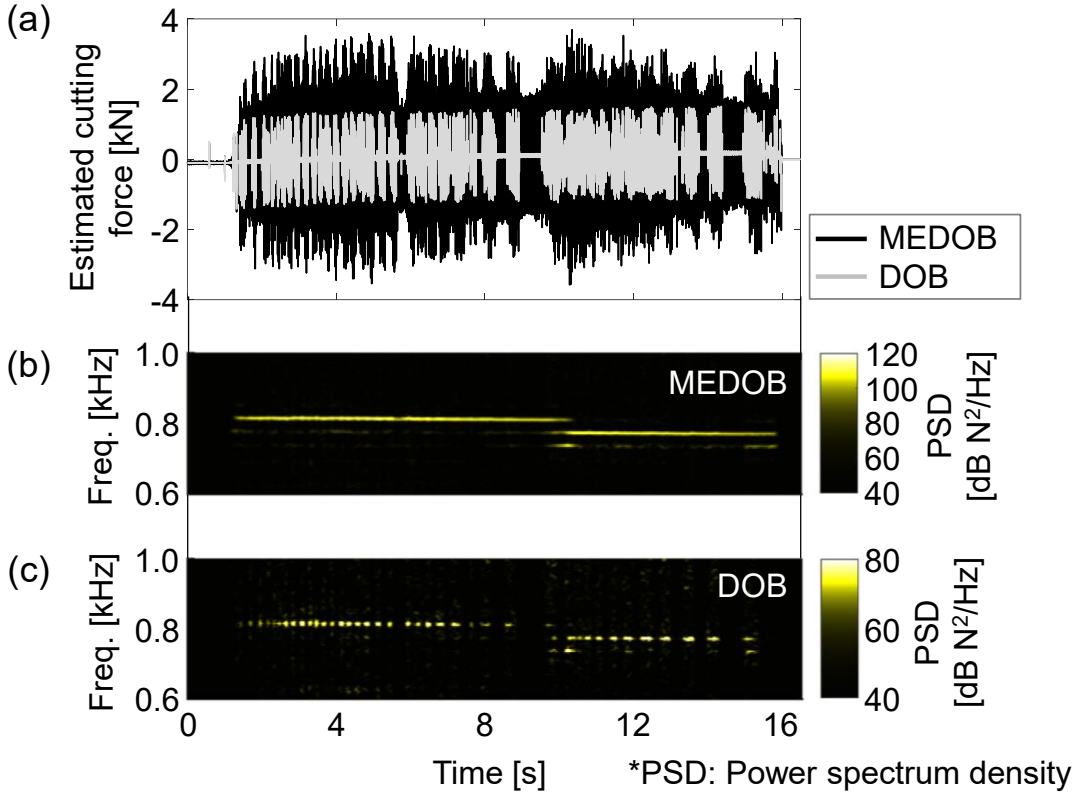

Fig. 6-7 Comparison of experimental result in Y1-axis with 0.2 mm width of cut (a) machined surface (b) time-frequency analysis result of estimated cutting force by MEDOB (c) time-frequency analysis result of estimated cutting force by DOB

acceleration pickup. Though chatter frequency components are also included in DOB, the determination of a suitable threshold is more challenging. The vibration generated at the cutting point was attenuated through transmission to the motor angle due to the damping property of the mechanical components, such as the rolling guideway, nut-screw interface, screw, and support bearings. Therefore, the sensitivity of the cutting force to the rotary encoder signal is lower than that to the linear encoder signal, which makes the differences between the estimation result of DOB and MEDOB.

Fig. 6-7 shows the estimated cutting force components in the Y1-axis where a sliding guideway is employed. When MEDOB is applied, the chatter frequency components are clearly observed as with the X1-axis, where a rolling guideway is used. As shown in Table 6-1, resolution of the rotary encoder for Y1-stage is higher than that for X1-stage. Thus, it is expected that angular response in Y1-axis is more sensitive to chatter than that in X1-axis. However, time-domain data of DOB approaches intermittently zero. In addition, as presented in the time-frequency analysis result, the chatter frequency components repeatedly appear and disappear, similar to the stick-slip phenomenon. The vibrations generated at the cutting point were not transmitted to the motor angle because of the higher damping capacity of the sliding guideway. Therefore, in-process chatter

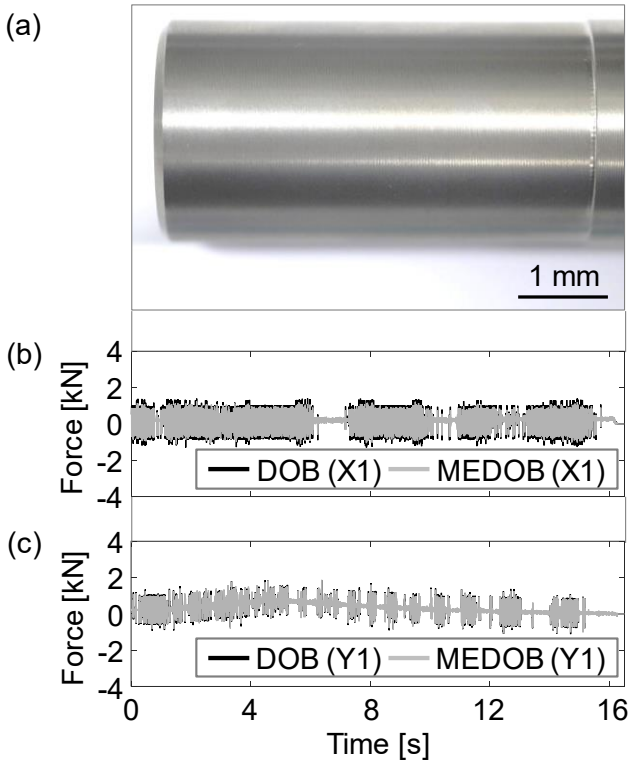

Fig. 6-8 Machined surface and estimated cutting forces with 0.3 mm width of cut (a) machined surface (b) time domain data of estimated cutting force in X1-axis (c) time domain data of estimated cutting force in Y1-axis

monitoring is further difficult, when the variation of the cutting force and the motor angle are low. The use of a linear encoder near the cutting point can increase sensitivity to chatter regardless of guideway type.

Fig. 6-8 shows the machined surface and the estimated cutting forces under stable cutting conditions. In the stable case, there are no significant differences between the estimated cutting force by MEDOB and DOB, because comparatively low frequency components are dominant. In order to quantify and compare the variation of the estimated cutting force between stable and unstable cases, the moving variance [74] was calculated. The moving variance uses the theorem that the variance of a population corresponds to the total power spectrum density of all frequency components, except for the DC component of the population. As shown in Fig. 6-9, the moving variance of MEDOB is significantly different between the unstable and stable cases in contrast to DOB. By applying MEDOB, monitoring of chatter would improve regardless of the guideway type.

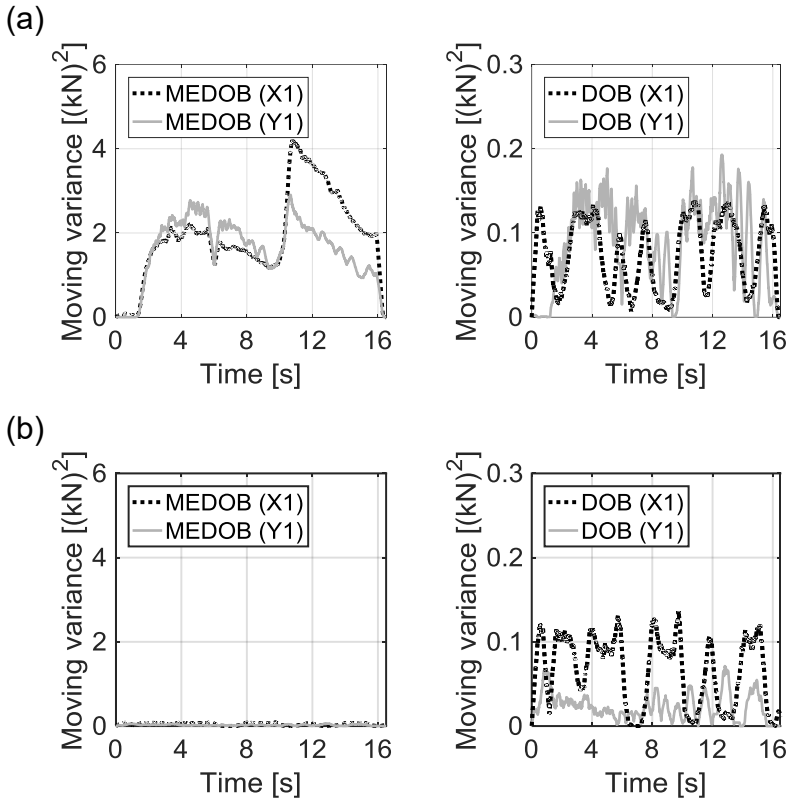

Fig. 6-9 Moving variance of estimated cutting forces (a) unstable case (depth of cut: 0.2 mm) (b) stable case (depth of cut: 0.3 mm)

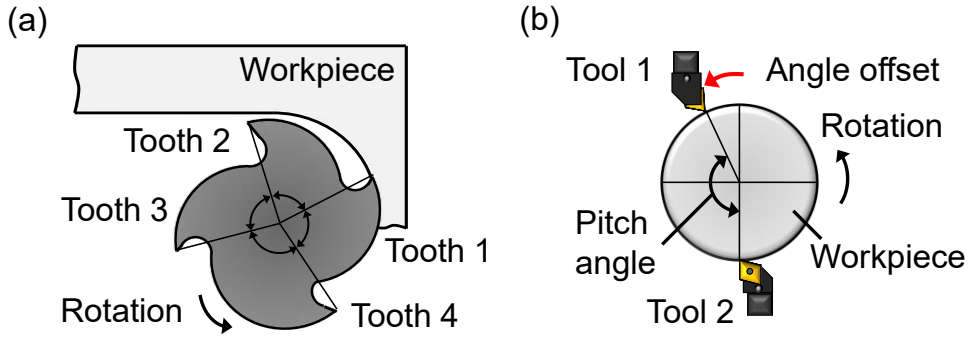

Fig. 6-10 Comparison of (a) milling with variable pitch tool and (b) unequal pitch turning

6.4 Proposal of chatter avoidance technique by unequal pitch turning

6.4.1 Concept of unequal pitch turning

As mentioned in Chapter 1, chatter in milling can be avoided by using a properly designed variable pitch tool. With variable pitch, the phase difference between inner and outer modulation is altered from that in regular pitch tool. In this research, unequal pitch turning is introduced, considering the similarity of the processes as shown in Fig.

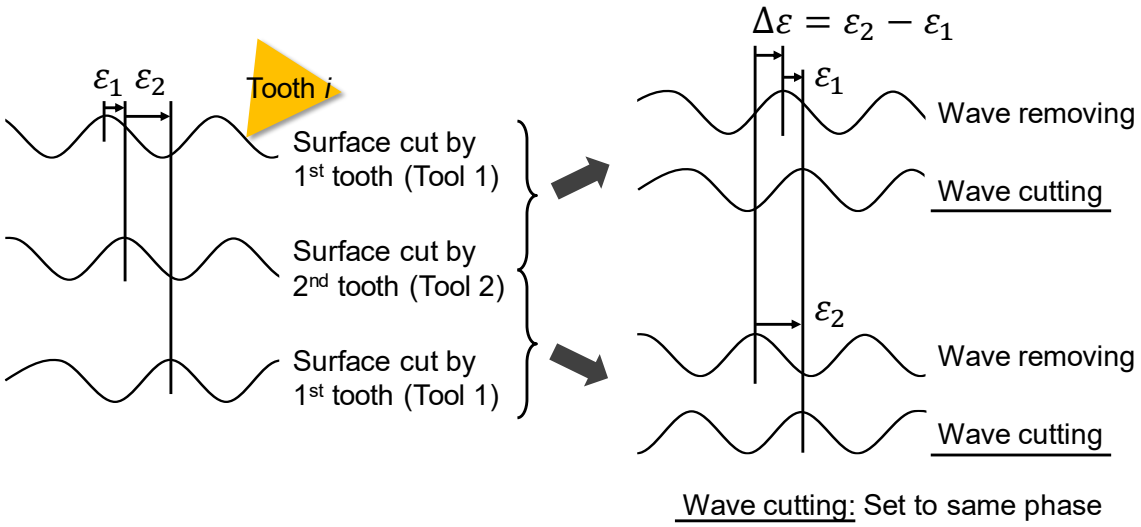

Fig. 6-11 Schematic of regenerative effect in milling with variable pitch tool

6-10. In milling with variable pitch tool, the tooth-pass period is altered. In unequal pitch turning, on the other hand, the time period between two successive cuts is altered by moving cutting point in circumferential direction. Both cutting methods aim to change the period so as to cancel out the regenerative effect. Thus, design method of pitch angle in milling with variable pitch tool is applicable to that in unequal pitch turning. As presented in Chapter 1, the pitch angle of the variable pitch tool is designed so that the phase difference becomes π. Shamoto et al. developed a simple method to optimize the pitch angle of the variable pitch tool [102]. As shown in Fig. 6-11, surface cut by each tooth can be divided into two components: wave removing and wave cutting. The wave removing corresponds to the regenerative vibration of previous tooth. The wave cutting corresponds to present tooth vibration. In Fig. 6-11, the waves cutting are set to same phase; therefore, phase difference between the waves removing influence on stability to chatter, while the wave cutting components does not. The regenerative effect can be canceled out, when the phase difference between regenerative waves $\Delta\varepsilon$ satisfies following equation:

$$\Delta\varepsilon = 2\pi\left(m + \frac{1}{2}\right) \tag{6-1}$$

where $m = 0, 1, 2\cdots$. Considering similarity in mechanics, 1st tooth and 2nd tooth of variable pitch tool shown in Fig. 6-11 can be interpreted as tool 1 and tool 2 in unequal pitch turning. Thus, chatter in parallel turning is avoided when the optimum pitch angle between two tools can be selected, which satisfies Eq. (6-1).

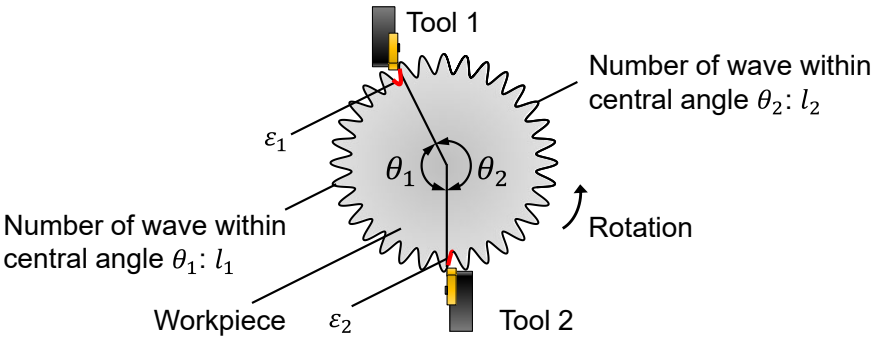

Fig. 6-12 Schematic of wavy surface left on machined workpiece

6.4.2 Optimization of pitch angle

When the chatter occurs, the wavy surfaces remain on the workpiece as shown in Fig. 6-12. Because the chatter develops at single frequency in many cases, the variation period of wavy surfaces corresponds to the chatter frequency. Thus, phase of the chatter frequency component left on one circumference of the workpiece φ can be expressed as follows:

$$\varphi = (f_c \times 2\pi) \div \frac{S}{60} \tag{6-2}$$

where the spindle speed is S min^{-1}, and the chatter frequency is f_c Hz. Phase of the chatter frequency component within central angle θ_1 and θ_2 can be calculated as follows:

$$\begin{aligned} \varphi_1 &= \varphi \times \frac{\theta_1}{2\pi} \\ &= \frac{60}{S}\theta_1 f_c \end{aligned} \tag{6-3}$$

$$\begin{aligned} \varphi_2 &= \varphi \times \frac{\theta_2}{2\pi} \\ &= \frac{60}{S}\theta_2 f_c \\ &= \frac{60}{S}(\theta_1 + \Delta\theta) f_c \end{aligned} \tag{6-4}$$

where $\Delta\theta(=\theta_2 - \theta_1)$ is optimum pitch angle difference.

Phase of the chatter frequency component within central angle θ_1 and θ_2 can be expressed by using number of waves (l_1, l_2) and phase difference (ε_1, ε_2) as follows:

$$\varphi_1 = 2\pi l_1 + \varepsilon_1 \tag{6-5}$$

$$\varphi_2 = 2\pi l_2 + \varepsilon_2 \tag{6-6}$$

By combining Eq. (6-3) ~ (6-6), the following equations are introduced:

$$2\pi l_1 + \varepsilon_1 = \frac{60}{S}\theta_1 f_c \tag{6-7}$$

$$2\pi l_2 + \varepsilon_2 = \frac{60}{S}(\theta_1 + \Delta\theta) f_c \tag{6-8}$$

Therefore, the phase difference between the regenerative waves $\Delta\varepsilon(=\varepsilon_2 - \varepsilon_1)$ can be calculated as follows:

$$2\pi(l_2 - l_1) + \varepsilon_2 - \varepsilon_1 = \frac{60}{S}\Delta\theta f_c$$

$$\therefore \Delta\varepsilon = \frac{60}{S} f_c \Delta\theta \tag{6-9}$$

As mentioned in the last section, the regenerative effect is canceled when the phase difference $\Delta\varepsilon$ is set to odd multiple of π. By substituting Eq. (6-1) into Eq. (6-9), the optimum pitch angle difference $\Delta\theta$ that can suppress the chatter can be introduced as follows:

$$\Delta\theta = 2\pi\left(m + \frac{1}{2}\right)\frac{S}{60 f_c} \tag{6-10}$$

As referred from Eq. (6-10), spindle speed S and chatter frequency f_c need to be determined to calculate the optimum pitch angle difference $\Delta\theta$. Although the spindle speed is regarded as known value, it is preferable to measure the chatter frequency in-process. This is because the chatter frequency can vary during the process (e.g. Fig. 6-5). Therefore, in this dissertation, the chatter frequency was measured in-process from the estimated cutting force.

In contrast to the chatter avoidance techniques using the SLD, the unequal pitch turning method does not require to consider dynamics of the tool system, the workpiece, and its variation due to the material removal. In the method, the phase shit between the regenerative waves are focused rather than variation in the chip thickness. Variation in dynamics can be captured by measuring the chatter frequency during the process, and the in-process chatter avoidance is possible by adaptively changing the pitch angle difference in response to the chatter frequency.

6.4.3 Construction of in-process chatter avoidance system

When conducting frequency analysis, Fast Fourier Transform (FFT) is usually employed. However, it is not necessarily suitable for implementing control system because of its huge calculation load, which is also true of short time Fourier transform (STFT). On the other hand, chatter generally develops around the resonance frequency of the mechanical component, and the resonance frequency can be theoretically calculated based on the material property. Assuming the workpiece as cantilever, natural frequency of the first bending mode f_n can be predicted as follows:

$$f_n = \frac{\eta^2}{2\pi L^2}\sqrt{\frac{EI}{A\rho}} \tag{6-11}$$

Measurement range of the chatter frequency can be limited by using the predicted natural frequency. When monitoring power spectrum of specific frequency component, sliding discrete Fourier transform (SDFT [103]) is applicable on behalf of STFT. Calculation algorithm of SDFT is written as follows:

$$S_k[n] = S_k[n-1]e^{j2\pi k} + y[n+N] - y[n] \tag{6-12}$$

where $S_k[n]$ is the discrete Fourier transform from $y[n]$ to $y[n+N-1]$, $y[n]$ is the analyzed signal, and k is the frequency. By conducting the SDFT for multiple frequencies, it is possible to determine frequency of the most dominant component within specific frequency range, which is regarded as the chatter frequency in this research.

Off-line and on-line (i.e. SDFT) frequency analysis results of the estimated cutting force in Y1 axis are shown in Fig. 6-13. Experimental conditions are listed in Table 6-3. Based on the material property of the workpiece and its projection length, natural frequency of the first bending mode is predicted as 533 Hz. Considering chatter

Table 6-3 Experimental conditions for in-process measurement of chatter frequency

Spindle speed [min^{-1}]	1200
Depth of cut in each tool [mm]	0.2
Feed rate [mm/rev]	0.15
Material of workpiece	JIS SUS303
Diameter of workpiece [mm]	ϕ24.9
Projection length [mm]	180
Analyzed frequency range in SDFT [Hz]	500 - 700
Frequency resolution of SDFT [Hz]	1.0
Calculation interval of SDFT [Hz]	2.25

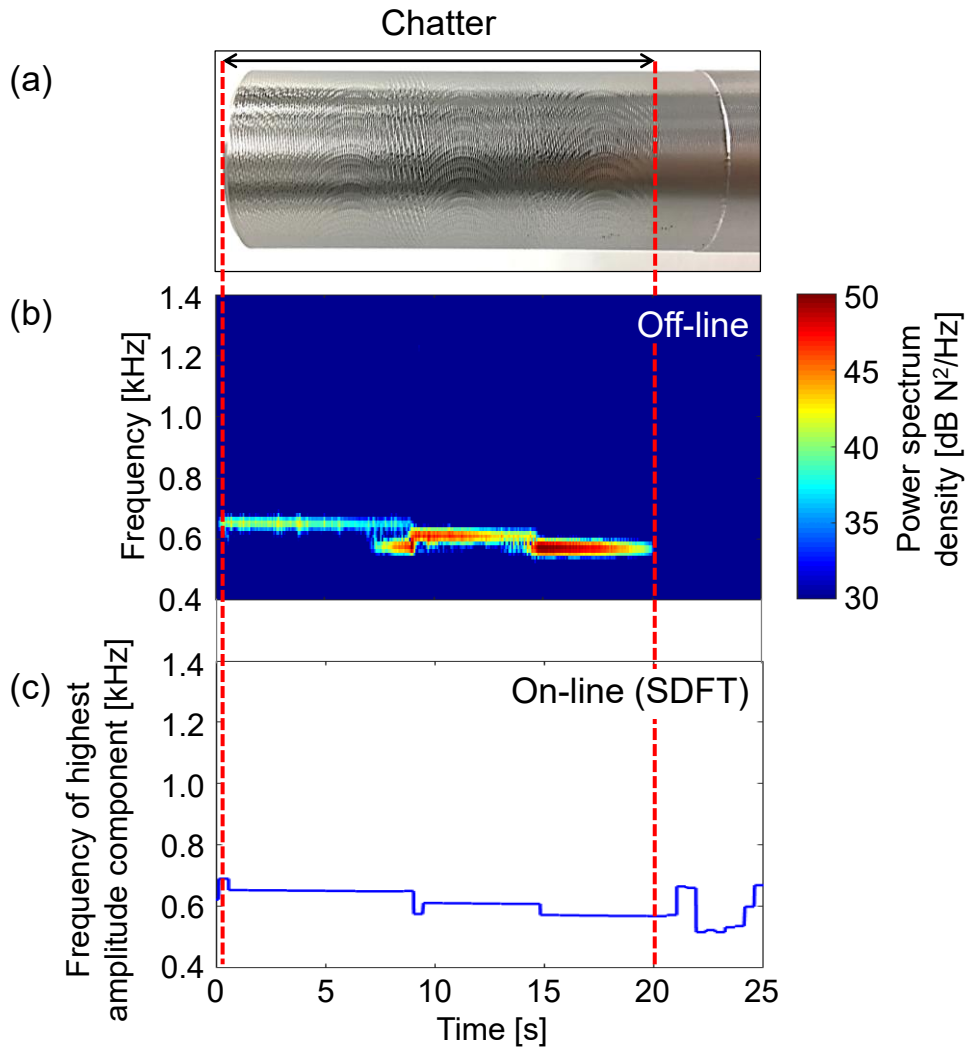

Fig. 6-13 Comparison of off-line and on-line frequency analysis result (a) machined surface (b) time-frequency analysis result of estimated cutting force (c) calculated chatter frequency by SDFT

frequency can change during the process, frequency range of SDFT analysis is set to 500 – 700 Hz. As shown in Fig. 6-13, on-line analysis result approximately coincided with off-line analysis result using SDFT in chatter region. In Fig. 6-14, relation between measurement error of the chatter frequency f_c and calculation error of the pitch angle difference $\Delta\theta/2$ is described. The calculation process is presented in the following. At first, three cases were assumed that the chatter frequencies were 560 Hz, 600 Hz, and 640 Hz and the spindle speed was 1200 min^{-1}. Second, $\Delta\theta/2$ was calculated around each chatter frequency (i.e. 550-570 Hz, 590-610 Hz, 630-650 Hz) based on Eq. (6-10). Next, $\Delta\theta/2$ at each chatter frequency (i.e. 560 Hz, 600 Hz, 640 Hz) was calculated, and was subtracted from $\Delta\theta/2$ that was calculated at the second step. As a result, Fig. 6-14 was obtained. Seen from the figure, calculation error of $\Delta\theta/2$ was less than or comparable to 0.1° within $\pm$10 Hz measurement error of the chatter frequency. Measurement error of the chatter frequency can be regarded as sufficiently small, and its influence on the

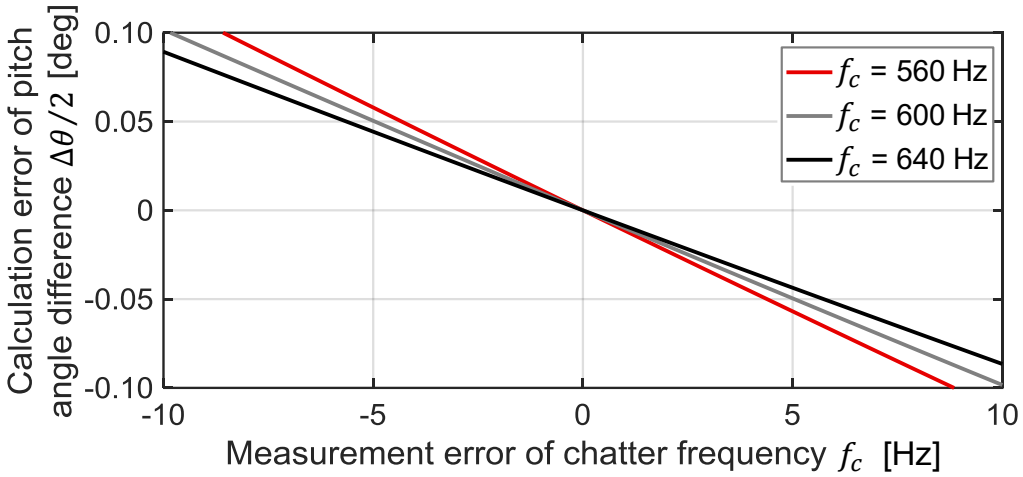

Fig. 6-14 Calculation error of pitch angle difference $\Delta\theta/2$ responding to measurement error of chatter frequency f_c

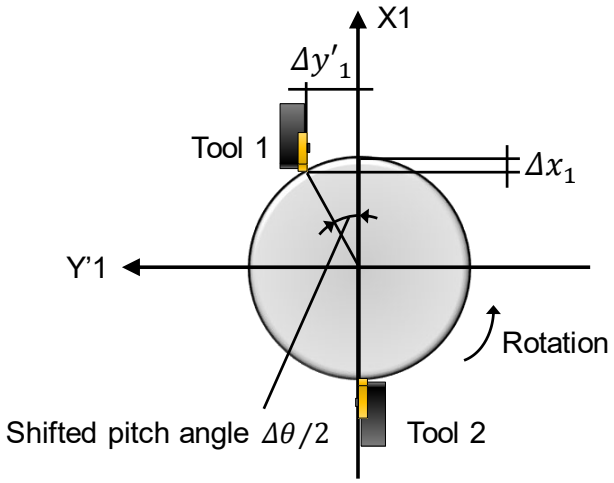

Fig. 6-15 Shifted pitch angle and quantity of turret 1's movement

chatter avoidance is negligible, which will be confirmed in the next section.

In order to avoid chatter as fast as possible, it is desired to reduce calculation cycle of SDFT. However, calculation interval of SDFT is limited to 2.25 Hz (i.e. 444 ms) due to the calculation load. In addition, the number of analyzable cutting force component is also limited to one. Thus, estimated cutting force component in Y1 axis was analyzed in the in-process chatter avoidance test shown in section 6.5.3.

6.5 Chatter avoidance test

6.5.1 Unequal pitch turning at optimum pitch angle difference

Validity of the proposed unequal pitch turning method was evaluated by performing parallel outside turning tests. In the cutting tests, width of cut was set to 0.2 mm and projection length of the workpiece was 160 mm. The other cutting conditions are listed in Table 6-2. At first, conventional equal pitch turning was performed, and chatter

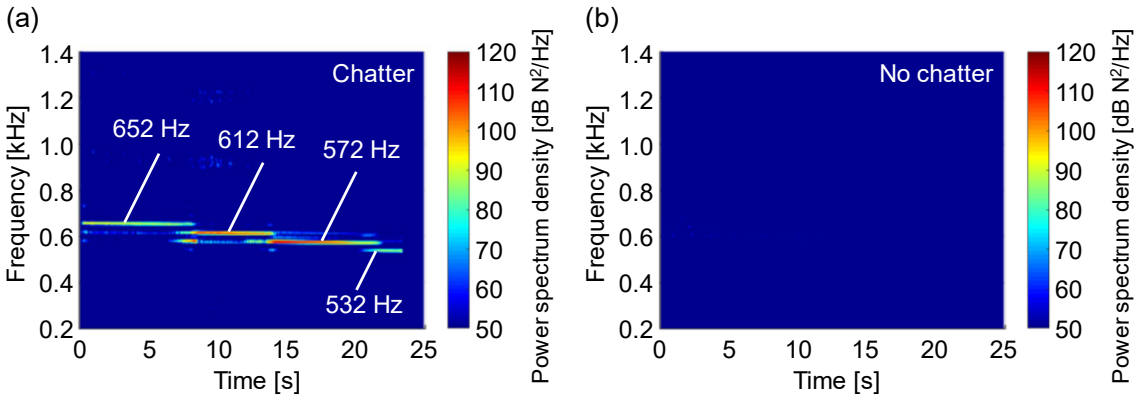

Fig. 6-16 Time-frequency analysis results of estimated cutting force (a) equal pitch turning (b) unequal pitch turning

Fig. 6-17 Machined surface of workpiece (a) equal pitch turning (b) unequal pitch turning

frequency was measured after the process. The optimum pitch angle difference $\Delta\theta$ was also determined by referring Eq. (6-10), and an integer m was set to 0. Secondly, unequal pitch turning was performed without changing cutting condition except for the pitch angle between two tools. Note that only turret 1 was moved in circumferential direction at $\Delta\theta/2$ so that the pitch angle difference between two tools was $\Delta\theta$ as shown in Fig. 6-15. The tool 1 was moved by Δx_1 and $\Delta y'_1$ in X1Y'1 plane, while the posture of the tool 1 was not changed.

As shown in Fig. 6-16 (a), chatter occurred with the frequency of 652 Hz just after start of cutting. Then the dominant chatter frequency shifted to 612 Hz, 572 Hz and 532 Hz. When calculating the pitch angle difference, the chatter frequency was set to 652 Hz, and the optimum pitch angle difference $\Delta\theta$ was calculated as 5.52°. In Fig. 6-16 (b),

time-frequency analysis result in unequal pitch turning was presented. As shown in the figure, characteristic frequency components were not observed. The cutting force variation with the frequency of 612 Hz, 572 Hz and 532 Hz was suppressed as well as that of 652 Hz. By employing the unequal pitch turning, surface roughness Ra is improved from 6.02 μm to 1.54 μm, and chatter marks vanished as shown in Fig. 6-17.

6.5.2 Robustness of pitch angle difference

As shown in the last section, chatter can be avoided even if the chatter frequency changes during the process. That suggests the pitch angle difference that can suppress chatter has some frequency ranges. When calculating the optimum pitch angle difference $\Delta\theta$, an integer m was set to 0 so that the phase difference $\Delta\varepsilon$ became π. On the other hand, the chatter is theoretically avoidable when the phase difference $\Delta\varepsilon$ becomes 3π, 5π .... In this section, the robustness of the unequal pitch turning was experimentally evaluated by changing pitch angle difference. At first, the pitch angle was continuously changed to evaluate whether the process became stable at the point where the phase difference $\Delta\varepsilon$ became odd multiple of π. Second, the stability was experimentally evaluated at the conditions where the phase differences were near π. The shifted pitch angle and the quantity of movement of turret 1 are shown in Table 6-4.

The first experimental result is shown in Fig. 6-18. The shifted pitch angles $\Delta\theta/2$ corresponding to the phase difference $\Delta\varepsilon = 3\pi$, 5π, 7π are approximately 8.2°, 13.8°, 19.3°, respectively. Seen from the figure, the chatter could be avoided in the vicinity of the pitch angle difference where the phase difference was an odd multiple of π. However, loud noise was produced in the experiment, which was not reflected to the time-frequency analysis result of the estimated cutting force. As mentioned before, the cutting point of the tool 1 changed on the X1Y'1 plane without changing its posture. Thus, rake angle gradually changed to negative direction as increase of the pitch angle difference, which resulted in producing larger cutting force and loud noise. In the experimental setup, the optimum pitch angle difference should be set so that the phase difference comes close to π.

The second experiment results are shown in Fig. 6-19. When calculating the optimum pitch angle difference $\Delta\theta$, the chatter frequency was assumed to 652 Hz. The chatter was avoided when the phase difference $\Delta\varepsilon$ was from 0.7π to 1.1π. The process is likely to be stable when the phase difference is lower than π. This is because the machine structure does larger work than the cutting process as explained in Fig. 1-5 (b).

Fig. 6-20 summarizes relation between the phase difference and the pitch angle difference, which is introduced from Eq. (6-9). As shown in the figure, the higher the chatter frequency f_c is, the larger the phase difference is under the same pitch angle

Table 6-4 Shifted pitch angle and quantity of movement of turret 1 in each condition

$\Delta\varepsilon$ [rad]	0.5π	0.6π	0.7π	0.8π	0.9π	1.1π	1.15π	1.2π
$\Delta\theta/2$ [deg]	1.38	1.66	1.94	2.21	2.49	3.05	3.19	3.32
d [mm]	23.4	23.7	24.1	24.5	24.5	22.9	22.5	24.9
Δx_1 [μm]	3.4	5.0	6.9	9.1	11.6	16.2	17.4	20.9
$\Delta y'_1$ [μm]	281.8	343.3	407.9	472.4	532.2	609.2	626.0	721.0

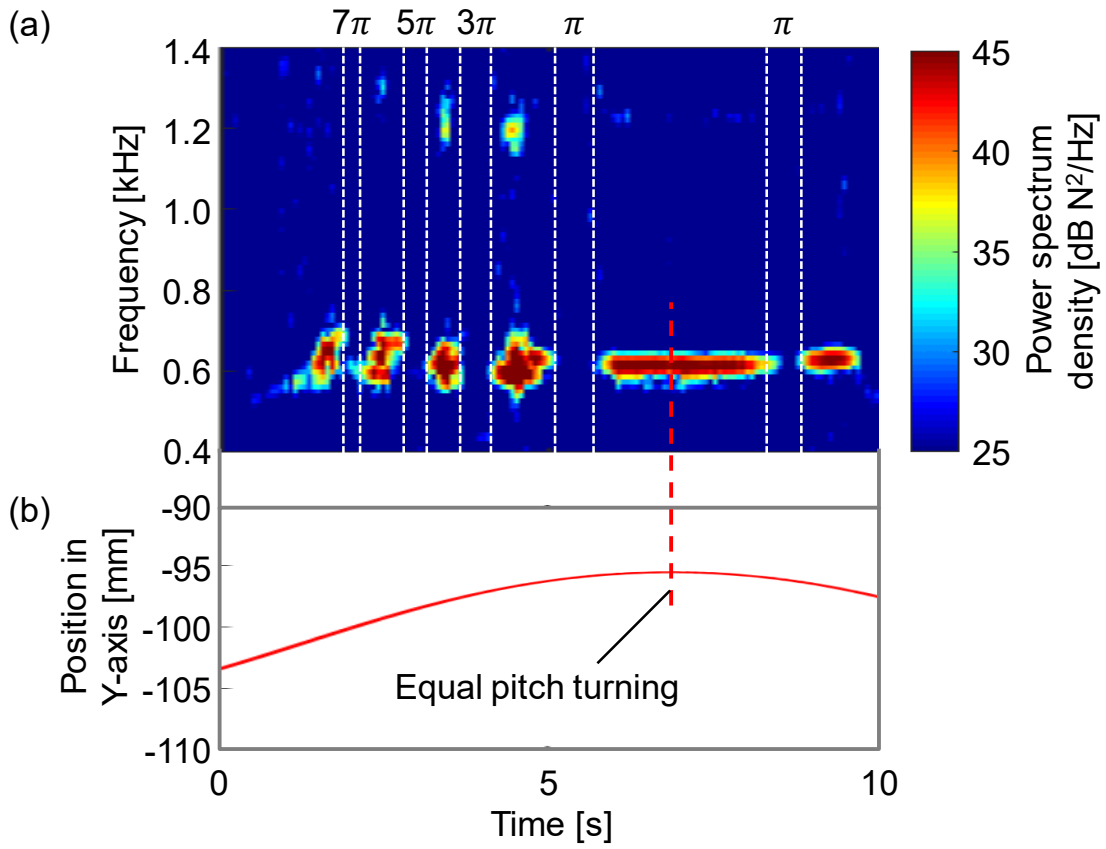

Fig. 6-18 Experimental result under continuous movement of pitch angle (a) time-frequency analysis result (b) motion trajectory of turret 1 in X1-axis

difference. Thus, it is preferable to select the pitch angle difference $\Delta\theta$ based on the largest chatter frequency in order to keep phase difference $\Delta\varepsilon$ not greater than π. When the spindle speed is low, the small pitch angle difference is enough for canceling the regenerative effect. However, the range of the pitch angle difference that can cancel the regenerative effect is narrower compared with the case of the high spindle speed.

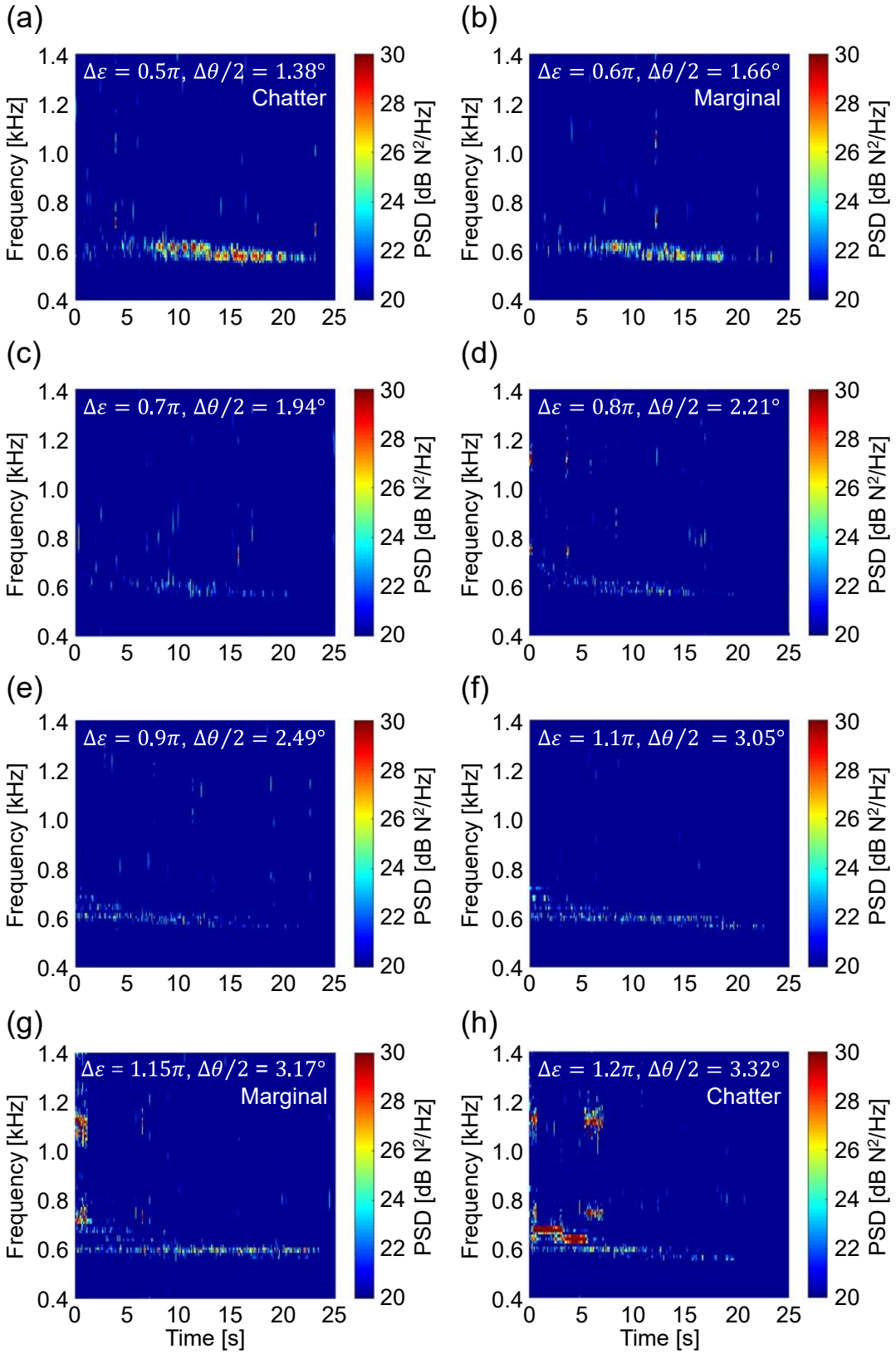

Fig. 6-19 Time-frequency analysis results of estimated cutting force responding to phase difference $\Delta\varepsilon$ and pitch angle difference $\Delta\theta$ (PSD: Power Spectrum Density) (a) $\Delta\varepsilon$ =0.5π (b) $\Delta\varepsilon$ =0.6π (c) $\Delta\varepsilon$ =0.7π (d) $\Delta\varepsilon$ =0.8π (e) $\Delta\varepsilon$ =0.9π (f) $\Delta\varepsilon$ =1.1π (g) $\Delta\varepsilon$ =1.15π (h) $\Delta\varepsilon$ =1.2π

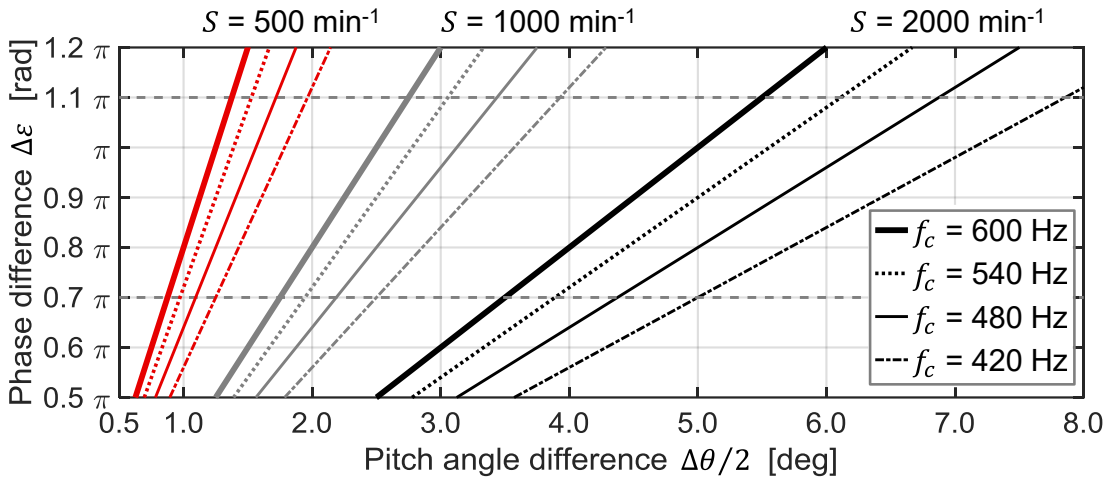

Fig. 6-20 Relation between pitch angle difference and phase difference in unequal pitch turning responding to spindle speed and chatter frequency

Table 6-5 Experimental conditions for in-process chatter avoidance test

Spindle speed [min^{-1}]	1200
Depth of cut in each tool [mm]	0.2
Feed rate [mm/rev]	0.15
Material of workpiece	JIS SUS303
Diameter of workpiece [mm]	ϕ22.1
Projection length [mm]	160
Predicted resonance frequency of first bending mode [Hz]	599
Analyzed frequency range in SDFT [Hz]	550 - 750
Frequency resolution of SDFT [Hz]	1.0
Calculation interval of SDFT [Hz]	2.25
Control interval of pitch angle [s]	1.0 s

6.5.3 Chatter avoidance based on in-process measurement of chatter frequency

Based on the in-process chatter avoidance system constructed in section 6.4.3, the outside parallel turning was carried out at the conditions shown in Table 6-5. Control interval of the pitch angle was set to 1.0 s so that additional vibration was not induced by feed motion. In the cutting test, the cutting method was changed from equal pitch turning to unequal pitch turning during the process.

The experimental result is shown in Fig. 6-21. As shown in Fig. 6-21 (a) and (b), chatter with the frequency of 738 Hz developed in the region where conventional equal pitch turning was carried out. In Fig. 6-21 (c), the shifted pitch angle $\Delta\theta/2$ and the position responses of the X1- and Y'1-direction are presented. In the figure, the displacement in X1- and Y'1-directions at equal pitch turning region are calibrated to zero. In addition,

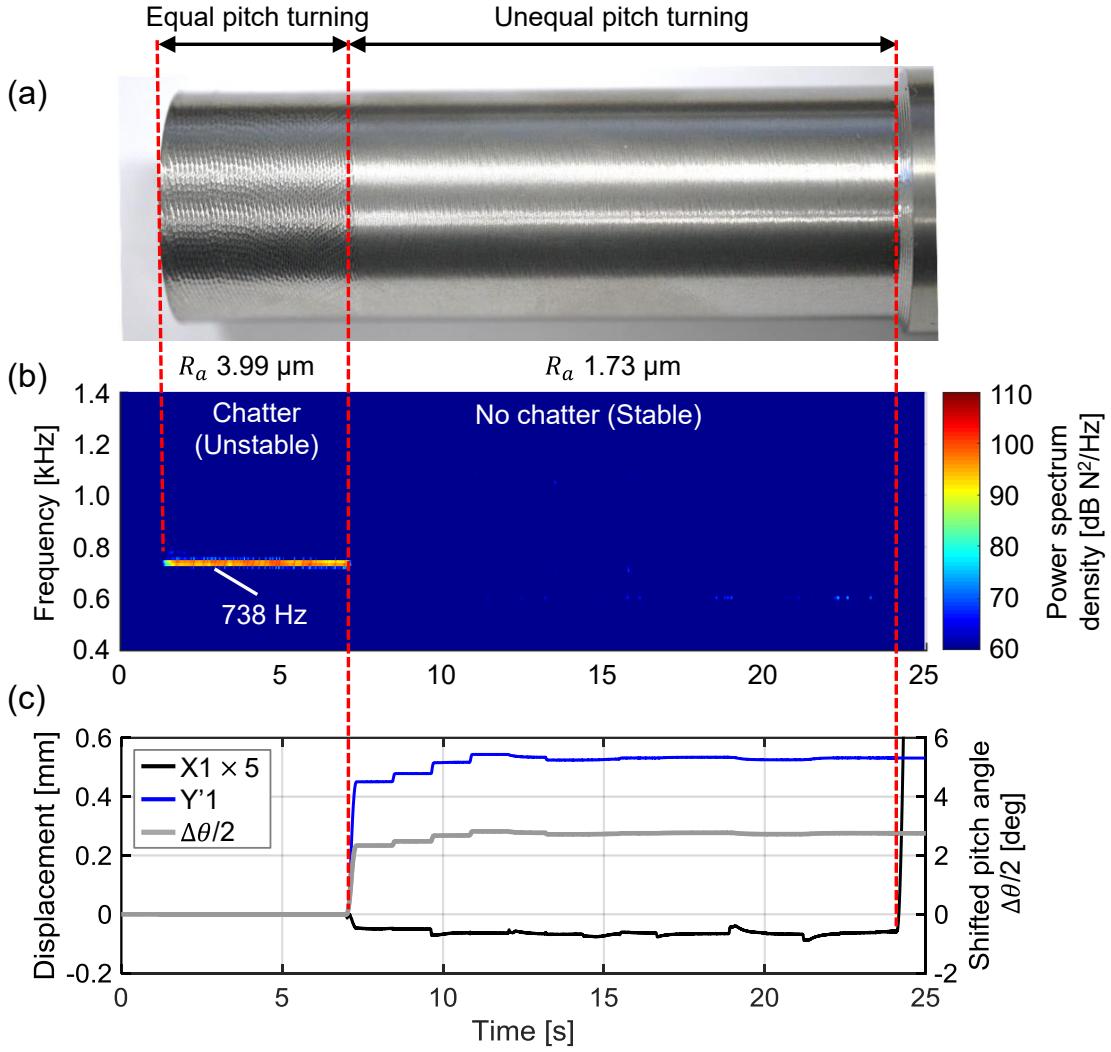

Fig. 6-21 Experimental result of in-process chatter avoidance test (a) machined surface (b) time-frequency analysis result (c) position responses and shifted pitch angle

the displacement in X1-direction was multiplied by five times to make it see well. After the shifted pitch angle $\Delta\theta/2$ was changed from 0°, the chatter frequency component was promptly diminished. By slightly changing the cutting point in circumferential direction, approximately 0.5 mm in this case, the chatter in parallel turning can be avoided.

6.6 Summary

This chapter describes the chatter monitoring in parallel turning and its avoidance technique applying the estimated cutting force. The contents are summarized as follows.

1. In the DOB-based cutting force estimation using inner information of the servomotor, monitoring of the chatter might be difficult when the angle of the servomotor changed little due to the damping property of the sliding guideway. On the other

hand, MEDOB can clearly capture the dominant chatter frequency components regardless of guideway type.

2. Unequal pitch turning method was introduced, considering the similarity of the processes between the parallel turning with the unequal pitch angle and the milling using the irregular pitch tool. The pitch angle is changed so that the phase difference between the regenerative waves becomes π.
3. In the proposed method, the optimum pitch angle difference is calculated from the spindle speed and the chatter frequency. At the same time, the proposed method does not require to consider dynamics of the tool system, the workpiece, and its variation due to the material removal. In addition, it is possible to apply the proposed method when the chatter occurs due to the flexibility of the workpiece, which is out of focus in existing chatter avoidance technique in parallel turning.
4. By performing the unequal pitch turning with the optimum pitch angle, it was possible to avoid the chatter even if the chatter frequency varied during the process. In the experimental setup, the chatter could be avoided when the phase difference was set between 0.7π and 1.1π. When in-process measurement of the chatter frequency is possible based on the estimated cutting force, the chatter can be avoided during the process by adoptively changing the pitch angle.

7. Conclusions

In this dissertation, sensorless cutting force estimation techniques for the ball-screw-drive system were developed, based on disturbance observer using multiple encoder signals. In addition, in-process chatter avoidance technique for parallel turning was developed, applying the estimated cutting force.

In Chapter 1, process monitoring techniques for self-optimizing machine tools and chatter avoidance techniques were explained. Considering cost, sustainability, and application to existing machine tools, sensorless cutting force estimation was focused in this dissertation, and state-of-the-art technologies were explained. Problems of existing chatter avoidance technique in parallel turning were explained and necessity of in-process chatter avoidance technique was presented.

In Chapter 2, two sensorless cutting force estimation methods were proposed, using the inner information of the full-closed control system: the current reference, the motor angle and the stage position.

First, the dual-inertia model of the ball-screw-driven stage was presented, which was used for estimating the cutting force. In addition, inevitable modeling error of the dual-inertia model was explained because of ignoring several structural modes, such as the torsional, the pitching and the yawing modes.

Second, estimating equation of the cutting force was derived by applying multi-encoder based disturbance observer (MEDOB). By considering dynamic interaction between rotation and translation in the MEDOB-based estimation method, it is possible to enhance estimation bandwidth of the cutting force compared with the conventional DOB-based estimation method. Since the cutting force is estimated by extracting rigid body motion in the MEDOB-based method, the stiffness value is unnecessary in estimating the cutting force. The MEDOB-based cutting force estimation is essentially the same as mode-decoupled cutting force estimation in the rigid body mode.

Third, compensation method of phase lag elements in the control system was explained, which was non-negligible in estimating high-frequency cutting force. By delaying the signals so that the total amount of the phase lag became equal, the phase lags can be compensated, such as delay in servo amplifier, numerical differential, and signal transmission.

Next, mode-decoupled cutting force estimation technique was explained, which independently estimated the cutting force component in the rigid body and the vibration mode. By using the modal matrix, the dual-inertia model can be decoupled into two

independent modes. In the vibration mode, cutting force is estimated based on the relative displacement, velocity, and acceleration between the stage and the motor.

Finally, estimating principle in triple-inertia system was presented, considering expansion to multi-inertia system. The estimation error of the cutting force can increase near the resonance frequency when there is discrepancy in degrees of freedom between the plant model and the observer.

In Chapter 3, the specification and the structure of the control system of the simulator and the experimental setup were presented, which were used for evaluating the estimation performance of the cutting force. In addition, the frequency response of the experimental setup and position dependent characteristics of the disturbance force were analyzed in detail, which influenced estimation performance of the cutting force. Owing to the position dependent and the repeatable characteristics of the disturbance force, comparatively low frequency components can be eliminated by performing the idling test. The low frequency variations come from the mechanical elements, such as ball-screw and the motor. On the other hand, high frequency variations resulting from the encoder need to be eliminated by signal processing.

In Chapter 4, the influence of the error factors in sensorless cutting force estimation was evaluated based on the time domain simulation and the actual end milling tests. Specifically, the following error factors were considered in the simulation: the difference of the estimation method (i.e. DOB, MEDOB), the identification error of the movable mass, the quantization error of the angle measurement, and the synchronization errors due to the phase lag elements.

According to the simulation result, measurement error of acceleration or identification error of the movable mass increases the estimation error in high frequencies. In the ball-screw-drive system, the resolution of the rotary encoder is important as well as that of linear encoder, because vibration amplitude of the angle response against the cutting force drastically decreases in high frequencies.

The modeling errors of the observer, including identification and synchronization errors, limit estimation bandwidth of the cutting force. They can evoke estimation error of milling force at the instant when the cutting force becomes local maximum value and cutting edge comes out of the workpiece. In addition, insufficient resolution of encoder evokes high frequency noises especially during air cutting region in intermittent cutting, which develop near the frequency of the higher harmonics.

By constructing the estimation system that considered above error factors, the estimation bandwidth by the MEDOB-based method increased compared with the conventional DOB-based method. It was possible to estimate high-frequency variation of

the actual cutting force with the frequency of 333 Hz, was comparable to previous work evaluated in the linear motor driven stage. The standard deviation of the estimation errors was less than or comparable to 10 N under the evaluated cutting condition.

Though it is difficult to predict amplitude of high frequency noises from the interpolation error of the encoder, their frequencies are predictable considering the feed rate and the signal period. In addition, the torsional vibration of the screw-system can be excited by the cutting force and appears in the estimated cutting force as the high frequency noises. By applying notch filters, the high frequency noises can be eliminated and it is possible to enhance the estimation accuracy.

In Chapter 5, the validity of the mode-decoupled method was evaluated, in which the cutting force component in the rigid body and the vibration mode were independently estimated. Estimation performance of both feed and cross-feed components were evaluated particularly under the low inertia ratio condition.

Because the proportion of the motor thrust force is low under the low inertia ratio condition, the cutting force estimation in the vibration mode is less influenced by the variation of the motor thrust force. On the other hand, the elastic force, corresponding to the relative displacement between the motor and the table, presented high proportion in the wide frequency range. Thus, the position dependency in the relative displacement and the identification accuracy of the stiffness value can influence on the estimation accuracy in the vibration mode.

The experimental results indicated that the temporal variation of the feed force could be estimated in the vibration mode as well as the MEDOB-based method (i.e. in the rigid body mode). Owing to the relative motion-based cutting force estimation, it is possible to decrease high frequency noises due to the output error of the rotary encoder in the experimental setup.

In the vibration mode, it is possible to estimate cross-feed component of the cutting force including higher harmonics, even if the cutting force is less than the maximum static friction force. That is an advantage over the current signal-based estimation technique including the observer-based approach. The relative motion-based estimation is particularly effective when estimating the cross-feed components. Both the standard deviation and mean value of the estimation errors were less than or comparable to 10 N under the evaluated cutting condition.

In Chapter 6, the chatter monitoring and its avoidance technique in parallel turning were described. The cutting force observers were implemented to the control system of the prototype multi-tasking machine tool, and the cutting force components in parallel turning were monitored based on the servo information. Based on the estimated cutting

force, the most dominant chatter frequency was computed during the process and the chatter was avoided by changing the pitch angle responding to the chatter frequency.

In conventional DOB-based cutting force estimation, monitoring of the chatter might be difficult when the motor angle changes little due to damping of mechanical components. By using the position response from the linear encoder in addition to the angle response, on the other hand, MEDOB can clearly capture the dominant chatter frequency components both in rolling and sliding guideways.

In order avoid the chatter in parallel turning, the unequal pitch turning method was proposed. In the method, the pitch angle between two tools are set to unequal value so that the phase difference between the regenerative waves becomes π. By considering the relation between the phase difference and the pitch angle, the optimum pitch angle difference can be calculated from the spindle speed and the chatter frequency. The proposed method does not require the modal parameters of the mechanical components, and it is possible to apply when flexibility of the workpiece is problematic.

The experimental result indicated that it was possible to avoid the chatter by applying the proposed method when the phase difference between the regenerative waves could be set between 0.7π and 1.1π in the experimental setup. By applying the estimated cutting force, the chatter frequency can be calculated during the process. It is possible to adoptively avoid the chatter even if the chatter frequency varies during the process.

To respond to mass customization, the flexibility and the robustness of the production system are further required, and the importance of self-optimizing production system is increasing. In field of machine tool, condition monitoring and stabilization techniques based on it are required, which are indispensable to detection of abnormal cutting and process optimization. Against this background, this dissertation provides sensorless cutting force estimation methods for the process monitoring in the ball-screw-drive system and stabilizing machining method. The error factors in the cutting force estimation were also evaluated, which were non-negligible but were not evaluated with integrative manner. By making use of angle and position responses, it is possible to estimate both feed and cross-feed components of the cutting force. With the integration of the proposed unequal pitch turning and the estimated cutting force, it is possible to avoid destabilization of the process, which can be a part of self-optimizing machine tool in the future.

The proposed techniques can be installed into the ball-screw-driven machine tools with full-closed controlled, which is beneficial for making the existing machine tools be intelligent. In addition to provide methodology to increase accuracy and bandwidth of the cutting force estimation, probable error factors and compensation methods were also provided, which might be problematic in terms of practical application.

In this dissertation, the estimation performance of the cutting force was basically evaluated by assuming dynamic behavior of the ball-screw-driven stage as the dual-inertia system. To extend to the multi-inertia model, using additional sensors, is promising approach to further enhance estimation accuracy and bandwidth, which is particularly remarkable at the spindle side. Process monitoring at the spindle side has advantage in the robustness of the mass variation in the workpiece. Integration of general servo information of the machine tool (e.g. current, angle, position) and additional information (e.g. acceleration at the spindle housing) is worth consideration in future works.

In the mode-decoupled estimation technique, motion of the feed drive is decoupled into rigid body mode and one or more vibration modes. In other words, the Multi-Degree-of-Freedom (MDoF) plant (multi-inertia plant) can be decoupled into multiple equivalent Single-Degree-of-Freedom (SDoF) plants. Thus, it is possible to directly apply existing process monitoring technique constructed in the SDoF system to the MDoF system. As a result, process monitoring in the MDoF system can be easier and simpler by monitoring in the equivalent SDoF system.

Appendix

A) Equivalence of MEDOB-based estimation and mode-decoupled estimation in the rigid body mode

Modal displacement in the rigid body mode x_{rigid} is introduced by referring Eq. (2-39) as follows:

$$x_{rigid} = \frac{1}{\alpha+1}(x_m + \alpha x_t) \tag{A-1}$$

Because inertia ratio α is denoted as $\alpha = M_t/(J_r R^2) = M_t/M_r$, modal mass M_{rigid} and modal damping C_{rigid} in the rigid body mode are rewritten by referring Eq. (2-41).

$$\begin{aligned} M_{rigid} &= (\alpha+1)M_r \\ C_{rigid} &= \alpha_c(\alpha+1)M_r \end{aligned} \tag{A-2}$$

The equation for cutting force in the rigid body mode (Eq. (2-43)) is rearranged by using Eq. (A-1), Eq. (A-2), and $\alpha = M_t/M_r$ as follows:

$$\begin{aligned} F_{cut(rigid)} &= \frac{K_t I_a^{ref}}{R} - (\alpha+1)M_r \cdot \frac{a_m + \alpha a_t}{\alpha+1} - \alpha_c(\alpha+1)M_r \cdot \frac{v_m + \alpha v_t}{\alpha+1} - \frac{T_{fric}}{R} - F_{fric} \\ &= \frac{K_t I_a^{ref}}{R} - M_r a_m - M_t a_t - \alpha_c M_r v_m - \alpha_c M_t v_t - \frac{T_{fric}}{R} - F_{fric} \end{aligned} \tag{A-3}$$

By substituting Eq. (2-30) into Eq. (A-3), the following equation is obtained.

$$F_{cut(rigid)} = \frac{K_t I_a^{ref}}{R} - M_r a_m - M_t a_t - C_r v_m - C_t v_t - \frac{T_{fric}}{R} - F_{fric} \tag{A-4}$$

By referring Eq. (2-8) and Eq. (2-24), the parameters for rotational elements written as translational terms were rearranged to rotational terms as follows:

$$\begin{aligned} F_{cut(rigid)} &= \frac{K_t I_a^{ref}}{R} - \frac{J_r}{R^2} R\alpha_m - M_t a_t - \frac{D_r}{R^2} R\omega_m - C_t v_t - \frac{T_{fric}}{R} - F_{fric} \\ &= \frac{1}{R}\left(K_t I_a^{ref} - J_r \alpha_m - D_r \omega_m - T_{fric}\right) - M_t a_t - C_t v_t - F_{fric} \end{aligned} \tag{A-5}$$

The estimating equation in the rigid body mode is the same as that applying MEDOB, Eq. (2-20).

B) Calculation procedure of transfer function of cutting force observer considering identification error of movable mass

As for the mechanical parameters such as the movable mass, it is possible to calculate frequency response of the observer by transfer function on behalf of conducting time-domain simulation. In this regard, single input and single output system between reference and estimated cutting force is assumed for calculating the transfer function. Estimating equation of the cutting force written in Eq. (4-2), which considers the identification error of the movable mass, is rearranged to Laplace domain as follows:

$$\hat{F}_{cut} = \frac{g_{cut}}{s + g_{cut}} \left\{ \frac{1}{R} K_t I_a^{ref} - \frac{1}{R} (J_r s^2 + D_r s)\theta_m - (QM_t s^2 + C_t s) x_t \right\} \tag{B-1}$$

By considering $J_r = M_r / R^2$ and referring Eq. (2-6) and Eq. (B-1) is rearranged as follows:

$$\hat{F}_{cut} = \frac{g_{cut}}{s + g_{cut}} \left\{ \frac{1}{R} K_t I_a^{ref} - M_t \left(\frac{1}{\alpha} s^2 + 2\zeta_r \omega_t s \right) \cdot R\theta_m - M_t (Qs^2 + 2\zeta_t \omega_t s) \cdot x_t \right\} \tag{B-2}$$

According to Eq. (2-4), both $R\theta_m$ and x_t can be expressed by using I_a^{ref} and F_{cut}. Thus, $\hat{F}_{cut}$ can be rewritten by substituting Eq. (2-4) into Eq. (B-2) as follows:

$$\begin{aligned} \hat{F}_{cut} = {} & \frac{g_{cut}}{s + g_{cut}} \cdot \frac{2(1-Q)\alpha\zeta_k \omega_t s^2 + (1-Q)\alpha\omega_t^2 s}{D(s)} \cdot \frac{K_t}{R} I_a^{ref} \\ & + \frac{g_{cut}}{s + g_{cut}} \left\{ \frac{\omega_t (s^2 + 2\alpha\zeta_r \omega_t s)(2\zeta_k s + \omega_t)}{sD(s)} \right. \\ & \left. + \frac{(Qs^2 + 2\zeta_t \omega_t s)\{s^2 + 2\alpha(\zeta_r + \zeta_k)\omega_t s + \alpha\omega_t^2\}}{sD(s)} \right\} F_{cut} \end{aligned} \tag{B-3}$$

For simplification, single input and single output system from the cutting force reference F_{cut} to the estimated cutting force $\hat{F}_{cut}$ is assumed, and the terms of I_a^{ref} in Eq. (B-3) are ignored in the following calculation. By expanding Eq. (B-3), the transfer function of $\hat{F}_{cut} / F_{cut}$ can be analytically calculated as follows:

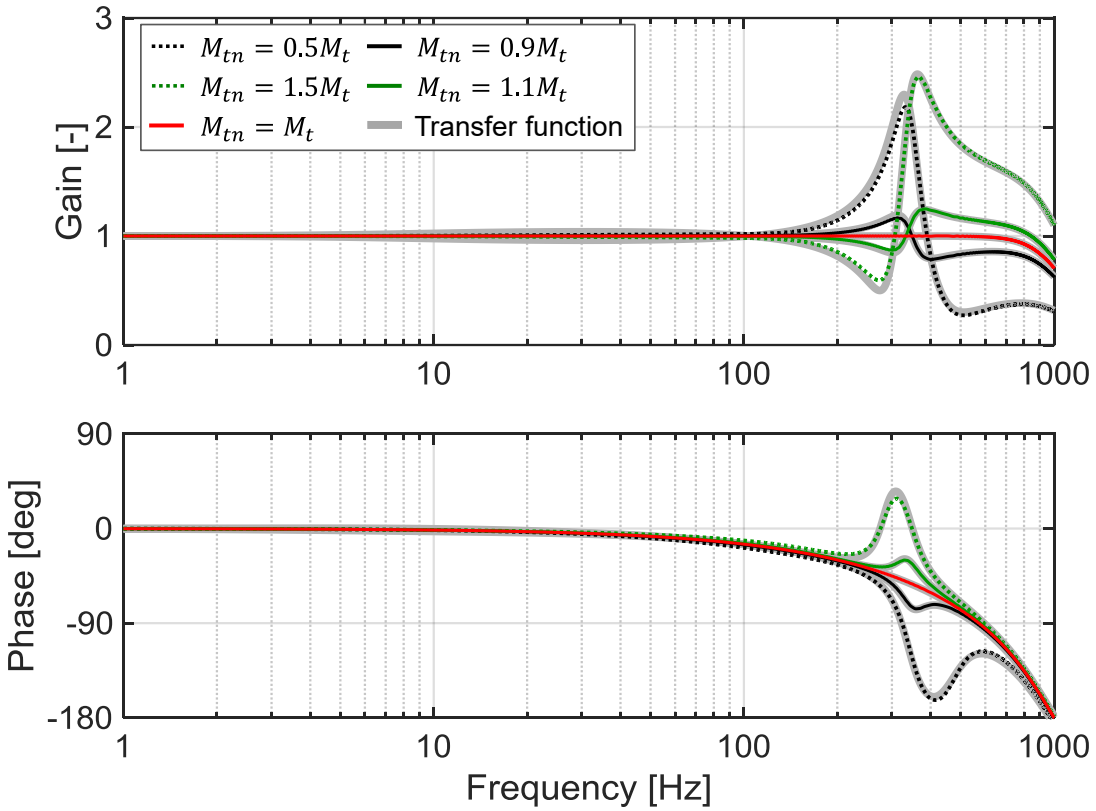

Fig. B-1 Comparison of FRF calculated from time domain simulation shown in section 4.2.2 and transfer function shown in Appendix

$$\frac{\hat{F}_{cut}}{F_{cut}} = \frac{g_{cut}}{s + g_{cut}} \cdot \frac{a_3 s^3 + a_2 s^2 + a_1 s + a_0}{D(s)} \tag{B-4}$$

where

$$\begin{aligned} a_3 &= Q \\ a_2 &= 2\omega_t\{\alpha\zeta_r + (Q\alpha + 1)\zeta_k + \zeta_t\} \\ a_1 &= \omega_t^2\{4\alpha(\zeta_t\zeta_r + \zeta_k\zeta_t + \zeta_r\zeta_k) + Q\alpha + 1\} \\ a_0 &= 2\alpha\omega_t^3(\zeta_r + \zeta_t) \end{aligned} \tag{B-5}$$

When there is no identification error of the movable mass, that is $Q = 1$, the second term on the right hand side of Eq. (B-4) becomes 1. In that case, frequency response of the cutting force observer corresponds to that of low-pass filter, $g_{cut}/(s + g_{cut})$.

As shown in Fig. B-1, it is possible to evaluate the identification error of the movable by using transfer function as well as the time domain simulation.

References

[1] Y. Altintas, A. Verl, C. Brecher, L.G. Uriarte, G. Pritschow, Machine tool fe ed drives, *CIRP Annals - Manufacturing Technology*. Vol.60, No.2, pp. 779–7 96, (2011). doi:10.1016/j.cirp.2011.05.010.

[2] https://www.dmgmori.co.jp/en/products/machine/id=1542, June 12, 2017, *DMG MORI's homepage*.

[3] http://www.okuma.co.jp/english/product/new/laserex/index.html, June 12, 2017, *Okuma's homepage*.

[4] R. Schmitt, C. Brecher, B. Corves, T. Gries, S. Jeschke, F. Klocke, et al., Se lf-optimising Production Systems, *Integrative Production Technology for Hig h-Wage Countries*, Springer Berlin Heidelberg, Berlin, Heidelberg, (2012). p p. 737–738. doi:10.1007/978-3-642-21067-9_6.

[5] Y. Altintas, C. Brecher, M. Weck, S. Witt, Virtual Machine Tool, *CIRP Anna ls - Manufacturing Technology*. Vol.54, No.2, pp. 115–138, (2005). doi:10.101 6/S0007-8506(07)60022-5.

[6] Y. Altintas, P. Kersting, D. Biermann, E. Budak, B. Denkena, I. Lazoglu, Vi rtual process systems for part machining operations, *CIRP Annals - Manufa cturing Technology*. Vol.63, No.2, pp. 585–605, (2014). doi:10.1016/j.cirp.2014. 05.007.

[7] H. Noda, Platform for smart factory with IoT technology and activities with CNC and Robots, *The 17th International Machine Tool Engineers' Confere nce (IMEC)*, Tokyo, pp. 47–66, (2016).

[8] K. Horibe, T. Muraki, Digital Manufacturing by Utilizing Digital Data Integ ration and IoT, *Journal of the Japan Society for Precision Engineering*. Vol. 83, No.1, pp. 36–41, (2017). doi:10.2493/jjspe.83.36. (in Japanese)

[9] R. Teti, K. Jemielniak, G. O'Donnell, D. Dornfeld, Advanced monitoring of machining operations, *CIRP Annals - Manufacturing Technology*. Vol.59, No. 2, pp. 717–739, (2010). doi:10.1016/j.cirp.2010.05.010.

[10] H.-C. Möhring, O. Bertram, Integrated autonomous monitoring of ball screw drives, *CIRP Annals - Manufacturing Technology*. Vol.61, No.1, pp. 355–35 8, (2012). doi:10.1016/j.cirp.2012.03.138.

[11] B. Denkena, T. Mörke, M. Krüger, J. Schmidt, H. Boujnah, J. Meyer, et al., Development and first applications of gentelligent components over their lif ecycle, *CIRP Journal of Manufacturing Science and Technology*. Vol.7, No.2, pp. 139–150, (2014). doi:10.1016/j.cirpj.2013.12.006.

[12] J. V Abellan-Nebot, F.R. Subrión, A review of machining monitoring system s based on artificial intelligence process models, *The International Journal*

of Advanced Manufacturing Technology. Vol.47, No.1–4, pp. 1–21, (2009). doi:10.1007/s00170-009-2191-8.

[13] J. Tlusty, G.C. Andrews, A Critical Review of Sensors for Unmanned Machining, *CIRP Annals - Manufacturing Technology*. Vol.32, No.2, pp. 563–572, (1983). doi:10.1016/S0007-8506(07)60184-X.

[14] I. Inasaki, *Machining system*, Yokendo, Tokyo, pp. 126-127, 158, (2009). (in Japanese)

[15] M. Fujishima, K. Ohno, S. Nishikawa, K. Nishimura, M. Sakamoto, K. Kawai, Study of sensing technologies for machine tools, *CIRP Journal of Manufacturing Science and Technology*. Vol.14, pp. 71–75, (2016). doi:10.1016/j.cirpj.2016.05.005.

[16] A. Matsubara, S. Ibaraki, Monitoring and Control of Cutting Forces in Machining Processes: A Review, *International Journal of Automation Technology*. Vol.3, No.4, pp. 445–456, (2009). doi:10.20965/ijat.2009.p0445.

[17] M.B. Jun, O. Burak Ozdoganlar, R.E. DeVor, S.G. Kapoor, A. Kirchheim, G. Schaffner, Evaluation of a spindle-based force sensor for monitoring and fault diagnosis of machining operations, *International Journal of Machine Tools and Manufacture*. Vol.42, No.6, pp. 741–751, (2002). doi:10.1016/S0890-6955(01)00156-0.

[18] F. Klocke, O. Adams, T. Auerbach, S. Gierlings, S. Kamps, S. Rekers, et al., New concepts of force measurement systems for specific machining processes in aeronautic industry, *CIRP Journal of Manufacturing Science and Technology*. Vol.9, No.1, pp. 31–38, (2015). doi:10.1016/j.cirpj.2015.01.006.

[19] A. Albrecht, S.S. Park, Y. Altintas, G. Pritschow, High frequency bandwidth cutting force measurement in milling using capacitance displacement sensors, *International Journal of Machine Tools and Manufacture*. Vol.45, No.9, pp. 993–1008, (2005). doi:10.1016/j.ijmachtools.2004.11.028.

[20] J.H. Kim, H.K. Chang, D.-C. Han, D.Y. Jang, S.I. Oh, Cutting force estimation by measuring spindle displacement in milling process, *CIRP Annals - Manufacturing Technology*. Vol.54, No.1, pp. 67–70, (2005). doi:10.1016/S0007-8506(07)60051-1.

[21] A.A.D. Sarhan, A. Matsubara, M. Sugihara, H. Saraie, S. Ibaraki, Y. Kakino, Monitoring method of cutting force by using additional spindle sensors, *JSME International Journal Series C*. Vol.49, No.2, pp. 307–315, (2006). doi:10.1299/jsmec.49.307.

[22] P. Albertelli, M. Goletti, M. Torta, M. Salehi, M. Monno, Model-based broadband estimation of cutting forces and tool vibration in milling through in-process indirect multiple-sensors measurements, *The International Journal of*

Advanced Manufacturing Technology. Vol.82, No.5–8, pp. 779–796, (2016). doi:10.1007/s00170-015-7402-x.

[23] S.A. Spiewak, Acceleration based indirect force measurement in metal cutting processes, *International Journal of Machine Tools and Manufacture*. Vol. 35, No.1, pp. 1–17, (1995). doi:10.1016/0890-6955(95)80005-0.

[24] M. Mitsuishi, T. Nagao, Y. Hatamura, S. Warisawa, Real-Time Machining State Detection Using Multiaxis Force Sensing, *CIRP Annals - Manufacturing Technology*. Vol.41, No.1, pp. 505–508, (1992). doi:10.1016/S0007-8506(07)61255-4.

[25] Y. Usui, S. Miyazawa, N. Sawai, Estimation of Cutting Force from Machine Tool Conditions such as Distortion and Vibration., *Journal of the Japan Society for Precision Engineering*. Vol.63, No.11, pp. 1605–1608, (1997). doi:10.2493/jjspe.63.1605. (in Japanese)

[26] H.-C. Möhring, K.M. Litwinski, O. Gümmer, Process monitoring with sensory machine tool components, *CIRP Annals - Manufacturing Technology*. Vol.59, No.1, pp. 383–386, (2010). doi:10.1016/j.cirp.2010.03.087.

[27] Y. Altintas, Prediction of Cutting Forces and Tool Breakage in Milling from Feed Drive Current Measurements, *Journal of Engineering for Industry*. Vol.114, No.4, pp. 386–392, (1992). doi:10.1115/1.2900688.

[28] J.M. Lee, D.K. Choi, J. Kim, C.N. Chu, Real-Time tool breakage monitoring for NC milling process, *CIRP Annals - Manufacturing Technology*. Vol.44, No.1, pp. 59–62, (1995). doi:10.1016/S0007-8506(07)62275-6.

[29] G.D. Kim, C.N. Chu, Indirect cutting force measurement considering frictional behaviour in a machining centre using feed motor current, *The International Journal of Advanced Manufacturing Technology*. Vol.15, No.7, pp. 478–484, (1999). doi:10.1007/s001700050092.

[30] R. Sato, M. Hasegawa, S. Keiichi, Cutting force monitoring based on the frequency analysis of feed motor torques, *Journal of SME Japan*. Vol.2, pp. 7–12, (2013).

[31] K. Ohnishi, M. Shibata, T. Murakami, Motion control for advanced mechatronics, *IEEE/ASME Transactions on Mechatronics*. Vol.1, No.1, pp. 56–67, (1996). doi:10.1109/3516.491410.

[32] H. Shinno, H. Hashizume, H. Yoshioka, Sensor-less Monitoring of Cutting Force during Ultraprecision Machining, *CIRP Annals - Manufacturing Technology*. Vol.52, No.1, pp. 303–306, (2003). doi:10.1016/S0007-8506(07)60589-7.

[33] M. Takei, D. Kurihara, S. Katsura, Y. Kakinuma, Hybrid Control for Machine Tool Table Applying Sensorless Cutting Force Monitoring, *International Journal of Automation Technology*. Vol.5, No.4, pp. 587–593, (2011). doi:10.20

965/ijat.2011.p0587.

[34] S. Ibaraki, T. Okuda, Y. Kakino, M. Nakagawa, T. Matushita, Disturbance Estimation on a Hexapod-Type Parallel Kinematic Machine Tool by Using A Disturbance Observer, *Transactions of the Japan Society of Mechanical Engineers Series C*. Vol.70, No.694, pp. 1764–1769, (2004). doi:10.1299/kikaic.70.1764. (in Japanese)

[35] Y.-H. Jeong, D.-W. Cho, Estimating cutting force from rotating and stationary feed motor currents on a milling machine, *International Journal of Machine Tools and Manufacture*. Vol.42, No.14, pp. 1559–1566, (2002). doi:10.1016/S0890-6955(02)00082-2.

[36] R. Koike, Y. Kakinuma, T. Aoyama, Drill fracture detection by integrating disturbance observer and rotational digital filter, *CIRP Journal of Manufacturing Science and Technology*. Vol.7, No.3, pp. 177–184, (2014). doi:10.1016/j.cirpj.2014.04.001.

[37] B.Y. Lee, Y.S. Tarng, Drill fracture detection by the discrete wavelet transform, *Journal of Materials Processing Technology*. Vol.99, No.1–3, pp. 250–254, (2000). doi:10.1016/S0924-0136(99)00432-X.

[38] X. Li, R. Du, B. Denkena, J. Imiela, Tool Breakage Monitoring Using Motor Current Signals for Machine Tools With Linear Motors, *IEEE Transactions on Industrial Electronics*. Vol.52, No.5, pp. 1403–1408, (2005). doi:10.1109/TIE.2005.855656.

[39] Y. Altintas, I. Yellowley, J. Tlusty, The Detection of Tool Breakage in Milling Operations, *Journal of Engineering for Industry*. Vol.110, No.3, pp. 271, (1988). doi:10.1115/1.3187881.

[40] S. Tönissen, R. Koike, Y. Kakinuma, T. Aoyama, F. Klocke, Monitoring of tool collision in drilling by disturbance observer, *CIRP Journal of Manufacturing Science and Technology*. Vol.7, No.3, pp. 274–282, (2014). doi:10.1016/j.cirpj.2014.05.004.

[41] R. Koike, Y. Kakinuma, T. Aoyama, K. Ohnishi, Tool Collision Detection in High-speed Feeding based on Disturbance Observer, *Procedia CIRP*. Vol. 14, pp. 478–483, (2014). doi:10.1016/j.procir.2014.03.104.

[42] S. Ibaraki, M. Sakahira, H. Saraie, A. Matsubara, Y. Kakino, On the Monitoring of Cutting Forces in End Milling Processes: An Estimation Method by Geometrically Combining Force Vectors of Servo Motors and a Spindle Motor, *Journal of the Japan Society for Precision Engineering*. Vol.70, No.8, pp. 1091–1095, (2004). doi:10.2493/jspe.70.1091. (in Japanese)

[43] D. Kono, A. Matsubara, T. Shirai, K. Hoshide, T. Miura, T. Togashi, Analysis of Positional Deviation Caused by Position-Dependent Disturbances in Bal

l Screw Drive, *Journal of the Japan Society for Precision Engineering*. Vol.82, No.6, pp. 589–594, (2016). doi:10.2493/jjspe.82.589.

[44] T. Miura, A. Matsubara, D. Kono, K. Otaka, K. Hoshide, Design of high-precision ball screw based on small-ball concept, *Precision Engineering*. Vol.47, pp. 452–458, (2017). doi:10.1016/j.precisioneng.2016.09.020.

[45] Y. Altintas, P.K. Chan, In-process detection and suppression of chatter in milling, *International Journal of Machine Tools and Manufacture*. Vol.32, No. 3, pp. 329–347, (1992). doi:10.1016/0890-6955(92)90006-3.

[46] S. Smith, J. Tlusty, Efficient Simulation Programs for Chatter in Milling, *CIRP Annals - Manufacturing Technology*. Vol.42, No.1, pp. 463–466, (1993). doi:10.1016/S0007-8506(07)62486-X.

[47] T. Insperger, G. Stépán, Updated semi-discretization method for periodic delay-differential equations with discrete delay, *International Journal for Numerical Methods in Engineering*. Vol.61, No.1, pp. 117–141, (2004). doi:10.1002/nme.1061.

[48] T. Insperger, B.P. Mann, G. Stépán, P.V. Bayly, Stability of up-milling and down-milling, part 1: alternative analytical methods, *International Journal of Machine Tools and Manufacture*. Vol.43, No.1, pp. 25–34, (2003). doi:10.1016/S0890-6955(02)00159-1.

[49] Y. Altintas, E. Budak, Analytical Prediction of Stability Lobes in Milling, *CIRP Annals - Manufacturing Technology*. Vol.44, No.1, pp. 357–362, (1995). doi:10.1016/S0007-8506(07)62342-7.

[50] E. Budak, Y. Altintas, Analytical Prediction of Chatter Stability in Milling—Part I: General Formulation, *Journal of Dynamic Systems, Measurement*, and Control. Vol.120, No.1, pp. 22, (1998). doi:10.1115/1.2801317.

[51] A. Comak, O. Ozsahin, Y. Altintas, Stability of Milling Operations With Asymmetric Cutter Dynamics in Rotating Coordinates, *Journal of Manufacturing Science and Engineering*. Vol.138, No.8, pp. 081004-1-0810047-1, (2016). doi:10.1115/1.4032585.

[52] J. Munoa, X. Beudaert, Z. Dombovari, Y. Altintas, E. Budak, C. Brecher, et al., Chatter suppression techniques in metal cutting, *CIRP Annals - Manufacturing Technology*. Vol.65, No.2, pp. 785–808, (2016). doi:10.1016/j.cirp.2016.06.004.

[53] A. Matsubara, S. Tsujimoto, D. Kono, Evaluation of dynamic stiffness of machine tool spindle by non-contact excitation tests, *CIRP Annals - Manufacturing Technology*. Vol.64, No.1, pp. 365–368, (2015). doi:10.1016/j.cirp.2015.04.101.

[54] Y. Altıntas, S. Engin, E. Budak, Analytical Stability Prediction and Design

of Variable Pitch Cutters, *Journal of Manufacturing Science and Engineering*. Vol.121, No.2, pp. 173-178, (1999). doi:10.1115/1.2831201.

[55] E. Budak, An Analytical Design Method for Milling Cutters With Nonconstant Pitch to Increase Stability, Part I: Theory, *Journal of Manufacturing Science and Engineering*. Vol.125, No.1, pp. 29-34, (2003). doi:10.1115/1.1536655.

[56] E. Budak, An Analytical Design Method for Milling Cutters With Nonconstant Pitch to Increase Stability, Part 2: Application, *Journal of Manufacturing Science and Engineering*. Vol.125, No.1, pp. 35-38, (2003). doi:10.1115/1.1536656.

[57] N. Suzuki, R. Ishiguro, T. Kojima, Design of irregular pitch end mills to attain robust suppression of regenerative chatter, *CIRP Annals - Manufacturing Technology*. Vol.65, No.1, pp. 129–132, (2016). doi:10.1016/j.cirp.2016.04.041.

[58] S. Turner, D. Merdol, Y. Altintas, K. Ridgway, Modeling of the stability of variable helix end mills, *International Journal of Machine Tools and Manufacture*. Vol.47, No.9, pp. 1410–1416, (2007). doi:10.1016/j.ijmachtools.2006.08.028.

[59] A.R. Yusoff, N.D. Sims, Optimisation of variable helix tool geometry for regenerative chatter mitigation, *International Journal of Machine Tools and Manufacture*. Vol.51, No.2, pp. 133–141, (2011). doi:10.1016/j.ijmachtools.2010.10.004.

[60] A. Ito, E. Shamoto, Proposal of Low-Radial and High-Axial Immersion Machining of Hard Materials with Highly-Varied-Helix End Mill, *Journal of the Japan Society for Precision Engineering*. Vol.81, No.9, pp. 867–874, (2015). doi:10.2493/jjspe.81.867. (in Japanese)

[61] S.D. Merdol, Y. Altintas, Mechanics and Dynamics of Serrated Cylindrical and Tapered End Mills, *Journal of Manufacturing Science and Engineering*. Vol.126, No.2, pp. 317-326, (2004). doi:10.1115/1.1644552.

[62] Z. Dombovari, Y. Altintas, G. Stepan, The effect of serration on mechanics and stability of milling cutters, *International Journal of Machine Tools and Manufacture*. Vol.50, No.6, pp. 511–520, (2010). doi:10.1016/j.ijmachtools.2010.03.006.

[63] G. Stepan, J. Munoa, T. Insperger, M. Surico, D. Bachrathy, Z. Dombovari, Cylindrical milling tools: Comparative real case study for process stability, *CIRP Annals - Manufacturing Technology*. Vol.63, No.1, pp. 385–388, (2014). doi:10.1016/j.cirp.2014.03.137.

[64] S. Smith, J. Tlusty, Stabilizing Chatter by Automatic Spindle Speed Regula

tion, *CIRP Annals - Manufacturing Technology*. Vol.41, No.1, pp. 433–436, (1992). doi:10.1016/S0007-8506(07)61238-4.

[65] E. Al-Regib, J. Ni, S.H. Lee, Programming spindle speed variation for mach ine tool chatter suppression, *International Journal of Machine Tools and M anufacture*. Vol.43, No.12, pp. 1229–1240, (2003). doi:10.1016/S0890-6955(03) 00126-3.

[66] M. Zatarain, I. Bediaga, J. Muñoa, R. Lizarralde, Stability of milling proces ses with continuous spindle speed variation: Analysis in the frequency and time domains, and experimental correlation, *CIRP Annals - Manufacturing Technology*. Vol.57, No.1, pp. 379–384, (2008). doi:10.1016/j.cirp.2008.03.067.

[67] S. Seguy, T. Insperger, L. Arnaud, G. Dessein, G. Peigné, On the stability o f high-speed milling with spindle speed variation, *International Journal of Advanced Manufacturing Technology*. Vol.48, No.9–12, pp. 883–895, (2010). d oi:10.1007/s00170-009-2336-9.

[68] K. Shimana, E. Kondo, H. Karashima, N. Kawagoishi, Fast Detection of Ch atter in End-Milling Using Pseudo Auto-Correlation Function, *International Journal of Automation Technology*. Vol.6, No.6, pp. 728–735, (2012). doi:10.2 0965/ijat.2012.p0728.

[69] X.Q. Li, Y.S. Wong, A.Y.C. Nee, Tool wear and chatter detection using the c oherence function of two crossed accelerations, *International Journal of Mac hine Tools and Manufacture*. Vol.37, No.4, pp. 425–435, (1997). doi:10.1016/S 0890-6955(96)00030-2.

[70] H. Cao, K. Zhou, X. Chen, Chatter identification in end milling process bas ed on EEMD and nonlinear dimensionless indicators, *International Journal of Machine Tools and Manufacture*. Vol.92, pp. 52–59, (2015). doi:10.1016/j.ij machtools.2015.03.002.

[71] G.R. Frumuşanu, A. Epureanu, I.C. Constantin, Method for early detection of the regenerative instability in turning, *The International Journal of Adv anced Manufacturing Technology*. Vol.58, No.1–4, pp. 29–43, (2011). doi:10.1 007/s00170-011-3383-6.

[72] M. Lamraoui, M. Thomas, M. El Badaoui, F. Girardin, Indicators for monito ring chatter in milling based on instantaneous angular speeds, *Mechanical Systems and Signal Processing*. Vol.44, No.1–2, pp. 72–85, (2014). doi:10.101 6/j.ymssp.2013.05.002.

[73] Y. Kakinuma, Y. Sudo, T. Aoyama, Detection of chatter vibration in end mil ling applying disturbance observer, *CIRP Annals - Manufacturing Technolog y*. Vol.60, No.1, pp. 109–112, (2011). doi:10.1016/j.cirp.2011.03.080.

[74] R. Koike, Y. Kakinuma, T. Aoyama, K. Ohnishi, Development of Chatter Vi

bration Detection utilizing Disturbance Observer (2nd Report), *Journal of the Japan Society for Precision Engineering*. Vol.81, No.7, pp. 692–698, (2015). doi:10.2493/jjspe.81.692.

[75] E. Budak, E. Ozturk, Dynamics and stability of parallel turning operations, *CIRP Annals - Manufacturing Technology*. Vol.60, No.1, pp. 383–386, (2011). doi:10.1016/j.cirp.2011.03.028.

[76] C. Brecher, A. Epple, S. Neus, M. Fey, Optimal process parameters for parallel turning operations on shared cutting surfaces, *International Journal of Machine Tools and Manufacture*. Vol.95, pp. 13–19, (2015). doi:10.1016/j.ijmachtools.2015.05.003.

[77] E. Ozturk, A. Comak, E. Budak, Tuning of tool dynamics for increased stability of parallel (simultaneous) turning processes, *Journal of Sound and Vibration*. Vol.360, pp. 17–30, (2016). doi:10.1016/j.jsv.2015.09.009.

[78] M.J. Reith, D. Bachrathy, G. Stepan, Optimal Detuning of a Parallel Turning System—Theory and Experiments, *Journal of Dynamic Systems, Measurement, and Control*. Vol.139, No.1, pp. 014503-1 - 014503-7, (2016). doi:10.1115/1.4034497.

[79] C. Brecher, Y. Trofimov, S. Bäumler, Holistic modeling of process machine interactions in parallel milling, *CIRP Annals - Manufacturing Technology*. Vol.60, No.1, pp. 387–390, (2011). doi:10.1016/j.cirp.2011.03.025.

[80] E. Budak, A. Comak, E. Ozturk, Stability and high performance machining conditions in simultaneous milling, *CIRP Annals - Manufacturing Technology*. Vol.62, No.1, pp. 403–406, (2013). doi:10.1016/j.cirp.2013.03.141.

[81] E. Shamoto, T. Mori, K. Nishimura, T. Hiramatsu, Y. Kurata, Suppression of regenerative chatter vibration in simultaneous double-sided milling of flexible plates by speed difference, *CIRP Annals - Manufacturing Technology*. Vol.59, No.1, pp. 387–390, (2010). doi:10.1016/j.cirp.2010.03.028.

[82] E. Shamoto, T. Mori, B. Sencer, N. Suzuki, R. Hino, Suppression of regenerative chatter vibration in multiple milling utilizing speed difference method – Analysis of double-sided milling and its generalization to multiple milling operations, *Precision Engineering*. Vol.37, No.3, pp. 580–589, (2013). doi:10.1016/j.precisioneng.2013.01.003.

[83] U. Karagüzel, E. Uysal, E. Budak, M. Bakkal, Analytical modeling of turn-milling process geometry, kinematics and mechanics, *International Journal of Machine Tools and Manufacture*. Vol.91, pp. 24–33, (2015). doi:10.1016/j.ijmachtools.2014.11.014.

[84] R. Yan, X. Tang, F.Y. Peng, Y. Wang, F. Qiu, The effect of variable cutting depth and thickness on milling stability for orthogonal turn-milling, *The Int*

ernational Journal of Advanced Manufacturing Technology. Vol.82, No.1–4, pp. 765–777, (2016). doi:10.1007/s00170-015-7418-2.

[85] C. Mitsantisuk, M. Nandayapa, K. Ohishi, S. Katsura, Design for Sensorless Force Control of Flexible Robot by Using Resonance Ratio Control Based on Coefficient Diagram Method, *Automatika – Journal for Control, Measurement, Electronics, Computing and Communications*. Vol.54, No.1, pp. 62–73, (2013). doi:10.7305/automatika.54-1.311.

[86] D.A. Vicente, R.L. Hecker, F.J. Villegas, G.M. Flores, Modeling and vibration mode analysis of a ball screw drive, *The International Journal of Advanced Manufacturing Technology*. Vol.58, No.1–4, pp. 257–265, (2012). doi:10.1007/s00170-011-3375-6.

[87] S. Frey, A. Dadalau, A. Verl, Expedient modeling of ball screw feed drives, *Production Engineering*. Vol.6, No.2, pp. 205–211, (2012). doi:10.1007/s11740-012-0371-0.

[88] K.K. Varanasi, S. a. Nayfeh, The Dynamics of Lead-Screw Drives: Low-Order Modeling and Experiments, *Journal of Dynamic Systems, Measurement, and Control*. Vol.126, No.2, pp. 388, (2004). doi:10.1115/1.1771690.

[89] M.F. Zaeh, T. Oertli, J. Milberg, Finite Element Modeling of Ball Screw Feed Drive Systems, *CIRP Annals - Manufacturing Technology*. Vol.53, No.1, pp. 289–292, (2004). doi:10.1016/S0007-8506(07)60700-8.

[90] C.E. Okwudire, Y. Altintas, Hybrid Modeling of Ball Screw Drives With Coupled Axial, Torsional, and Lateral Dynamics, *Journal of Mechanical Design*. Vol.131, No.7, pp. 71002, (2009). doi:10.1115/1.3125887.

[91] A. Kamalzadeh, D.J. Gordon, K. Erkorkmaz, Robust compensation of elastic deformations in ball screw drives, *International Journal of Machine Tools and Manufacture*. Vol.50, No.6, pp. 559–574, (2010). doi:10.1016/j.ijmachtools.2010.03.001.

[92] R. Sato, M. Tsutsumi, Mathematical Model of Feed Drive Systems Consisting of AC Servo Motor and Linear Ball Guide, *Journal of the Japan Society for Precision Engineering*. Vol.71, No.5, pp. 633–638, (2005). doi:10.2493/jspe.71.633. (in Japanese)

[93] Y. Kakino, A. Matsubara, Z. Li, D. Ueda, H. Nakagawa, T. Takeshita, et al., A Study on the Total Tuning of Feed Drive Systems in NC Machine Tools (1st Report), *Journal of the Japan Society for Precision Engineering*. Vol.60, No.8, pp. 1097–1101, (1994). doi:10.2493/jjspe.60.1097. (in Japanese)

[94] K. Ohnishi, N. Matsui, Y. Hori, Estimation, identification, and sensorless control in motion control system, *Proceedings of the IEEE*. Vol.82, No.8, pp. 1253–1265, (1994). doi:10.1109/5.301687.

[95] M. Matsuoka, T. Murakami, K. Ohnishi, Vibration suppression and disturbance rejection control of a flexible link arm, *Proceedings of IECON '95 - 21st Annual Conference on IEEE Industrial Electronics*. Vol.2, pp. 1260–1265, (1995). doi:10.1109/IECON.1995.483978.

[96] S. Katsura, J. Suzuki, K. Ohnishi, Pushing Operation by Flexible Manipulator Taking Environmental Information Into Account, *IEEE Transactions on Industrial Electronics*. Vol.53, No.5, pp. 1688–1697, (2006). doi:10.1109/TIE.2006.881960.

[97] A. Matsubara, S. Ibaraki, Y. Kakino, M. Endo, M. Umemoto, Vibration Control of Feed Drive in NC Machine Tools by Dual Actuation. 1st Report. Damping Control of 2 Mass System by Relative Velocity Feedback., *Journal of the Japan Society for Precision Engineering*. Vol.69, No.3, pp. 422–426, (2003). doi:10.2493/jjspe.69.422. (in Japanese)

[98] P. Van Loon, *Modal parameters of mechanical structures*, K.U. Leuven, (1974).

[99] A. Nagamatsu, *Introduction to modal analysis*, *Corona publishing*, Tokyo, pp. 362-367, (1993). (in Japanese)

[100] S. Katsura, K. Ohnishi, Absolute Stabilization of Multimass Resonant System by Phase-Lead Compensator Based on Disturbance Observer, *IEEE Transactions on Industrial Electronics*. Vol.54, No.6, pp. 3389–3396, (2007). doi:10.1109/TIE.2007.903931.

[101] Y. Altintas, *Manufacturing Automation: Metal Cutting Mechanics, Machine Tool Vibrations, and CNC Design*, Cambridge University Press, Cambridge, pp. 35-46, (2012).

[102] E. Shamoto, K. Kageyama, T. Moriwaki, Suppression of Regenerative Chatter Vibration with Irregular Pitch End Mill : Construction of Analytical model and Optimization of Pitch Angle, *Proceedings of JSME Kansai Branch Annual Meeting*, The Japan Society of Mechanical Engineers, pp. (3-5)-(3-6), (2002) (in Japanese)

[103] E. Jacobsen, R. Lyons, The sliding DFT, *IEEE Signal Processing Magazine*. Vol.20, No.2, pp. 74–80, (2003). doi:10.1109/MSP.2003.1184347.

Acknowledgement

This dissertation is summary of my research from 2012 to 2017 as a member of laboratory for manufacturing science in Keio University. Owing to the helps from people and environments, I could manage to attain progress in research. Firstly, I would like to express the deepest applications to my supervisor, Associate Professor Dr. Yasuhiro Kakinuma. He gave me a motivation to go Ph.D. program and enthusiastically supported me throughout this research. In addition, he gave me various opportunities to enhance the ability as researcher, such as participating conferences, writing journal articles, applying grant, and engaging in collaborative research with both academia and industry. I would like to show sincere gratitude to Emeritus Professor Dr. Tojiro Aoyama. His comments in research meeting were helpful to keep direction of my research.

I would like to show my gratitude to Professor Dr. Hideki Aoyama, Professor Dr. Toshisyuki Murakami, and Professor Dr. Jiwang Yan in Keio University who provided me with beneficial comments and suggestions in writing this dissertation.

I would like to express heartfelt gratitude to Takamichi Ito, Dr. Jun Fujita, Atsushi Tada, Hirohiko Matsuzaki, Masato Inatsu, Makoto Sawazaki and Yasunori Kato from Toshiba Co. Ltd., for their technical supports. Owing to their assistance, the prototype machine tool could be developed and I succeeded in more accurate and wideband cutting force estimation. I would like to thank Yutaka Nagai, Dr. Satoru Arai, Keisuke Matsumura, and Masahiro Nobutomo from NSK Ltd. for providing high-precision ball-screws and linear guideways. In addition, I also appreciate in analyzing friction characteristics in detail and providing us technical data of them. In constructing the control system of the experimental setup, Junji Tachibana, Takashi Ikeda, and Naoki Kudoh from PMAC Japan Co. Ltd., kindly and politely supported me, and I would like to express them to deep gratitude. Owing to their technical supports, I can start operation of the experimental setup in a short time and construct real-time cutting force estimation system. I would like to show appreciation to Shu Shirakawa from Heidenhain Co. for providing optical linear encoders and valuable comments relating to measurement error of position/angle response.

Development of chatter avoidance system is collaborative research among Nakamura-Tome Precision Industry Co. Ltd., Nagoya University, Tokyo Institute of Technology, PMAC Japan Co. Ltd., and Keio University. Kenichi Nakanishi and Manabu Sawada from Nakamura-Tome Precision Industry Co. Ltd., made efforts in preparing the prototype multi-tasking machine tool and gave me technical advice in experimental verification. I am grateful for their contribution. I would like to express deep appreciation to Associate Professor Dr. Norikazu Suzuki in Nagoya University and Associate Professor Dr. Hayato Yoshioka in Tokyo Institute of Technology for providing me with

meaningful comments regarding development of chatter avoidance system.

My appreciation goes to former and current students in the laboratory, Hiroko Miyazaki, Yuta Mizumoto, Takashi Kadota, Shinya Sakata, and Shuntaro Yamato. I would also like to thank Dr. Ryo Koike for giving me profitable comments relating my research and supporting me to prepare for this dissertation. I am grateful for Michie Ishiwata for her continuous contributions to keep research environments.

I would also like to acknowledge to financial supports by the Grant-in-Aid for JSPS Research Fellow from the Japan Society for the Promotion of Science, and by Machine Tool Engineering Foundation.

Finally, I would like to express special thanks to my parents for their continuous supports.

August, 2017
Yuki Yamada